8-2009

SYNthesis OF POLYMERS FEATURING NOVEL DIPHOSPHINES

Eleanor Tennyson
Clemson University, etennys@clemson.edu

SYNTHESIS OF POLYMERS FEATURING NOVEL DIPHOSPHINES

A Thesis
Presented to
the Graduate School of
Clemson University

In Partial Fulfillment
of the Requirements for the Degree
Masters of Science
Chemistry

---

by
Eleanor G. Tennyson
August 2009

Accepted by:
Dr. Rhett C. Smith, Committee Chair
Dr. Gautam Bhattacharyya
Dr. Jason McNeill

ABSTRACT

This report details the synthesis of functionalized platinum-based metallopolymers featuring *m*-terphenyl-scaffolded and light-harvesting phosphine ligands. Substituents placed on both the phosphine and pendant alkynyl units can enhance the optical activity of the metallopolymers depending on their inherent properties. The presence of the platinum metal atom can be exploited to increase conductivity of the molecule and promises to be a unique and valuable modification for polymers to be used in light emitting diodes and photovoltaics. Light-harvesting phosphines prepared in the course of the metallopolymer development have also been used to prepare luminescent polyelectrolytes that prove valuable for well-defined composite film formation by a simple layer-by-layer deposition protocol.

DEDICATION

To my family. To my parents, MTR and GET, for constantly encouraging and supporting me in any and all endeavors I choose and for providing me with the opportunities to pursue my aspirations. To my older brother, AGT, for guiding me how to survive and hold my own in a demanding discipline; you have provided the chemistry shoes I want to and strive to fill. To my little brother, GTT – "Isabelle," for always being there to listen, laugh and distract me from the omnipresent research obstacles; Broder, you always know how to make everything better.

Finally, to my friends, most notably SEP, AMV and CEQ, without whom my sanity would not have remained intact. While you, SEP, are a self-proclaimed "non-science kid," I would not have survived this without our necessary, almost daily, chats. In fact, I cannot imagine surviving my chemistry career, or any future professional endeavors, without you. You truly are the best in every sense of the word. AMV—no hay palabras; you have provided me with a paramount respite from the lab, writing and locura in general. I do not know what I would have done not having known you throughout this process and, most certainly, far into the future—and I am so glad that is what it is. And to CEQ—I am not really sure what happens to our brains when we are together but I am eternally thankful for it; on countless occasions, you have picked me up off the floor with laughtercizes. We may have the crazy, but I wouldn't have it any other way. And while I may have lost some sanity in the process of the following work, because of all of you, I am so much better, hello much better!

ACKNOWLEDGMENTS

The author of this manuscript would like to thank Dr. Rhett C. Smith for all of his ingenuity, troubleshooting and encouragement throughout. This work would not have been possible without his patience and incredible teaching prowess. Thank you for being the greatest bossman and The Papa Smith.

TABLE OF CONTENTS

LIST OF ABBREVIATIONS

λ_{em} – wavelength of emission

λ_{max} – wavelength of maximum absorbance

τ – lifetime

Φ – quantum yield

$CDCl_3$ – chloroform-d_1

DCM – dichloromethane

DMF – *N*,*N*-dimethylformamide

DMSO-d_6 – dimethylsulfoxide-d_6

E – energy

$h\nu$ – photon

HCl – hydrochloric acid

HPLC – high-performance liquid chromatography

HOMO – highest occupied molecular orbital

IPCE – incident photon to electron conversion efficiency

k_r – radiative rate of decay

k_{nr} – nonradiative rate of decay

LBL – layer-by-layer

LED – light-emitting diode

LUMO – lowest unoccupied molecular orbital

MEH-PPV – poly[2-methoxy,5-(2'-ethylhexyloxy)-1,4-phenylene-vinylene]

MeOH – methanol

n-BuLi – *n*-butyllithium

NaOH – sodium hydroxide

NMR – nuclear magnetic resonance

OCP – organic π-conjugated polymer

OLED – organic light-emitting diode

ORTEP – Oak Ridge Thermal Ellipsoid Plot

P3MT – poly(3-methylthiophene)

PAA – poly(acrylic acid)

PCBM – [6,6]-phenyl-C_{61}-butyric acid methyl ester

PDB – 2-(4-biphenylyl)-5-(4-tert-butylphenyl)-1,3,4-oxadiazole

PL – photoluminescence

PMAA – poly(methyl methacrylate)

PPP – poly(*p*-phenylene)

PPV – poly(*p*-phenylene vinylene)

PtOEP – 2,3,7,8,12,13,17,18-octaethyl-21H,23H-porphine platinum(II)

ROMP – ring opening metathesis polymerization

S – singlet state

S_0 – singlet ground state

S_1 – singlet excited state

SAXS – small angle X-ray scattering

T – triplet state

T_0 – triplet ground state

T_1 – triplet excited state

TCSPC – time-correlated single-photon counting

THF – tetrahydrofuran

TLC – thin layer chromatography

TMS – trimethylsilyl

UV-vis – ultra-violet visible

VT-NMR – variable temperature nuclear magnetic resonance

LIST OF TABLES

LIST OF SCHEMES

LIST OF FIGURES

LIGHT-HARVESTING POLYMERIC MOLECULES: OPTIMIZING THE INTERACTIONS BETWEEN LIGHT AND MATTER

Light is an intricate and complex phenomenon that has been studied since the emergence of scientific disciplines. Even in prehistory, visual clues from everyday life demonstrated how integral light was to life on Earth; those plants and animals that grow in sunlight seem to flourish more than those shielded from light. The success of so many life processes is based upon these complicated interactions between light and matter. Beginning with the interaction between light and small molecules, one can garner a profound understanding as to how light drives complex phenomena in matter. Scaling up these interactions to a macromolecular scale demonstrates how, by harvesting the ability of light to induce important chemical processes, the energy of light is crucial for biological processes and modern technology.

1.1 Interaction between Light and Small Molecules

Initial investigations into the nature of light engaged many physicists in a debate as to whether light behaved as a wave or as a particle. Notable early discoveries in this investigation were made by scientists such as Christiaan Huygens and Isaac Newton. However, the theory of light that still studied today is based largely on work by James Maxwell and Albert Einstein. Maxwell, extending the work of others on the nature of light as a wave, derived his famous equations that describe light in terms of electromagnetic radiation.[1] Nearly forty years later, Max Planck proposed that light was present in quantized energy packets though he admitted an inability to fully comprehend the physical consequences of this. Shortly after Planck's hypothesized energy quantization for light came the cornerstone experiment by Albert Einstein that elucidated

the photoelectric effect. This investigation by Einstein showed that light indeed behaved as a particle as it was capable of ejecting electrons from a metal surface which could, in turn, induce current.[2] Further, Einstein agreed with Planck that these energy packets, quanta as Einstein called them, were in discrete energies. Quanta came to be known as photons and describe the particle nature of light. Thus light can be described as both a particle and wave; this wave-particle duality of light was later studied by Louis de Broglie and applied to other particles besides light. He found that all matter behaved as waves and this behavior could be described with a specific wavelength (de Broglie wavelength).[3] As a result, the initial discoveries of the wave-particle duality of light led de Broglie to his famous formula that explains the wavelike properties of all matter (confirmed for electrons in 1927).

While light can behave as both a wave and a particle, the primary interest to the current investigation is the interaction between light as photons and molecules. While often called particles, photons are truly pseudoparticles since they do not have a resting mass. Yet in all other regards they behave as any other particles encountered in chemistry. Most importantly, photons are able to move freely and exist with certain well defined energies. This frequency of the photon is a paramount property that significantly influences its interaction with all molecules. To better understand the interplay between light and matter of the complex polymers detailed in the current work, it is best to first start with the series of events that occur when light interacts with small molecules.

When a molecule is irradiated with light, it may absorb the energy of the incident light if it is the appropriate energy. Moreover, certain photons with the correct frequency are able to promote an electron to an excited state after absorption of light (Figure 1.1).

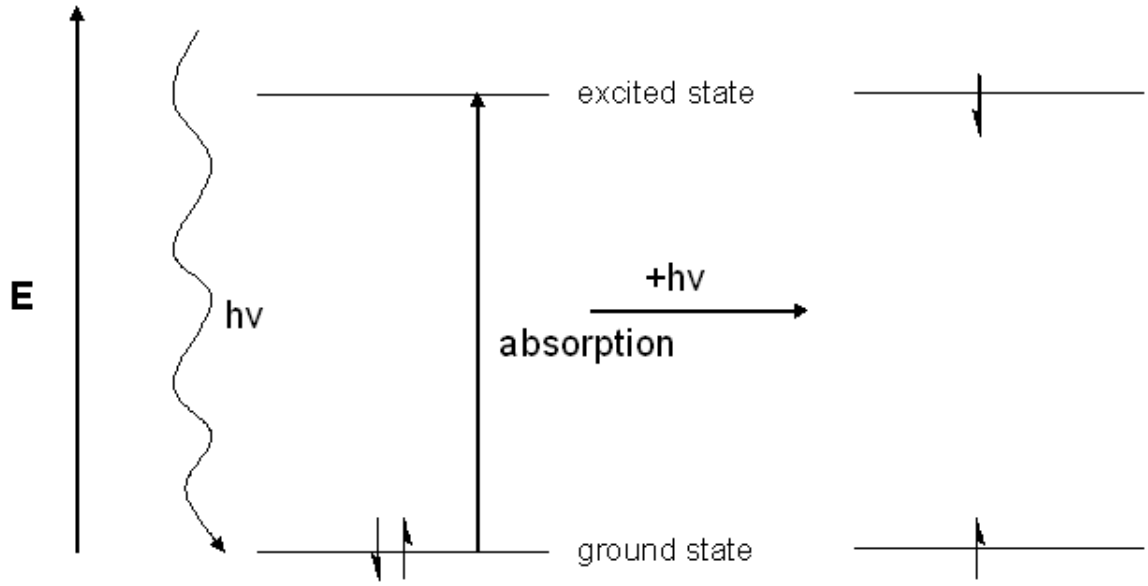

Figure 1.1. Simplified scheme showing the absorption of light by a molecule and subsequent electronic transition.

First, it is important to note that the absorption process occurs so quickly that nuclei do not move (Franck-Condon Principle); thus, absorption of light is thought of as a purely electronic transition from a ground state to excited state (without altering the vibrational levels during excitation). Moreover, if the electronic transition happens concomitantly with a vibrational level transition, the wavefunctions must overlap significantly to favor this process. Examination of a Morse potential diagram shows that absorption occurs without changing the internuclear distance (Figure 1.2); more importantly, the wavefunctions for each vibrational level show that certain transitions are more probable than others. That is, the better overlap between the ground and excited state wavefunction, the higher probability for this electronic transition and thus a more intense absorption peak observed.

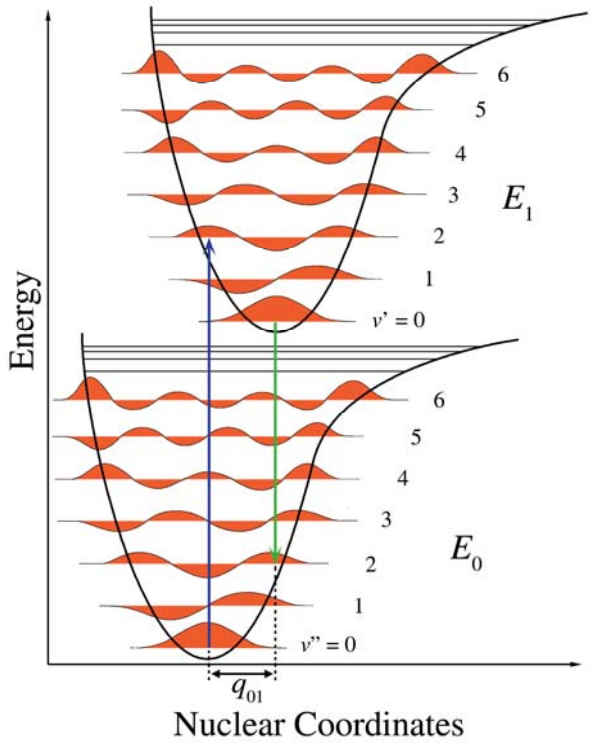

Figure 1.2. Morse potential diagram for ground and excited states to demonstrate the Franck-Condon principle.[4]

For all molecules, there is a specific frequency of light that gives a maximum absorbance. That is, some wavelength of light is most efficiently absorbed by the molecule of interest; this energy corresponds to the most probable electronic transition based on the overlap of the ground and excited state wavefunctions. Most often with small unconjugated molecules, the maximum absorbance occurs with photons of high energy. The physical meaning of this is that it requires much more energy to promote an electron to the excited state in a small molecule as compared to a larger compound with π-conjugation. Moreover, because the color of an object is directly related to the wavelength of light it absorbs, it follows that these small molecules are often colorless because their maximum absorption is not in the visible region (roughly 400 to 700 nm). It

is at this point that it is paramount to consider the nature of the electrons in both the ground and excited state. Most small organic molecules have a singlet ground state; moreover, the selection rules for electronic transitions dictate that the spin of the electron should not change.[5] Thus, absorption and subsequent excitation of the electron must also proceed without changing the spin of the electron. As a result, absorption processes involve an electronic transition from the singlet ground state (S_0) to the singlet excited state (S_1). After the absorption process, the molecule loses some of the harvested energy to vibrational relaxation and excited state energy reorganization processes; the amount of energy lost to these events is called the Stokes shift.

The above description of the absorption of light is certainly an oversimplified one as is the following discussion of the processes that may occur after absorption. After absorption of incident light, small molecules possess extra internal energy that was provided by the photon. There are a number of potential outcomes for this energy, all of which fall into one of two categories: radiative or nonradiative decay. Nonradiative decay involves the molecule releasing the energy from the exited state without emitting light; this can include losing the energy as heat or even in collisions with other small molecules. On the other hand, radiative decay of the excited state energy produces light. There are a number of radiative outcomes for the absorbed energy, the most common of which are fluorescence and phosphorescence (Figure 1.3).

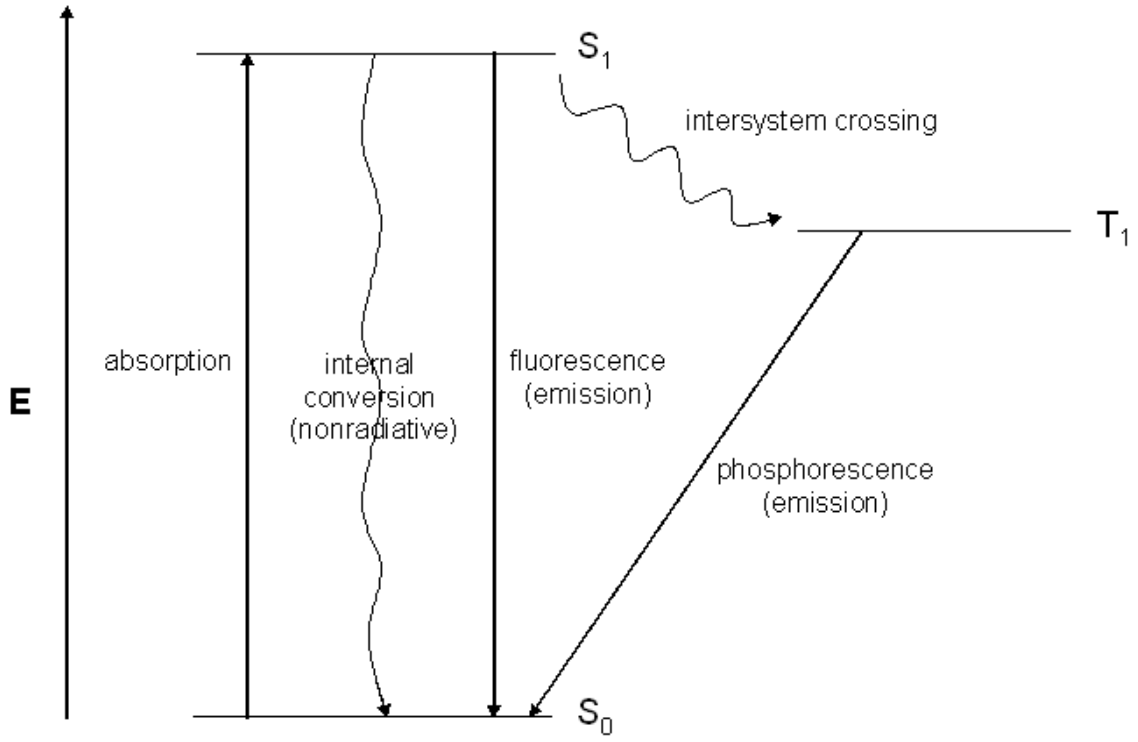

Figure 1.3. Simplified Jablonski Diagram showing the potential fates of the excited state energy after absorption.

Fluorescence is one of the potential consequences following vibrational relaxation after exciting a small molecule with incident light. The process of fluorescence is defined as the radiative decay when the electron in the excited state relaxes back down to the ground state and while doing so emits light at a certain frequency. Thus, the emissive release of the excited state energy by fluorescence ($S_1 \rightarrow S_0$) produces light with lower energy than the photon that was absorbed. As a result, the light released with fluorescence is at longer wavelengths than that of the incident photon. This property of fluorescence allows for tunable emission if a certain colored material is to be made with the molecule of interest.

Another potential emissive release of the excited state energy is via phosphorescence. Phosphorescence is a radiative process that occurs when the electron relaxes from the triplet excited state (T_1) to the singlet ground state. Because the radiation originates from the triplet excited state, it is first necessary for the excited state to undergo a spin-forbidden intersystem crossing (with attendant flipping of the electron) so that the triplet state becomes populated. Not surprisingly then, the electron undergoes another change in spin during emission ($T_1 \rightarrow S_0$) (phosphorescence) and so this process is also spin-forbidden. A direct consequence of these necessary spin flips is that phosphorescence is a much slower and less efficient radiative pathway than fluorescence. Typical rates of fluorescence are on the order of 10^8 s^{-1} with lifetimes around 10 nanoseconds.[6] Because fluorescence or nonradiative decay occurs so quickly after absorption, there is not enough time for intersystem crossing to yield a significant population of the triplet excited state. As a result, rarely do small organic molecules exhibit notably high phosphorescence quantum yields at room temperature.

Absorption and fluorescence are processes of particular relevance when examining molecules that are targeted as materials used for technological purposes. Certain devices such as light-emitting diodes (LEDs) and photovoltaics require specifically tailored absorption and emission properties; thus, it is critical to synthesize materials that are readily tunable to absorb and emit differently and more efficiently. In addition, the process of phosphorescence can be an appealing property for some materials and, in such cases, it is also critical to improve the efficacy of this radiative process as well. Scaling up the size of molecules provides a more diverse array of possible absorption and emission properties than small molecules can provide. More specifically,

examining the photophysics of organic conjugated polymers demonstrates an exciting ability to create materials that require lower energy photons for excitation and emit radiation in a controllable way.

1.2 Organic Conjugated Polymers and Their Photophysical Properties

The ground to excited state electronic transition described in the previous section can be described in terms of molecular orbital theory as promotion of an electron from the highest occupied molecular orbital (HOMO) to the lowest unoccupied molecular orbital (LUMO). When π-conjugation is present in a molecule, the energy difference between the HOMO and LUMO decreases compared to less conjugated analogues; this is primarily because, as delocalization extends further over a molecule, the energy of the HOMO increases while the energy of the LUMO decreases.[7] A direct consequence of this is that the energy required to excite an electron from the ground to excited state decreases as conjugation increases. Moreover, if the excitation source is light, conjugated molecules do not require as high of energy photons as smaller, nonconjugated molecules do. In turn, conjugated molecules absorb more strongly at longer wavelengths since less energy is required to promote the electron into the excited state. As one could imagine, further extension of the conjugation lowers the S_0-S_1 energy gap even more; this fact is particularly useful for designing materials with targeted absorption or emission at a specific wavelength of light.[8]

That increasing the conjugation length of organic molecules shifts the wavelength of maximum absorbance more into the red region is readily demonstrated from a simple example. For example, benzene exhibits an absorbance maximum (λ_{max}) around 180 nm in its electronic absorption,[9] while naphthalene exhibits an absorbance maximum around

270 nm and anthracene, comprised of three fused aromatic rings, has its λ_{max} at around 360 nm (Figure 1.4).[9]

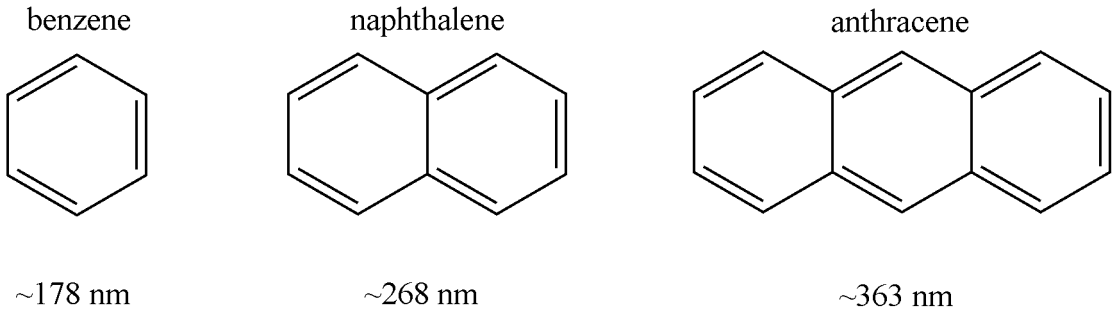

Figure 1.4. Structures and approximate wavelengths of maximum absorbance for benzene, naphthalene and anthracene demonstrating the effect of conjugation on energy of light most efficiently absorbed.

The use of organic π-conjugated polymers (OCPs) in LEDs and photovoltaics is an area of ongoing interest for researchers. Being able to maximize the efficiency of these devices requires the OCP to be intricately tuned to absorb and emit the exact wavelengths necessary for these applications. As a result, recent investigations have focused on synthesizing OCPs from copolymers or specifically functionalized monomers to achieve the desired photophysical properties. For example, a series of poly(*p*-phenylene) polymers (Figure 1.5) with systematic variation of functional groups were synthesized to examine the effects of increasing and interrupting conjugation on photophysical properties.[10]

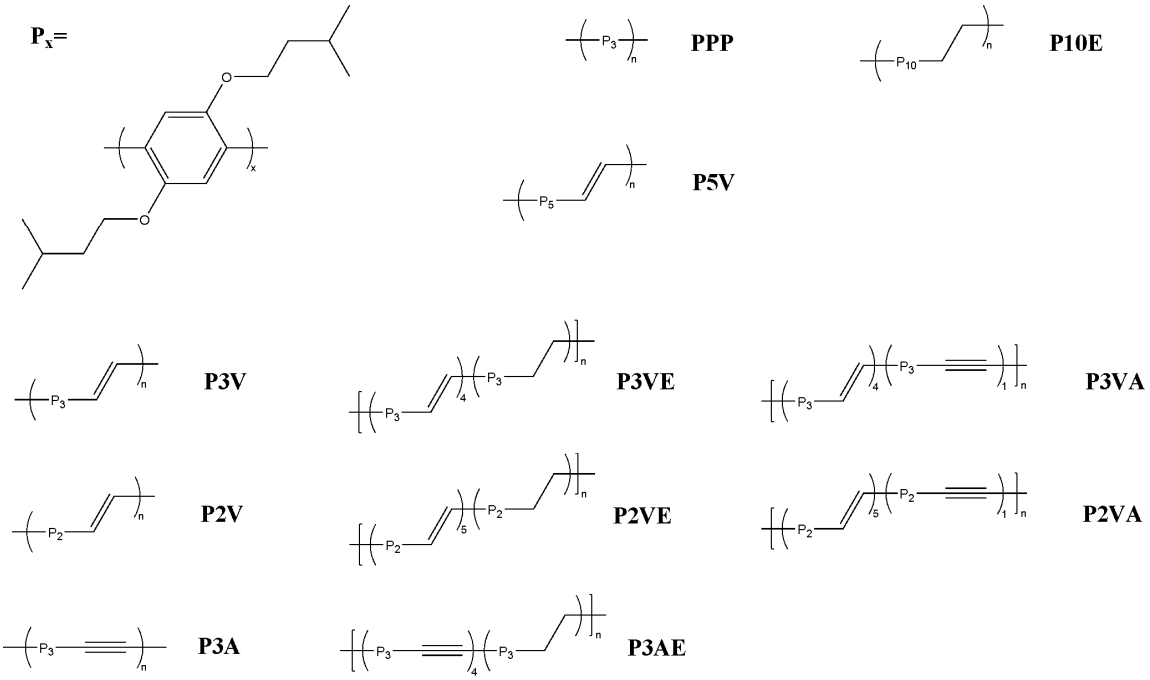

Figure 1.5. Poly(*p*-phenylene) polymers used in the study by Remmers and coworkers.

Remmers and coworkers found that increasing the proportion of vinylene units within the polymer backbone led to progressive bathochromic (to lower energy wavelength) shifting of the absorbance maximum. This decrease in energy gap is directly due to the fact that increasing the fraction of vinylene moieties lengthens the effective conjugation length.

Not only do organic conjugated polymers shift the absorption properties towards lower energy wavelengths, they also effect changes in the photoluminescence processes (fluorescence and phosphorescence). Intuitively, it should follow that if the absorption red-shifts as conjugation extends through the molecule, then radiative emission must also be shifted towards longer wavelengths as a result of the Stokes shift to the red region typical of fluorescence (*vide supra*). As briefly discussed above, much of the interest in OCPs as practical materials originates from the emissive processes that occur after

excitation. Thus, for materials that are targeted for light-emitting devices, it is necessary to create an excited state (exciton) of the polymer that will relax primarily by radiative decay. One of the potential downfalls when considering luminescence efficiency of highly conjugated polymers is that these excitons can be delocalized over extended regions of conjugation and may persist for extended periods of time owing to intra- and interchain excited state transfer.[11] The ability of excitons to migrate increases the probability for quenching of excited state energy. Moreover, previous studies have shown that recombination of excited states limits the efficiency of OCPs in practical applications such as LEDs.[12] Interrupting the conjugation can create exciton traps that reduce the likelihood of nonradiative relaxation and thus increase photoluminescence efficiency. In the aforementioned study,[10] it was found that interrupting the conjugation in poly(*p*-phenylene) copolymers (Figure 1.5) with ethylene increases the photoluminescence efficiency of the polymer. Thus, the photoluminescence efficiency of LED-targeted organic π-conjugated polymers can be enhanced by non-conjugated moieties since they act as excited state traps preventing quenching and nonradiative decay. Though a note of caution is in order because interrupting conjugation can also impact charge carrier mobility, interchain morphology and absorbance maxima.

Because increasing conjugation allows more exciton mobility, it follows that the lifetime of the excited state can be extended with more delocalization. Long-lived excited states also lead to an increased probability of intersystem crossing to the triplet excited state. As a result, with more conjugation, phosphorescence becomes a more accessible radiative pathway for excited state energy emission. Although the previous section would suggest that this would be a detriment to luminescence efficiency, an investigation by Xu

and Holdcroft demonstrate that phosphorescence can become an accessible radiative pathway in π-conjugated organic polymers. [13] They examined several types of poly(3-hexylthiophene) polymers (with differing regiochemistry and molecular weights) and attributed the observed low energy photoluminescence emission at 826 nm to the spin-forbidden phosphorescence process. The phosphorescence lifetime was found to be on the order of 15 μs, much longer than typical fluorescence lifetimes (~10 ns). The use of higher energy light (from laser) to excite the polymers into a higher energy singlet state facilitates subsequent intersystem crossing to access the triplet state. They argue that emission at 826 nm must be phosphorescence because: 1) intensity increases as the excitation energy is increased; 2) the lifetime is on the order of microseconds and 3) the photoluminescence is quenched by oxygen.† Furthermore, the presence of a larger atom (sulfur) in poly(3-hexylthiophene) enhances spin-orbit coupling to relax the forbiddenness of intersystem crossing to the triplet state. This phenomenon, called the "heavy atom effect" is widely observed (see Section 1.3).[14] This investigation demonstrates that conjugated polymers offer another form of optical activity that can be useful for photovoltaics and LEDs.

The above studies demonstrate that increased conjugation in organic polymers is useful for absorbing strongly in the ultraviolet and visible region (for photovoltaics) but it is also known that extended conjugation can cause a decrease in photoluminescent quantum yields. Clearly, there is a delicate balance between functionalization and conjugation that must be achieved to design more efficient and specialized organic polymers to be used in modern technology. One such route of current interest is to

† Oxygen is an efficient quencher of phosphorescence radiative emission.

introduce heavy atom transition metals into polymer backbones to examine the effects of the metal's presence on the conjugation and thus photophysical properties of the material.

1.3 Incorporation of a Transition Metal Changes Light-Harvesting Behavior of OCPs

Spin-orbit coupling is a quantum mechanical phenomenon that permits excited states of different multiplicity to mix despite it being a forbidden process.[15] In terms of photophysical processes, spin-orbit coupling allows certain radiative pathways to become accessible since the spin-forbidden transitions (such as intersystem crossing to the triplet state) can be achieved. The incorporation of heavy atoms (notably platinum, iridum, ruthenium and osmium) into the molecule or polymer chain is thus a viable strategy for enhancing intersystem crossing and consequently phosphorescent emission. Here it is useful to examine the equations that dictate the radiative and nonradiative rates of phosphorescence. The radiative and nonradiative decay rates of phosphorescence (k_r and k_{nr}, respectively) are directly related to the triplet excited state lifetime (τ_T) and the phosphorescence quantum efficiency (Φ_P):

$$k_{nr} = (1- \Phi_P) / \tau_T \quad (1)$$

$$k_r = \Phi_P / \tau_T \quad (2)$$

Compounds or polymers with enhanced spin-orbit coupling (from heavy atoms) have been found to have phosphorescence radiative decay (k_r) rates larger than analogous molecules without the heavy atom. Moreover, because these faster rates are accompanied by shorter triplet excited state lifetimes (τ_T), it follows that larger phosphorescence quantum yields are obtained with heavy-atom containing compounds and polymers.

Early investigations into the heavy-atom effect dealt with small molecules and polymers with sulfur or a halogen serving as the heavy atom. One of the first observations[16] of the heavy-atom effect was made by McClure in 1949. In this study, it was found that substituting aromatic compounds with halogens resulted in an increase in the transition probability from singlet to triplet excited state. In essence, the synthesized halogenated organic molecules had significantly long fluorescence lifetimes and efficient intersystem crossing. Two phenomena operate here: (1) the longer the fluorescence lifetime, the more probability for this excited state energy to transition to the triplet state and then emit radiatively from there; (2) because heavy atoms are present, the spin-orbit coupling is enhanced and intersystem crossing is more efficient.

While the majority of early investigations into the heavy-atom effect on photophysics were concerned with sulfur and halides, recent work has been extended to transition metal incorporation into conjugated polymers. One of the most common metals employed to promote the heavy-atom effect is platinum. The first study on any platinum-containing conjugated polymer was in 1977; in this study, Sonogashira and coworkers synthesized simple platinum acetylide polymers with the platinum atom in a square planar geometry with *n*-butylphosphine ligands on the metal (Figure 1.6).[17] While this study was only aimed at synthesizing a platinum-containing polymer without any accompanying photophysical study, interest grew in discerning the effect of the heavy platinum atom on the optical properties of such polymers.

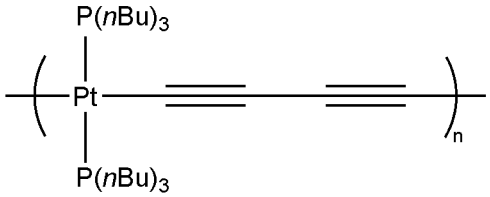

Figure 1.6. First platinum-acetylide polymer as synthesized by Sonogashira and coworkers.

Understanding the effect of platinum incorporation on the photophysics of organic molecules and polymers has grown considerably since this phenomenon was first described. Ground and excited states each contain numerous vibrational states and the absorption and emission processes become more complicated when vibrational levels are taken into account. Incorporating these vibrational levels gives rise to a more detailed Jablonski diagram (Figure 1.7). The spin-orbit coupling that is necessary to partially allow the S→T intersystem crossing transition is often effected by vibrational coupling. Vibrational coupling allows for a mixing between $\pi \rightarrow \pi^*$ transition and excited states such that orbital angular momentum is changed.[18] Effectively this is the spin-orbit coupling necessary for increased population of the triplet excited state. It has been found that the presence of a platinum atom in an emissive polymeric material yields rates[19] of intersystem crossing approaching 10^{11} s^{-1} thereby making the triplet state more easily accessed (competitive with fluorescence). The nonradiative decay from the accessed triplet state is governed by a simple energy gap law;[18] more efficient phosphorescence is derived from a higher-lying triplet excited state.

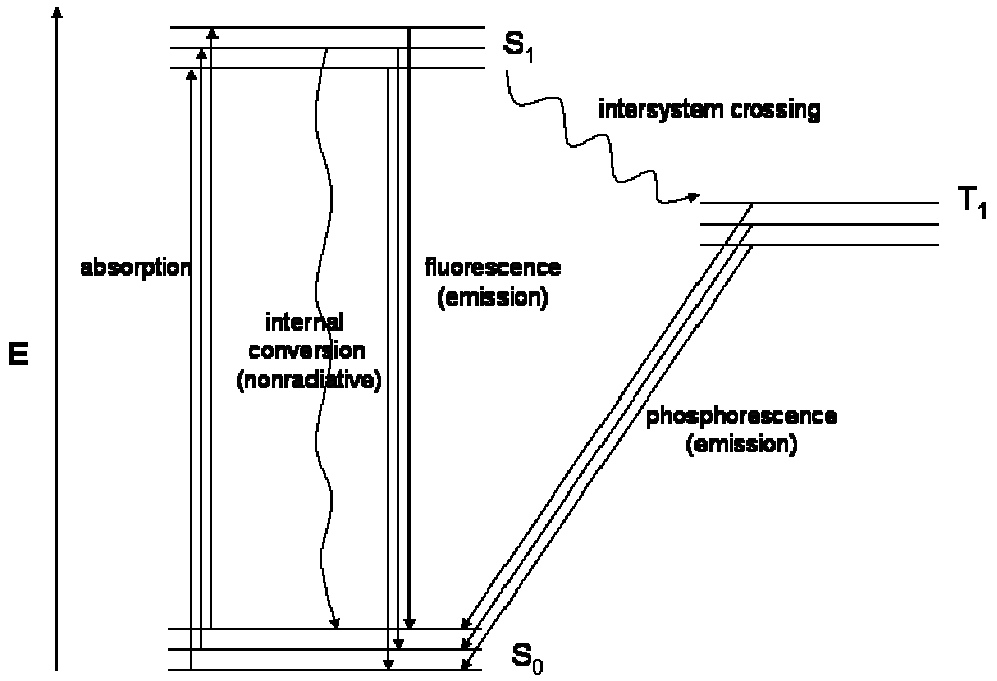

Figure 1.7. Jablonski diagram showing potential absorption and emission transitions including vibrational levels.

To better understand the impact of conjugation length on the photophysical properties of platinum-based organic polymers, the absorption and photoluminescence of platinum-acetylide oligomers of varying length have been examined (Figure 1.8).[20]

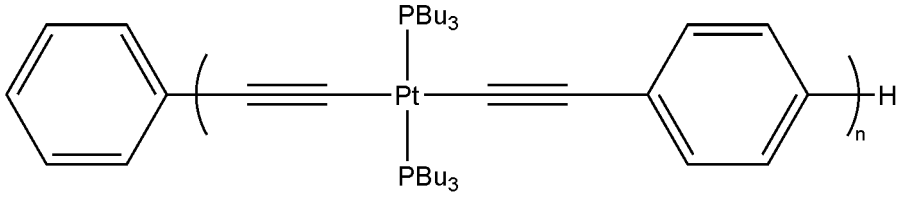

n = 1-5, 7

Figure 1.8. Platinum-acetylide oligomers examined by Liu and coworkers; length of oligomers varies from only one monomer unit to seven.

Room temperature studies on these oligomers revealed that the predominant band in the absorption spectrum is that of the $\pi \rightarrow \pi^*$ transition corresponding to longitudinal energy transfer across the conjugated oligomer. The higher energy, less intense bands in the absorption spectrum are attributed to transitions localized on benzene monomers that do not participate in delocalization across the oligomer. Moreover, the fact that the predominant $\pi \rightarrow \pi^*$ transition is at a similar energy to that for previously studied platinum-acetylide polymers suggests these oligomers are a good model for longer polymeric molecules; this study may also suggest the effective conjugation length in platinum-containing polymers is localized over only a few repeat units. The important finding of this study is that the fluorescence quantum yield in these oligomers is much lower than that of the phosphorescence quantum yield; this implies that intersystem crossing is efficient and favored in these platinum-acetylide oligomer models. In addition, the red-shifting of fluorescence occurs up until the oligomer length reaches about five units long, indicating that the length of conjugation participating in the excited state energy transfer is about six. From the transition energies, it was concluded that the singlet excited state is delocalized while the triplet excited state is considerably localized. However, because phosphorescence intensity still depended on the number of monomers, the triplet excited state still is affected by oligomer chain length.

A more recent study sought to elucidate the delocalization extent of triplet excited states in platinum-acetylide oligomers via variable temperature photophysical experiments and computational methods.[21] The platinum-acetylide oligomers in this investigation were the same oligomers whose structures are provided in Figure 1.8. Using transient absorption spectroscopy to probe the triplet-triplet energy transition, the nature

of the triplet excited state was discerned. This technique showed that all of the oligomers exhibited a strong emission peak at about 650 nm in the transient absorption spectrum after excitation with a 355 nm laser (which generates a triplet excited state). The emission at 650 nm is due to phosphorescence. Moreover, there was no red- or blue-shifting of this peak as the length of the oligomers was changed, suggesting localization on a single chromophore in the platinum-acetylide oligomer. In this investigation, the triplet exciton-localization segment of the oligomers consisted of two platinum-based monomers and two phenylacetylene monomers. Low temperature studies and quantum calculations further indicate that the triplet excited state energy depends on the conformation of the oligomer. These results provide researchers with an insight as to the nature of the triplet excited state as well as how to design platinum-based polymers with specific conformations to effect the desired photoluminescence.

The incorporation of heavy metals into polymer chains effects interesting changes in conductivity and optical activity of the material. Heavy metal atoms (both early and late transition metals) have access to a variety of stable oxidation states. Depending on the nature of inclusion, a transition metal positioned within the π-conjugated backbone of a conducting polymer may not hinder extension of electrical communication through the metal-derivative subunit.[22] The presence of the metal atom can even enhance the conductivity of the material by decreasing the band gap of the material. Incorporating a platinum metal into certain thiophene-based oligomers (Figure 1.9), for example, decreases the band gap energy of **PtTH2** by 0.33 eV relative to **Th2**, the metal-free analog.[23] Moreover, the presence of the transition metal in the oligomer was found to decrease the transition energy compared to the analogous thiophene oligomer. Because

the transition energy further decreases as the chain length increases, the authors conclude that the platinum metal does not disrupt conjugation and still permits delocalization of the excited state energy.

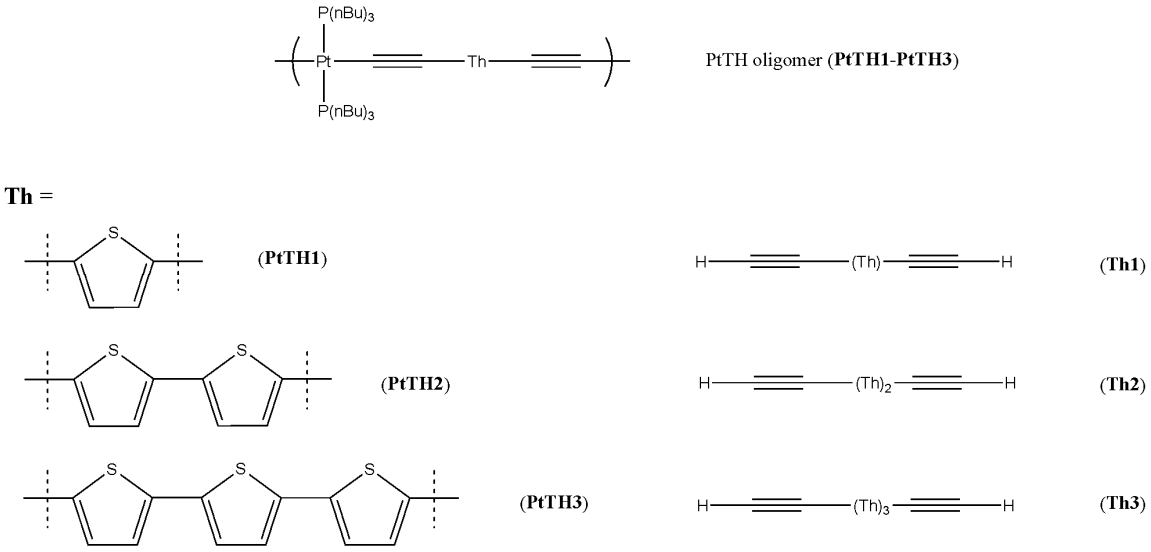

Figure 1.9. Platinum-based oligomers and non-metallated analogous oligothiophenes studied to discern the effect of heavy metal incorporation on conjugation and photophysics.

Because the flow of electrons is not disrupted by the metal atom, it is interesting to examine the optical properties that result from heavy metal incorporation into organic chromophores. In some cases, the heavy metal atom allows semiconducting polymers to be more effective electrical conductors and light emitting complexes than their nonmetallic analogs. The successful synthesis of platinum-based polymers proposed in the current work (*vide infra*) would preface the genesis of a wide range of uniquely-structured materials with potentially enhanced conductivity and photoluminescence quantum efficiency.

1.4 Tuning Organometallic CPs to Alter Band Gap Energy

Because the photophysical properties of all polymers depend on the energy difference between the ground state and excited state, it is possible to synthesize materials that exhibit specifically targeted absorption and fluorescence by manipulating these orbital energy levels. The energy difference between the ground and excited state has thus far been discussed primarily as the difference between S_0 and S_1 (or T_0 and T_1 when concerned with phosphorescence). However, as noted previously, the ground and excited state can be thought of as the HOMO and LUMO of the polymeric material, respectively. Often when moving into the realm of practical materials such as photovoltaics and LEDs, it is convenient to think about this transition energy difference in terms of classical semiconductor band gap theory. In this area, molecules and macromolecules are characterized according to their potential for conducting electrons.

In band gap theory, there exist three major classes of materials that are useful for describing the conductivity of compounds: insulators, conductors and semiconductors. Insulators are materials that do not permit the free movement of electrons and thus cannot conduct electric current (charge per unit time). On the other hand, conductors permit electrons to move freely throughout the material of interest. These rudimentary definitions give rise to band gap theory, which is commonly invoked to explain the conductive properties of any given substance.

The classification of materials into these three groups is founded upon on the energy difference between the electron-filled valence band and the empty conduction band in the material of interest (Fig 1.10).[24]

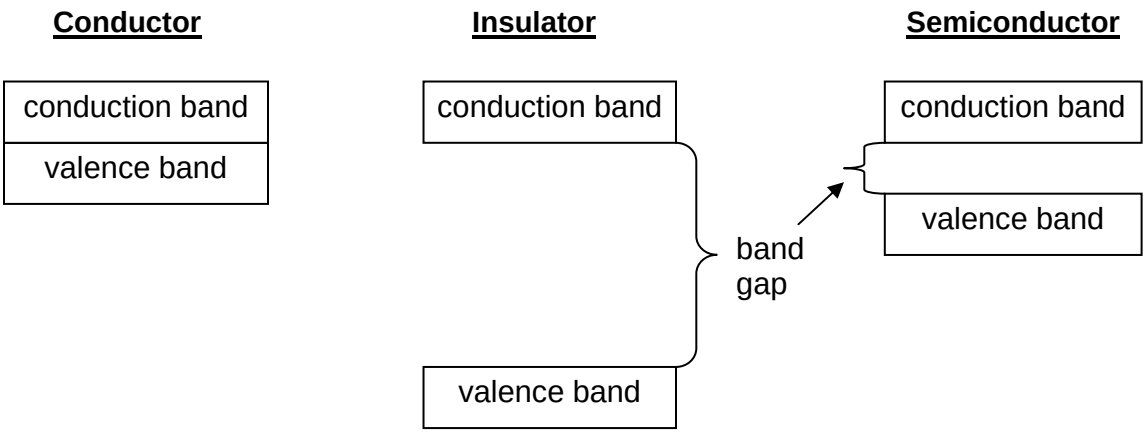

Figure 1.10. General depiction of the band gap for the three classes of materials. Notice the lack of band gap in the conductor class.

In lieu of the terminology that has been used thus far, it is important to point out that the valence band correlates with the HOMO of the molecule of interest while the conduction band correlates with the LUMO. The ability of a material to conduct electricity relies on the difference in energy between the conduction band and the valence band. A number of initiators are possible for promoting an electron: incident light, electrical stimulus and even heat. The promotion of electrons into the conduction band permits electron movement in both the upper and lower band (as a hole is left behind in the valence band upon excitation). Conductors require minimal to no energy to allow free electron motion while insulators do not permit electron movement at all as the band gap is too large. Because of the small energy difference between the valence and conduction band in conductors, however, electron movement can occur even when it is undesired. Semiconductors are the material of interest for this investigation as they will conduct electricity when an electron is excited from the valence band. This property is of

particular utility because the conductivity can be triggered when desired but inhibited in the absence of electron promotion.

Because the chemical nature of the absorption and emission process is founded upon electron transitions between the ground and excited state, it is not hard to imagine that organic polymers find utility in devices that require electrical conductivity. Altering electron donicity of functional groups on the polymer alters the HOMO and LUMO levels and thus the conductivity and wavelengths of absorption and emission. A simple example is provided by an early investigation that demonstrated how charge transfer in organic polymers can be enhanced by functionalization of monomeric units.[25] Specifically, copolymerization of trinitrostyrene and 4-vinylpyridine yielded polymers with significantly enhanced charge-transfer as gauged by strong and broad absorbances. These values were compared with those of trinitrotoluene and various amines which served as monomer models. The greatly enhanced absorbance and extinction coefficient suggest a significant interaction between donor (4-vinylpyridine) and acceptor (trinitrostyrene) moieties in the trinitrostyrene/4-vinylpyridine copolymer. This early study demonstrated that functionalization of monomers or selective copolymerization can alter the charge-transfer events that give rise to photophysical properties and conduction.

The discovery that polymers can be modified to selectively change the absorption, emission and charge-transfer processes led researchers to tune polymers to exhibit the desired photophysics. The previously noted study[11] is another example of a variety of poly(*p*-phenylene vinylene) copolymers with differing HOMO-LUMO energy gaps. In this investigation, a PPV derivative with interruptions in the conjugation shows a blue-shift in the absorbance spectrum, reflecting an increase in the band gap energy. The

authors explain that this shift results from conjugation interruptions by twisting of the polymer. Previous studies have shown that poly[(2,5-dimethyl-*p*-phenylene)vinylene] has a larger band gap than PPV because allylic strain disrupts the conjugation by preventing the polymer from achieving planarity.[26] Thus, by introducing certain steric constraints into a polymer backbone, the energy of light that is absorbed can be controlled. This indicates that the band gap energy is being tuned as a direct result of functionalizing the polymer in such a way that steric clashes disrupt planarity. Initial successes in band gap engineering have led to increasing intricacy in polymer structure to affect their photophysical behavior.

Functionalization allows not only for tuning of an OCP's band gap, but can also affect its photoluminescence efficiency. This aspect is well illustrated by a variety of poly(*p*-phenylene) polymers (Figure 1.5).[10] A particularly interesting result of this study is that a solid state photoluminescence of the poly(*p*-phenylene) polymer **P10E** was significantly red-shifted versus the analogous solution phase spectrum (Figure 1.11).

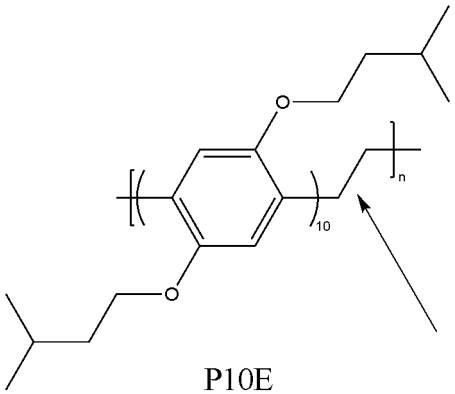

P10E

Figure 1.11. Polymer **P10E** that exhibits significant red-shifting in solid-state as compared to solution phase, as measured by UV-vis spectroscopy. The arrow denotes the bond that can manifest as a vinylene impurity, which results from the polymerization conditions.

The red-shift is attributed to a higher concentration of vinylene "impurities" in the polymer backbone in the solid state as compared to the dilute solution. Random, infrequent presence of a double bond in the highlighted position (Figure 1.11) does not significantly affect the absorption or fluorescence of dilute solutions of **P10E**. However, in solid state photophysical studies, there is a strong red-shifting in the emission wavelength ($\Delta\lambda$ = 56 nm); the authors suggest that, because the excited state energy transfer to the vinylene impurities is more efficient in the solid-state, the emission is red-shifted as it becomes more dominated by this chromophore emission. It is also possible that the red-shifting is merely a consequence of enhanced chain aggregation and excimer formation in the solid-state that is not as probable in dilute solutions. Thus, the maximum emission wavelength and intensity of a polymer can also be shifted according to the monomer's photophysical characteristics. This investigation also demonstrated that the monomer identity affects the photoluminescence efficiency. Further insights are provided

when examining a material analogous to **P10E**, but in which every fourth vinylene unit is replaced by an acetylene unit (**P3V** versus **P3VA**, respectively—Figure 1.12). This change in structure results in a red-shift ($\Delta\lambda$ = 18 nm) in the photoluminescence spectrum.

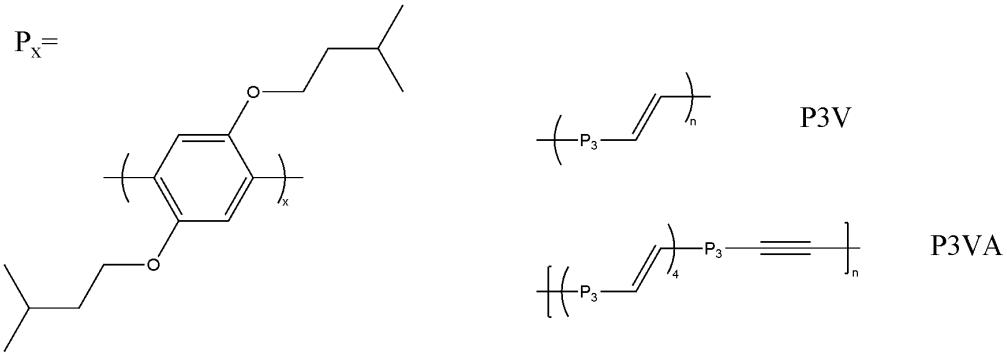

Figure 1.12. Poly(*p*-phenylene) type polymers **P3V** and **P3VA**.

The acetylene moiety has an excited state with lower energy than the vinylene; excited state energy prefers to emit (either radiatively or nonradiatively) from the lowest available energy level. As a result, the excited state energy seeks out the acetylene "impurities" in **P3VA** and decays from an excited state delocalized over a molecular segment that includes the triple bond, often nonradiatively, instead of radiative decay from the vinylene moiety. Thus, emission from the acetylene excited state is lower in energy (red-shifted) and the quantum yield is lowered. Remmers and coworkers demonstrate that "impurities" in the polymer backbone allow for tunable emission and photoluminescence efficiency based on the monomer identity and polymeric functionalization.

Other investigations were aimed at investigating platinum-containing polymers to determine how the metal influences the effective conjugation length of the polymeric

backbone as well.[23] One such study examined a variety of platinum and palladium containing poly-ynes to discern whether the metal interrupts the conjugation or participates in the delocalization. They found that the platinum or palladium d orbitals mix with the p orbitals from the acetylide ligand in the polymeric structure. Moreover, using computational techniques and spectroscopic methods, it was predicted that the triplet excited state extends over one repeating units while the singlet excited state spans about two repeating units within the polymer chain. These results agree well with previous work indicating that the triplet excited state is very localized compared to the singlet excited state.[21] However, an important finding was that the platinum and palladium do not disrupt the conjugation of the polymer, but still provide enhanced phosphorescence.

A related study by Wilson and coworkers examined various acetylide-based polymers with *trans*-tributylphosphine present in each repeating unit (Figure 1.13).[18]

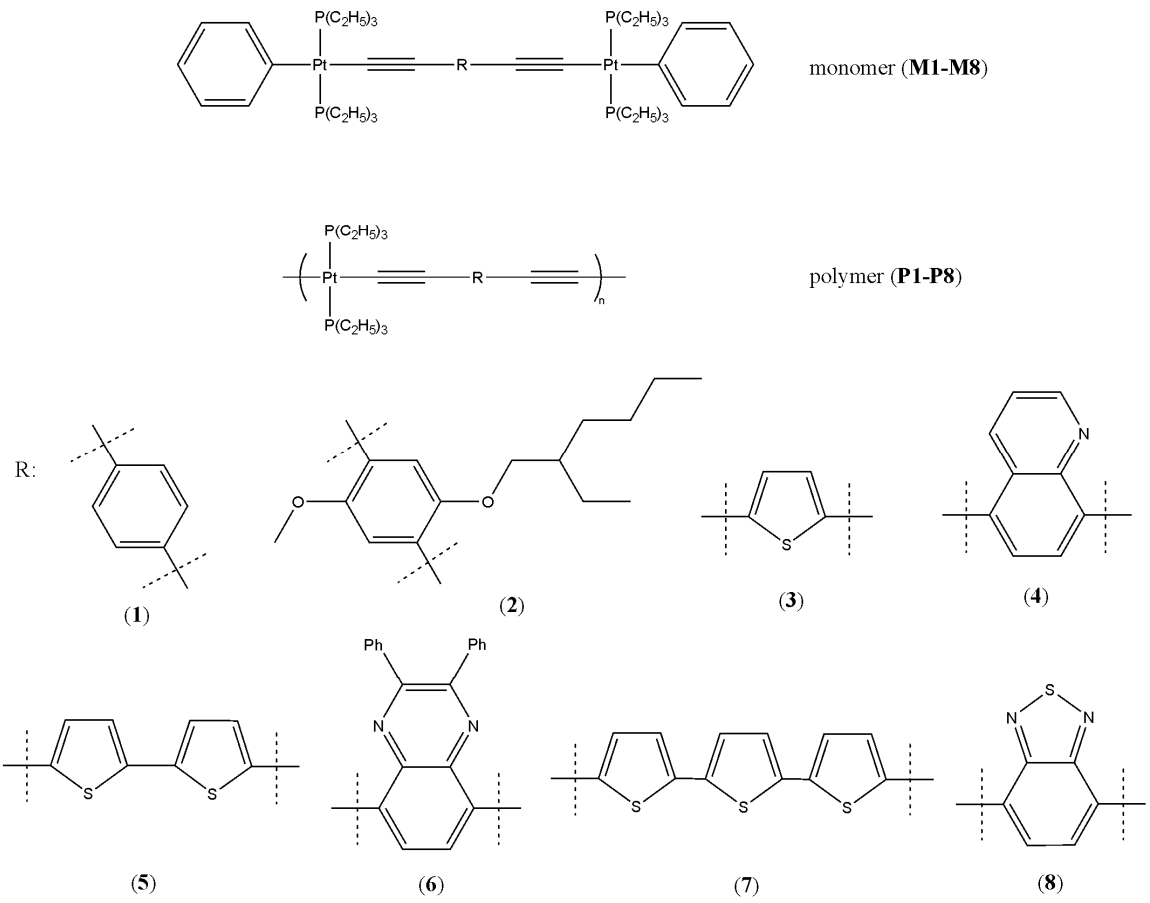

Figure 1.13. Platinum-containing polymers and monomers from the study by Wilson and coworkers.

Of particular interest are the absorption and phosphorescence emission behavior of these polymers, which reflect how accessible the triplet state becomes with the presence of the platinum atom. Incorporation of the platinum increases the phosphorescence radiative decay rate up to four-fold as compared to the analogous monomers (i.e., **P1** versus **M1**). Moreover, the rate of nonradiative decay from the triplet excited state is directly related to the energy of the triplet state. A significant pathway for nonradiative emission is through vibrational modes, leading to energy transfer to other monomers, neighboring polymer chains or even solvent molecules. Thus, if the triplet

excited state is low-lying, it is much easier to transfer the excited state energy to other moieties than if the triplet state were high in energy. As a result, as the triplet excited state energy is raised, the phosphorescence quantum yield also increases. It follows that if the polymer's flexibility can be reduced, it will reduce the likelihood for vibrationally induced nonradiative decay. Thus, the platinum metal makes the triplet excited state more accessible and if the polymer is also rigidified, phosphorescence should be more prevalent and efficient.

Finally, the effect of through-space conjugation should be noted as it applies to the efficiency of metallopolymer conductivity and light emissive properties. For example, when within ~2.8 Å of each other and stacked in a face-to-face manner, phenyl rings can engage in through space conjugation, as evident in various [2.2]paracyclophane derivatives.[27] As a result, the ability to permit free electron movement can be enhanced in polymers (and metallopolymers) that take advantage of proximity effects that allow another pathway for conjugation.

The studies summarized in this section demonstrate how specific functionalization of organic polymers can be used to tune the absorption and emission properties of a material. Monomer identity and side chain functionalities can dictate the wavelength and intensity of light emitted after absorption processes. Moreover, the incorporation of heavy atoms, transition metals especially, enhances spin-orbit coupling that can improve the accessibility of the triplet state. As a result, these transition-metal containing conjugated polymers can be synthesized such that radiative emission from the triplet state (phosphorescence) is the dominant form of photoluminescence. It has also been shown that interrupting the conjugation in these polymers provides excited state

energy traps that can significantly improve the efficiency of photoluminescence by reducing the likelihood of nonradiative decay. Finally, because the band gap energy (difference between the valence and conduction band levels) can be tuned according to monomer identity and functionalization, the conductivity of these polymeric materials can be tailored for the desired electrical application. These findings have brought organic conjugated polymers to the forefront of research concerning optoelectronic and photovoltaic devices. Even more recently, transition-metal containing organic polymers have become attractive macromolecules for these devices since phosphorescence is a more viable radiative pathway with the presence of the transition metal. Significant research has been dedicated to optimizing organic and organometallic polymers for practical uses in devices such as solar cells and light-emitting diodes, as discussed in the following section.

1.5 Organic and Organometallic CPs in Modern Technology

The practical applicability of organic conjugated polymers (OCPs) and transition-metal containing organic conjugated polymers is primarily in the area of optoelectric devices (of particular importance are solar cells and LEDs). While the basic details of how absorption, emission and charge carrier mobility scale with metal incorporation have all been reviewed in Sections 1-4 of this chapter, very little has been said about how specifically these polymers find versatile use in modern technology. It is therefore necessary to discuss the chemical and mechanical processes that occur in these devices; understanding these events will elucidate why OCPs and transition-metal containing OCPs are excellent candidates for the materials that constitute these LEDs and solar cells.

Finally, it is important to examine which types of polymers have been used in these applications to understand how improvements can be made.

1.5.1 Photovoltaic Devices and Organic/Organometallic Polymers

Emerging concerns about clean and renewable energy first led researchers to investigate the possibility of harvesting light energy from the sun and converting it into electricity and energy suitable for everyday life. Because charge transfer is paramount to their efficiency, solar cells that garner energy from the sun must consist of donor and acceptor molecules that aid in the transfer of electrons and thus promote conduction of electrical current.[28] While it is crucial that the charge transfer proceeds readily at the junction between the donor and acceptor moieties within a solar cell, it is especially important that the donor strongly absorbs light energy from the sun, as illustrated by the solar spectrum (Figure 1.14).

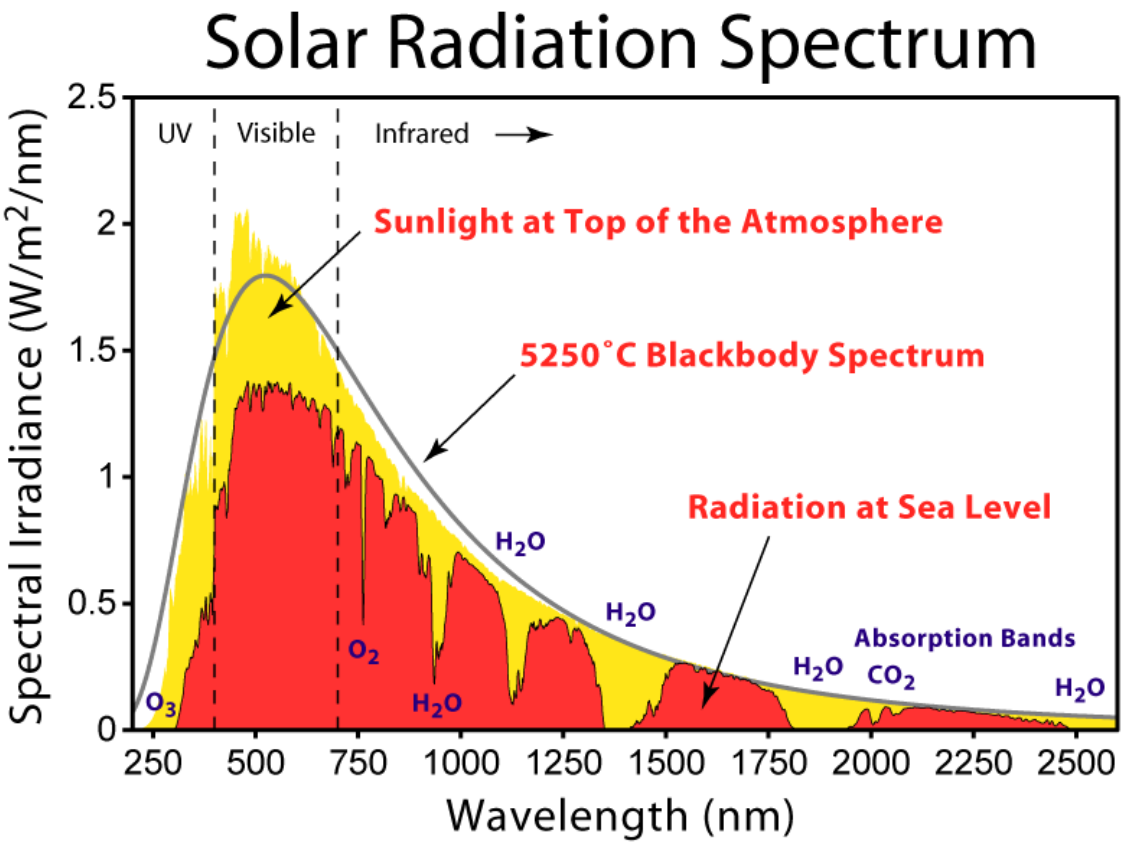

Figure 1.14. Spectrum demonstrating the spectral profile of sunlight at sea level.[29]

Finally, it should be noted that since the band gap dictates which incident light can be absorbed (must be higher energy than band gap to promote electron), it is important to be able to optimize the energy difference between the HOMO and LUMO in polymers to be used for photovoltaics.

Initial investigations into creating solar cells were focused on using crystalline silicon materials; soon after their inception, silicon materials were doped with atoms (phosphorous or boron) to enhance their conductivity.[30] The p-doped materials typically feature boron atoms within the silicon crystalline material to provide extra holes, thus increasing electron affinity. Conversely, n-doped silicon features atoms such as

phosphorous, which provides extra electrons to further enhance the material's ability to conduct electrons. This doping was used to enhance the conductivity of early solar cells that were synthesized from crystalline silicon. Both n-type and p-type silicon crystalline layers were combined to form p-n junctions that permitted free movement of photogenerated excited electrons. More recently, OCPs and metallated OCPs have become attractive substitutes since their band gap can be tuned depending on monomer identity and functionalization, and because they can be easily processed compared to silicon-based materials.

As noted above, there has recently been a shift in interest from the previously used inorganic crystalline solar cells to bulk heterojunction solar cells that often incorporate organic polymers. The current model of bulk heterojunction photovoltaic operation relies on four events in the conversion of solar energy into harvestable electrical current;[31] it is important to note that all solar cells contain donor and acceptor components that meet at some heterojunction. Moreover, the photovoltaic device contains a cathode and anode that ultimately allow for electrical current generation after photoexcitation. First in this process is the promotion of an electron from one of the materials (often an organic or organometallic conjugated polymer) to an excited state by incident light. This process generates excitons (excited states) within the material that comprises the solar cell. Following the absorption of sunlight, the excited states move towards the oppositely charged electrode to generate exciton-hole pairs. In the third step, there is a charge transfer (electron movement) from the donor to the acceptor component that occurs at the heterojunction. Finally, the transfer of the formal charge from donor to acceptor causes a cascade of electron (and hole) movement to the appropriate electrode to

result in a buildup of charge. This charge collection is essentially a potential that has been formed across the solar cell device and can thus be harvested as electricity. The general schematic for these four processes are depicted in Figure 1.15.

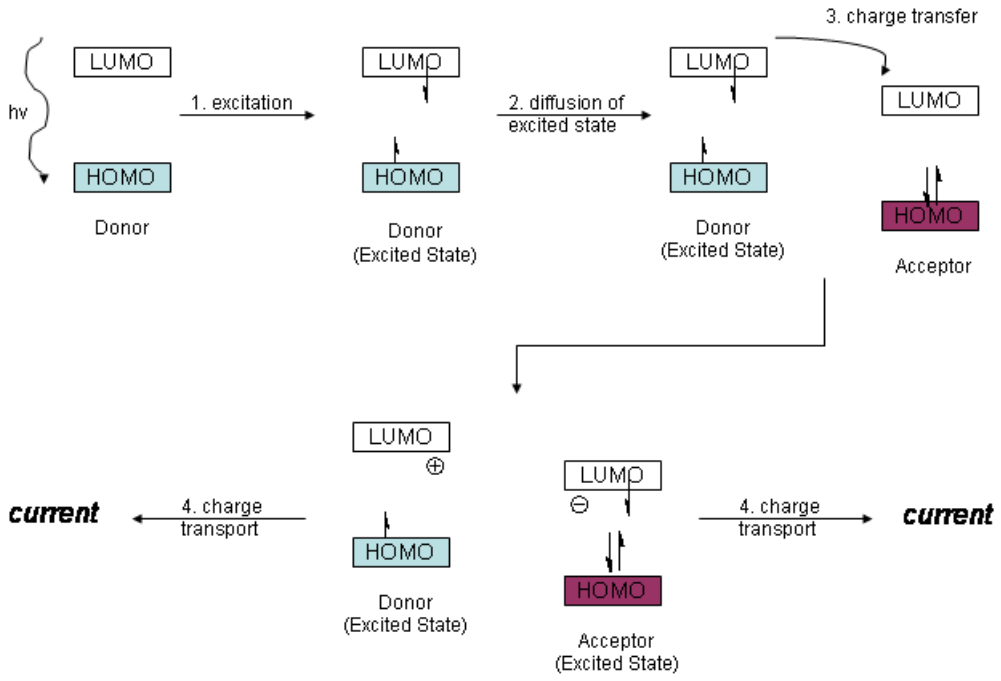

Figure 1.15. Simplified schematic for four major events in the conversion of solar energy into electrical current; figure adapted from Thompson and Frechét.[31]

The first organic polymer studied for its potential use in solar cells was polyacetylene.[32] Polyacetylene can be doped with aluminum (p-type doping) to enhance conductivity of photogenerated excited states. In the doped form, the absolute quantum efficiency was around 10% but the efficiency in converting the incident light energy into electrical current was only around 0.30% at the polyacetylene-aluminum junction.

However, this study also found that molecular oxygen inhibited the quantum efficiency at the polymer-metal junction. Thus, while this study demonstrates that OCPs can be used to harvest light energy and convert it into electrical current, the fact that the material is not exceptionally stable to atmospheric conditions where the solar cell will be used limits its practical applicability in photovoltaics.

After the initial discovery that conjugated organic polymers have utility in photovoltaic devices, countless investigations ensued that were concerned with devising OCPs with applicability to solar cells. Shortly after the initial studies on polyacetylene/aluminum photodiodes, polythiophene and poly(3-methylthiophene) were studied to discern their photophysical applications (Figure 1.16).[33]

Figure 1.16. Structure of polythiophene and poly(3-methylthiophene) (P3MT).

In this study, they found that polythiophene and poly(3-methylthiophene) can be electrochemically grown and then sandwiched between aluminum and gold or platinum layers to yield a solar cell type device. Both polymers behave as p-type semiconductors and can achieve up to 4% power efficiency when irradiated with light at a wavelength of 470 nm. This value is well within the range of light emitted by the sun, and so these polymers are certainly attractive candidates for solar cell use. However, the 4% efficiency of converting light to electrical current is still a modest number for the optimal operating efficiency of a solar cell. The efficiency of the cells also degrades after prolonged

exposure to incident light, possibly due to decomposition of the aluminum layer and not the organic polymer. It was found that the photocurrent half-life is dependent upon the power of the light source: four hours at 60 mW/cm^2, three and a half hours at 0.3 μW/cm^2 and a half-hour at 8 μW/cm^2. Ultimately, this study showed a significant improvement over the polyacetylene/aluminum solar cell material reported only three years earlier. Moreover, this investigation marks a shift in thinking from the traditional inorganic-based solar cells to those containing conjugated organic molecules and polymers that are the foundation of bulk heterojunction solar cells.

Researchers began to combine organic polymers with other conjugated moieties to enhance the efficiency of materials to be used in solar cell applications. For example, Sariciftci and coworkers examined poly[2-methoxy,5-(2'-ethylhexyloxy)-1,4-phenylene-vinylene] (MEH-PPV) which shared a junction with a fullerene derivative, [6,6]-phenyl-C_{61}-butyric acid methyl ester (PCBM), to determine the effect of the fullerene on the polymer efficiency as a photodiode (Figure 1.17).[34]

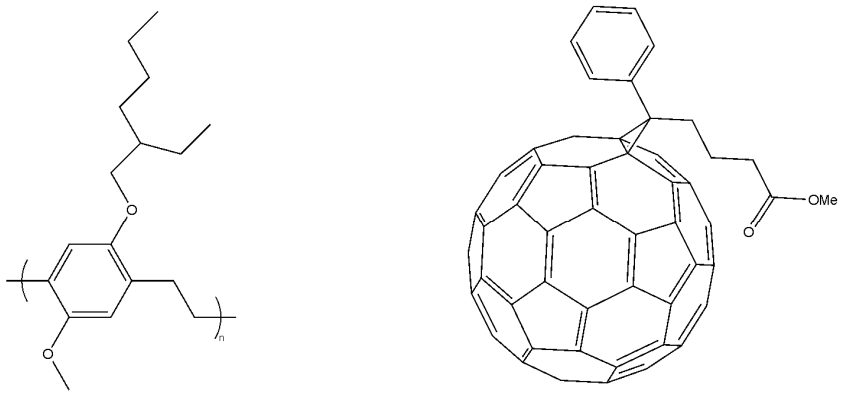

Figure 1.17. Structure for poly[2-methoxy,5-(2'-ethylhexyloxy)-1,4-phenylene-vinylene] (MEH-PPV) and [6,6]-phenyl-C_{61}-butyric acid methyl ester (PCBM).

The above investigation found that the fullerene/polymer junction itself was especially photosensitive and acted as an efficient conductor of photogenerated current. Moreover, Sariciftci and coworkers argue that the photoexcitation and generation of separable charges occurs at the heterojunction between the fullerene and polymer. These results show that combining organic conjugated polymers with other highly conjugated complexes can produce photosensitive materials which also undergo different excitation events (now charge separation generated at the heterojunction).

In addition to organic conjugated polymers, OCPs with transition metals have become attractive macromolecules for solar cells. Since it has been shown that metals can dope OCPs to make them more applicable to photovoltaics, it should be no surprise that many researchers are now focused on synthesizing metal-containing organic polymers to enhance photovoltaic performance. Of particular interest is including transition metals, especially platinum, into the polymer backbone in order to determine whether conductivity and photoefficiency (absorption, quantum yield, etc.) is improved. These investigations are aimed at studying how the presence of the transition metal affects charge separation in the photovoltaic device. One pioneering study utilized 2,1,3-benzothiadiazole monomers capped with platinum-containing donor monomers (Figure 1.18), which had modest power efficiency at best in the range of 1-1.4%.[35]

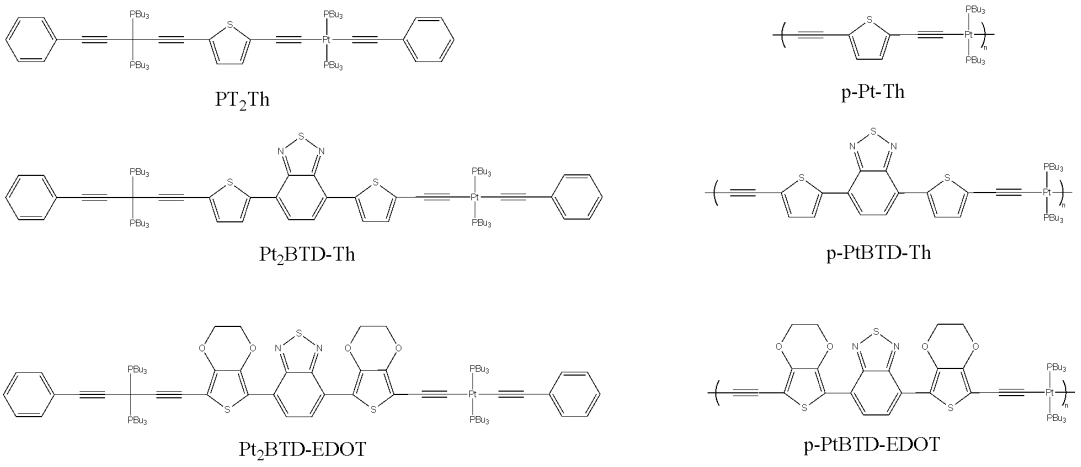

Figure 1.18. Polymers and monomers used in the investigation by Mei and coworkers to examine the effect of platinum on band gap energy.

They explain that in these systems with low band gap energies (~1.9 to ~2.1 eV), the platinum makes the triplet excited state significantly more accessible. However, because the band gap is so low, the triplet excited state energy cannot undergo photoinduced electron transfer to the [6,6]-phenyl-C_{61}-butyric acid methyl ester (PCBM) moiety at the heterojunction. Moreover, it was suggested that charge separation and photoconduction events in these devices are a direct result of the singlet excited state. As a result, accessing the triplet state will not enhance the efficiency of solar cells unless the donor and acceptor triplet excited state energy levels can be relatively similar.

1.5.2 Light-emitting Diodes and Organic/Organometallic Conjugated Polymers

Because the absorption and subsequent radiative and nonradiative decay pathways are fundamentally electronic transitions, it follows that photophysical events can be effected by electrochemically stimulating a semiconducting material. In essence, this is the basic process that governs the operation of light-emitting diodes. The following

schematic shows the chemical and physical events that occur within the LED when the device has electrical current introduced (Figure 1.19).

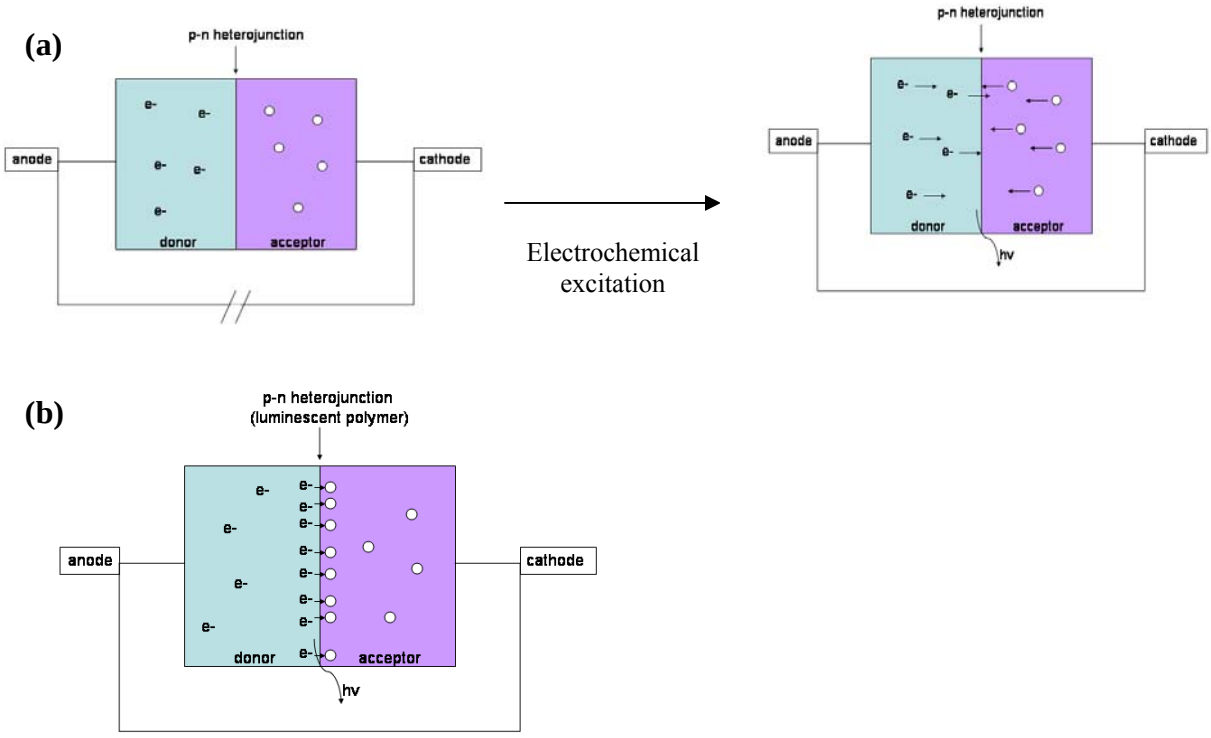

Figure 1.19. General schematic for LED operation after excitation of the semiconducting materials with electricity **(a)** and for charge recombination at the heterojunction that leads to luminescence **(b)**.

Thus, it is not only important for both the donor and acceptor components to be seminconducting materials, but also for these materials to emit light at the targeted wavelength. However, it is crucial for the donor and acceptor materials to favor radiative emission over nonradiative decay pathways (such as vibrational relaxation or intermolecular nonradiative recombination events) for these semiconductors to be of utility in LED devices. As with solar cells, n-type and p-type doping enhances the conduction of electrical current that allows for the generation of excited states. The

heterojunction allows for charge transfer from the donor to the acceptor component, which is often selected for desired electroluminescent color.

Early solid-state LEDs were constructed from inorganic semiconducting materials such as gallium arsenide.[36] In these first electroluminescent devices, the gallium arsenide emitted light in the infrared region with moderate efficiency. Later investigations found that doping the gallium arsenide with phosphorous yielded materials that emit light in the visible (red) region. Moreover, the relative amount of phosphorous compared to the gallium content allowed the material to be tuned to emit certain wavelengths of light. These phosphorous doped gallium arsenide inorganic layers were the first commercially available light-emitting diodes but suffered from poor quantum efficiency. This was primarily a result of the index of refraction of the material leading to a loss of emitted light. Later investigations found that doping the gallium arsenide with zinc oxide yielded light-emitting diodes with improved efficiency. While these initial investigations demonstrated the relative ease in making light-emitting diodes, the expensive nature of these materials coupled with the low photoluminescence yield led researchers to investigate other viable molecules for electroluminescent devices such as LEDs. Therefore, it is not surprising that the synthesis of materials with specific conductivity and photophysical properties (emission wavelength, intensity and efficiency) is a major focus of current LED-based investigations. Organic and organometallic polymers are ideal candidates for LEDs because they can be easily-synthesized highly emissive materials with excellent processibility photophysical properties that can be intricately tuned based on the polymer conformation, functionalization and interaction with other molecules.

Because organic conjugated polymers often display high quantum yields for fluorescence and phosphorescence, and because they can be engineered to absorb and emit specific wavelengths of light, these polymeric materials soon became the focus of LED-based research. The main property that makes organic conjugated polymers useful for LEDs is their conjugated semiconducting nature. Delocalization over the macromolecule allows for excited state energy to travel across the polymer which results in unique photophysical properties. The luminescent events of solid-state LEDs is driven by recombination (and subsequent radiative emission) of charges at the heterojunction after excited state generation and charge movement.[12] Electronic excitation can be achieved by pushing an electric current through the polymeric material or even incident light can be used as an excitation source.

One of the early successes in investigating the applicability of OCPs to LEDs came from a study on poly(*p*-phenylene vinylene), or PPV, as an electroluminescent material.[12] The electroluminescence of PPV is due to radiative recombination of electrons and holes generated by the excitation event. However, the quantum efficiency of the PPV films were only around 0.05%. This value corresponds roughly to the amount of luminescence per excitation event. Thus, though the devices showed an electroluminescence quantum yield of around 8%, the efficiency with which electricity is converted into light was poor in this study. The authors concluded that the low efficiency was likely due to nonradiative recombination sites (acetylene defects in the polymer commonly seen with Gilch polymerization used to synthesize PPV) known to greatly reduce quantum efficiency.

Son and coworkers expanded on the initial investigations into PPV as a light-emitting material by introducing *cis*-linkages to interrupt the conjugation in the PPV polymer in hopes that nonradiative recombination sites were reduced and thus the overall photoluminescence and quantum efficiency improved.[37] Particularly noteworthy from this study is that LEDs consisting of PPV embedded between either 2-(4-biphenylyl)-5-(4-tert-butylphenyl)-1,3,4-oxadiazole (PDB) or poly(methyl methacrylate) (PMAA) and an aluminum electrode showed significant improvement in quantum efficiency. The external quantum efficiency of these LEDs approached 0.44% which is significantly better than those previously seen by Burroughes and coworkers. These results demonstrate that interrupting the conjugation of OCPs can help localize excited states, thus limiting the nonradiative recombination.

As detailed before, the incorporation of metals into polymer chains allows for more efficient phosphorescence light emission. For every singlet excited state generated electrochemically, there are three triplet excited states accessible. Moreover, nonradiative decay pathways that result in nonproductive loss of triplet excited state energy are disfavored because the phosphorescence lifetime is so short that nonradiative recombination events are significantly reduced. Thus, the applicability of highly conjugated metallopolymers to LEDs is especially profound. Not only may the metallopolymers be conductive, but also the material will permit more efficacy of the light emission.

One of the earliest investigations into incorporating a heavy metal into OCPs for LED purposes examined the effect of using 2,3,7,8,12,13,17,18-octaethyl-21H,23H-porphine platinum(II) (PtOEP) in electroluminescent materials.[38] This study doped tris-

(8-hydroxyquinoline) aluminum with the PtOEP and measured the photoluminescent properties and quantum efficiency. Surprisingly, the incorporation of the highly phosphorescent PtOEP increased the quantum efficiency of the aluminum-based LED to near 4%. However, one of the drawbacks of this doping is that large concentrations of PtOEP actually leads to a deteriorations of quantum efficiency, likely due to nonradiative recombinations between donor and acceptor molecules (quenching). And while this study did not specifically examine the effect of platinum-doping of OCPs, it certainly demonstrates that the incorporation of a transition metal into an LED material can improve quantum efficiency significantly.

A more recent investigation into incorporating platinum into LED-bound OCPs examined the photophysical and LED applicability of platinum-containing poly-ynes.[39] These polymers contain an electron-deficient bithiazole which is aimed at enhancing the conductivity of the poly-yne backbone; this functionalization caused emission of green light after excitation. However, the authors did not report the quantum efficiencies so no comparison to non-metallated OCP-based LEDs can be made. This study does demonstrate, however, that incorporation of a platinum metal into the highly conjugated polyyne does not disrupt the conjugation in any way that is detrimental to photoluminescence emission intensity.

Much of the research concerned with platinum-containing OCPs is focused on platinum-acetylide polymers and their applicability to LEDs. One of the most insightful early investigations into platinum-acetylide polymers was aimed at determining how the spin-orbit coupling enhanced by the heavy metal affected photoluminescence in light-emitting devices. In this study, the photophysical properties of a phosphine-bound

platinum-acetylide polymer with repeating 2,3-diphenylquinoxaline units were compared those of the monomer (Figure 1.20).[40]

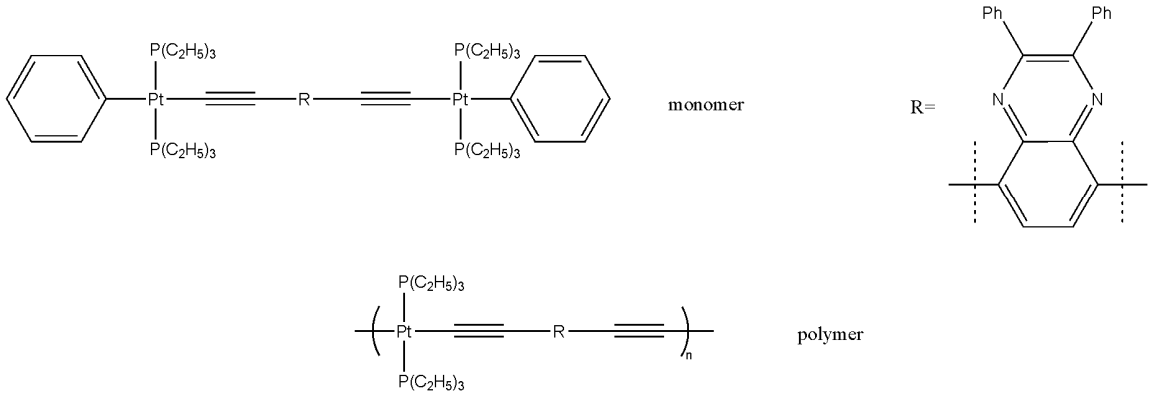

Figure 1.20. Platinum-acetylide monomer and polymer examined by Wilson and coworkers for potential LED applicability.

Although the triplet emission (phosphorescence) occurs from a lower-lying excited state, fluorescence is more prevalent even though intersystem crossing is hypothesized to be near unity due to the platinum metal. This is because phosphorescence emissive rates (10^3 s^{-1}) are still much slower than the nonradiative decay rates (~10^5 – 10^6 s^{-1}) from the triplet states in these platinum-based polymers. More specifically, this study is concerned with determining the singlet generation fraction for both the polymer and monomer to discern the effects of extended conjugation. In this investigation, the polymer singlet generation fraction (~54%) is significantly higher than that observed in the monomer (~22%). This means that there is a difference in the electron-hole generation and recombination in polymers with extended conjugation as compared to smaller molecules with the same type of delocalization. In small molecules, electron-hole capture occurs when the two oppositely charged moieties are within a distance over which electrostatic or Coulombic interactions are operative. Because delocalization is not

a key component of electron-hole capture in small molecule-based devices, spin wavefunction overlap is not important; thus, the capture process in these cases is spin-independent. However, with extended conjugation, electrons and holes must move greater distances where capture can occur by way of electron hopping. Moreover, these oppositely charged species often reside on the same polymeric chain; in this case, it is now important to account for the spin wavefunctions of these excited species because their interaction is a direct result of overlap of these wavefunctions. As such, the electron-hole capture in polymeric species *is* spin-dependent. Therefore, the recombination events that ultimately lead to emission in LEDs depend on the nature of the material (i.e., whether it is highly conjugated). This investigation demonstrates that even though phosphorescence can be harvested efficiently from platinum-acetyilde polymers due to enhanced triplet excited state population, the quantum-mechanical processes that account for emission may still favor singlet generation and consequent fluorescence.

The purpose of the current work is to investigate novel platinum-containing polymers in hopes of devising materials that will be of particular utility in photovoltaic and light-emitting devices. The introduction of the heavy platinum atom is aimed at enhancing spin-orbit coupling and making the triplet state more accessible in the polymeric material. Linear highly conjugated phosphine monomers are used in the polymerization process to afford polymer materials with relative ease and efficiency. The photophysical properties of the polymers will be compared to those of the phosphine monomer to examine the effects of extended conjugation and transition-metal incorporation. It is our hope that these results, with further investigations into the more

mechanical limitations of the polymers, can be of particular utility in both harvesting natural light energy as well as producing highly efficient light-emitting devices

REFERENCES CITED

(1) Maxwell, J. C. "A Dynamical Theory of the Electromagnetic Field" *Philos. Trans. R. Soc. London, A* **1865**, *155*, 459-512.

(2) Einstein, A. "Concerning an Heuristic Point of View toward the Emission and Transformation of Light" *Am. J. Phys.* **1965**, *33*, 1-16.

(3) McQuarrie, D. A.; Simon, J. D. *Physical Chemistry: A Molecular Approach*; University Science Books: Sausalito, California, 1997.

(4) Morse Potential Diagram from http://upload.wikimedia.org/wikipedia/commons/0/0e/Franck-Condon-diagram.png retrieved on 20 March 2009.

(5) Pilar, F. L. *Elementary Quantum Chemistry*, Second ed.; Courier Dover Publications: Massachusetts, 2006.

(6) Lakowicz, J. R. *Principles of Fluorescence Spectroscopy*, Third ed.; Springer Science and Business Media: New York, 2006.

(7) Bruice, P. Y. *Organic Chemistry*, Third ed.; Prentice Hall: New Jersey, 2001.

(8) Kraft, A.; Grimsdale, A. C.; Holmes, A. B. "Electroluminescent Conjugated Polymers--Seeing Polymers in a New Light" *Angew. Chemie Int. Ed.* **1998**, *37*, 402-428.

(9) V. Talrose, A.N. Yermakov, A.A. Usov, A.A. Goncharova, A.N. Leskin, N.A. Messineva, N.V. Trusova, M.V. Efimkina, UV/Visible Spectra" in **NIST Chemistry WebBook, NIST Standard Reference Database Number 69**, Eds. P.J. Linstrom and W.G. Mallard, National Institute of Standards and Technology, Gaithersburg MD, 20899, http://webbook.nist.gov, (retrieved February 28, 2009).

(10) Remmers, M.; Neher, D.; Grner, J.; Friend, R. H.; Gelinck, G. H.; Warman, J. M.; Quattrocchi, C.; dos Santos, D. A.; Brdas, J.-L. "The Opticals, Electronic, and Electroluminescent Properties of Novel Poly(*p*-phenylenevinylene)-Related Polymers" *Macromolecules* **1996**, *29*, 7432-7445.

(11) Burn, P. L.; Kraft, A.; Baigent, D. R.; Bradley, D. D. C.; Brown, A. R.; Friend, R. H.; Gymer, R. W.; Holmes, A. B.; Jackson, R. W. "Chemical Tuning of the Electronic Properties of Poly(*p*-phenylenevinylene)-Based Copolymers" *J. Am. Chem. Soc.* **1993**, *115*, 10117-10124.

(12) Burroughes, J. H.; Bradley, D. D. C.; Brown, A. R.; Marks, R. N.; Mackay, K.; Friend, R. H.; Burns, P. L.; Holmes, A. B. "Light-emitting Diodes Based on Conjugated Polymers" *Nature* **1990**, *347*, 539-541.

(13) Xu, B.; Holdcroft, S. "First Observation of Phosphorescence from π-Conjugated Polymers" *J. Am. Chem. Soc.* **1993**, *115*, 8447-8448.

(14) Lower, S. K.; El-Sayed, M. A. "The Triplet State and Molecular Electronic Processes in Organic Molecules" *Chem. Rev.* **1966**, *66*, 199-241.

(15) Koziar, J. C.; Cowan, D. O. "Photochemical Heavy-Atom Effects" *Acc. Chem. Res.* **1978**, *11*, 334-341.

(16) McClure, D. S. "Triplet-Singlet Emissions in Organic Molecules" *J. Chem. Phys.* **1949**, *17*, 905-913.

(17) Sonogashira, K.; Takahashi, S.; Hagihara, N. "A New Extended Chain Polymer, Poly[*trans*-bis(tri-*n*-butylphosphine)platinum 1,4-butadiynediyl]" *Macromolecules* **1977**, *10*.

(18) Wilson, J. S.; Chawdhury, N.; Al-Mandhary, M. R. A.; Younus, M.; Khan, M. S.; Raithby, P. R.; Kohler, A.; Friend, R. H. "The Energy Gap Law for Triplet States in Pt-Containing Conjugated Polymers and Monomers" *J. Am. Chem. Soc.* **2001**, *123*, 9412-9417.

(19) Guo, F.; Kim, Y.-G.; Reynolds, J. R.; Schanze, K. S. "Platinum-acetylide Polymer Based Solar Cells: Involvement of the Triplet State for Energy Conversion" *Chemical Commun.* **2006**, 1887-1889.

(20) Liu, Y.; Jiang, S.; Glusac, K.; Powell, D. H.; Anderson, D. F.; Schanze, K. S. "Photophysics of Monodisperse Platinum-Acetylide Oligomers: Delocalization in the Singlet and Triplet Excited States" *J. Am. Chem. Soc.* **2002**, *124*, 12412-12413.

(21) Glusac, K.; Kose, M. E.; Jiang, H.; Schanze, K. S. "Triplet Excited State in Platinum-Acetylide Oligomers: Triplet Localization and Effects of Conformation" *J. Phys. Chem.* **2997**, 929-940.

(22) Chawdhury, N.; Kohler, A.; Friend, R. H.; Wong, W.-Y.; Lewis, J.; Younus, M.; Raithby, R. R.; Corcoran, T. C.; Al-Mandhary, M. R. A.; Khan, M. S. "Evolution of Lowest Singlet and Triplet Excited States with Number of Thienyl RIngs in Platinum Poly-ynes" *J. Chem. Phys.* **1999**, *110*, 4963-4970.

(23) Beljonne, D.; Wittman, F.; Kohler, A.; Graham, S.; Younus, M.; Lewis, J.; Raithby, P. R.; Khan, M. S.; Friend, R. H.; Bredas, J. L. "Spacial Extent of the Singlet and Triplet State Excitons in Transition Metal Containing Poly-ynes" *J. Chem. Phys.* **1996**, *105*, 3868-3877.

(24) Huheey, J. E.; Keiter, E. A.; Keter, R. L. *Inorganic Chemistry: Principles of Structure and Reactivity*, Fourth ed.; HarperCollins: New York, 1993.

(25) Yang, N. C.; Gaoni, Y. "Charge-Transfer Interaction in Organic Polymers" *J. Am. Chem. Soc.* **1964**, *86*, 5022-5023.

(26) Martens, J. F.; Marseglia, E. A.; Bradley, D. D. C.; Friend, R. H.; Burn, P. L.; Holmes, A. B. "The Effect of Side Groups on the Structure and Ordering of Poly(*p*-phenylenevinylene) Derivatives" *Synthetic Metals* **1993**, *55*, 449-452.

(27) Bazan, G. C. "Novel Organic Materials through Control of Multichromophore Interactions" *J. Org. Chem.* **2007**, *72*, 8615-8635.

(28) Shah, A.; Torres, P.; Tscharner, R.; Wyrsch, N.; Keppner, H. "Photovoltaic Technology: The Case for Thin-Film Solar Cells" *Science* **1999**, *285*, 692-698.

(29) Solar Radiation Spectrum from http://globalwarmingart.com/images/4/4c/Solar_Spectrum.png retrieved on 28 February 2009.

(30) Doping Silicon: Diodes and Transistors from http://electronics.howstuffworks.com/diode1.htm retrieved on 20 March 2009.

(31) Thompson, B. C.; Frechét, J. M. J. "Polymer-Fullerene Composite Solar Cells" *Angew. Chemie Int. Ed.* **2008**, *47*, 58-77.

(32) Weinberger, B. R.; Gau, S. C.; Kiss, Z. "A Polyacetylene:Aluminum Diode" *Appl. Phys. Lett.* **1981**, *38*, 555-558.

(33) Glenis, S.; Horowitz, G.; Tourillon, G.; Garnier, F. "Electrochemically Grown Polythiophene and Poly(3-methylthiophene) Organic Photovoltaic Cell" *Thin Solid Films* **1984**, *111*, 93-103.

(34) Sariciftci, N. S.; Braun, D.; Zhang, C.; Srdanov, V. I.; Heeger, A. J.; Stucky, G.; Wudl, F. "Semiconducting Polymer-Buckminsterfullerene Heterojunctions: Diodes, Photodiodes, and Photovoltaic Cells" *Appl. Phys. Lett.* **1993**, *68*, 585-587.

(35) Mei, J.; Ogawa, K.; Kim, Y.-G.; Heston, N. C.; Arenas, D. J.; Nasrollahi, Z.; McCarley, T. D.; Tanner, D. B.; Reynolds, J. R.; Schanze, K. S. "Low-band-gap Platinum Acetylide Polymers as Active Materials for Organic Solar Cells" *Appl. Phys. Interfaces* **2009**, *1*, 150-161.

(36) Kazan, B. "Material Aspects of Display Devices" *Nature* **1980**, *208*, 927-936.

(37) Son, S.; Dodabalapur, A.; Lovinger, A. J.; Galvin, M. E. "Luminescence Enhancement by the Introduction of Disorder into Poly(*p*-phenylenevinylene)" *Science* **1995**, *269*, 376-378.

(38) Baldo, M. A.; O'Brien, D. F.; You, Y.; Shoustikov, A.; Sibley, S.; Thompson, M. E.; Forrest, S. R. "Highly Efficient Phosphorescent Emission from Organic Electroluminescent Devices" *Nature* **199**, *395*, 151-154.

(39) Wong, W.-Y.; Zhou, G.-J.; He, Z.; Cheung, K.-Y.; Ng, A. M.-C.; Djurisic, A. B.; Chan, W.-K. "Organometallic Polymer Light-Emitting Diodes Derived from a Platinum(II) Polyyne Containing the Bithiazole Ring" *Macromolecular Chemistry and Physics* **2008**, *209*, 1319-1322.

(40) Wilson, J. S.; Dhoot, A. S.; Seeley, A. J. A. B.; Khan, M. S.; Kohler, A.; Friend, R. H. "Spin-Dependent Exciton Formation in π-Conjugated Compounds" *Nature* **2001**, *413*, 828-831.

CHAPTER TWO

PLATINUM-BASED ETHYNYLBENZENE POLYMERS WITH *META*-TERPHENYL SCAFFOLDS

2.1 Rigid Scaffolds in Organometallic Conjugated Polymers

As discussed in Chapter 1, the flexibility of an organic conjugated polymer has significant effects on its photophysical behavior.[1] More specifically, rigidifying an OCP reduces the likelihood that excited state energy (garnered from absorption processes) is lost to vibrational relaxation or other nonradiative decay pathways. And because the conjugated polymer is less flexible, the effective conjugation length increases, leading to a red-shift in both the absorption and emission parameters as compared to less rigid analogues. In addition, limiting the mobility of the polymer raises the energy of the triplet excited state which has been shown to produce more efficient phosphorescence (larger values of Φ_P) processes.[1] Thus, it is desirable to synthesize highly conjugated polymers with limited bond rotation and vibrational freedom to enhance their applicability in photovoltaic and light-emitting devices.

In this chapter, novel strategies to increase the rigidity of organometallic conducting metallopolymers shall be discussed. While there are countless methods of rigidifying organometallic polymers and copolymers, the focus of the current investigation is to utilize an *m*-terphenyl scaffolded diphosphine that *trans*-spans the transition metal. Terphenyl scaffolds first became of interest in transition-metal coordination complexes after much research had been done on terdentate “pincer” ligands (Figure 2.1).

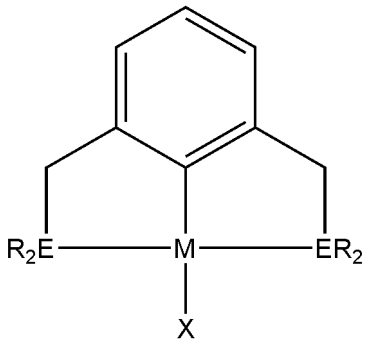

Figure 2.1. General schematic for a transition metal complex with an *m*-xylyl pincer ligand scaffold.

These pincer ligands afford much stability to the metal-carbon bonds within the complex because the multiple binding sites from the ligand result in the chelate effect.[2, 3] Moreover, the unique conformations that can be achieved with the presence of a pincer ligand have given rise to many unique catalysts comprised of transition-metal pincer complexes. The pincer scaffold limits most of the rotational freedom at the metal center leaving only a few torsional and vibrations modes of flexibility. The chelate effect and rigidification brought about by the terdentate pincer complex is clearly advantageous; however, there is only one site (X) for polymeric growth from the transition metal which, at first glance, appears to limit the diversity of polymers that can be synthesized when using the traditional pincer scaffold as a rigid building block. Yet numerous studies have circumvented this problem through the utility of functionalized pincer ligands that can allow polymerization from multiple sites.

One method of incorporating the rigid terdentate pincer complexes into polymers has been to functionalize preformed pincer complex with a polmerizable moiety. A recent

example of this strategy is the preparation of **Pinc1** by ring opening metathesis polymerization (ROMP) of a pincer-substituted norbornene derivative (Figure 2.2).[4]

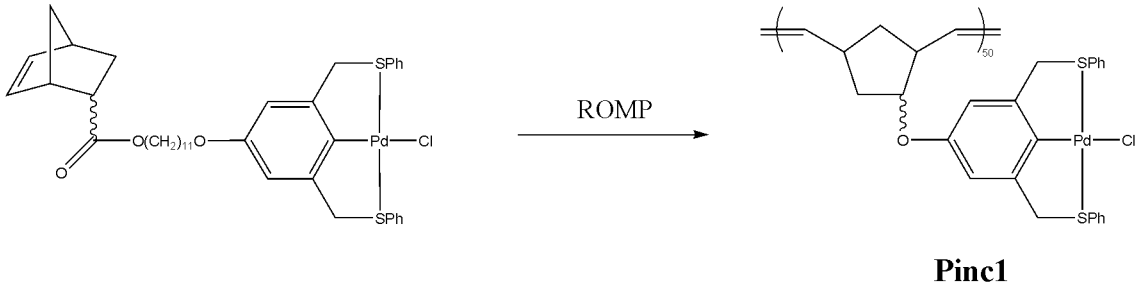

Pinc1

Figure 2.2. Organic polymer with pincer-type metallated ligands present on each monomer unit.

This polymer was not explored in terms of its photophysical behavior, but instead was synthesized in order to understand the self-assembly and catalytic properties (for Heck coupling) garnered by the polymer with the inclusion of the pincer-type transition metal moiety. The synthesized polymer can then perform Heck coupling readily by a simple one-pot procedure that combines the pincer-based containing polymer with an aryl halide and alkene to afford the desired polymer (Figure 2.3). A variety of different Heck heterocoupling reactions were investigated and the pincer-based polymer afforded the desired products with yields ranging from 92-99%.

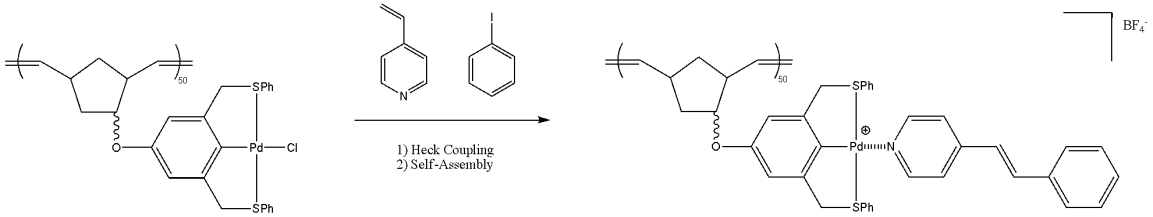

Figure 2.3. One-pot synthesis of pincer-based polymer with Heck coupling product coordinating to the transition metal.

While the above study demonstrates that pincer-scaffolded complexes have been used in polymerizations in general, it is more pertinent to the current study to review prior work on pincer-based polymers with unique optical properties. One such investigation used a bimetallic pincer complex to afford coordinatively cross-linked polymer, **PVP:Pin1** (Figure 2.4).[5]

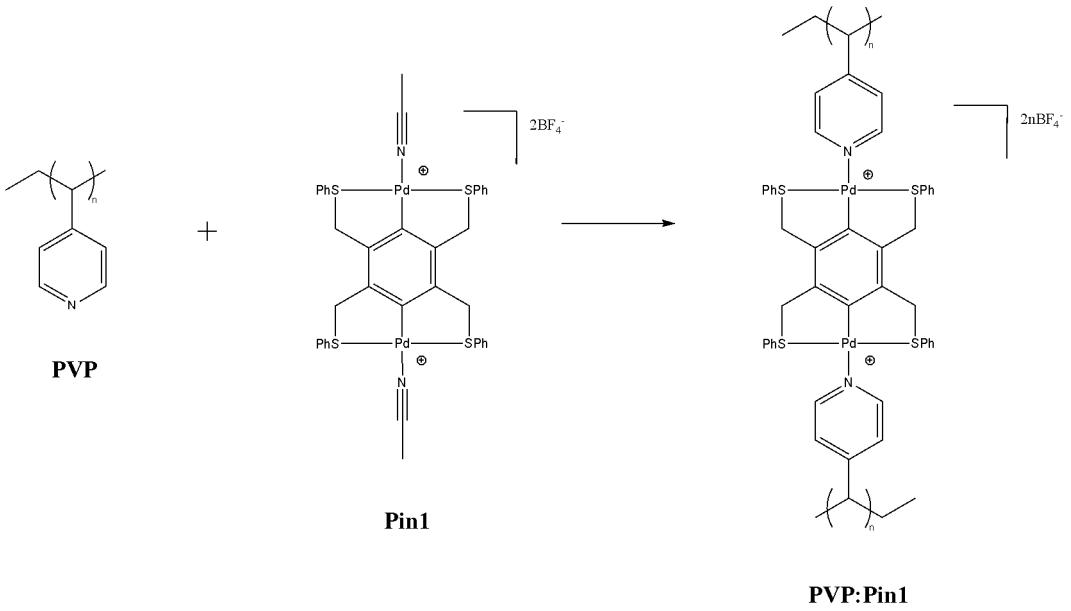

Figure 2.4. Synthesis of bimetallic pincer complex containing polymer **PVP:Pin1**.

The **PVP:Pin1** polymerization is a reversible process; that is, the polymer forms when **PVP** and **Pin1** (both solvated in acetonitrile) are deposited onto a quartz substrate. This process was tracked by UV-vis spectroscopy to examine the optical properties of the resultant **PVP:Pin1** polymeric layer that formed. The absorbance maximum red-shifts upon formation of the **PVP:Pin1** complex primarily because the nitrile ligands are easily displaced by the incoming pyridine moieties. More specifically, the coordination of the nitrogen to the pincer complex extends the effective conjugation length relative to both **PVP** and **Pin1** monomers and therefore is the primary cause of the red-shifting in

absorbance. However, it should be noted that a dichloro analog of the bimetallic pincer complex (**Pin1-Cl$_2$**) could be reacted with a simple dialkyne to afford a polymer with the pincer type functionality within the polymeric backbone at each repeating unit (Scheme 2.1).

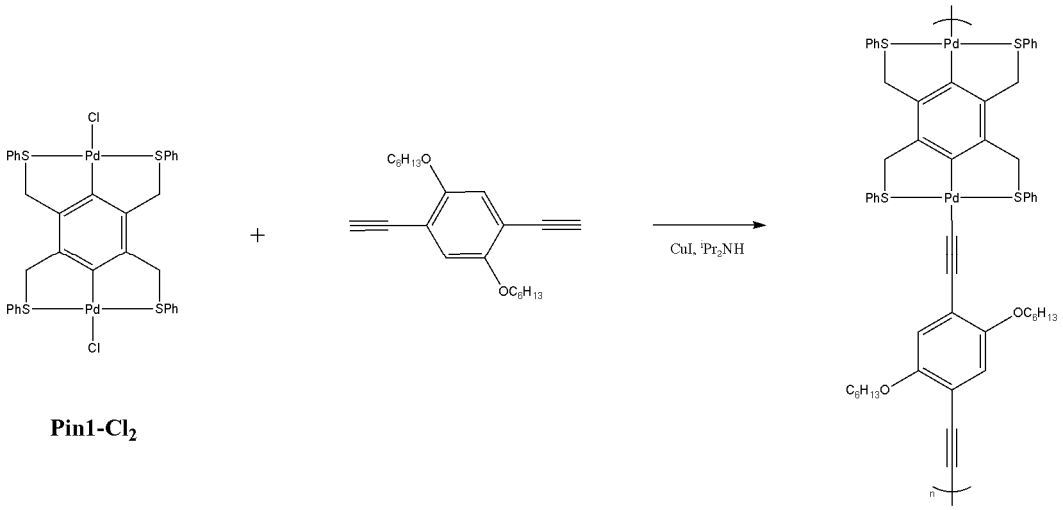

Pin1-Cl$_2$

Scheme 2.1. Polymer afforded by reaction of bimetallic pincer (**Pin1-Cl$_2$**) and 2,5-dihexyloxy-1,4-diethynylbenzene.

In contrast to pincer ligands, *m*-terphenyl scaffolds that bind through phosphine moieties provide some rigidity to transition metal complexes while only occupying two of the four coordination sites for square planar d^8 transition metals. Nickel- and palladium-based scaffolded complexes have been synthesized and studied in detail in order to elucidate their structural nuances (Figure 2.5).[6] Therefore, incorporation of *m*-terphenyl derivatized scaffolds in organometallic polymers is an appealing field of research that informs the current investigation.

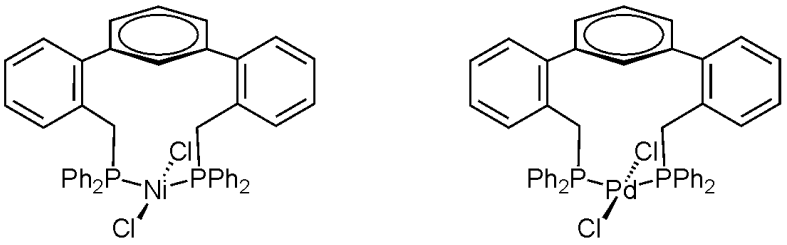

Figure 2.5. Nickel- and palladium-based transition metal complexes with *m*-terphenylphosphine scaffolds.

The most prevalent application of *m*-terphenyl scaffolds to date has been to exploit their steric bulk to provide kinetic stabilization to a variety of otherwise reactive species. Terphenyls have proven useful in stabilizing otherwise unisolable transition metal complexes as well as anionic species and radicals.[7, 8] More recently, there has been a focus on diversifying *m*-terphenyls by substitution of the flanking aryl rings, thereby providing a variety of interesting materials for a myriad of applications (Figure 2.6).

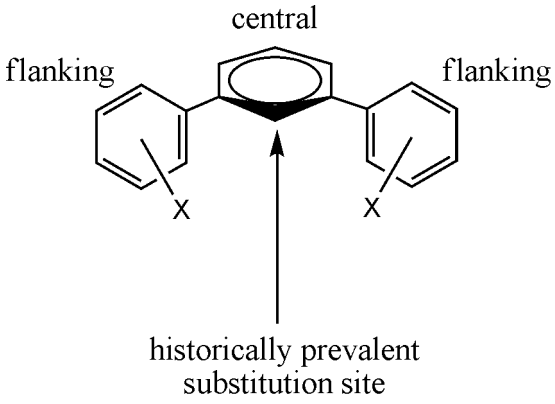

Figure 2.6. General structure for a simple *m*-terphenyl scaffold with central and flanking aryl rings labeled appropriately; particularly noteworthy are the substitution sites (X) which will be studied in the current work.

Because the focus of the current work is to synthesize rigid transition-metal containing polymers, it seems appropriate to focus on terphenyl scaffolded ligands that are compatible with the transition metal of interest, notably platinum. Several reports have described *m*-terphenyl scaffolded phosphines; the binding of an *m*-terphenylphosphine to nickel and palladium was investigated in hopes of creating terdentate scaffolded transition metal complexes (Figure 2.5).[6] This study accomplished a *trans*-spanning bidentate ligand complex, and elucidated conformational nuances of the *trans*-scaffolded palladium complex, confirming its limited flexibility (Figure 2.7).

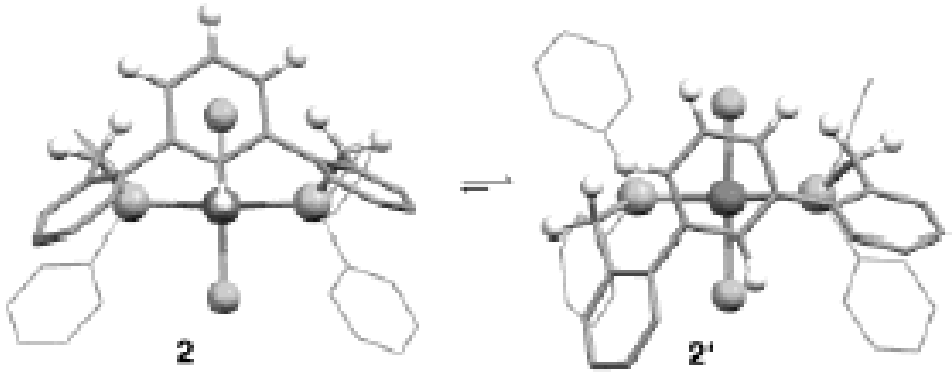

Figure 2.7. Isomers of palladium metal complex with *m*-terphenylphosphine bidentate scaffold; figure taken from 2004 publication by Smith and Protasawiecz.[6]

It was found that torsional mobility of the terphenyl scaffold allows for interconversion between palladium complexes **2** and **2'**. These results demonstrate that the *m*-terphenylphosphine, when bound to a transition metal, enforces some rigidity in the complex but still is able to undergo minor motions that slightly distort the geometry. Later investigations proved that halide elimination from the central benzene ring in the *m*-terphenyl scaffold can proceed readily (using palladium(0) dibenzylideneacetone as

the palladium-bearing reagent) to afford terdentate pincer type transition metal complexes (Figure 2.8).[9]

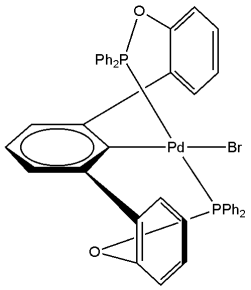

Figure 2.8. Palladium complex with terdentate *trans*-spanning *m*-terphenylphosphine type scaffold.

This new class of terdentate *m*-terphenyl scaffolded transition metal complexes was shown to have structural rigidity even up to 130 °C. These results are of particular relevance to the current discussion because they demonstrate limited flexibility about the transition metal even in applications where heat is generated (solar cells and light-emitting diodes often suffer from this).

The focus of the current study is to synthesize a platinum-containing metallopolymer with a rigid *m*-terphenylphosphine scaffold (Figure 2.9) that limits bond vibration and rotations while hopefully raising the triplet excited state in energy to reduce nonradiative emission.

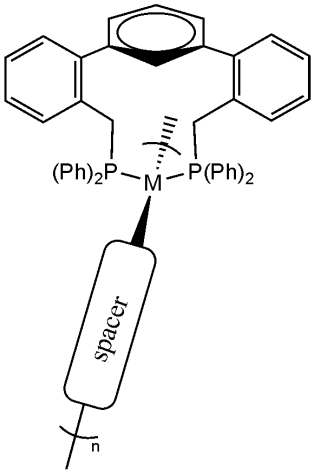

Figure 2.9. *m*-Terphenylphosphine scaffold that is of interest in producing rigid polymers; the terphenylphosphine is *trans*-spanning a square planar transition metal for illustrative purposes.

Moreover, the presence of the heavy platinum metal is aimed at enhancing the population of the triplet state thereby further promoting phosphorescence which can be of particular utility in light-emitting devices.

2.2 Synthesis of Polymer Precursors

The typical starting materials for synthesis of platinum-acetylide polymers are of the general form $[PtCl_2(PR_3)_2]$, so complex **2** was targeted (Figure 2.10).

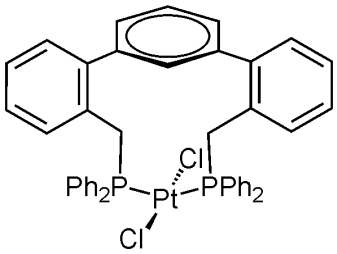

Figure 2.10. Complex **2** that is to be the precursor to the targeted platinum-acetylide oligomers and polymers.

Generation of complex **2** relies on reaction of *m*-terphenylphosphine (**1**) with dichlorobis(benzonitrile) platinum. The *m*-terphenylphosphine **1** is synthesized readily by first generating lithium diphenylphosphide and then adding brominated terphenyl (**A**) following the reported method (Scheme 2.2).[6]

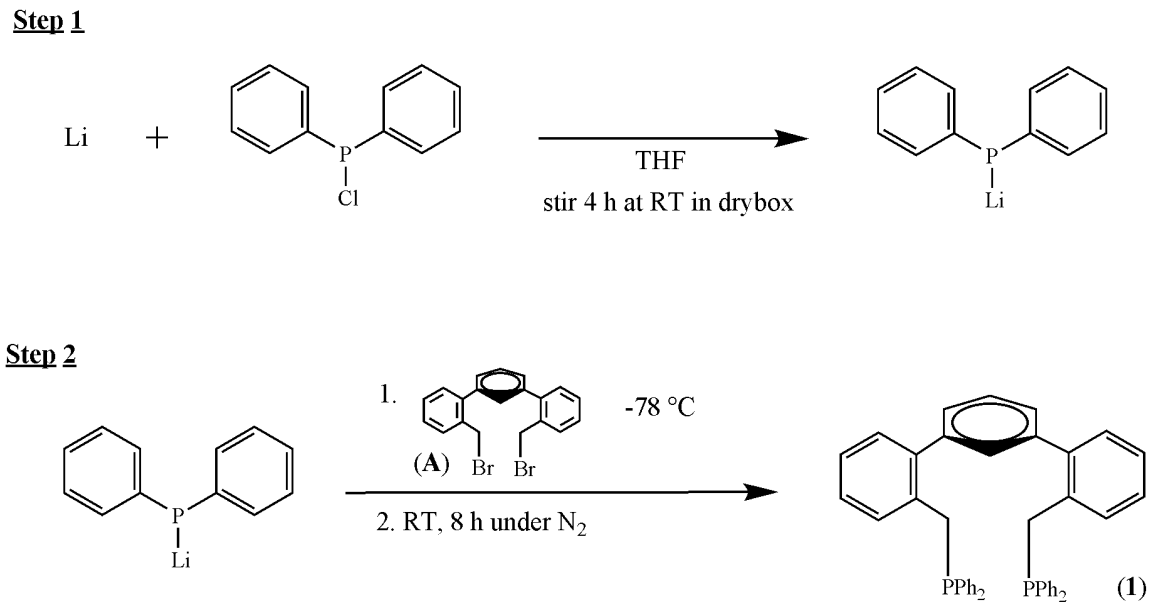

Scheme 2.2. Synthesis of *m*-terphenylphosphine material **1**.

Compound **1** can then be reacted with a platinum species to generate a scaffolded dichloroplatinum species **2** (Scheme 2.3). The two chlorides on this species are easily displaced by an incoming acetylide and so provide an attractive starting material to platinum-based polymers.

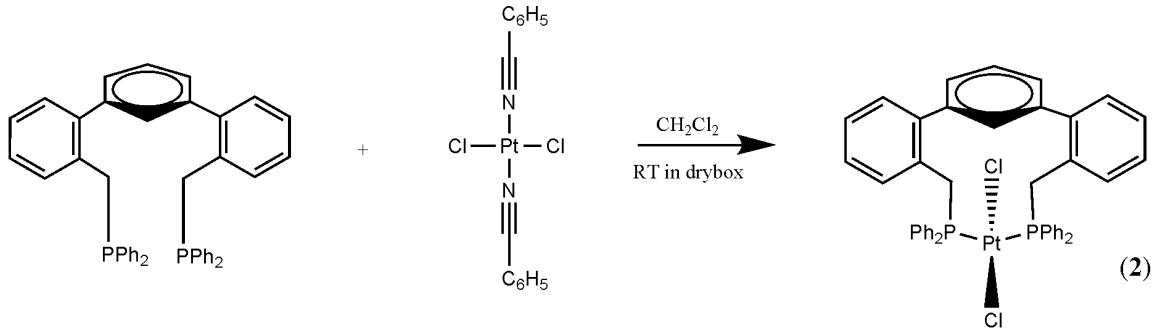

(**2**)

Scheme 2.3. Synthetic pathway to terphenylphosphine based dichloroplatinum starting complex **2**—also referred to as *trans*-[(**1**)$PtCl_2$].

Synthesis of platinum starting material **2** is readily achieved under mild conditions via a simple transmetallation mechanism. In this vein, benzonitrile is the only side product generated and is easily removed by washing with pentane. The bidentate *m*-terphenylphosphine scaffold provides stability to the platinum metal such that it is air-stable in both solid-state and solvated. Phosphorous-31 NMR is demonstrative of successful synthesis of complex **2**. The *m*-terphenylphosphine has a ^{31}P chemical shift of –8.8 ppm; after reaction with *trans*-dichlorobis(benzonitrile)platinum, the obtained yellow solid exhibits at ^{31}P resonance at 11.2 ppm in the ^{31}P spectrum. Moreover, the strong central peak at 11.2 ppm for complex **2** is flanked by two platinum satellites at 22.0 and 0.46 ppm, indicating new connectivity between the platinum metal center and phosphorous atoms from the terphenyl. The coupling constant ($^1J_{Pt\text{-}P}$) for complex **2** (2616 Hz) is diagnostic of the anticipated *trans*-binding mode, as illustrated by other *trans*-bis(phosphine)$PtCl_2$ complexes (Figure 2.11).[10, 11]

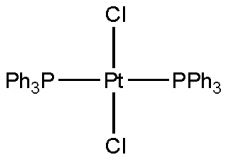

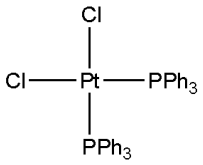

$^{1}J_{\text{Pt-P}} = 2637$ Hz $^{1}J_{\text{Pt-P}} = 3637$ Hz

Figure 2.11. *Cis* and *trans* isomers for a platinum-acetylide complex with associated platinum-phosphorous coupling constants.

Further confirmation of the *trans*-binding mode of the *m*-terphenylphosphine scaffold is given by the crystal structure of **2** (Figure 2.12) with the accompanying refinement details (Table 2.1).

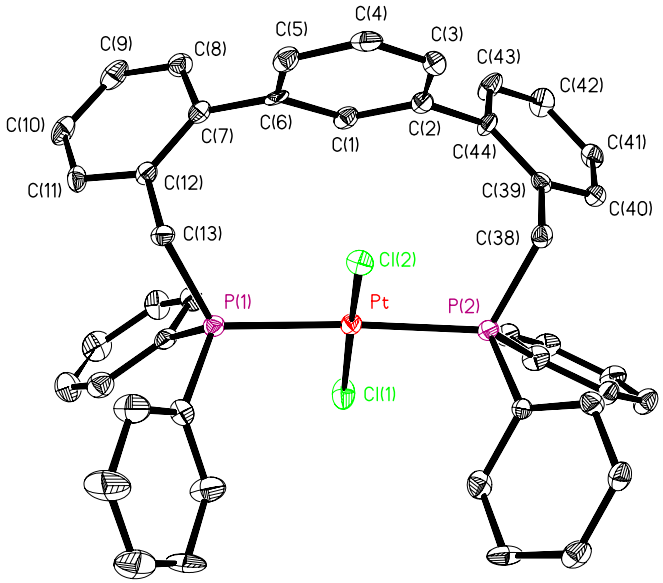

Figure 2.12. ORTEP drawing (30% probability ellipsoids) of the molecular structure of **2**. Hydrogen atoms are omitted for clarity.

Empirical formula	$C_{44}H_{36}Cl_2P_2Pt$
Formula weight (g/mol)	892.66
Temperature (K)	153 (2)
Wavelength (Å)	0.71073
Crystal system	Monoclinic
Space group	$P2_{1/n}$
Unit cell dimensions	
a (Å)	13.042(3)
b (Å)	10.284(2)
c (Å)	27.826(6)
α (deg)	90.00
β (deg)	101.25(3)
γ (deg)	90.00
Volume (Å3)	3660.5(13)
Z	4
Calculated density (Mg/m3)	1.620
Absorption coefficient (mm-1)	4.098
F(000)	1768
Crystal size (mm)	0.24 × 0.19 × 0.12
Crystal color and shape	yellow chip
Θ range for data collection (deg)	2.73 - 25.10
Limiting indices	-12 < h < 15
	-8 < k < 12
	-33 < l < 33
Reflections collected	21267
Independent reflections	6318
Completeness to *Θ*	25.10 (96.9 %)
Max. transmission	0.6391
Min. transmission	0.4396
Refinement method	Full-matrix least-squares on *F*2
Data / restraints / parameters	6318/0/442
Goodness of fit on *F*2	1.164
Final R indices ($I > 2\sigma(I)$)	
R1	0.0453
wR2	0.0883
R indices (all data)	
R1	0.0602
wR2	0.0964

Table 2.1. Refinement details for crystal structure of **2**.

2. 3 Synthesis of Pt-Acetylides Containing *m*-Terphenyl Phosphines

The polymer precursor **2** can be used to create platinum complexes that contain platinum atoms connected to an ethynyl moiety. In this step, the two chloride ligands are displaced by acetylide groups of varying functionalities (Scheme 2.4). This Sonogashira/Hagihara type coupling is the basis for our proposed polymerization

pathway and promises significant utility in synthesizing the desired functionalized platinum polymers.

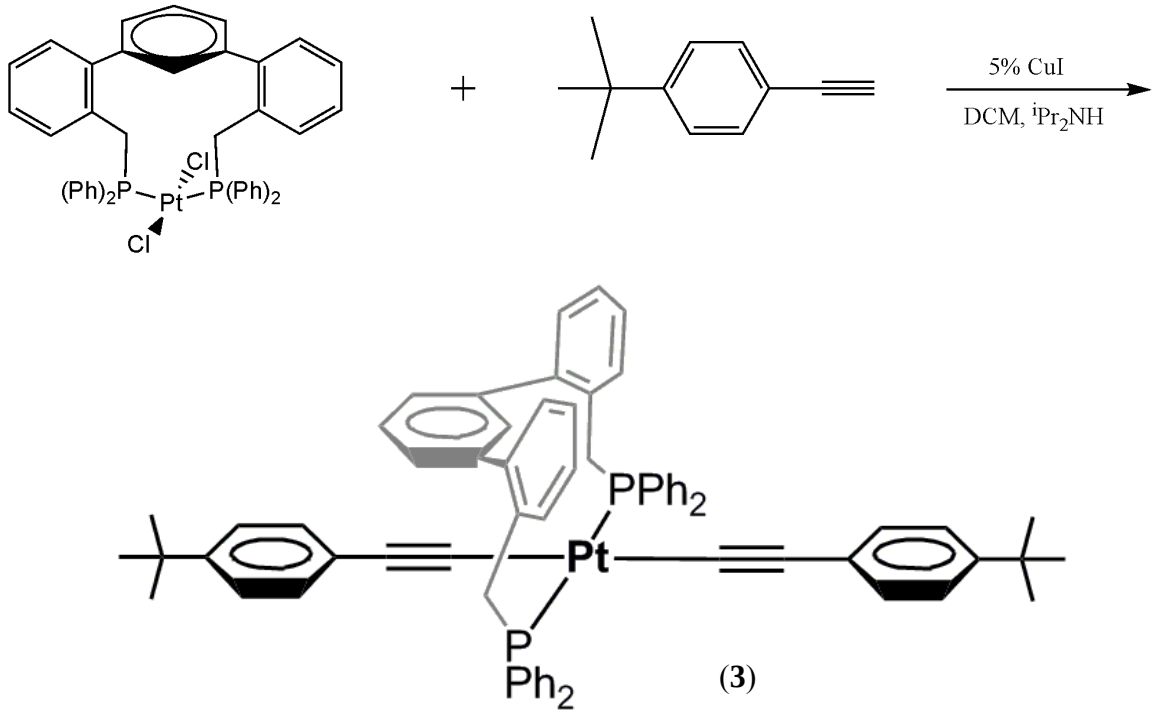

Scheme 2.4. Synthetic pathway to model compound **3** which demonstrates the success in the ligand exchange between chloride and acetylide ligands on the platinum metal center.

The preliminary investigation of synthesizing complex **3** afforded information regarding the reaction conditions necessary for successful synthesis. As the starting material **2** was a yellow solid, it was predicted that compound **3** would also be yellow in color because no substituents with strong absorbances in the visible spectrum were being added to **2**. Moreover, previous investigations[11] have found a wavelength of maximum absorbance of 350 nm for the *trans*-platinum triphenylphosphine-based complex shown below which features a chromophore π-system nearly identical to that of **2** (Figure 2.13).

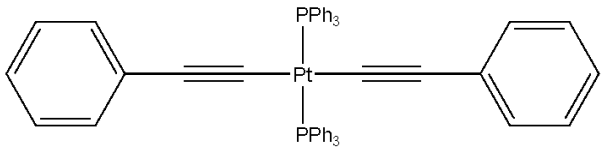

Figure 2.13. *Trans*-platinum acetylide type complex with triphenylphosphine ligands.

When initial attempts (heating to 70 °C) afforded a deep purple material, it seemed that excessive heat interfered with the desired reaction. Most likely the 4-*tert*-butylphenylacetylene self-dimerized at such high temperatures, at a rate exceeding that of the ligand exchange between the terminal alkyne and the chlorides on the platinum in complex **2**. Subsequent syntheses of model compound **3** were performed in the same molar ratios according to the same initial procedure but without heating. These investigations yielded the expected pale yellow solid without the need for separation from colored side products. Phosphorous-31 NMR spectra featured a chemical shift for **3** at 11.2 ppm; this chemical shift is the same as that of the *trans*-[(**1**)$PtCl_2$] (*vide supra*). However, coupling constant in the model complex **3** ($^1J_{Pt\text{-}P}$ = 2751 Hz) is larger than that of starting material **2** ($^1J_{Pt\text{-}P}$ = 2616 Hz). Relatively small changes in coupling between the dichloro and diethynyl complexes are typical as demonstrated by a $^1J_{Pt\text{-}P}$ of 2385 Hz for *trans*-[$(Et_3P)_2PtCl_2$] compared to a $^1J_{Pt\text{-}P}$ of 2370 Hz for the diethynylbenzene analog, *trans*-[$(Et_3P)_2Pt(C{\equiv}C\text{-}Ph)_2$].[12, 13] It is a well-documented fact that increasing the length of a bond results in smaller ^1J coupling constants because more distance now separates the two nuclei.[14] It is possible that the small change in coupling constant (larger in **3** relative to **2**) is due to the fact that the platinum-acetylide bond is longer than a platinum-chloride bond, and so the platinum-phosphorous bond shortens to compensate in the model

complex **3**. These predictions will be further probed by X-ray crystallographic data on **3** should crystals be obtained.

The synthesis of the platinum model compound **3** demonstrates that the ligand exchange between chlorides and acetylides at the platinum center proceeds readily at room temperature and that this synthetic scheme can be used for the assembly of platinum-ethynyl bonds on platinum precursors that include the terphenyl phosphine. Moreover, reagents with two accessible alkynes can reasonably be expected to afford polymers with repeating platinum-based terphenylphosphine monomeric units via a similar procedure. However, future investigations should seek to elucidate the solid-state and solution-state structures and photophysics of **3** and related complexes, since these characteristics might help in predicting polymer conformations and thus potential fluxionalities.

2.4 Polymerization of *trans*-[(1)$PtCl_2$] with 1,4-diethynyl-2,5-dihexyloxybenzene

As the model compound (*vide supra*) demonstrated that ligand exchange between acetylides and chlorides is possible at the platinum center, it became of interest to examine the reactivity of the dichloroplatinum complex **2** with reagents that contained two acetylene groups to determine if polymerization proceeds at the platinum center. This polymerization couples the dichloroplatinum complex **2** to 1,4-diethynyl-2,5-dihexyloxybenzene in the presence of 5% copper iodide catalyst (Scheme 2.5).

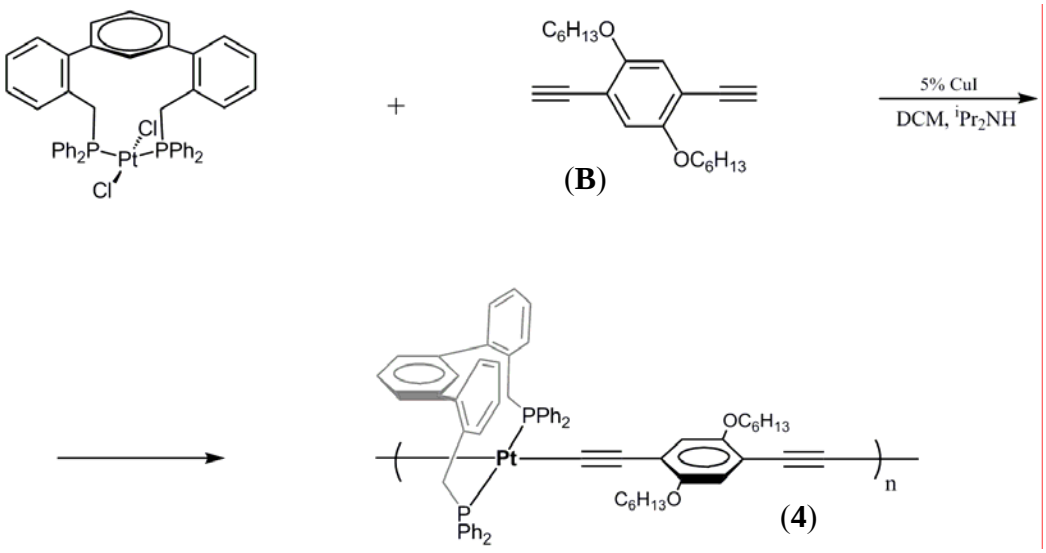

Scheme 2.5. Synthesis of platinum-based polymer containing alkoxybenzene functionalized acetylene units.

Before polymerization, it was necessary to prepare the desired 1,4-diethynyl-2,5-dihexyloxybenzene (**B**). This dialkyne is readily synthesized by Sonogashira coupling of trimethylsilylacetylene with 2,5-dihexyloxybenzene followed by base-induced deprotection of the TMS groups (Scheme 2.6).

Step 1

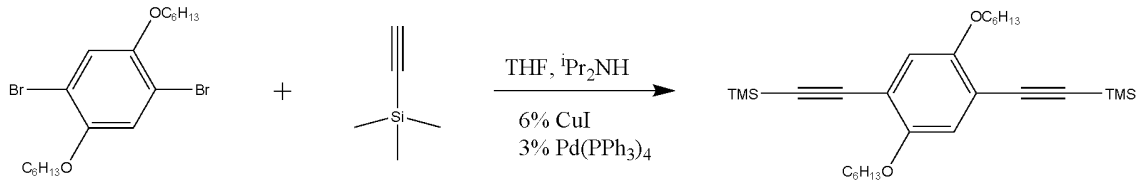

Step 2

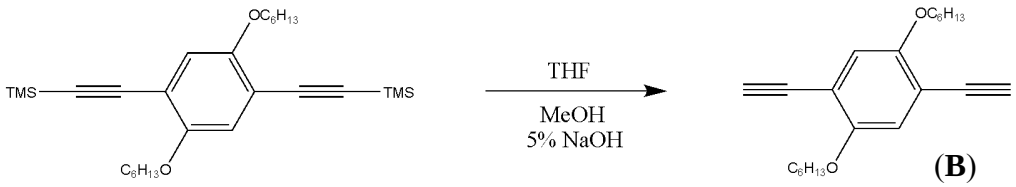

Scheme 2.6. Synthesis of TMS-protected analog of **B** and subsequent deprotection under basic conditions.

Initial attempts to create polymer **4** proved unsuccessful, partially because it was believed that the alkyne degraded before use. However, while terminal alkynes are generally unstable and can undergo self-polymerizations fairly readily, the dialkyne **B** in this investigation can be stored for extended periods of time as long as it is stored away from light and heat. Compound **B** can then be used in the polymerization reaction with **2** to afford polymer **4** (Scheme 2.5). These initial investigations elucidated potential purification methods in the event that polymer **4** was made but simply impure. Because investigations of complex **3** showed the product could be purified by passing crude **3** through a short column of silica gel using chloroform as the eluting solvent to remove ammonium salts that had been produced in the reaction, this method was used to purify the crude polymer **4**. Significant improvements in purity of the model compound **3** can

also be garnered from this crude mini-column method but this procedure afforded no improvement in the purity of the alkoxy polymer **4**. However, at this time, an absorption spectrum for the metallopolymer in a solution of dichloromethane showed a maximum absorbance of 370 nm.

After multiple failed attempts to synthesize the metallopolymer **4**, new batches of the *trans*-[(**1**)$PtCl_2$] and dialkyne **B** were made, purified and used immediately to discern whether starting material degradation was responsible for polymerization inhibition. It was also possible that some NMR silent impurities in either or both of the starting materials could prevent successful synthesis of the desired polymer **4** due to imbalanced stoichiometry. This later attempt at metallopolymer **4** appeared to proceed successfully as demonstrated by ^{31}P NMR resonances and couplings compared to the starting material **2**.

After isolation, the polymer is a brown orange glassy solid with excellent film-forming properties. The ^{31}P NMR spectrum of this crude alkoxy polymer **4** (Fig A-17) looks nearly identical to that of the starting dichloroplatinum **2** (Fig A-14). This is to be expected as there is no change in phosphorous connectivity in the polymerization detailed in Scheme 2.3. Therefore, there likely will be no definitive proof of polymer synthesis via ^{31}P NMR analysis. The slight change in the phosphorous-platinum coupling constant when comparing starting dichloroplatinum **2** ($J_{P\text{-}Pt}$ = 2630 Hz) and alkoxy polymer **4** ($J_{P\text{-}Pt}$ = 2626 Hz) is not large enough to be significant (only 4 Hz) especially when chemical shifts are reported with an intrinsic associated error of 0.1 ppm (~12 Hz for ^{31}P).

This new batch of alkoxy polymer **4** was also analyzed in terms of its absorption and photoluminescence properties, especially since the targeted devices (solar cells and/or light-emitting diodes) rely heavily on these photophysical characteristics.

Preliminary examination of the crude polymer fluorescence was performed by placing it under an ultraviolet lamp which demonstrated only modest fluorescence; however, cooling to liquid nitrogen temperature produced much more intense photoluminescence (Figure 2.14). Often the intensification of photoluminescence at low temperatures indicates that phosphorescence is a viable radiative pathway for the excited state energy. This is because the triplet excited state lifetime is much longer than is the case for the singlet excited state and therefore phosphorescence is more likely to be quenched before radiative decay (i.e., by oxygen dissolved in the solvent).[15] Low temperatures reduce the likelihood of quenching by oxygen (even in mM concentrations) as well as decrease nonradiative decay rates compared to radiative decay from the triplet excited state (phosphorescence).

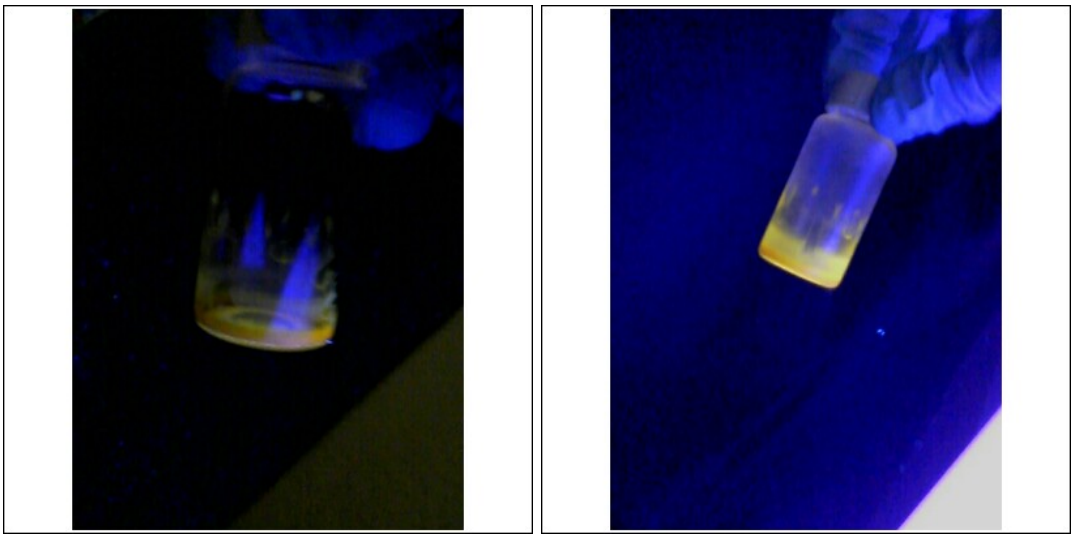

Figure 2.14. Alkoxy polymer **4** as seen under an ultraviolet lamp (254 nm) at room temperature (left) and after being cooled to 77 K (right).

More detailed UV-vis and fluorescence spectroscopy demonstrate a λ_{max} of 357 nm and a λ_{em} of 415 nm (dilute solution, λ_{ex} = 357 nm) as shown below (Figure 2.15). Moreover, the photoluminescence quantum yield of metallopolymer **4** (in dichloromethane) was found to be 0.12%.

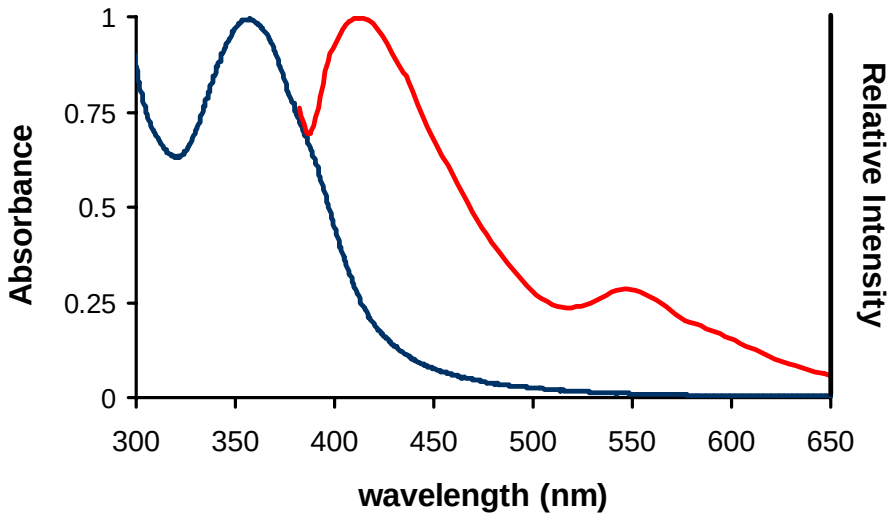

Figure 2.15. Absorbance (blue) and photoluminescence (red) spectra of platinum-based alkoxy polymer **4**.

Because the solution was prepared under an inert atmosphere, it is not possible to determine whether photoluminescence is due to fluorescence or phosphorescence from these photophysical studies. However, lifetime measurements performed in the future will elucidate the nature of the photoluminescence; longer lifetimes (on the order of μs) will be strong evidence for phosphorescence as the major form of radiative decay. A platinum acetylide polymer similar in structure (without the *m*-terphenyl scaffold) to alkoxy polymer **4** has been found to exhibit a wavelength of maximum absorbance on the same order as seen here (Figure 2.16).[16] This polymer shows a wavelength of maximum

absorbance around 380 nm and strong emission at ~520 nm which is more intense at low temperatures. The energy of emission for this platinum-acetylide polymer is at a much lower energy wavelength than is seen for **4**, but it is interesting to note the intensity dependence on temperature seen with $(Pt\text{-}TBT)_n$ as well.

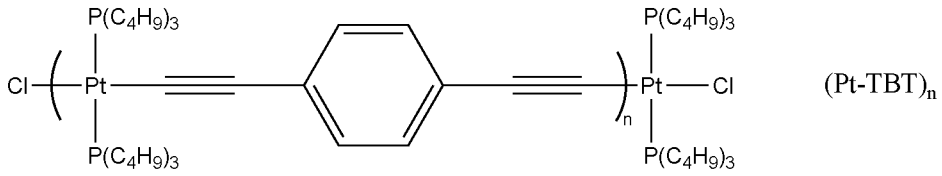

Figure 2.16. Platinum acetylide polymer with maximum absorbance similar to alkoxy polymer **4**.

A platinum-acetylide polymer (**P13**) similar in structure to $(Pt\text{-}TBT)_n$ was synthesized with electron donating methoxy groups on the diethynylbenzene spacers to examine their effect on the photophysical parameters of the polymer (Figure 2.17).[17]

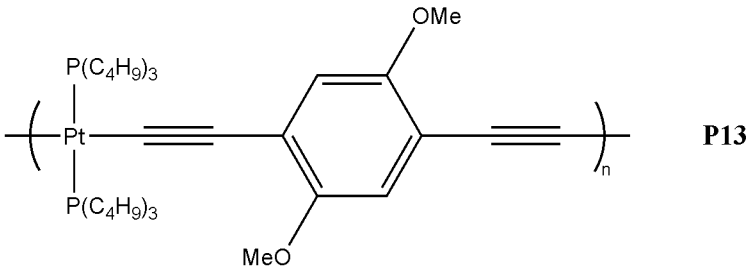

Figure 2.17. Platinum-acetylide polymer with diethynylbenzene spacer functionalized with methoxy groups.

This methoxy analog of the $(Pt\text{-}TBT)_n$ shows a λ_{max} of around 400 nm and a λ_{em} of 590 nm. These values show that incorporation of electron-donating methoxy groups red-shift the polymer's absorption and emission maxima relative to the unsubstituted

analogous polymer (i.e., **P13** versus $(Pt\text{-}TBT)_n$). However, there are important differences between the photophysical parameters of **4** and those of **P13**. The wavelength of maximum absorbance for the alkoxy polymer **4** is at a slightly higher energy (by ~40 nm) than **P13**; moreover, the emission maximum of **4** is significantly blue-shifted (by ~175 nm) compared to **P13**. Band gaps for materials whose π-systems are not as coplanar are higher in energy (blue-shifted) and are more likely to decay nonradiatively. The blue-shift in absorption and emission maxima, concomitant with the significantly low quantum yield ($\Phi = 0.12\%$), could imply a decrease in coplanarity in **4** as compared to **P13**. This is possibly due to the long solublizing hexyloxy chains introducing some steric clash limiting the twisting freedom of **4** and perhaps locking the polymer into a noncoplanar conformation. In addition, the terphenyl scaffold present in **4** that is not in **P13** is a bulky bidentate ligand that could aid in this "conformational locking" if the hexyloxy chains are pushed away from the encumbering *m*-terphenyl.

Estimation of the band gap for **4** can be made from the onset of absorbance (gauged around 440 nm); according to this analysis, the band gap energy is around 2.8 eV. Smaller energy differences between the HOMO and LUMO correlate with more efficient semiconducting materials that are to be used in photovoltaics and light-emitting devices. While electrochemical studies have not yet been performed on polymer **4**, some general comparison to other platinum-containing metallopolymers' band gaps can be made to discern whether **4** is a potentially promising material for photovoltaic or LED purposes. Some platinum-containing thiophene based metallopolymers have been found to have low band gap energies on the order of 1.9 and 2.1 eV (Figure 2.18).[18]

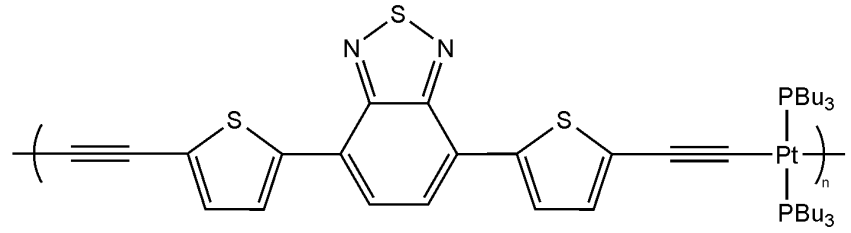

p-PtBTD-Th

E_g = 2.07 eV

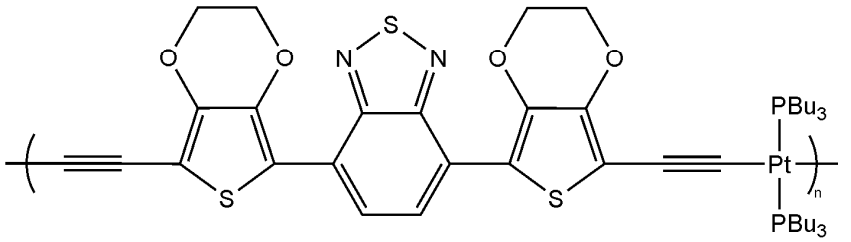

p-PtBTD-EDOT

E_g = 1.93 eV

Figure 2.18. Thiophene metallopolymers with associated bandgaps that are targeted as potential photovoltaic or LED materials.

These polythiophene polymers exhibit promising emissive properties as well as semiconducting behavior. Moreover, this investigation finds that to enhance triplet state emission, it is necessary for the band gap energies to be above 2.1 eV so that charge separation can be achieved. In lieu of these results, it appears that polymer **4** has a band gap energy on the order of what would be beneficial for conductive and light-emitting devices—especially if phosphorescence were desired.

The synthesis of **4** appears to be operative at least according to the previous procedure on an NMR scale. However, the characterization of complex **4** proves to be much more difficult than that of the model compound **3**. Due to the highly conjugated nature of metallopolymer **4**, the aromatic region in the ^{1}H NMR will be hard to analyze

and assign definitive integrations. Moreover, the aromatic region in the ^{13}C NMR of what is presumed to be polymer **4** has significant line broadening that may be an indication of successful polymerization.[19] Alternatively, the broadening in both the ^{1}H and ^{13}C NMR spectra seem to imply fluxionality in the terphenyl scaffold that bridges the platinum metal center. A palladium analog of the dichloroplatinum **2** synthesized by Smith and coworkers[6] demonstrates significant broadening in the ^{1}H NMR which is attributable to the twisting motion of the terphenyl scaffold that broadens the benzylic protons (Figure 2.7). Currently it appears as though the latest attempt at polymerization has been successful in affording platinum alkoxy polymer **4**; it is of particular interest to perform high resolution mass spectrometry or related technique to obtain the molecular weight for the unique polymer presented here.

2.5 Synthesis of a Functionalized *m*-Terphenylphosphine

As explained before, small molecules and organic π-conjugated polymers can often undergo nonradiative decay by vibrational relaxation after excitation (either photo- or electrochemical excitation). This non-emissive decay of the excited state energy leads to a decrease in both photoluminescence intensity and overall quantum yield; moreover, the dissipation of the excited state energy implies a decrease in conductance of the material. For polymeric materials that are used for semiconductive or light-emitting materials, it is thus necessary to maximally preserve the excited state energy before that energy is needed for the device purpose. Because flexibility of the polymeric material gives rise to the bond vibration relaxation mechanism, it seems that rigidifying organic and organometallic polymers will reduce this form of non-emissive decay. In addition, limiting the fluxionality of polymers targeted for photovoltaics and light-emitting devices

can essentially lock a molecule into a more planar structure which has been shown to be directly correlated with a lower band gap energy.[20] Thus, by rigidifying a polymer, the effective conjugation length can be extended which enhances conductivity, photoluminescence quantum yield and red-shifts absorbance and emission wavelengths.

Some of the most well-known OCPs studied in terms of the relationship between conformation and photophysics are polythiophenes. One of the first elucidations of the importance of morphology came from a study on poly(3-methylthiophene), P3MT, conductivity in thin films.[21] In this investigation, the conductivity of P3MT was studied as a function of film thickness in electrochemical manipulations. Because electropolymerization was used to generate the P3MT, halting the polymerization progress at certain stages yielded polymer films of varying thickness. The authors found that thicker films suffered from a decrease in electrical conductivity as compared to the thinner P3MT polymers. More specifically, P3MT that was ~200 nm thick demonstrated a conductivity of around 1.98×10^3 S/cm compared to 1.47×10^3 S/cm for a P3MT film of ~380 nm. In addition, decreasing polymer thickness led to red-shifting of absorbance maximum; 6 nm P3MT had a wavelength of maximum absorbance of 552 nm compared to 510 nm for a P3MT film about 190 nm thick. These results demonstrate that P3MT film thickness is directly correlated to the photophysical and conductive properties of the polymers. Moreover, the authors rationalize these trends by explaining that increasing the polymer thickness causes a more disordered macromolecular structure (as a result of both inter- and intramolecular forces) which reduces the effective conjugation length. Conversely, the thin P3MT films remain more organized and planar thereby increasing the delocalization over the polymer and lowering the band gap energy. As a result, this

effective “rigidification” of P3MT demonstrates that photophysical and conductive properties can be enhanced by controlling the polymer conformation.

Polythiophene copolymers have also been synthesized in an effort to reduce polymer mobility and hopefully enhance conductivity and photophysical behavior. An early investigation attempted to make poly(thienylene vinylene) in order to compare its conductivity and optical properties to the “parent” poly(thiophene) molecule.[22] Poly(thienylene vinylene) was found to have a band gap around 1.7 eV both from doping experiments and absorption onset estimation. This value is considerably lower than the band gap energy of poly(thiophene) found on the order 2 eV.[23] The ethylene linkages in a polythiophene backbone limit the rotational freedom of the thiophene moieities. A direct result of the inhibited bond rotation is that the poly(thienylene vinylene) molecule is more rigid than the parent poly(thiophene) thereby causing an increase in effective conjugation length. Thus, poly(thienylene vinylene) is a better semiconducting material because of a decrease in band gap energy as a result of the ethylene linkages limiting fluxionality and/or reducing the incidence of steric clash in the polymer backbone.

Owing to the increase in conductivity and photoluminescence efficiency improvements in rigidifying OCPs, researchers have begun to investigate the effects of limiting the mobility of organometallic polymers targeted for photovoltaics and light-emitting diodes. As previously discussed, phosphorescence is an attractive form of radiative decay from the excited state in polymers that contain a heavy atom (such as a transition metal) that enhances spin-orbit coupling. Moreover, because phosphorescence is a spin-forbidden process, it often times is much slower than nonradiative decay pathways which operate on the order of 10^8 s^{-1} as a general estimate.[15] As such, it is

necessary to reduce the likelihood of nonradiative decay to make phosphorescence a more competitive emission outcome.

An aforementioned study found that materials having higher-energy triplet states demonstrate correspondingly higher phosphorescence efficiency and radiative rates in platinum-containing polyacetylides.[1] The authors explain that the nonradiative decay rate (from the triplet state) is directly related to the band gap energy of the platinum-acetylide polymer; lower-lying triplet states are more susceptible to nonradiative excited state energy decay. Therefore, to harvest the spin-forbidden photoluminescence from the triplet state, structural modifications to the platinum-containing OCP were made to increase the triplet state energy. By calculating triplet state energies and rates of phosphorescent radiative decay, it was found that the higher-lying triplet states produces phosphorescence with the greatest efficiency. For example, **P2** with a triplet energy of 2.4 eV has a much faster radiative decay rate than **P7** with a triplet energy of 1.53 eV (Figure 2.19).

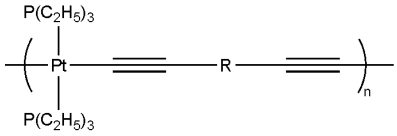

general polymer structure

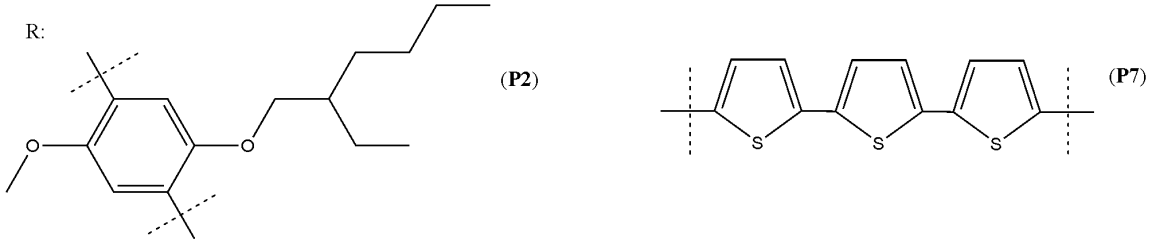

(**P2**) (**P7**)

Figure 2.19. Platinum-acetylide polymers used to investigate the connection between triplet energy level and phosphorescence radiative decay rates.

These results demonstrate that phosphorescence can be harvested more efficiently from organometallic polymers when the triplet state energy is higher; however, it should be noted that this increase in triplet energy will likely decrease the conductivity of the material. Moreover, rigidifying the metallopolymer causes the triplet energy to increase while at the same time reducing excited energy loss to bond vibrations. However, this technique certainly increases the band gap energy of the polymeric material which will reduce its semiconducting efficacy.

The above studies demonstrate that rigidification of OCPs and organometallic polymers can significantly alter the conductivity and light-emitting behavior of the material by effecting changes in the band gap energy. Limiting the vibrational relaxation of the polymer by reducing rotational and vibrational modes extends the effective conjugation length and lowers the band gap energy; as a result, more rigid OCPs appear to be better semiconductors. However, rigidifiying metallopolymers can increase the triplet state energy thereby making phosphorescence more efficient but possibly decreasing conductivity. It is therefore necessary to alter the OCP or metal-containing OCP according to the requirements of the targeted device. The current investigation aims to discern the effect of further rigidifying the *m*-terphenylphosphine scaffolded polymer **4** to determine whether photophysical characteristics and conductivity are enhanced with even less fluxionality in the polymeric backbone.

While the synthesis of *m*-terphenyl scaffolded metallopolymers similar to the alkoxy polymer **4** (*vide supra*) is interesting in and of itself, the potential to build polymers off the terphenyl scaffold promises enhanced optical properties compared to the structure with monomeric units repeating only between platinum centers. That is, the

ability to synthesize "double-decker" polymers is of particular interest to our synthetic investigations (Scheme 2.7).

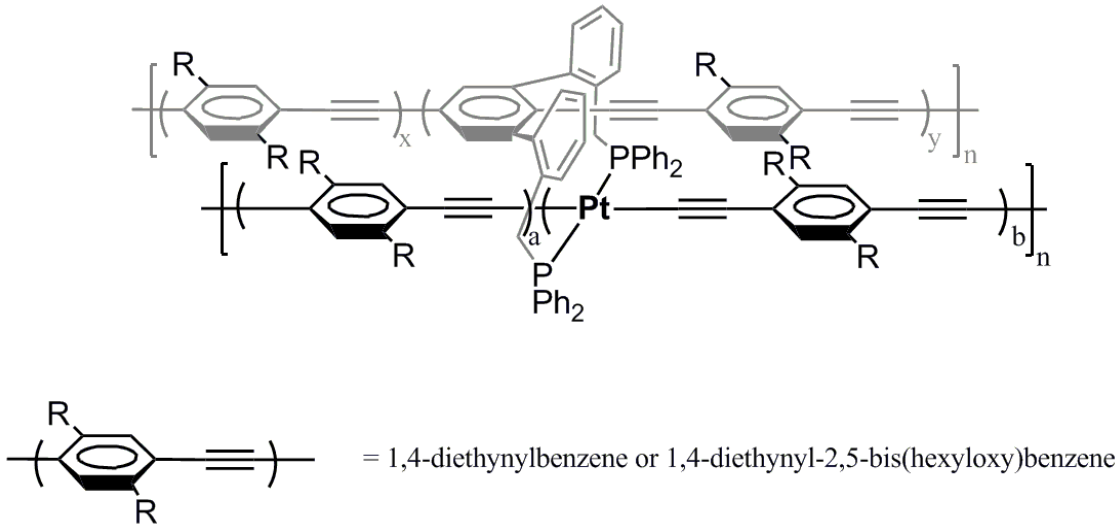

Scheme 2.7. Proposed structure for a platinum-based metallopolymer with polymeric chains emanating from the platinum center and the terphenyl scaffold.

The current section is aimed at describing the synthesis of the functionalized *m*-terphenylphosphine scaffolded platinum precursor that is necessary for subsequent polymerizations.

2.6 Synthesis of a Functionalized *m*-Terphenylphosphine Scaffold

Since the polymer of interest requires a terphenyl scaffold that is halogenated on the central benzene ring, it is necessary to first synthesize such a functionalized *m*-terphenylphosphine. In the present investigation, an *m*-terphenylphosphine that is dihalogenated (**9**) will be synthesized (Scheme 2.8).

Step 1

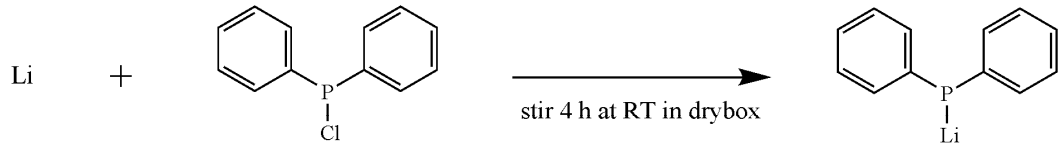

Step 2

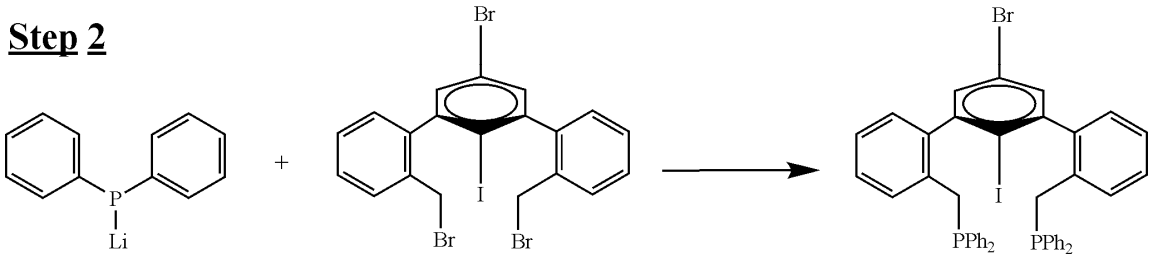

(**9**)

Scheme 2.8. Synthesis of terphenylphosphine **9**.

Once the functionalized terphenylphosphine has been isolated and purified, it can be reacted with dichlorobis(benzonitrile)platinum in the same manner as with the simple terphenylphosphine to yield *trans*-[(**9**)$PtCl_2$] (**10**) (Scheme 2.9).

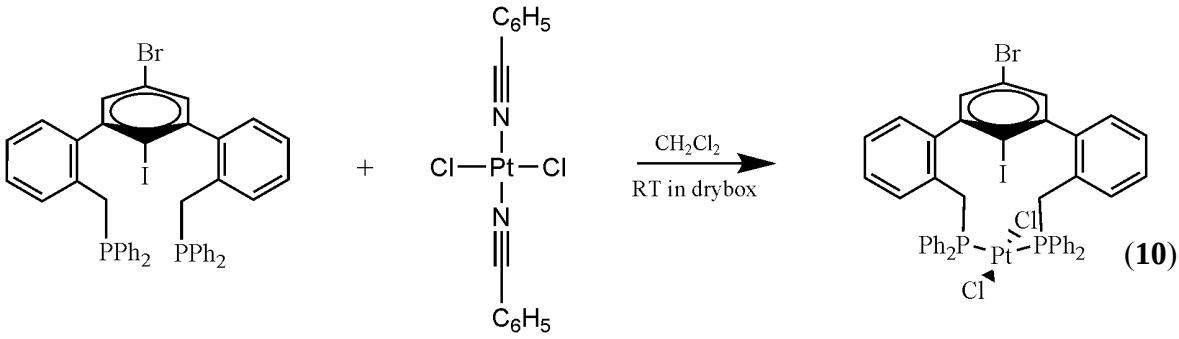

(**10**)

Scheme 2.9. Synthesis of functionalized terphenyl-scaffolded platinum **10**.

Synthesis of *m*-terphenylphosphine scaffold **9** proceeds with similar ease and efficiency as that seen with **1**. The resultant product is a beige white solid that is easily

characterized by standard spectroscopic techniques. Its use in synthesizing the polymer precursor **10** seemed promising to eventually afford the desired functionalized polymer.

The synthesis of *trans*-[(**9**)$PtCl_2$] (**10**) proved to more difficult than anticipated given the relative ease by which the production of *trans*-[(**1**)$PtCl_2$] proceeds (*vide infra*). Various reaction conditions were examined to determine whether the process could be driven to completion to afford **10**. Without any success at affording a pure platinum-containing starting material, the potential for synthesizing the desired scaffolded polymer seemed remote; reevaluation of the purity of **9** was performed to discern if it was interfering with synthesis of **10**. Closer examination of the spectral data available for the functionalized terphenylphosphine **9** indicates an equilibrium barrier is likely interfering with our desired reaction. The ^{31}P NMR of **9** shown in Figure 2.20 demonstrates two phosphorous resonances (–9.68 and –10.12 ppm) which correspond to different conformations (*syn* and *anti*) for the *m*-terphenylphosphine **9** (Scheme 2.10).

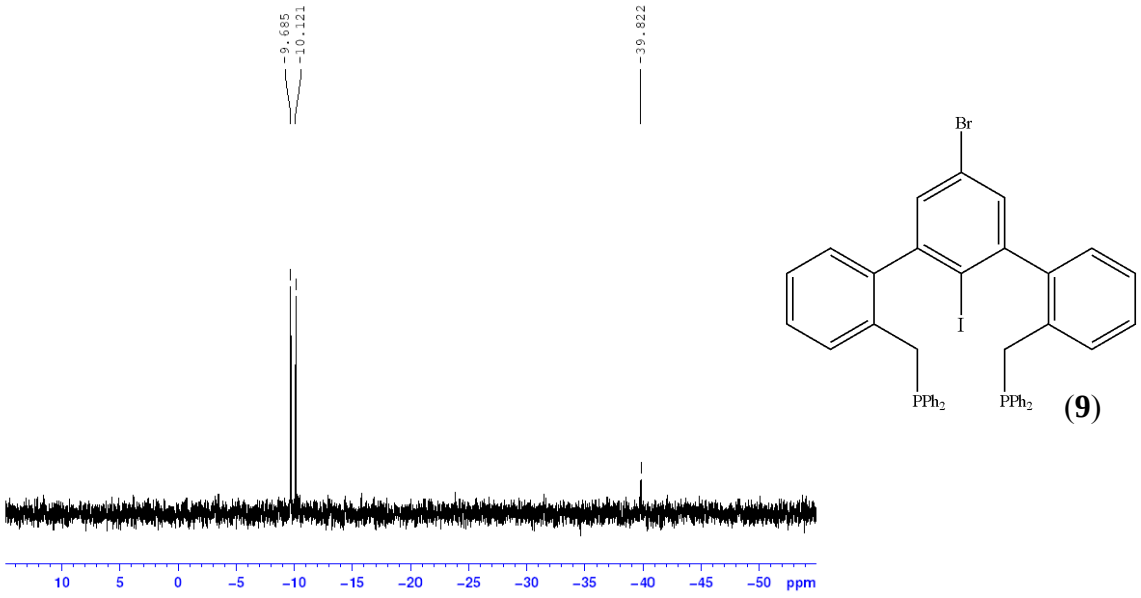

Figure 2.20. Phosphorous-31 NMR of functionalized *m*-terphenylphosphine **9** showing the presences of two atropisomers.

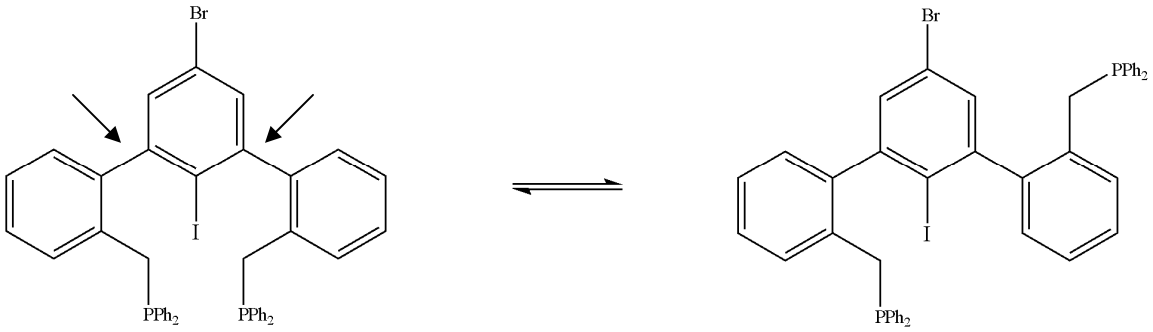

Scheme 2.10. Equilibrium for the *syn* (left) and *anti* (right) atropisomers possible for *m*-terphenylphosphine **9**. Arrows indicate bonds about which hindered rotation is observed.

The monobrominated terphenyl analog of **9** (**9-Br**, Scheme 2.11) has been studied by Protasiewicz and coworkers in terms of its atropisomerism.[9]

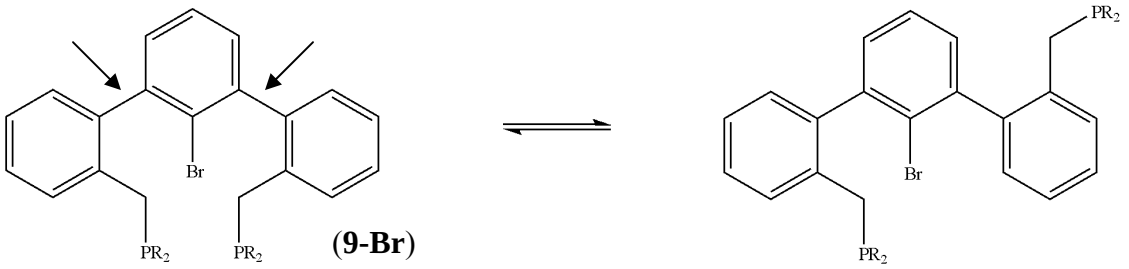

Scheme 2.11. Functionalized terphenylphosphine with sterically hindered rotation as examined by Protasiewicz and coworkers. Arrows indicate bonds about which hindered rotation is observed.[9]

Both **9** and **9-Br** demonstrate sterically hindered rotation (atropisomerism) about the highlighted bonds as a result of the large halogens on the central aryl ring. Moreover, the rotation is slow enough to be seen on the NMR timescale to allow investigation of solvent and temperature dependence on the atropisomerism. As the *anti* form of the functionalized terphenylphosphine **9** will not bridge a platinum metal as is required for

our polymerizations, it is necessary to optimize the reaction conditions so that there is no barrier to rotation and thus efficient isomerism between the *syn* and *anti* forms of **9**. Thus, the following section addresses a variable temperature NMR study to determine the temperature at which rotation about the highlighted bonds (in our analog) is essentially free.

As detailed previously, the ^{31}P NMR spectrum of the functionalized terphenylphosphine **9** displays two prominent resonances consistent with the *syn* and *anti* isomers possible for the compound (Fig A-29). The *anti* isomer will not produce a terphenyl-scaffolded platinum dichloro species because the phosphine moieties are no longer close to each other in space and therefore do not promote *trans*-binding to one platinum metal atom. This is especially detrimental to our current investigation because the *anti* isomer is more energetically favorable as the bulky diphenylphosphine groups are positioned in such a way as to minimize steric penalties. However, because it is an equilibrium, when some of the *syn* isomer bridges a platinum metal, there can be an conversion from *anti* to *syn* in the equilibrium according to Le Châtelier's principle. As a result, more *syn* will be present and then react with the platinum species to yield the desired terphenyl-scaffolded platinum material until eventually all the terphenylphosphine **9** is consumed to give the desired **10**. Yet the hindered rotation in the equilibrium (Scheme 2.10) implies that interconversion between the *syn* and *anti* forms requires a significant energy input.

A convenient and efficient technique for determining the energy required for isomer interconversion is that of variable temperature NMR (VT-NMR). The method relies on finding the temperature of the sample at which the two isomer peaks coalesce

into one broad peak. This technique is similar to the classic experiment in which VT-NMR is performed to find the energy barrier to rotation to *N,N*-dimethylacetamide.[24] Once this temperature is recorded, a simple mathematical manipulation can be performed to elucidate the free energy of rotation about the sterically hindered bond (equation 1), where T_c is the coalescence temperature (in K) and ν_a and ν_b are the NMR chemical shifts in Hz.[25]

$$\Delta G^{\neq} = (19.1 \times 10^{-3})(T_c)[9.97 + \log(T_c) - \log(\nu_a - \nu_b)] \qquad \textbf{(equation 1)}$$

For the *m*-terphenylphosphine[9] depicted in Scheme 2.10, a VT-NMR experiment was performed with the aim of determining to examine the temperature at which rotation about the bonds of interest is essentially unhindered (T_c) which can then be used to estimate the free energy of activation ($\Delta G^{\neq}$).

The VT-NMR of the functionalized terphenylphosphine **9** did not yield any crucial information about the energetics of the atropisomerism equilibrium (Figure A-33). While the intensity of both ^{31}P resonances decreases slightly as the temperature increases, there is no change in the height of one atropisomer peak relative to the other. Moreover, and perhaps more importantly, the two peaks do not move closer to each other even as the temperature approaches 80 °C. Essentially there appears to be no coalescence, albeit incomplete, even to this temperature. Owing to the probehead limitations (cannot exceed 90 °C), it is not possible to discern where coalescence occurs for the terphenylphosphine **9** because it appears to be well above 80 °C. Using equation 1, this implies that the free energy to rotation ($\Delta G^{\neq}$) is at least 73 kJ/mol. Only the iodine is sterically hindering the interconversion between *syn* and *anti* isomers, but the bromine could play a minor role in

hindering the rotation in the other direction. This would mean that whether the diphenylphosphine arm rotated forward or backward in the *anti* isomer, it would still encounter steric clash when attempting to isomerize to the *syn* form. However unlikely, it could also be possible that there is no rotation about the highlighted bond (*vide supra*) and that the conformers may be locked into either the *syn* or *anti* form. The inability to optimize reaction conditions to favor the *syn* isomer of **9** will preclude the ability to make the proposed "double-decker" polymers because there will be no method to successful synthesis of the platinum starting material *trans*-[(**9**)$PtCl_2$] (**10**). However, replacement of the iodine with a 4-*tert*-butylphenylacetylene may reduce the steric hindrance to rotation and thus allow an ethynyl-substituted analog of **10** to be afforded and then used in polymerizations.

2.7 Miscellaneous Terphenyls and Alkynes to be used in Later Syntheses

This brief section merely details the purity and modification of a few functionalized terphenyls and acetylide donors to be used in later polymerization reactions. The incorporation of various functional groups, such as halogens or nitro groups, will change the optical properties of the metallopolymers and so are attractive compounds for incorporation into a platinum-based polymer.

Trimethyl((4-nitrophenyl)ethynyl)silane (Figure 2.21), which had been stored in the freezer, was examined by ^1H NMR to determine its purity.

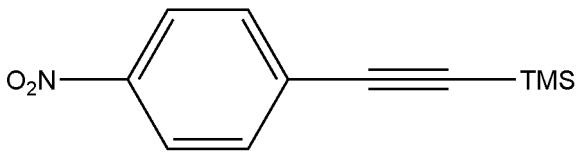

Figure 2.21. TMS-protected ethynylbenzene with a *para*-nitro group functionalization.

The nitro group would effect changes in the optical properties of the metallopolymer and so determining if it interferes with the ligand exchange reaction is first necessary. Thus, it will be used in making a model compound similar to complex **3**. After drying under vacuum for 2 h, ^{1}H NMR of the trimethyl((4-nitrophenyl)ethynyl)silane (Fig A-19) showed a 1:1 integration of the two phenyl resonances. The purity of the TMS-protected acetylide source was determined to be acceptable for the next step in creating a nitro-functionalized platinum-model compound.

Two functionalized terphenyls were examined by ^{1}H NMR to determine their purity for later use as polymerization precursors (Figure 2.22).

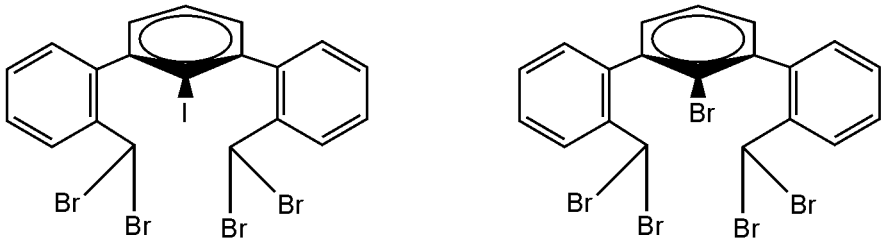

(**6**) (**7**)

Figure 2.22. Terphenylphosphine precursors with central aryl halogenated either by an iodide or bromide.

The first compound, a tetrabrominated terphenyl with a single iodide (**6**) showed clean proton resonances with anticipated integrations and can be used without further purification (Fig A-20). Proton NMR of a tetrabrominated terphenyl with a bromide on the central aryl ring (**7**) showed significant amounts of succinamide present at 2.6 ppm and so purification of this compound was necessary. Compound **7** was mixed with ~5 mL of MeOH, pulverized and the solid was isolated by vacuum filtration and dried under

vacuum for 2 h. This procedure was repeated twice until the ^{1}H NMR spectrum (Fig A-21) indicated acceptable purity for compound **7** to be used in the next step.

Finally, a brominated terphenyldialdehyde (**8**) that had been previously synthesized was worked up for generation of a monobrominated terphenyl (Figure 2.23).

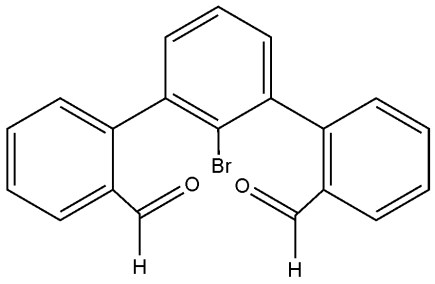

(**8**)

Figure 2.23. Monobrominated terphenylphosphine precursor **8**.

Compound **8** was an orange liquid phase on top of a silver gray solid (likely Ag(0) generated in the course of the reaction) and the solid was removed by vacuum filtration to yield a yellowish orange oil. After evaporation of the solvent, the resultant orange residue was dissolved in 30 mL of dichloromethane and ~1 mL of 10% HCl was added and the reaction mixture was stirred for 48 h. At that time, the reaction mixture was washed with water (3 x 10 mL) and the organic layer dried over anhydrous magnesium sulfate overnight. The solvent was then evaporated off to leave a bright orange viscous liquid and initial ^{1}H NMR showed significant amounts of solvent present. The crude product was washed with diethyl ether (3 x 10 mL) and again the solvent was removed *in vacuo* but now to yield a pale yellow-white solid. Proton NMR showed a clean product with a strong aldehyde peak at 9.8 ppm (Fig A-22).

Pure compound **8** was then reduced with sodium borohydride. First, methanol (750 mL) was dried by placing of magnesium turnings (50 g) with iodide chips (5 g) in a

1L roundbottom flask. The methanol was then distilled from this violent reaction mixture while under positive nitrogen pressure and placed in an ice bath; only around 100 mL of anhydrous methanol was collected from this procedure. Then, in the dry box, sodium borohydride (0.017 g, 0.447 mmol) was added to about 3 mL of THF in a roundbottom flask and sealed with a septum for bringing out of the drybox. Compound **7** (0.163 g, 0.447 mmol) was added to ~1 mL THF and ~2 mL of anhydrous methanol using Schlenk techniques. This mixture was then transferred via syringe to the sodium borohydride slurry and the reaction was stirred at room temperature for ~24 h. At that time, 1 mL of 15% HCl was added to the reaction mixture which then stirred for another ten minutes. Then ~5 mL of diethyl ether was added to the reaction mixture and then the solution was washed with water (3 x 10 mL), the organic layer dried with anhydrous magnesium sulfate and concentrated by rotary evaporation to give a barely detectable amount of a pale white residue. As there was no visible product to be isolated, the residue was combined with diethyl ether and pentane to try to precipitate out more desired product. This mixture was left in the freezer and still has not produced measurable product so no spectral analysis can be presented. However, this procedure should allow for a monobrominated (Br on the central aryl ring) scaffold to be generated and then used for phosphine synthesis and later creation of a model platinum compound.

2.8 Conclusions

Synthesis of *trans*-[(**1**)$PtCl_2$] appears to operate via a ligand exchange at the platinum center between dichlorobis(benzonitrile)platinum and *m*-terphenylphosphine. This complex is especially stable due to the *m*-terphenyl scaffolding that *trans*-spans the platinum center. Moreover, owing to promising results in ligand exchange between the

chloride on trans-[(**1**)$PtCl_2$] and 4-*tert*-butylphenylacetylene, polymerization has been performed and optimized. It appears that an *m*-terphenylphosphine scaffolded platinum acetylide polymer (**4**) can be made by performing a ligand exchange between *trans*-[(**1**)$PtCl_2$] and the dialkyne **B**. This polymer, which is a glassy orange solid, demonstrates absorbance and emission similar to platinum-acetylide polymers already targeted for photovoltaic and light-emitting devices. Moreover, the intensification at low temperatures offers a promising alternative to materials that are currently used in LEDs that require low operating temperatures. Band gap estimation of **4** based on absorbance data appears to suggest that this stable metallopolymer may find excellent use in devices that require semiconducting polymers with unique photophysical characteristics. More in depth electrochemical investigations are necessary to determine the precise energy of the HOMO and LUMO to further elucidate whether **4** will be a truly versatile material in modern photovoltaics and light-emitting devices.

The synthesis of a functionalized scaffolded polymer analogous to the alkoxy polymer **4** would be of particular interest to examine the effects of rigidifying the metallopolymer in terms of its conductivity and photoluminescence. Not only would polymerizations from the platinum and *m*-terphenylphosphine scaffold rigidify the polymer, it would also provide a favorable π-π stacking interaction between upper and lower chains. In essence, this "double-decker" polymer would be highly conjugated on the top and bottom polymer chains as well as able to engage in through-space conjugation. And as seen previously, the platinum metal would enhance spin-orbit coupling while still preserving conjugation thereby making this functionalized "double-decker" polymer truly unique in the class of platinum-acetylide polymers. While the

photophysical and conductive traits of this polymer would be significantly edifying as to the effects of rigidification concomitant with through-space conjugation, it thus far seems exceedingly difficult to make the necessary polymer precursor, *trans*-[(**9**)$PtCl_2$] (**10**) because **9** cannot be isolated in only the *syn* conformer.

Future studies should utilize an NMR instrument equipped with a probehead that has less stringent temperature limitations. It is necessary to first discern the coalescence temperature of **9** to determine at which point (if any) the rotation about the central phenyl ring is no longer sterically inhibited. Once this temperature is identified, following the same reaction protocol as detailed in Scheme 2.5 at the appropriate temperature should afforded the desired "double-decker" metallopolymer.

Experimental

General Considerations

All air-sensitive reactions were performed using standard Schlenk techniques or in an MBraun UNILab glovebox under nitrogen. Anhydrous solvents were purchased from Fisher Scientific and further dried and degassed using an MBraun solvent purification system. All other reagents were used as received unless otherwise specified. NMR spectra of interest were obtained on a Bruker Avance 300 (operating at 300, 75.4, and 121.4 MHz for ^{1}H, ^{13}C, and ^{31}P nuclei, respectively) or Bruker Avance 500 spectrometer (operating at 500, 125.7, and 202.4 MHz for ^{1}H, ^{13}C, and ^{31}P nuclei, respectively). NMR spectral data are reported in ppm referenced to residual solvent signal (^{1}H and ^{13}C) or 85% phosphoric acid (^{31}P). UV-vis absorption spectra were acquired on a Cary 50 Spectrophotometer while photoluminescence (PL) spectra were obtained on a Varian Eclipse fluorimeter.

2,6-bis(2-((diphenylphosphino)methyl)phenyl)benzene (1)

Desired phosphine **1** was synthesized using previously reported literature procedures.[6] In the drybox, freshly cut lithium wire (0.147 g, 21.1 mmol) and chlorodiphenylphosphine (0.557 g, 2.52 mmol) in 20 mL of tetrahydrofuran were stirred for 4 h to afford a deep red solution. At that time, the red solution was decanted away from the excess lithium wire and removed from the drybox in a 100 mL round bottom flask. At –78 °C, a solution of **A** (0.5 g, 1.2 mmol) in 8 mL of THF was added via syringe to the dark red reaction mixture. Immediately after adding the halogenated terphenyl, the dry ice bath was removed and the reaction was allowed to stir for 16 h under positive nitrogen pressure. After stirring overnight, the THF was removed and the crude phosphine dissolved in about 10 mL of diethyl ether, washed three times with degassed water and the ether was then removed *in vacuo*. Analysis of the resultant off-white crystalline solid by ^{1}H and ^{31}P NMR (Fig A-1 and A-2) indicated the desired **1** was synthesized and purified effectively. ^{1}H NMR (300 MHz, $CDCl_3$) δ: 7.4-7.0 (m, 32H), 3.4 (s, 2H); ^{31}P NMR (121.4 MHz, $CDCl_3$) δ: –8.8.

***trans*-[(1)$PtCl_2$] (2)**

Starting dichloroplatinum complex **2** was synthesized in the drybox by placing dichlorobis(benzonitrile)platinum (0.300 g, 0.635 mmol) in dichloromethane (~20 mL) followed by dropwise addition of a solution of **1** (0.399 g, 0.636 mmol) in about 20 mL of dichloromethane. Completion of dropwise addition yielded a yellow solution and the reaction mixture stirred for 94 h at room temperature in the drybox. Product was characterized by ^{1}H and ^{31}P NMR and shown to be pure enough to bypass recrystallization (Fig A-3 and A-4). ^{1}H NMR (300 MHz, $CDCl_3$) δ: 8.5-6.7 (m, 29H), 6.1

(s, 1H) 5.1-4.7 (s, 2H), 3.7-3.2 (s, 2H); ^{31}P NMR (121.4 MHz, $CDCl_3$) δ: 11.16 (t, $J_{P\text{-}Pt}$ = 2616 Hz). Elemental Analysis (%): Calc. for $C_{44}H_{36}Cl_2P_2Pt$: C, 59.20; H, 4.06; Cl, 7.94; P, 6.94; Pt, 21.85; Found: C, 59.20; H, 4.06, N, 0. In future syntheses where significant impurities were present, compound **2** was easily recrystallized by diffusion of diethyl ether into a dichloromethane solution of **2**.

^{31}P NMR spectrum for this batch showed no starting phosphine for the reaction mixture which has a characteristic chemical shift of –8.8 ppm (Fig A-2). The synthesis and isolation of complex **2** proceeds with relative efficiency and can be stored in the drybox until the next step in the polymer synthesis. Any minor impurities can be removed by recrystallization as noted above.

***trans*-[(1)PtCl$_2$] model compound (3)**

Complex **3** was made by first transferring dichloroplatinum **2** (0.568 g, 0.636 mmol) into a pressure tube in the drybox; any residue left in the vessel that previously contained **2** was rinsed with a minimal amount of toluene. Then 4-*tert*-butylphenylacetylene (0.302 g, 1.91 mmol) was added dropwise to the pressure tube while stirring. Copper iodide (0.018 g, 5% mol catalyst) was transferred to the reaction mixture using ~5 mL of diisopropylamine. The pressure tube was then brought out of the drybox and heated to 70°C and stirred for 5 d at which point there was a purple metallic liquid atop a yellow granular solid. ^{31}P NMR of the purple liquid phase showed minor integration for the chemical shift characteristic of complex **2** (spectra not provided), so the reaction mixture was diluted with dichloromethane, washed with water and the solvent was rotovapped off. ^{1}H and ^{31}P NMR indicated dichloromethane still present so crude product **3** was dried under vacuum for 2 h.

Complex **3** was purified by column chromatography using 1:1 mixture of hexane to dichloromethane. The pale yellow fractions presumably contained the compound **3** of interest and were collected using a 1.2:1 mixture of hexane:dichloromethane. ^{1}H and ^{31}P NMR spectra of fraction 11 (fraction size = 10 mL) showed eluting solvent still present so crude product dried under vacuum for 4 h and submitted for purer ^{1}H, ^{31}P and ^{13}C NMR spectral analysis (Fig A-5, A-6, A-7). ^{1}H NMR (300 MHz, $CDCl_3$) δ: 8.1-7.9 (s, 1H), 7.5-6.9 (m, 10H), 6.8-6.2 (s, 1H), 5.1 (s, 1H), 3.1 (s, 1H), 1.4-1.2 (m, 18H); ^{31}P NMR (121.4 MHz, $CDCl_3$) δ: 11.17 (t, $J_{P\text{-}Pt}$ = 2751 Hz); ^{13}C NMR (75.4 MHz, $CDCl_3$) δ: 144.4, 142.3, 134 (br), 133.7, 133.3, 131-124 (br m), 119, 112.5, 29.2.

Syntheses of model compound **3** after this initial attempt were performed according to the same procedure but without heating to yield product **3** in decent enough purity to preclude column chromatography. Moreover, later syntheses demonstrated that purification of **3** occurs readily with the crude product recrystallizing by diffusion of pentane into a diethyl ether solution of product **3**.

TMS-protected 1,4-diethynyl-2,5-dihexyloxybenzene

Step 1 in the synthesis of the desired alkyne is the production of the TMS-protected 1,4-diethynyl-2,5-dihexyloxybenzene. This compound is made by first placing 1,4-dibromo-2,5-dihexyloxybenzene (2.021 g, 5 mmol) and $Pd(PPh_3)_4$ (0.173 g, 0.15 mmol) in 50 mL of tetrahydrofuran in a 150 mL pressure flask in the drybox. While the aforementioned solution stirred, trimethylsilylacetylene (0.982g, 10 mmol) and copper(I) iodide (0.057 g, 0.30 mmol) were placed in 50 mL of diisopropylamine. The trimethylsilylacetylene/copper iodide solution was then added to the reaction flask at a rate of 1 pipet/min while stirring to yield a brownish yellow solution. After completion,

the reaction mixture was brought out of the drybox and heated to 75 °C for 48 h. At that time, the solvent was removed by rotary evaporation and the resultant brick red solid was dissolved in 50 mL of toluene. The crude product in toluene was then passed through silica to remove any ammonium salts. Rotary evaporation of the solvent yielded the TMS-protected 1,4-diethynyl-2,5-dihexyloxybenzene which was a yellow solid. The resultant product was analyzed by ^{1}H NMR (Fig A-8). The ^{1}H NMR shows a 1:9 integration ratio of the aromatic protons relative to the methyl groups on the trimethylsilyl group indicating successful synthesis of the TMS-protected compound. ^{1}H NMR (300 MHz, $CDCl_3$) δ: 6.9 (s, 1H), 3.9 (quartet, 4H), 1.8 (m, 4H), 1.4 (m, 8H), 0.9 (m, 6H), 0.4 (s, 18H).

1,4-diethynyl-2,5-dihexyloxybenzene (B)

Before reaction between alkyne-containing compound and complex **2** can occur, the trimethylsilyl (TMS) protected 1,4-diethynyl-2,5-dihexyloxybenzene must be deprotected to afford compound **B** (Scheme 2.6). The deprotection was carried out, following a reported method,[26] by adding 1 mL of 20% (w/v) NaOH, 5 mL of THF and 2 mL of MeOH to 0.1 g of bis-TMS-protected analog of **B**. This solution was stirred for about 2 hours while wrapped in foil. At that time, TLC analysis showed consumption of starting material and presence of a new product so the reaction mixture was diluted with dichloromethane, washed with water (3 x 10 mL), dried over anhydrous magnesium sulfate and the solvent was removed by rotary evaporation. ^{1}H NMR analysis showed successful removal of the trimethylsilyl groups (Fig A-9) and compound **B** was stored in the drybox freezer for ~2 d before use in the polymerization. ^{1}H NMR (300 MHz, $CDCl_3$) δ: 6.9 (s, 1H), 3.9 (quartet, 4H), 3.3 (s, 2H), 1.8 (m, 4H), 1.4 (m, 8H), 0.9 (m, 6H).

In later procedures for deprotecting the TMS-analog, the crude reaction mixture was diluted with diethyl ether instead of dichloromethane and there appears to be no difference in purity or yield of the isolated dialkyne based on the solvent differences. Moreover, future deprotections that followed the same procedure but still had TMS protons present could be purified by washing with methanol and drying under vacuum. The subsequent syntheses showed that **B** remains pure for extended periods of time while stored in the drybox freezer when free of solvent and wrapped in foil.

Platinum-based 1,4-diethynyl-2,5-dihexyloxybenzene metallopolymer (4)

In the drybox, compound **2** (0.050 g, 0.056 mmol) was added to ~1 mL of dichloromethane in a small vial followed by dropwise addition of a mixture of 1,4-diethynyl-2,5-dihexyloxybenzene (0.018 g, 0.056 mmol) and copper iodide (1.2 mg, 5% mol cat.) in ~2 mL of diisopropylamine. The vial that contained the copper iodide and diethyne reagent was washed with dichloromethane and this solution was also transferred to the reaction vial while stirring. The mixture was allowed to stir for 1 d at room temperature in the drybox. At that time, ^{31}P NMR showed only starting material **2** present and so the reaction mixture was removed from the drybox and heated at 50 °C while stirring for about 36 h. Again, spectral analysis only showed resonances consistent with dichloroplatinum complex **2**.

As it was believed that the deprotected 1,4-diethynyl-2,5-dihexyloxybenzene had decomposed while stored in the drybox freezer, the reaction was carried out a second time but with immediate use of the deprotected dialkyne reagent after ^{1}H NMR analysis indicated the TMS groups had been removed from the acetylene moieties. This reaction differed enough that it will be detailed here. *Immediately* after the deprotection step, the

1,4-diethynyl-2,5-dihexyloxybenzene was pumped into the drybox for use. The dichloroplatinum complex **2** (0.050 g, 0.056 mmol) was dissolved in ~3 mL of dichloromethane and the 1,4-diethynyl-2,5-dihexyloxybenzene (0.018 g, 0.056 mmol) was added to this solution. Copper iodide (1.2 mg, 5% mol cat.) in 2 mL of diisopropylamine was transferred to the reaction mixture; the vial that contained the copper iodide and diisopropylamine was rinsed with another 2 mL of diisopropylamine and this was also transferred to the reaction mixture. The reaction mixture was stirred at room temperature in the drybox for ~36 h to yield an orange solution at which point ^{31}P NMR showed again only a chemical shift consistent with complex **2**. The reaction was transferred to a pressure tube and brought out of the drybox to stir while heating to 50 °C for 24 h. ^{1}H NMR of crude reaction mixture showed resonances different from complex **2** so purification was pursued. The crude product mixture was brought back into the drybox and washed with diethyl ether, the solvent was removed *in vacuo* to yield an orange-yellow solid with a glassy appearance. ^{1}H, ^{31}P and ^{13}C NMR spectra showed signals different from the starting complex **2** (Fig A-10, A-11, A-12) but required the NMR sample to prepared with all of the isolated solid. ^{1}H NMR (300 MHz, $CDCl_3$) δ: 9.2 (s, 1H), 8.1-6.2 (m, 5H), 6.1 (s, 1H), 3.7-3.3 (m, 2H), 1.8-0.8 (m, 12H); ^{31}P NMR (121.4 MHz, $CDCl_3$) δ: 11.12; ^{13}C NMR (75.4 MHz, $CDCl_3$) δ: 144.1, 142.3, 134 (br), 133.7, 132.5, 131-125 (br m), 67.7, 65.8, 53.4, 31.7, 29.2 (br m), 25.2, 24.9, 22.7, 19.0, 15.3, 14.0, 11.1.

After multiple attempts to create the desired polymer **4**, new batches of both the 1,4-diethynyl-2,5-dihexyloxybenzene and the dichloroplatinum complex **2** were made in hopes that either one or both of the starting materials had either decomposed or contained

NMR-silent impurities that were inhibiting polymerization. The ^{1}H, ^{31}P and ^{13}C NMR of this batch of dichloroplatinum **2** complex are provided to demonstrate definitive purity as far as NMR can probe (Fig A-13, A-14, A-15). ^{1}H NMR (300 MHz, $CDCl_3$) δ: 8.1 (s, 1H), 8.0-6.7 (m, 53H), 6.2 (d, 2H) 4.9 (s, 2H), 4.1 (s, 1H), 3.5 (s, 1H); ^{31}P NMR (121.4 MHz, $CDCl_3$) δ: 11.15 (t, $J_{P\text{-}Pt}$ = 2629 Hz); ^{13}C NMR (75.4 MHz, $CDCl_3$) δ: 144.1, 142.3, 134 (br), 133.7, 132.5, 131-125 (br m), 118.9, 112.8, 29.2.

The ^{1}H NMR of the dialkyne is not shown but appears as detailed before. As both starting materials appeared free of NMR-detectable impurities, the polymerization was attempted again. In the drybox, 1,4-diethynyl-2,5-dihexyloxybenzene (7.3 mg, 0.02 mmol) was placed in 3 mL of chloroform-d_1 and added to a 20 mL vial containing the dichloroplatinum **2** (20 mg, 0.02 mmol). Then 1 drop of diisopropylamine was added to the reaction vial and the reaction mixture was allowed to stir for 1 h at room temperature in the drybox. At that time, the reaction mixture was transferred via pipet to a vial containing copper(I) iodide (1 mg, 5 μmol) and the yellow solution was stirred for 48 h at room temperature in the box. After 48 h, the now dark orange reaction mixture was analyzed by ^{1}H, ^{31}P and ^{13}C NMR (Fig A-16, A-17, A-18). ^{1}H NMR (300 MHz, $CDCl_3$) δ: 8.1 (s, 3H), 8.0-7.0 (m, 85H), 6.1 (d, 4H), 4.0 (quartet, 4H), 3.7 (s, 7H), 3.0 (m, 24H), 1.8 (m, 5H), 1.5-0.7 (m, 208H); ^{31}P NMR (121.4 MHz, $CDCl_3$) δ: 11.14 (t, $J_{P\text{-}Pt}$ = 2626 Hz); ^{13}C NMR (75.4 MHz, $CDCl_3$) δ: 154.1, 144.1, 142.3, 134 (br), 133.7, 132.5, 131-125 (br m), 117.8, 113.0, 112.4, 82.3, 69.5, 67.1, 45.5, 31.7, 29.2 (br m), 25.2, 24.9, 22.4, 14.0. As the previous reaction was performed on an NMR tube scale, the purification was performed after the desired spectra were acquired. Platinum polymer **4** was washed three

times with water and the chloroform-d_1 was removed by rotary evaporation to yield a crude orange glassy solid.

To more quantitatively assess the optical properties of the terphenyl-scaffolded alkoxy polymer **4**, it was of interest to acquire UV-vis and Fluorescence spectra. However, it was first important to reprecipitate the polymer to remove any residual impurities. The crude orange polymer **4** was dissolved in 0.4 mL of dichloromethane and syringe transferred into a vial containing 3 mL of pentane to afford a yellow-orange precipitate. This suspension was centrifuged and the solvent decanted away from the resultant brown pellet that was the desired polymer **4** (2 mg). The purified polymer **4** was then dried *in vacuo*, brought into the box and dissolved in 10 mL of dichloromethane to make a stock solution of $2*10^{-4}$ M to be used for UV-vis and Fluorescence spectroscopy. After diluting the stock polymer solution to $2*10^{-5}$ M, an absorption spectrum was acquired of the polymer while under nitrogen atmosphere in a quartz cuvette (Fig B-2). A fluorescence spectrum of a polymer solution with concentration of $4*10^{-7}$ M was also acquired using 357.5 nm as the excitation wavelength.

Functionalized *m*-terphenylphosphine scaffold (9)

The synthesis of the functionalized terphenylphosphine **9** follows the procedure[6] used for making compound **1**. In the drybox, freshly cut lithium wire (0.992 g, 14.2 mmol) was added to 20 mL of THF followed by chlorodiphenylphosphine (0.391 g, 1.77 mmol) in a 50 mL roundbottom. The reaction mixture was stirred at room temperature for 4 h to yield a deep red solution. At that time, the red reaction mixture was decanted away from the excess lithium wire, transferred to a 100 mL roundbottom flask, brought out of the drybox and placed in an acetone dry ice bath. While at –78 °C, the dibrominated

terphenyl (0.5 g, 0.81 mmol) was added via syringe and the reaction mixture was allowed to warm to room temperature and then stir for 18 h under positive nitrogen pressure. At that time, the crude reaction mixture was pumped back into the box and the THF was removed *in vacuo*. The resultant pale yellow solid was dissolved in 10 mL of diethyl ether and the insoluble solid (presumably undesired lithium salt) was filtered via syringe. After removal of the diethyl ether, the crude beige solid presumed to be the terphenylphosphine **9** was analyzed by ^{1}H and ^{31}P NMR (Fig A-23 and A-24). ^{1}H NMR (300 MHz, $CDCl_3$) δ: 7.8 (s, 1H), 7.6 (s, 1H), 7.6-6.9 (m, 64H), 6.8 (s, 2H); ^{31}P NMR (121.4 MHz, $CDCl_3$) δ: –9.68, –10.1, –10.3, –39.8.

The ^{31}P NMR showed two resonances at –9.68 and –10.12 ppm corresponding to the *syn* and *anti* atropisomers of the desired phosphine **9**. However, a peak at –39.82 ppm was an impurity present in a significant amount. As a result, the crude beige solid was dissolved in 20 mL of diethyl ether in the drybox and then washed three times with degassed water using air-free techniques. The diethyl ether was then removed *in vacuo* and the beige solid analyzed by ^{31}P NMR again (Fig A-25). ^{31}P NMR (121.4 MHz, $CDCl_3$) δ: –9.69, –10.1, –39.8. As the air-free water wash did not remove the phosphorous-containing impurity at –39.82 ppm, it was assumed that this peak corresponds to a lithium diphenylphosphine that remained unreacted.

In order to reduce the amount of lithium diphenylphosphine impurities in the final functionalized terphenylphosphine **9**, the stoichiometry of the reaction was changed such that the ratio of dibrominated terphenyl to chlorodiphenylphosphine was as close to 1:2 as possible without obtaining monobrominated analogs of **9** as byproducts. As a result, another synthesis of **9** was set up with a molar ratio of 1:2.1 for the terphenyl to

chlorodiphenylphosphine stoichiometric amounts. Therefore, in the box, freshly cut lithium wire (0.992 g, 14.2 mmol) was added to a 50 mL roundbottom containing 20 mL of THF followed by the addition of chlorodiphenylphosphine (0.33 g, 1.69 mmol). The remainder of the reaction follows the procedure described in the preceding paragraph with the exception that the air-free water wash was omitted. ^{31}P NMR of the beige solid showed a clean spectrum with only a trace amount of the –39.82 ppm impurity (Fig A-26). ^{31}P NMR (121.4 MHz, $CDCl_3$) δ: –9.6, –10.1, –39.82 (trace amount). This functionalized terphenylphosphine **9** was deemed pure enough to proceed with the next step in the synthetic pathway to the "double-decker" polymer of interest.

***trans*-[(9)PtCl$_2$] (10)**

Functionalized dichloroplatinum complex **10** was synthesized in the drybox by adding a solution of functionalized terphenylphosphine **9** (56 mg, 0.12 mmol) in 5 mL of dichloromethane to a vial containing dichlorobis(benzonitrile)platinum (0.100 g, 0.12 mmol) already in 5 mL of dichloromethane. The resultant bright yellow reaction mixture was stirred at room temperature in the drybox for 24 h. At that time, the dichloromethane was removed *in vacuo* and the crude yellow solid was analyzed by ^{1}H and ^{31}P NMR (Fig A-27 and A-28). As the ^{31}P NMR showed multiple signals, including ^{31}P resonances consistent with starting material **9**, the NMR sample was heated to 60 °C with the goal of driving the reaction towards completion if there is a thermodynamic barrier as a result of the atropisomerism of **9**. After 2 h of heating at 60 °C, the NMR sample was analyzed by ^{31}P NMR again; however, this sample was too dilute for quick acquisition so an overnight ^{31}P NMR was necessary (Fig A-29). Again, there were numerous ^{31}P resonances in the spectrum indicating that heating was not effective at pushing the reaction towards

completion and thus synthesis of the desired functionalized terphenyl dichloroplatinum **10** has not yet been achieved.

VT-NMR of *m*-terphenylphosphine (9)

An NMR sample of the functionalized terphenylphosphine **9** was made by dissolving about 25 mg of the purified solid in 1 mL of toluene in the drybox. Toluene was used as its boiling point is 110 °C and would not present problems with sample boiling as the probehead temperature increased. A few drops of chloroform-d_1 was added for locking purposes. However, later a few drops of benzene-d_6 was added to the NMR sample because benzene-d_6 has six deuterium nuclei and thus provides a lock that is six times more sensitive than chloroform-d_1. (The instrument can lose the lock as the probehead and sample are heated and so having more deuterium nuclei is beneficial as it reduces the likelihood of losing the lock). The sample was placed into a Bruker Avance 300 MHz instrument and it was locked and shimmed. After that, simple ^{31}P NMR spectra were obtained at temperatures ranging from 25 °C to 78 °C with time in between experiments to allow for probehead temperature equilibration (Fig A-30).

REFERENCES CITED

(1) Wilson, J. S.; Chawdhury, N.; Al-Mandhary, M. R. A.; Younus, M.; Khan, M. S.; Raithby, P. R.; Kohler, A.; Friend, R. H. "The Energy Gap Law for Triplet States in Pt-Containing Conjugated Polymers and Monomers" *J. Am. Chem. Soc.* **2001**, *123*, 9412-9417.

(2) van der Boom, M. E.; Milstein, D. "Cyclometalated Phosphine-Based Pincer Complexes: Mechanistic Insight in Catalysis, Coordination, and Bond Activation" *Chem. Rev.* **2003**, *103*, 1759-1792.

(3) Albrecht, M.; van Koten, G. "Platinum Group Organometallics Based on 'Pincer' Complexes: Sensors, Switches, and Catalysts" *Angew. Chemie Int. Ed.* **2001**, *40*, 3750-3781.

(4) Pollino, J. M.; Weck, M. "Tandem Catalysis and Self-Assembly: A One-Pot Approach to Functionalized Polymers" *Org. Lett.* **2002**, *4*, 753-756.

(5) South, C. R.; Weck, M. "Bridged Coordination Polymer Multilayers with Tunable Properties" *Langmuir* **2008**, *24*, 7506-7511.

(6) Smith, R. C.; Protasiewicz, J. D. "A Trans-Spanning Diphosphine Ligand Based on a *m*-Terphenyl Scaffold and Its Palladium and Nickel Complexes" *Organometallics* **2004**, *23*, 4215-4222.

(7) Clyburne, J. A. C.; McMullen, N. "Unusual Structures of Main Group Organometallic Compounds Containing *m*-Terphenyl Ligands" *Coord. Chem. Rev.* **2000**, *210*, 73-99.

(8) Power, P. P. "Persistent and Stable Radicals of the Heavier Main Group Elements and Related Species" *Chem. Rev.* **2003**, *103*, 789-810.

(9) Ma, L.; Woloszynek, R. A.; Chen, W.; Ren, T.; Protasiewicz, J. D. "A New Twist on Pincer Ligands and Complexes" *Organometallics* **2006**, *25*, 3301-3304.

(10) Balema, V. P.; Wiench, J. W.; Pruskia, M.; Pecharsky, V. K. "Solvent-Free Mechanochemical Synthesis of Two Pt complexes: *cis*-$(Ph_3P)_2PtCl_2$ and *cis*-$(Ph_3P)_2PtCO_3$" *Chemical Commun.* **2002**, 1606-1607.

(11) Bemi, L.; Clark, H. C.; Davies, J. A.; Fyfe, C. A.; Wasylishen, R. E. "Studies of Phosphorus(III) Ligands and Their Complexes of Nickel(II), Palladium(II), and Platinum(II) Immobilized on Insoluble Supports by High-Resolution Solid-State Phosphorus-31 NMR Using Magic-Angle Spinning Techniques" *J. Am. Chem. Soc.* **1982**, *104*, 438-445.

(12) Grim, S. O.; Keiter, R. L.; McFarlane, W. "A Phosphorous-31 Nuclear Magnetic Resonance Study of Tertiary Phosphine Complexes of Platinum(II)" *Inorg. Chem.* **1967**, *6*, 1133-1137.

(13) Cairns, M. A.; Dixon, K. R.; Smith, M. A. R. "A New Synthesis of Platinum-Carbon Bonds" *J. Organomet. Chem.* **1977**, *135*, C33-C34.

(14) Autschbach, J.; Le Guennic, B. "Analyzing and Interpreting NMR Spin-Spin Coupling Constants Using Molecular Orbital Calculations" *J. Chem. Educ.* **2007**, *84*, 156-171.

(15) Lakowicz, J. R. *Principles of Fluorescence Spectroscopy*, Third ed.; Springer Science and Business Media: New York, 2006.

(16) Beljonne, D.; Wittman, F.; Kohler, A.; Graham, S.; Younus, M.; Lewis, J.; Raithby, P. R.; Khan, M. S.; Friend, R. H.; Bredas, J. L. "Spacial Extent of the Singlet and Triplet State Excitons in Transition Metal Containing Poly-ynes" *J. Chem. Phys.* **1996**, *105*, 3868-3877.

(17) Khan, M. S.; Al-Mandhary, M. R. A.; Al-Suti, M. K.; Corcoran, T. C.; Al-Mahrooqi, Y.; Attfield, J. P.; Feeder, N.; David, W. I. E.; Shankland, K.; Friend, R. H.; Kohler, A.; Marseglia, E. A.; Tedesco, E.; Tang, C. C.; Raithby, P. R.; Collings, J. C.; Roscoe, K. P.; Batsanov, A. S.; Stimson, L. M.; Marder, T. D. "Synthesis and Optical Characterization of Platinum(II) Poly-yne Polymers Incorporating Substituted 1,4-Diethynylbenzene Derivatives and an Investigation of the Intermolecular Interactions in the Diethynylbenzene Molecular Precursors" *New J. Chem.* **2003**, *27*, 140-149.

(18) Mei, J.; Ogawa, K.; Kim, Y.-G.; Heston, N. C.; Arenas, D. J.; Nasrollahi, Z.; McCarley, T. D.; Tanner, D. B.; Reynolds, J. R.; Schanze, K. S. "Low-band-gap Platinum Acetylide Polymers as Active Materials for Organic Solar Cells" *Appl. Phys. Interfaces* **2009**, *1*, 150-161.

(19) Komorski, R. A. "Line Broadening in the ^{13}C NMR Spectra of Bulk Polymers Above T_g" *J.Poly. Sci. B* **1983**, *21*, 2551-2559.

(20) Roncali, J. "Synthetic Principles for Bandgap Control in Linear π-Conjugated Systems" *Chem. Rev.* **1997**, *97*, 173-206.

(21) Yassar, A.; Roncali, J.; Garnier, F. "Conductivity and Conjugation Length in Poly(3-methylthiophene) Thin Films" *Macromolecules* **1989**, *22*, 804-809.

(22) Barker, J. "An Electrochemical Investigation of the Doping Processes in Poly(thienylene vinylene)" *Synthetic Metals* **1989**, *32*, 43-50.

(23) Tourillon, G.; Garnier, F. "Effect of Dopant on the Physicochemical and Electrical Properties of Organic Conducting Polymers" *J. Phys. Chem.* **1983**, *87*, 2289-2292.

(24) Gasparro, F. P.; Kolodny, N. H. "NMR Determination of the Rotational Barrier in *N,N*-dimethylacetamide" *J. Chem. Educ.* **1977**, *54*, 258-261.

(25) Wolf, C. *Dynamic Stereochemistry of Chiral Compounds*; RSC Publishing: Cambridge, UK, 2008.

(26) Swager, T. M.; Gil, C. J.; Wrighton, M. S. "Fluorescence Studies of Poly(*p*-phenyleneethynylene)s: The Effect of Anthracene Substitution" *J. Phys. Chem.* **1995**, *99*, 4886-4893.

CHAPTER THREE

PLATINUM AND PALLADIUM METALLOPOLYMERS FEATURING A LIGHT-HARVESTING DIPHOSPHINE MONOMER

3.1 Novel Staircase Platinum-Acetylide Organic Conjugated Polymers

As discussed in Chapter 1, the first platinum-acetylide polymer was synthesized by Sonogashira and coworkers[1] in 1977. Interest in metal-containing organic polymers even dates back further, however. Prior to metal-acetylide polymers, the only organometallic polymers successfully isolated and characterized were metallocene-based; the first widely studied metallopolymer of this class was poly(ferrocene) (Figure 3.1).

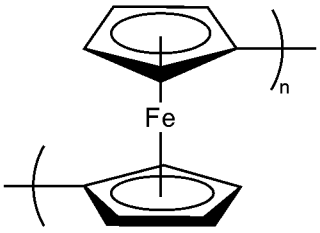

Figure 3.1. Structure the first widely studied and characterized metallopolymer, poly(ferrocene).

Poly(ferrocene) was first synthesized[2] via a radical polyrecombination mechanism using ferrocene and *tert*-butyl peroxide to afford the metallopolymer in low yields and very modest molecular weights. Initial investigations into the semiconducting behavior of poly(ferrocene) demonstrated poor conductivity values (10^{-7} to 10^{-9} S/cm); however, later studies unveiled that partially oxidized, more crystalline poly(ferrocene) has significantly improved conductivity (10^{-2} S/cm).[2] Thus, these results demonstrate that the nature of the transition metal, and its oxidation state, can have wide-reaching consequences on the conductivity of organometallic conducting polymers. While later investigations aimed at

optimizing the synthetic design of poly(ferrocene) and its functionalized analogues, shortly after work on poly(ferrocene) began, Sonogashira and coworkers reported the first successful platinum-acetylide synthesis. Researchers came to be enamored with elucidating the photophysical and conductivity consequences of incorporating a transition metal, such as platinum, into a highly-conjugated organic polymer, as the high conductivity of doped all-organic polymers was reported around this time.[3]

The platinum-acetylide polymer synthesized by Sonogashira and coworkers, however, was not characterized in terms of its photophysical properties or conductivity; instead, the focus was on demonstrating the successful synthesis and, albeit low, general molecular weight as determined by sedimentation equilibrium ($M_w \sim 11.9 - 12.2*10^4$). However, the general structure of a transition-metal containing poly-yne came to the forefront of poly(organometallic) syntheses and characterization. Simple platinum-acetylides of the structure first studied by Sonogashira and coworkers were found to have optical band gap energies ranging from 3.12 to 3.23 eV depending on the number of acetylene linkers between adjacent platinum atoms.[2]

Later investigations focused on metallopolymers that incorporate aryl groups within the polymer backbone to further enhance delocalization to effect desired conductivity and photoluminescence (Figure 3.2).

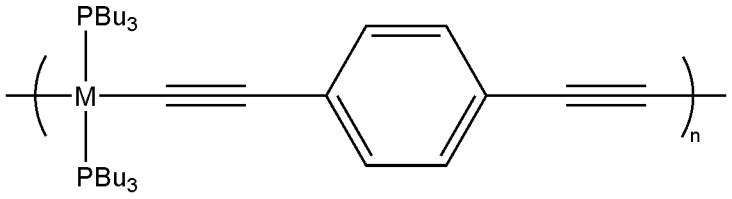

Figure 3.2. General structure for a metal-containing acetylide polymer incorporating phenyl groups.

A platinum-containing polymer of the structure depicted in Figure 3.2 was synthesized and compared to its monomers in terms of optical parameters.[4] This platinum based metallopolymer demonstrated a wavelength of maximum absorbance around 388 nm with a band gap energy of about 3.07 eV based on the onset of absorption. These band gaps of the polymer (**P1**) are significantly lower than those of the corresponding monomer (**M1**) (Figure 3.3).

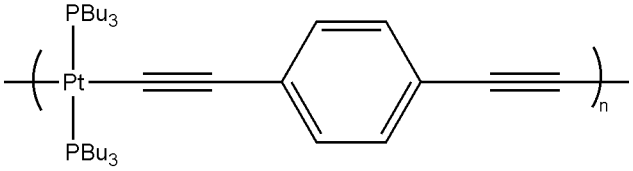

P1

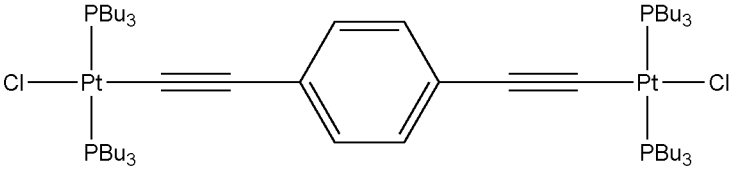

M1

Figure 3.3. Plantum-acetylide polymer and analogous monomer studied by Dray and coworkers.

Photoluminescence spectra for the polymer showed that it emits strongly at around 517 nm with a broad emission concomitant from 496 to 689 nm. The red-shifting

of photophysical properties of **P1** versus **M1** is attributed to the transition metal presence within the polymer backbone. Moreover, the authors explain that this change in the π-π* transition energy is demonstrative of π-metal mixing. This investigation also found that "doping" the polymer with iodine to oxidize the platinum to Pt(IV) caused an increase in the band gap energy by about 0.5 eV. In addition, photoluminescence spectra of **P1** demonstrated a near 15-fold enhancement of luminescence intensity upon cooling to 10 K. Conductivity measurements of the platinum poly-yne polymer revealed the material was a poor conductor. However, these preliminary photophysical results provided researchers with an impetus to functionalize and optimize the metal poly-yne structure to afford more conductive and uniquely emissive metallopolymers for material applications.

Not only were phenyl-containing platinum poly-ynes studied, but so were polymers of this general structure that incorporated anthracene and thiophene moieties within the polymer chain. Inclusion of anthracene into the poly-yne lowered the band gap energy to 2.48 eV while thiophene incorporation afforded polymers with band gap energy of 2.70 eV (Figure 3.4).[5] These results demonstrate that diversification of the polymer backbone can serve to further reduce the band gap energy of platinum poly-ynes as well as red-shift photophysical characteristics of the material.

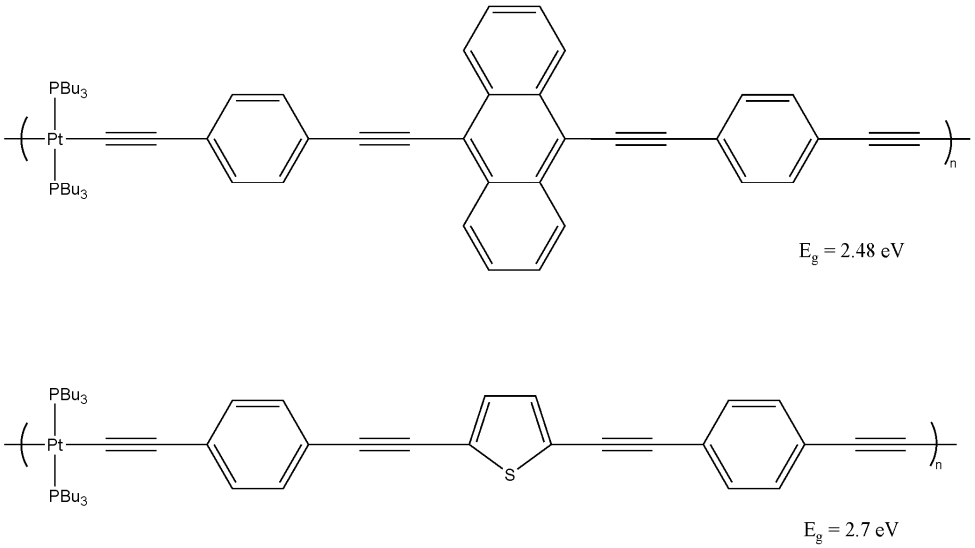

Figure 3.4. Anthracene- and thiophene-containing platinum poly-ynes with associated band gap energies as estimated by the onset of absorption.

Another synthetic method used to enhance the photophysical and conductivity properties of platinum poly-ynes is to use already functionalized dialkynes in the polymerization process. Most often employed is a dialkoxy dialkyne that will become the aryl spacer in the polymeric backbone. As discussed previously, the band gap energy of poly(2,5-dimethoxyphenylene vinylene) was found to be 0.4 eV lower than that of poly(*p*-phenylene vinylene). One motivating feature was therefore to gauge whether a similar red-shifting of the absorbance and photoluminescence could be effected in platinum poly-ynes. Many investigations have shown that alkoxy substitution on the phenyl moieties enhances solubility and processibility of these polymers for materials-based applications.

As detailed extensively in Chapter 1, polymers that contain heavy metal atoms promise unique optical properties with exceptionally efficient phosphorescence as a direct result of enhanced spin-orbit coupling. The more accessible triplet state in

platinum-containing poly-ynes allows for phosphorescence to become a more competitive pathway for radiative emission. As a general rule, the triplet emission yield (Φ_P) for poly(*p*-phenylene ethynylene) polymers is on the order of 0.1 or less.[6] Platinum-acetylide polymers of the structure depicted in Figure 3.5 showed significant enhancements of triplet state emission efficiency over non-metallated OCPs.

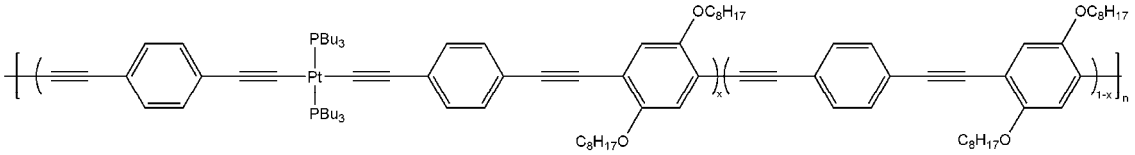

P1: x=1.00
P2: x=0.5
P3: x=0.25

Figure 3.5. Platinum-acetylide polymers with varying platinum content.

The authors find that the triplet yield depends on the platinum content within the polymeric backbone. More specifically, as more platinum-containing monomers are present within the chain (**P1** versus **P3**), the intersystem crossing efficiency increases thereby making triplet state radiative emission more competitive with fluorescence rates. Therefore, as platinum-loading of the poly(*p*-phenylene acetylene) increases, there is a marked decrease in fluorescence quantum yield accompanied by an increase in intersystem crossing rates (thereby leading to phosphorescent emissive decay). In addition, the photoluminescence spectra of **P1**-**P3** show qualitative evidence of the effect of the platinum content on radiative pathways. In **P1**, there are two strong emission maxima corresponding to fluorescence (450 nm) and phosphorescence (611 nm); with **P2**, there is a strong fluorescence emission (447 nm) accompanied by a small phosphorescence peak (612 nm). Finally, in **P3** (least platinum content), the

photoluminescence spectrum shows only a fluorescence emission (451 nm) with phosphorescence (628 nm) only appearing when the sample is cooled to 80 K. These results demonstrate that the platinum metal significantly enhances triplet state emission by making intersystem crossing more efficient (direct result of spin-orbit coupling). Moreover, the platinum content of the aryl-containing poly-ynes proves to be important for manipulating photoluminescent behavior and efficiency.

The bulk of the current work has focused on synthesizing polymers with the heavy metal atom, platinum, being *trans*-spanned by an *m*-terphenylphosphine scaffold. The aforementioned polymers with terphenylphosphine scaffolds contain repeating 1,4-diethynyl-2,5-dihexyloxybenzene monomeric units. It was our aim to increase the chromophore content of each monomeric unit to optimize the light-harvesting ability of the polymer. Thus, the following work focuses on generating polymers with linear phosphines that serve both as highly conjugated monomeric units and also a means to connect platinum nuclei (Scheme 3.1).

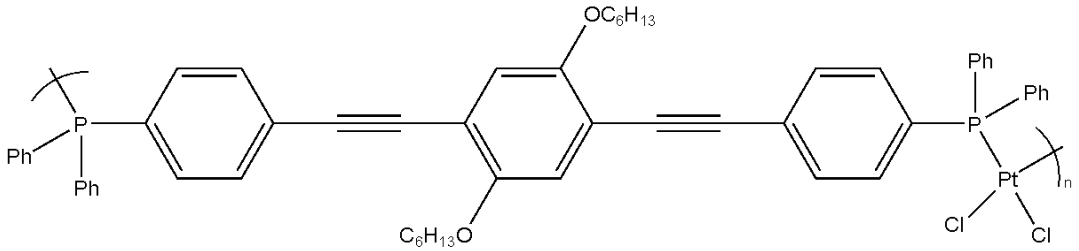

Scheme 3.1. Proposed staircase coordination polymer to be made with highly conjugated linear phosphines.

3.2 Synthesis of Linear Phosphine Oxide Analog to Desired Phosphine Fluorophore

As the phosphine used in the polymerization with platinum serves as the conjugated repeating monomeric unit, it is necessary to synthesize a linear phosphine that already has an appreciable amount of conjugation within its backbone (Scheme 3.2).

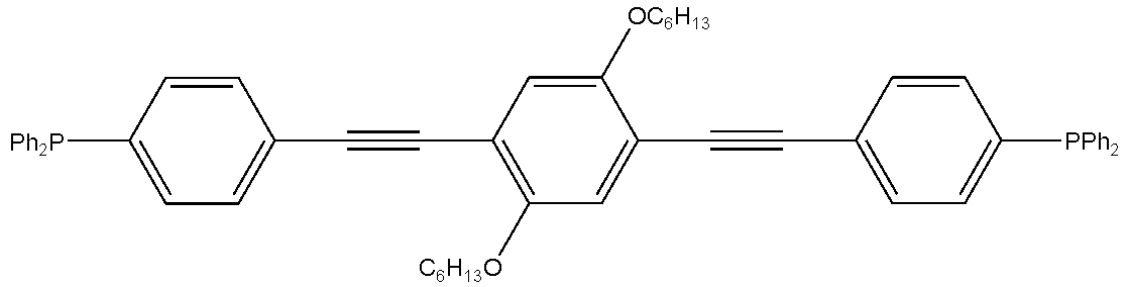

Scheme 3.2. Desired synthetic target: a linear, highly-conjugated diphosphine which will polymerize readily with platinum to afford the proposed staircase platinum polymer.

However, creating the above phosphine from the brominated analog, as outlined in Scheme 3.3, is not a viable synthetic route.

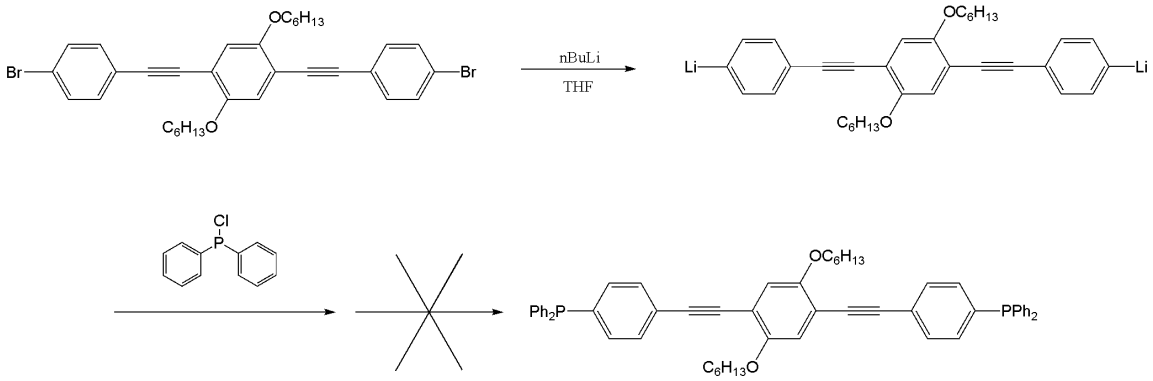

Scheme 3.3. Lithiation of dibrominated analog of desired phosphine that likely would not proceed.

It is very difficult to synthesize and purify a highly conjugated diphosphine using *n*-butyllithium to lithiate both ends of the molecule.[7] This is because a dianion is formed upon lithiation that can delocalize over the entire molecule. As a result, when the chlorodiphenylphosphine is added to make the desired phopshine it can be added to any of the carbon atoms within the conjugation path. Thus, the final product will be a mixture of compounds with the diphenylphosphine moiety at various places throughout the molecule instead of just at the desired terminal positions. Moreover, owing to the air-sensitive and water-sensitive nature of phosphines, it is exceptionally difficult to isolate the desired phosphine away from the phosphine side products. Instead, by utilizing coupling procedures, the phosphine oxide analog to the linear phosphine shown in Scheme 3.2 can be synthesized and purified in ambient conditions (Scheme 3.4). After the linear phosphine oxide is isolated and purified, it can then be reduced to the analogous phosphine which is used in the polymerization to yield the staircase platinum polymer.

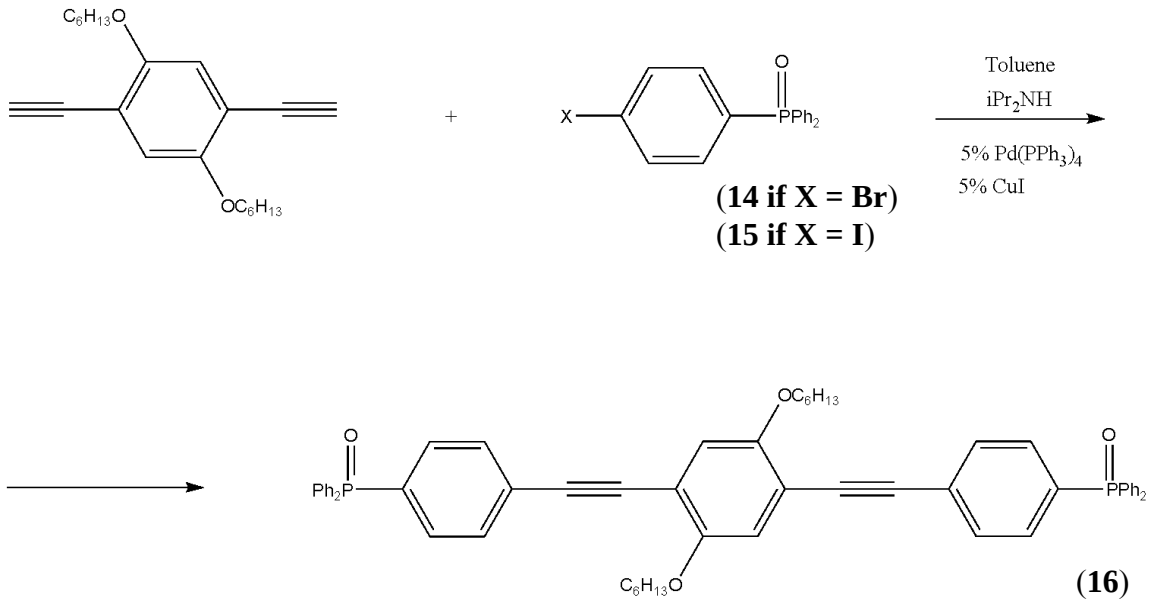

Scheme 3.4. Synthetic route to the phosphine oxide (**16**) analog of the desired linear phosphine using a Sonogashira coupling of an aryl halide (X = Br or I) to a terminal dialkyne.

Results and Discussion

While the synthesis of the light-harvesting phosphine oxide **16** proceeded as anticipated, the purification of it proves to be difficult. Performing column chromatography on the crude product is not feasible as the phosphine oxide adsorbs to the silica tightly enough that mobility is significantly impeded or even halted. Not only does this interfere with separation of product from impurities, it also impedes the ability to isolate the phosphine from the silica once impurities are removed. Moreover, as this compound is thus far unknown to the literature, it is necessary to obtain a pure sample of phosphine oxide **16** for more sophisticated characterization techniques such as X-ray crystallography.

The light-harvesting phosphine oxide (**16**) is a dark red to orange solid which absorbs strongly at 381 nm. Photoluminescence data of **16** shows a strong emission at 431 nm; most likely this emission is fluorescence because it is relatively high in energy. These investigations into the optical properties of the linear phosphine oxide monomer show that **16** absorbs strongly in the visible region which is expected as it is a highly conjugated molecule. Moreover, as the photoluminescence emission spectrum shows, compound **16** is highly luminescent. Therefore, this light-harvesting phosphine oxide is an excellent candidate for incorporation into a platinum-acetylide type polymer since it is already an efficient fluorophore.

3.3 Synthesis of a Fluorene-Based Light-Harvesting Phosphine Oxide

As the synthesis of phosphine oxide **16** provided appreciable yields and acceptable purity for further study, it was of interest to synthesize another phosphine oxide with an alternative chromophore. Phosphine oxide **18** was thus synthesized via a Suzuki coupling reaction between a fluorene-derived boronic ester (**17**) and the 4-bromophenyldiphenylphosphine oxide **14** (Scheme 3.5).

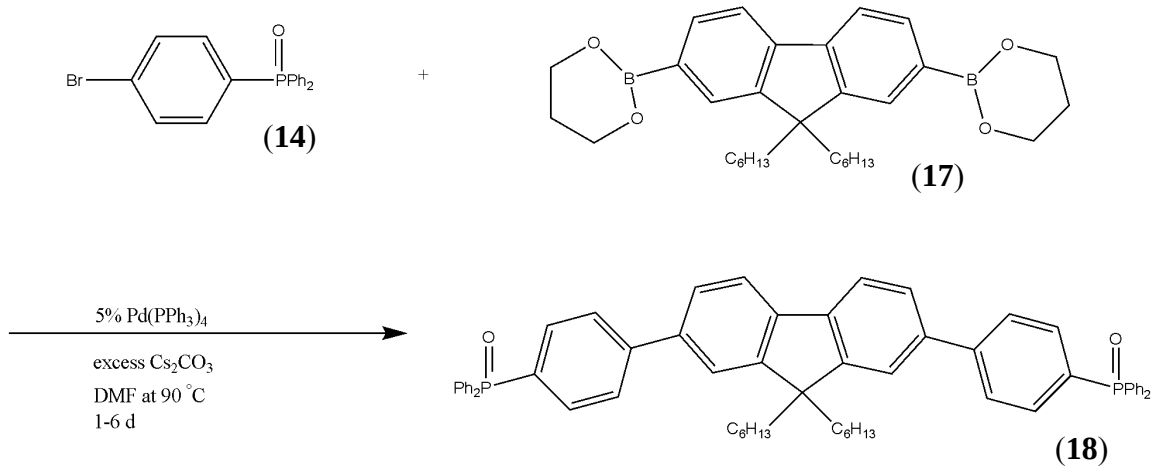

Scheme 3.5. Synthetic scheme for fluorene-based phosphine oxide **18**.

Results and Discussion

While the Suzuki coupling mechanism to yield phosphine oxide **17** appears to be operating adequately, purification of the crude product proves difficult. At this point in the investigation, it seems as though some *N*,*N*-dimethylformamide remains with the crude product after workup and it may be interfering with recrystallization. All purification attempts are referenced to a spectrum of pure phosphine oxide **17** synthesized by R. Gilliard (Fig A-51 and A-52); Gilliard's purified **17** is a colorless flaky crystalline solid. Alumina column chromatography affords phosphine oxide **17** with excellent purity but with very low yields. The same is the case for recrystallization attempts especially with pentane diffusing into a concentrated solution of **17** in tetrahydrofuran.

3.4 Synthesis of Light-Harvesting Phosphine Oxide (16) via 4-iodophenyldiphenylphosphine Oxide (15)

It should be detailed here that difficulties with the fluorene-based phosphine oxide synthesis prompted our investigation into using 4-iodophenyldiphenylphosphine oxide (**15**) in the coupling chemistry to afford the desired phosphine oxide. Iodoaryls are much better coupling partners in Pd-catalyzed carbon-carbon bond forming reactions than are aryl bromides; therefore, it was proposed that 4-iodophenyldiphenylphosphine oxide would give better yields under milder reaction conditions.

The Sonagashira coupling to afford phosphine oxide **16** (Scheme 3.2) first required preparation of phosphine oxide **15**. Surprisingly, **15** was not a known compound at the start of our study. The synthetic scheme to prepare **15** is the same as for preparing **14** (Scheme 3.6).

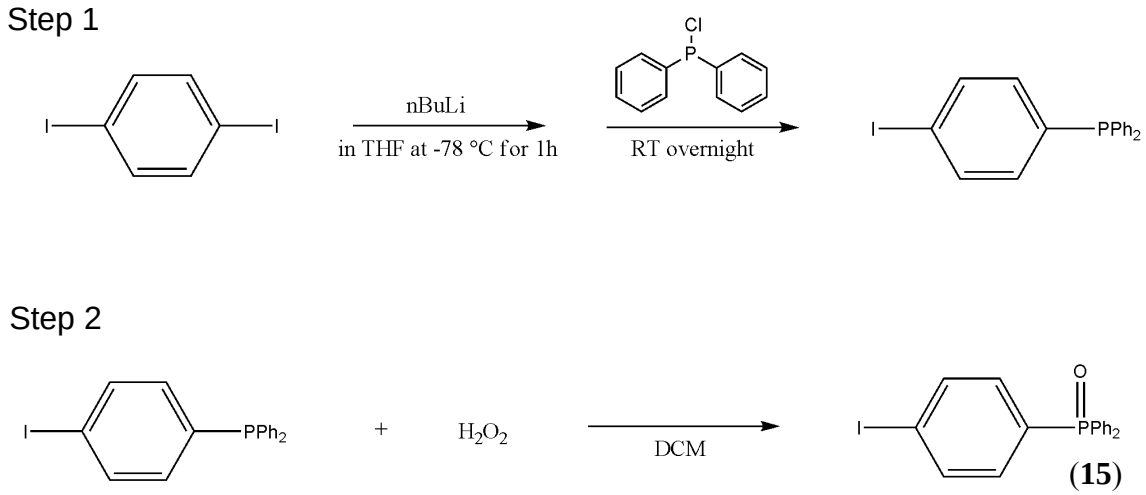

Scheme 3.6. Two-step synthesis of 4-iodophenyldiphenylphosphine oxide **15**.

Results and Discussion

The synthesis of 4-iodophenyldiphenylphosphine oxide **15** was easy and efficient and its purification of **15** proceeds by simple precipitation into pentane from diethyl ether. An analytically pure sample of **15** was obtained by B. Morgan, affording colorless crystals. The results of a single crystal X-ray diffraction study on these crystals are provided in Figure 3.6 and the ORTEP refinement details are given in Table 3.1.

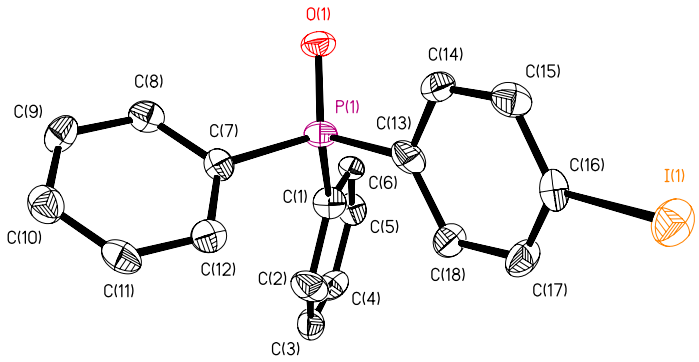

Figure 3.6. 50 % ORTEP diagram of **15**. Hydrogen atoms were omitted for clarity.

Empirical formula	$C_{18}H_{14}IOP$
Formula weight (g/mol)	404.16
Temperature (K)	153 (2)
Wavelength (Å)	0.71073
Crystal system	Monoclinic
Space group	$P2_{1/n}$
Unit cell dimensions	
a (Å)	6.1752(12)
b (Å)	15.139(3)
c (Å)	16.740(3)
α (deg)	90.00
β (deg)	94.39(3)
γ (deg)	90.00
Volume (Å3)	1560.4(5)
Z	4
Calculated density (Mg/m3)	1.720
Absorption coefficient (mm-1)	2.150
F(000)	792
Crystal size (mm)	0.12 × 0.07 × 0.05
Crystal color and shape	colourless chip
Θ range for data collection (deg)	2.44 – 25.10
Limiting indices	-7 < h < 7
	-17 < k < 18
	-13 < l < 19
Reflections collected	11282
Independent reflections	2777
Completeness to *Θ*	25.10 (99.9 %)
Max. transmission	0.9001
Min. transmission	0.7824
Refinement method	Full-matrix least-squares on *F*2
Data / restraints / parameters	2777/0/190
Goodness of fit on *F*2	1.059
Final R indices ($I > 2\sigma(I)$)	
R1	0.0646
wR2	0.1367
R indices (all data)	
R1	0.1053
wR2	0.1723

Table 3.1. Refinement details for the crystal structure of **15**.

Once isolated, **15** can be used for generating the light-harvesting phosphine oxide **16** in the same manner as described above (Scheme 3.4). The synthesis of linear phosphine oxide **16** proceeds under milder reaction conditions when using the iodo analog of the haloaryl diphenylphosphine oxide. Moreover, the product is pure by ^{31}P NMR with no purification necessary other than the described workup of the crude

reaction mixture. These results are not surprising as iodide is a better leaving group and so would require little to no heating for aryl halide coupling reactions. Future syntheses of phosphine oxides using the Sonogashira (and Suzuki) coupling procedures will utilize the 4-iodophenyldiphenylphosphine oxide **15**.

3.5 Reduction of Linear Phosphine Oxide 16 with Trichlorosilane

Reduction of the linear phosphine oxide **16** with trichlorosilane[7] will yield the analogous phosphine **18** which is a reactive species capable of undergoing ligand exchange with a platinum complex (Scheme 3.7).

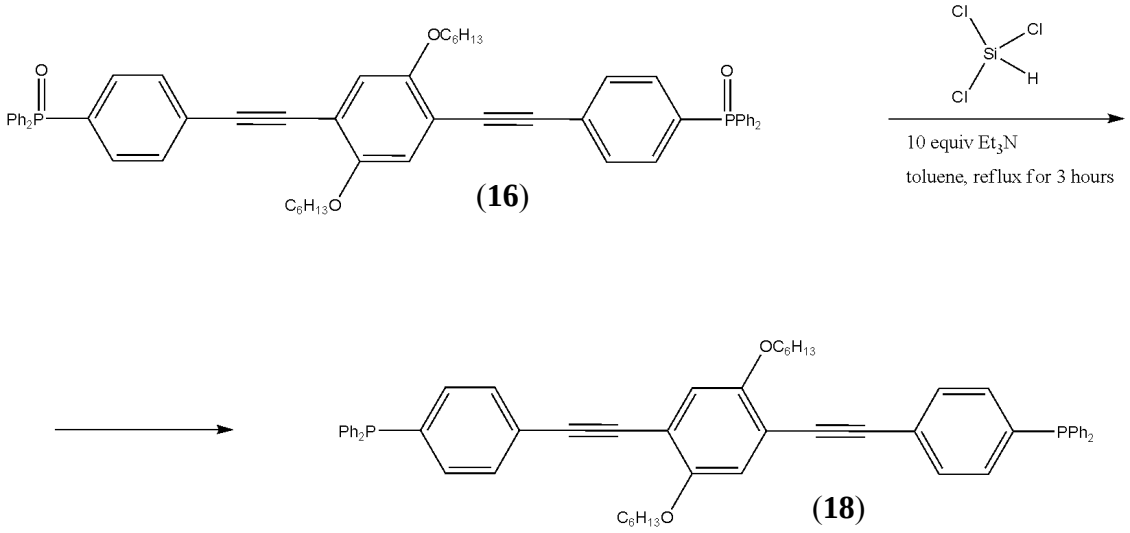

Scheme 3.7. Reduction of linear phosphine oxide **16** to give desired phosphine analog **18**.

Results and Discussion

The crude mixture resulting from reduction of **16** with trichlorosilane is a viscous red oil that often contains other phosphorous-based impurities. In early investigations, it was found that precipitation into acetonitrile from dichloromethane yields phosphine **18** in pure enough form to proceed with polymerization. Though, in some cases, this process was not sufficient to purify phosphine **18**. Since the material is air-sensitive, any

purification must be performed in the drybox or using standard Schlenk techniques. Preparatory thin-layer chromatography (TLC) on glass-backed silica plates using a 30% diethyl ether in hexane (v/v) yielded a phosphine **18** with improved purity. However, owing to the difficulty in performing such air-free purifications, later investigations focused on attaining exceptional purity of the linear phosphine oxide **16** before the reduction step.

So as to be able to compare with subsequent platinum-containing polymers, the linear phosphine **18** monomer was examined in terms of its photophysical parameters. It was found that the absorption of **18** (λ_{max} = 376 nm) is similar to that of phosphine oxide **16** (λ_{max} = 381 nm). Photoluminescence data (under air-free conditions) demonstrates an emission maximum of 426 nm which is slightly blue-shifted compared to the phosphine oxide **16** (λ_{em} = 432 nm). Once the linear phosphine **18** had been isolated, it was then reacted in a 1:1 ratio with dichlorobis(benzonitrile)platinum to yield a platinum polymer as depicted in Scheme 3.8 (*vide infra*).

3.6 Polymerization of Linear Phosphine with Platinum- and Palladium-Containing Metal Complexes

Ligand exchange between dichlorobis(benzonitrile)platinum (or palladium) and linear phosphine **18** should afford the desired neutral coordination metallopolymer (Scheme 3.8).

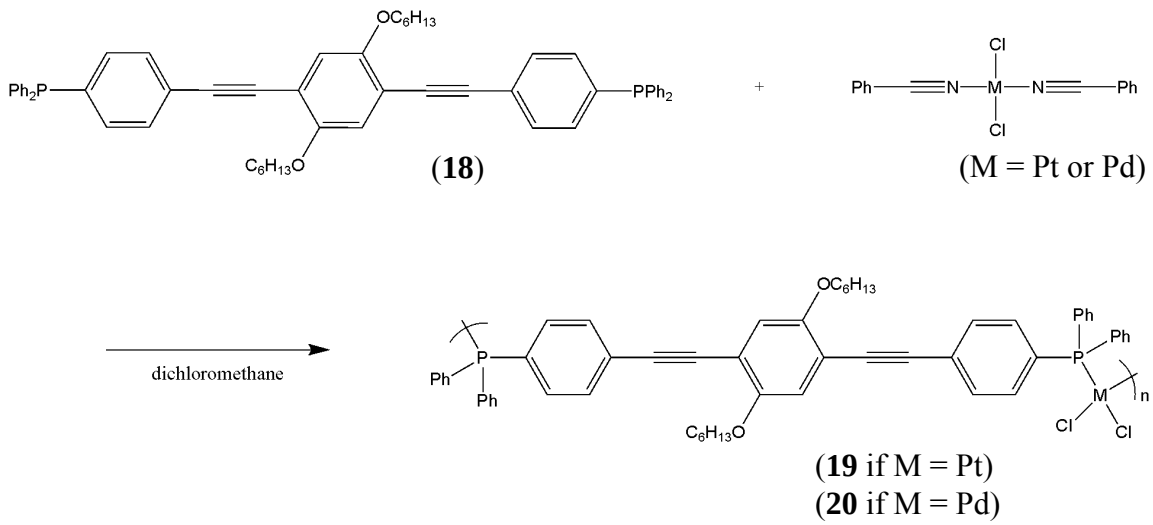

Scheme 3.8. General polymerization scheme to afford transition metal staircase polymer of interest.

The polymerization was also performed with dichlorobis(benzonitrile)palladium to examine the effect of the transition metal within the polymer on its physical and optical properties. It was believed that successful polymerization would afford a highly fluorescent polymer that would adopt a staircase structure as shown above. It should be noted that the polymer possesses single bonds with no impediments to rotation so there can be coiling within the polymer backbone.

Results and Discussion

Initial polymerization attempts to afford polymer **19** and **20** were performed with an 1.1% excess of phosphine **16**. The appearance of ^{195}Pt satellites in the ^{31}P NMR spectrum of **19** indicate phosphorous-platinum connectivity which is promising evidence that polymerization was successful as platinum atoms are connected by the linear phosphine **18** (Figure 3.7).

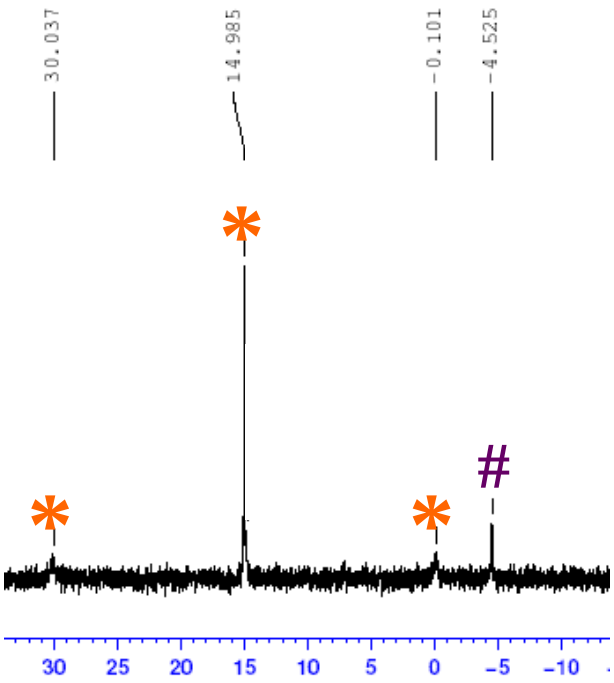

Figure 3.7. Phosphorous-31 NMR spectrum of platinum-based metallopolymer **19**; the internal phosphorous atoms (not end-groups) are denoted by asterisks while the end-group phosphorous atoms are marked with a pound symbol.

Phosphorous-31 NMR spectral data for both polymers **19** and **20** reveal interesting information about the coordination geometry as well as the molecular weights of the metallopolymers. Especially important is the fact that the phosphorous-platinum coupling constant ($^1J_{Pt\text{-}P}$ = 3657 Hz) is suggestive of *cis* coordination about the platinum atom as demonstrated by being a similar order of magnitude to that seen with *cis*-[$PtCl_2(PPh_3)_2$] ($^1J_{Pt\text{-}P}$ = 3673 Hz).[8] Moreover, the chemical shift of polymer **19** (δ ^{31}P = 15.0 ppm) is also comparable to that of *cis*-[$PtCl_2(PPh_3)_2$] (15.3 ppm)[8] further confirming that the phosphine coordination to the platinum atom is in a *cis* fashion after

polymerization. Similar analysis can be performed for the palladium polymer **20** utilizing the ^{31}P NMR spectral data (Figure 3.8).

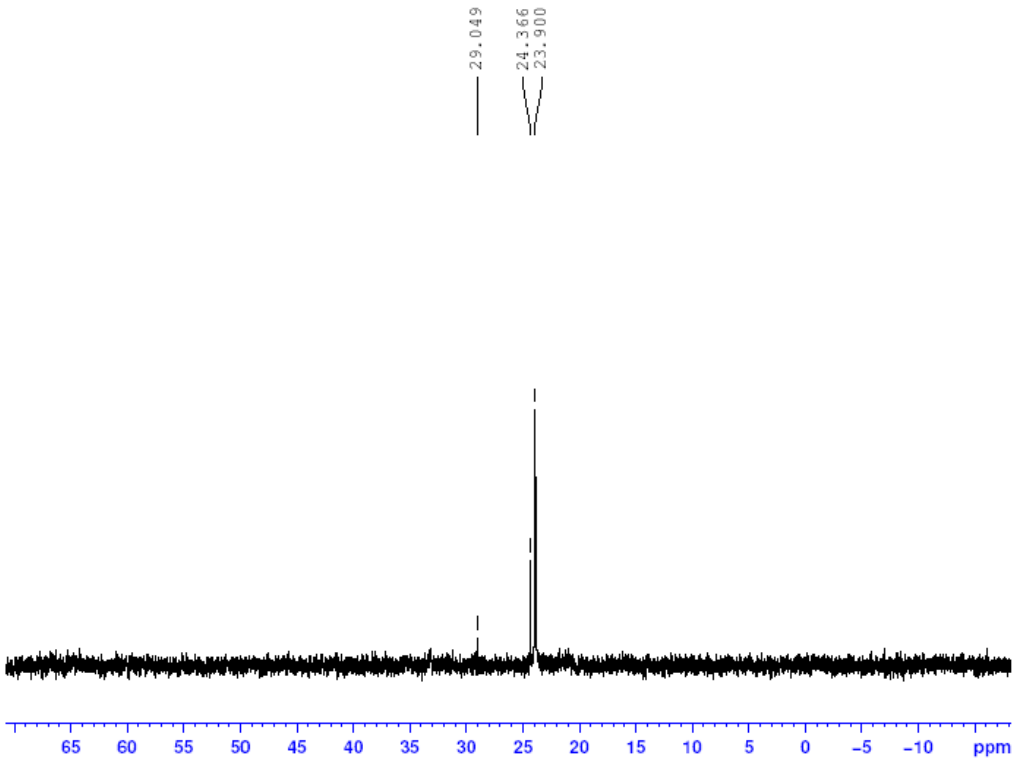

Figure 3.8. Phosphorous-31 NMR of palladium metallopolymer **20**.

Unlike platinum, palladium is an NMR-silent nucleus, so we do not have the benefit of a coupling constant to help elucidate whether *cis* or *trans* coordination is operative in **20**. Moreover, the chemical shift for **20** (δ ^{31}P = 23.9 ppm) is similar to that seen with both *trans*-[$PdCl_2(PPh_3)_2$] (24.2 ppm) and *cis*-[$PdCl_2(PPh_3)_2$] (22.4 ppm).[9] Therefore, it is uncertain whether the phosphine coordinates to the palladium in *cis* or *trans* manner. However, the use of identical precursor complexes and the relation of platinum and palladium within group 10 suggest that polymer **20** is also present in a *cis* configuration.

Not only can ^{31}P NMR data yield information as to the mode of coordination, but it also can be used to estimate the molecular weight of the metallopolymers. While ^{1}H NMR spectral data is conventionally used for molecular weight determinations, ^{31}P NMR integrations have been used[10] to estimate the degree of polymerization based on end-group versus internal phosphorous atom chemical shifts. For the case of the platinum polymer **19**, the peak at –4.5 ppm represents the two end-group phosphorous atoms while the peak at 15 ppm (with satellites included) corresponds to phosphorous atoms within the polymeric backbone (Figure 3.7). Integration of these peaks relative to each other reveals a degree of polymerization (n) of about 13 for the platinum based metallopolymer **19**. This value suggests a molecular weight (M_n) of about 15,000 g/mol for **19**. Similar treatment of the ^{31}P NMR spectrum for **20** yields a degree of polymerization (n) of about 14 (internal phosphorous atoms at 24.0 ppm compared to oxidized end-groups at 29.0 ppm). As a result, we can estimate the molecular weight of **20** to be around 17,000 g/mol.

The polymers were then analyzed by UV-vis and fluorescence spectroscopy to discern the differences in photophysical parameters between the phosphine monomer polymers **19** and **20**. Polymer **19** has a strong absorbance at 379 nm and a photoluminescence emission at around 435 nm. The phosphine **18** monomer absorbs strongly at 376 nm and emits at 426 nm. Thus, polymer **19** is slightly red-shifted in absorbance compared to the phosphine monomer and moderately red-shifted in terms of photoluminescence. This could be due to a push-pull type scenario generated by the presence of both the electron-donating hexyloxy groups and the electron-withdrawing platinum-bound phosphorous atoms. This, in turn, would lead to enhanced planarity and a

greater contribution of the quinoidal resonance structure to the molecule. As a result, red-shifting for **19** would be expected as compared to the phosphine monomer.

The optical properties of polymer **20** were also examined to determine if and how the metal identity affects the absorption, emission and band gap energies of the metallopolymer. Palladium-based polymer **20** has an absorption maximum at 378 nm and a very weak photoluminescence maximum at 431 nm. The palladium polymer **20** appears to be only slightly blue-shifted as compared to the platinum polymer **19** when observing wavelength of maximum absorbance; likely this difference is negligible. However, it appears that the palladium does effect changes in the photoluminescence activity of the polymer; that is, the palladium polymer **20** is much less photoluminescent than its platinum analog **19**. Comparison of the photophysical parameters of the phosphine **18** with the polymers demonstrates that photophysical parameters are generally red-shifted after polymerization (Table 3.2). Air-free photoluminescence lifetimes, as measured by time correlated single photon counting (TCSPC), demonstrate that the lifetime decreases in the polymer form. The lifetime could not be measure for the palladium-based polymer **20** as its photoluminescence was too weak to be amenable to TCSPC.

	λ_{max} (nm)	log ε	λ_{emit} (nm)	Φ	τ	E_g (eV)
16	381	4.62	432	0.620±0.002	1.7 ns	2.82
18	376	4.29	426	0.320±0.035	1.25 ns	2.85
P19 (Pt)	384	3.59	434	0.09±0.01	107 ps	2.83
P20 (Pd)	378	3.59	431	0.021±0.002	NA	2.80

Table 3.2. Photophysical parameters of interest for light-harvesting phosphine oxide **16**, light-harvesting phosphine **18**, platinum metallopolymer **19** and palladium metallopolymer **20**. Band gap energies are estimated from the onset of absorption.

The decreased photoluminescence lifetime of **19** versus **18** could be indicative of a number of photophysical events, such as heavy-atom quenching. However, it is clear that **19** undergoes relatively efficient photoluminescence (either from the singlet or triplet excited state) and this process is fast. Phosphorescence generally has longer lifetimes (often on the order of μs) than fluorescence so a lifetime of ~107 ps for polymer **19** indicates that fluorescence is the preferred pathway for radiative emission. This is not surprising because the platinum atom disrupts the conjugation of the molecule and thus photoluminescence of the polymer will be similar to that of the monomer **18**. Comparing the quantum efficiency (Φ) for platinum-polymer **19** compared to that of phosphine monomer **18** indicates that the polymeric species is much less efficient at photoluminescence. Moreover, it is important to note that the platinum-based polymer **19** is about four times more efficient in terms of photoluminescence as compared to the palladium-based polymer **20**.

Normalization of the photophysical data obtained for the above four species allows for convenient visual comparison of absorbance and emission maximum wavelengths. According to the absorbance data (Figure 3.9), the monomer phosphine **18** and both polymeric species (**18** and **19**) demonstrate very similar absorption properties.

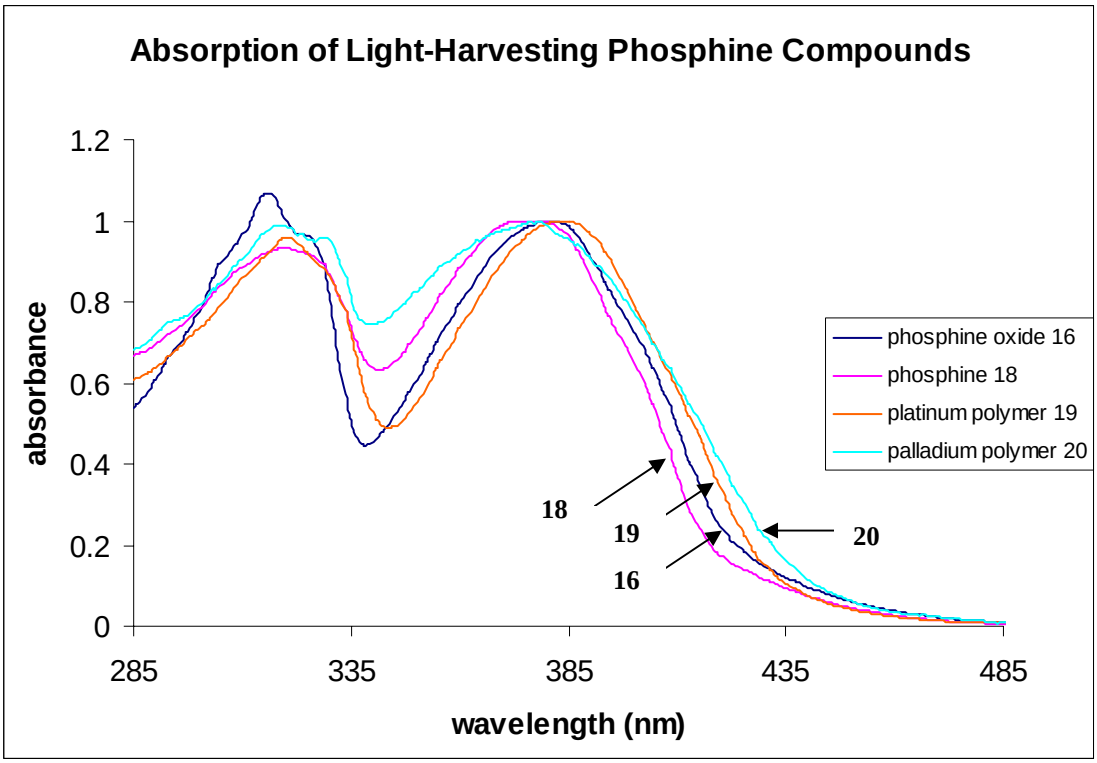

Figure 3.9. Normalized absorbance data for phosphine monomers and polymers.

The onset of absorption also allows for an estimation of the band gap energies for the polymeric species and analogous monomers (Table 3.2). While the band gap energy of the phosphine oxide is not necessarily important to the discussion of the polymeric materials, the phosphine **18** has an optical gap of around 2.85 eV. Polymerization with platinum to afford **19** lowers the band gap to 2.83 eV while the palladium-based polymer **20** has a band gap of around 2.80 eV. Thus, the difference in band gap energies of the metallopolymers compared to the phosphine monomer is very small, even negligible. The poly(*p*-phenylene vinylene) (PPV) polymer widely used in photovoltaics and light-emitting devices has a band gap energy of 2.5 eV which serves as a benchmark value to optimize when designing polymers for similar devices.[11] That the polymers synthesized

have band gap energies on the order of that seen with widely versatile PPV suggest they may be amenable to many modern technological devices requiring semiconducting polymeric materials. More sophisticated electrochemical measurements are necessary to make definitive assessments of the HOMO and LUMO energy level to fully elucidate the semiconducting abilities of polymers **19** and **20**.

The same data treatment can be used to generate a normalized plot of the photoluminescence data for the two phopshine monomers and platinum- and palladium-based polymers (Figure 3.10).

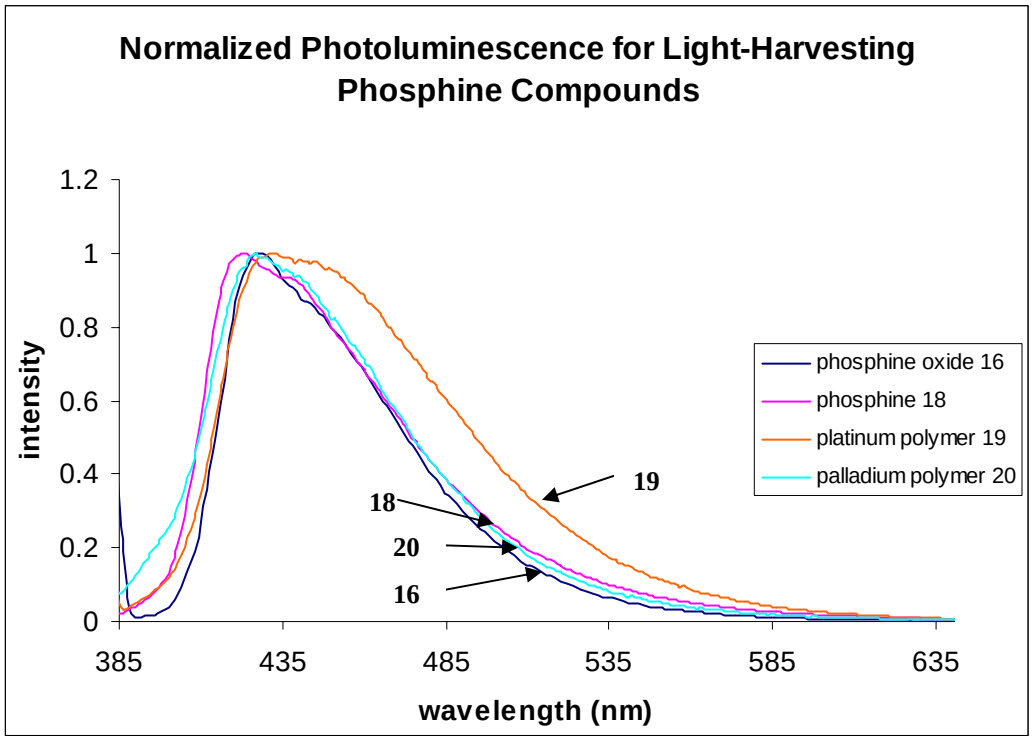

Figure 3.10. Normalized photoluminescence data for phosphine oxide **16**, phosphine **18**, platinum-based polymer **19** and palladium-based polymer **20**.

The photoluminescence maxima for the phosphine oxide, phosphine, platinum- and palladium-based polymers all appear at roughly the same wavelength (~430 nm).

However, the platinum-based polymer **19** shows a degree of broadening in the emission maximum which can be indicative of slower radiative decay than the other three species. Certainly the palladium-based polymer **20** had the lowest photoluminescence quantum yield which may imply that there are enhanced nonradiative recombination sites in the palladium polymer that are not present in the platinum polymer or phosphine-based monomers. However, it is possible that the palladium polymer **20** is more suited to photovoltaic devices because it may be an efficient semiconductor but a poor source of photoluminescence. Thus, based on these photophysical studies, it seems that the palladium-derived metallopolymer is not a suitable material for light-emitting devices but that the platinum-acetylide polymer synthesized here shows promise for such material applications.

Synthesis of polymer **19** was reattempted using a 1:1 ratio of phosphine **18** to platinum-material to see the effects of equimolar amounts of starting reagents. This procedure instantly produced a yellow orange viscous gel that was then dried *in vacuo* to afford a light orange glassy solid that was polymer **19b**. After numerous attempts, it was found that the afforded orange yellow solid was insoluble in all practical solvents. However, NMR samples consisting of polymer **19b** in chloroform-d_1, benzene-d_6 and DMSO-d_6 were heated to 65 °C in hopes of redissolving the polymer, and allowing slow gel formation for analysis by NMR spectroscopy. Even after 72 h of heating at this temperature, no solvation or regelling of polymer **19b** was noticeable for any of the solvents (Figure 3.11).

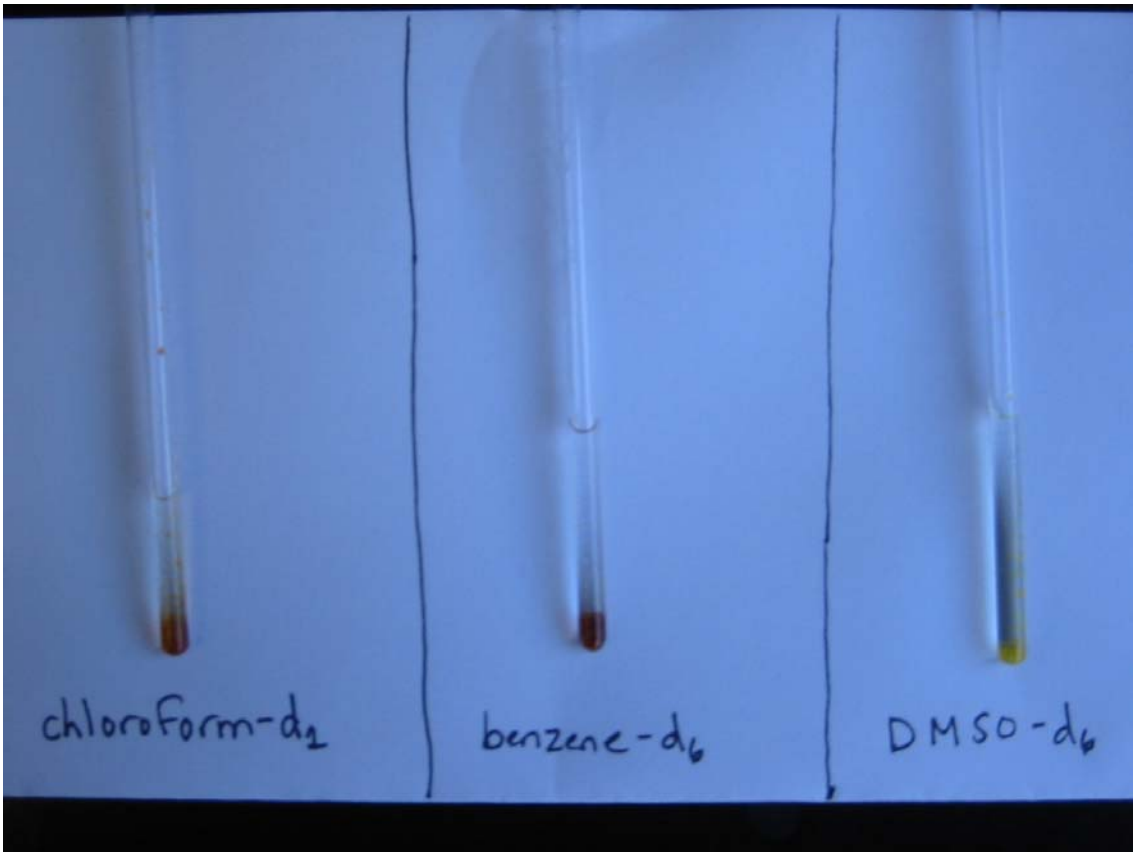

Figure 3.11. Depiction of the NMR samples of polymer **19b** after heating to 65 °C for 3 days showing no change in the solubility of the polymer.

Owing to the inability to analyze **19b**, the polymerization was performed again in an NMR tube as the reaction vessel with hopes of examining the resultant polymer gel. However, this time a 5% excess of phosphine **18** was used in order to shorten the polymer and intentionally make it a more soluble platinum-based polymer **19c**. While no ^{195}Pt satellites were observable after polymerization, the ^{31}P NMR shows a single broad resonance in the spectrum of polymer **19b** as made with excess phosphine. As it appeared that excess phopshine improved solubility of the polymer **19**, another polymerization was attempted with added trimethylphosphine meant to serve as end-capping groups, thus

further enhancing solubility by decreasing molecular weight. This reaction yielded a product medium that was not a gel as had been seen before with the polymerization attempts.

The ^{31}P NMR spectrum of the platinum-based polymer **19d** (made with excess phosphine or trimethylphosphine for end-group purposes) showed a very broad resonance consistent with that seen in the polymerization to yield **19c**; more importantly, addition of excess trimethylphosphine eventually yielded ^{31}P resonances that were consistent with the end-group phosphine moieties. However, the presence of oxidized species made it difficult to further analyze and characterize this polymer **19d**. Presumably, the increase in oxidized material was a result of the much greater sensitivity of trimethylphosphine to oxidation versus **18**. Yet the fact that excess phosphine yields more soluble (and thus processable) platinum-acetylide polymers is an especially important result of these initial synthetic attempts because it demonstrates the exchangeability of phosphines in this polymer. Such reversible coordination could be beneficial because this would allow **19** to act as a self-healing polymer following externally applied stress.

While an equimolar ratio of phosphine **18** to dichlorobis(benzonitrile)platinum affords a highly fluorescent gel that is likely polymer **19**, its insolubility presents problems as to characterization and purification. However, later investigations showed that an excess of phosphine **18** in the reaction conditions yields a more soluble polymer that is analyzable by standard NMR techniques although longer acquisition times are required. Moreover, providing the reaction medium with added trimethylphosphine to undergo phosphine exchange produces a polymer **19** that is even more amenable to solvation.

3.7 Conclusions

The above studies demonstrate that a highly conjugated light-harvesting phosphine fluorophore can be used as a repeating monomer unit in a platinum-acetylide type organic polymer. These polymers, based on the geometry about the phosphine moiety in the backbone, have distinct kinks in their structure owing to the steric bulk of the phenyl group on the phosphorous atom and to the *cis* coordination that is suggested by the ^{31}P NMR spectral parameters. However, as noted before, because there is free rotation in the bonds of the polymer backbone, these polymers may adopt a variety of conformations such as helices or random coils. They are therefore not exceptionally rigid-type polymers and will likely suffer from more excited state energy loss to bond vibrations and rotations than is the case for the *m*-terphenylphosphine scaffolded metallopolymers discussed in Chapter 2.

Thus far it appears that the presence of the platinum atom in the polymer backbone slightly red-shifts the absorption and emission wavelengths by extending the conjugation. Moreover, both the platinum- and palladium-based polymers are materials with band gap energies on the order of the widely used LED- and photovoltaic-targeted PPV. Cyclic voltammetry is necessary to definitively address the conductivity of polymers **19** and **20** to discern the level of the HOMO and LUMO (along with band gap energy verification). Based on the onset of absorption, however, it appears that polymerization of phosphine **18** with palladium affords a more conductive material but with very poor photoluminescence intensity. Conversely, the platinum-derived polymer **19** has a slightly larger band gap energy but is exceptionally photoluminescent. Based on these preliminary results, it seems that the polymer **19** is a better candidate for light-

emitting devices while polymer **20** may find particular utility in photovoltaic or other semiconducting materials that do not require photoluminescence.

Current studies are aimed at exchanging the chloride ligands present on the platinum atoms in **19** with various chromophores, notably acetylides such as those discussed in Chapter 1. Further addition of a chromophore to the platinum atom in place of the chloride ligands can increase the luminescent and light-harvesting properties of polymer **19** and perhaps even enhance its solubility depending on the chromophore chosen. Furthermore, this will provide a material with a heavy platinum atom embedded within the luminophore, allowing for efficient phosphorescence (see Chapter 1 for detailed discussion). There will also be an opportunity to observe processes that transfer excited state energy to the metal-appended fluorophore or vice versa.

3.8 Attempts to Synthesize Platinum-Containing Poly(*p*-phenylene vinylene) Polymer

Poly(*p*-phenylene) (PPP) is the predecessor to the first (and still widely used) semiconducting polymers used in modern photovoltaics and light-emitting devices; most often, the polymers seen in organic light-emitting diodes (OLEDs) are poly(*p*-aryl)s that derive some inspiration in their design from the initial investigations into PPP. Of particular importance to these fields are the organic polymer poly(*p*-phenylene vinylene) and its substituted analogues such as MEH-PPV, phenoxy-PPV and DSiPV (Figure 3.12).[12, 13]

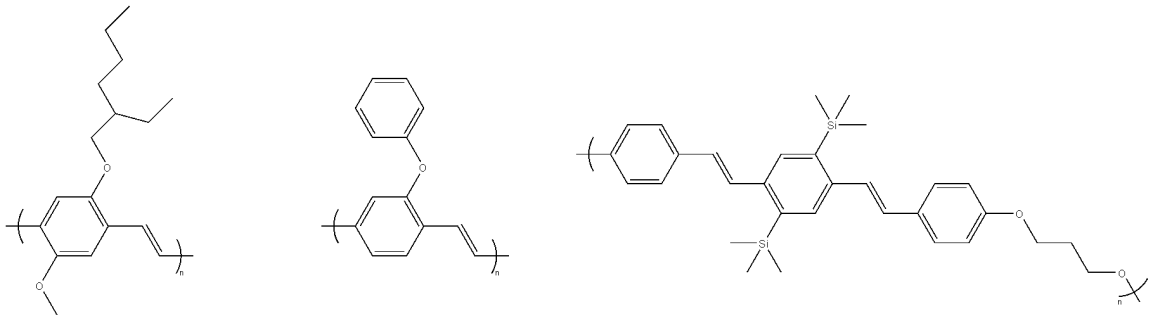

Figure 3.12. Structures for PPV-derived or inspired polymers MEH-PPV, phenoxy-PPV and DSiPV.

MEH-PPV and similar alkoxy-derivatives of PPV constituted a majority of the materials used for early OLEDs and continue to be some of the best materials in these applications. It is thus important to examine the photophysical properties of poly(*p*-phenylene) (PPP) in order to understand the shortcomings this polymer encountered in terms of its photophysics and conductivity that led researchers to investigate other light-emitting polymers such as poly(*p*-phenylene vinylene) (PPV). Moreover, the initial synthesis of PPV and characterization of its electroluminescent behavior informs how and why specifically researchers have introduced functionalization of polymer backbones to effect desired changes in the OCP behavior.

Poly(*p*-phenylene) (PPP) is a highly linear conjugated organic polymer that became of interest as a semiconducting material shortly after research on polyacetylene had begun.[14] While polyacetylene has a low band gap energy (~1.36 eV), it suffers from degradation when exposed to heat and other harsh conditions. However, the garnered stability from aromaticity in PPP makes this polymer more stable than polyacetylene

while presenting with a band gap energy still useful for devices that rely on conductivity (Figure 3.13).

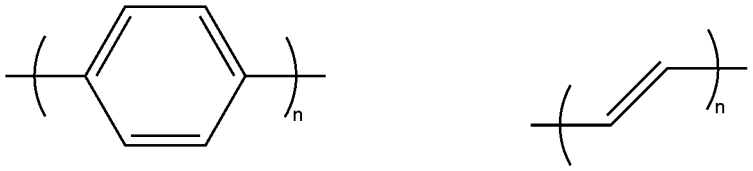

poly(*p*-phenylene) polyacetylene

Figure 3.13. Structure of poly(*p*-phenylene) and polyacetylene.

Early investigations found that PPP has a band gap energy of about 2.8 eV compared to that of around 1.4 eV for polyacetylene.[14] This increased band gap energy of PPP corresponds to light with a wavelength of ~443 nm, making PPP a potential material for blue light-emitting diodes. However, the increase in HOMO-LUMO gap for PPP as compared to polyacetylene will affect the polymer conductivity and thus applicability to electroluminescent and photovoltaic devices. In fact, no modern devices employ poly(*p*-phenylene) as the operating OCP; instead, many light-emitting diodes today utilize poly(*p*-phenylene vinylene) and its derivatives.

The parent poly(*p*-phenylene vinylene) (PPV), an insoluble bright yellow-green material having the structure shown in Figure 3.14, was first found to have electrochemically-induced luminescence in 1990.[15]

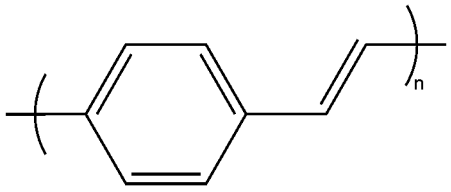

poly(*p*-phenylene vinylene)

Figure 3.14. Structure of poly(*p*-phenylene vinylene).

In this investigation, PPV was synthesized easily with soluble precursors and the resultant polymer was characterized spectroscopically and electrochemically. This initial synthesis was especially important because the PPV polymer was not a product of electropolymerization. While the unfunctionalized PPV polymer is insoluble, generally speaking, solution-based polymerizations afford polymeric materials that are more processable than electrochemically grown materials. Introduction of the double bond reduces any steric clashes between neighboring phenyls that are present in the PPP polymer. Moreover, this study demonstrated that PPV has a strong photoluminescence emission at around 2.2 eV which corresponds to a yellowish green color. Later investigations[11] characterize the band gap energy of PPV to be around 2.5 eV which is about 0.3 eV lower than that of PPP. Thus, the presence of the vinylene spaces between benzene rings lowers the HOMO-LUMO gap due to extension of the effective conjugation length. The advent of PPV was a notable development in the field of OLEDs because PPV was the first organic polymer used for an electroluminescent device.[15] The electrochemical stimulation of PPV induced photoluminescence with around 8% quantum efficiency and proved to be a breakthrough in the design of novel highly-conjugated organic polymers with emissive behavior.

Further investigations examined the effects of substitution of the phenyl rings in PPV to afford a myriad of unique light-emitting OCPs. For example, electron-donating methoxy groups present on the phenyl rings of poly(2,5-dimethoxyphenylene vinylene) (Figure 3.15)[14] leads to a material exhibiting a band gap energy on the order of 2.1 eV (cf. 2.5 eV for PPV).

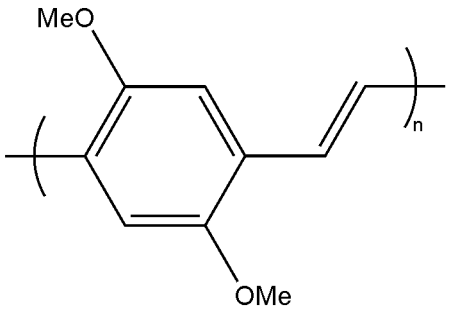

poly(2,5-dimethoxyphenylene vinylene)

Figure 3.15. Structure for the functionalized PPV derivative, poly(2,5-dimethoxyphenylene vinylene).

As a result, this methoxy-containing PPV will not only be useful for LEDs targeted for emission of lower energy light, but also the conductivity should improved versus the parent PPV as a result of the band gap energy decrease.

The fact that PPV-type π-systems provide advantageous band gap energies with improved semiconducting behavior has led to extensive variation of sidechains and incorporation of oligomeric PPV subunits into diverse π-systems. As detailed in previous chapters, the presence of heavy atoms can further improve photoluminescence efficiency and effect changes in emission wavelengths as a result of enhanced spin-orbit coupling, making introduction of a heavy atom such as a transition metal an appealing strategy to afford phosphorescent conjugated polymers. The current section describes efforts to synthesize a platinum-acetylide polymer modified to include disytrylbenzene moieties (like those crucial to the photophysical behavior of PPV). In addition, it is of interest to determine whether such a PPV-oligomer modified metallopolymer with a (phenylene vinylene)phosphine linker analogous to the PPE-oligomer modified **18** in Section 3.6 might afford advantageous conductivity and photoluminescence behavior over already

established PPV-type OCPs. We therefore targeted diphosphine **13**, which we envisioned would be an ideal precursor for polymers with the general structure of **PStb** (Scheme 3.9). Once the phosphine has been successfully synthesized and characterized, it can be used to undergo ligand exchange with dichlorobis(benzonitrile)platinum to afford the desired PPV-like metallopolymer.

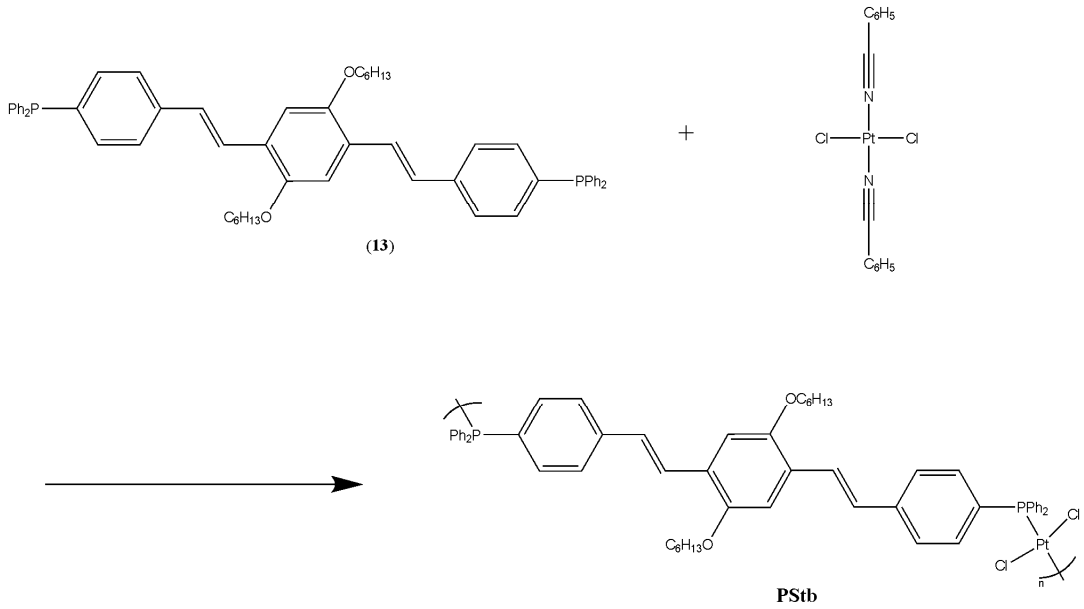

Scheme 3.9. Synthetic route to the functionalized platinum-containing PPV-type polymers (**PStb**) made with distyrylbenzene diphosphine **13**.

Since changing the functionality of the polymer chain for our metallopolymers seems to be of particular utility in optimizing the optical efficiency of these molecules, it was of interest to determine the effect of changing the spacer that bridges subsequent platinum atoms in the backbone. The incorporation of an already fluorescent linker is an attractive avenue as it promises to greatly enhance the optical properties of our metallopolymers.

We initially selected **EGT1** for the current study because it is synthesized readily by the Wittig Condensation of a dialdehyde to a phosphine salt in the presence of potassium *tert*-butoxide (Scheme 3.10).

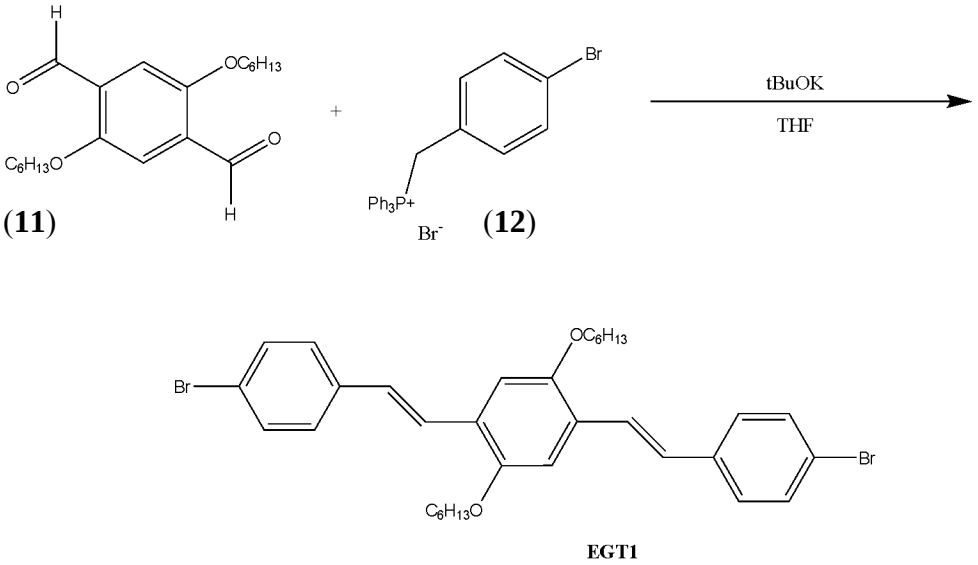

Scheme 3.10. Synthetic scheme for **EGT1**.

Results and Discussion

The ^{1}H NMR spectrum of **EGT1** showed that only the *E* isomer was formed, as gauged by a diagnostic vicinal coupling constant of $^{3}J_{HH}$ = 11 Hz for the olefinic protons; vinylic protons *cis* to each other have a vicinal coupling constant on the order of 15 Hz compared to that of around 8 Hz for those *trans* to each other.[16] This synthetic route appears to be stereospecific and no subsequent isomerization was necessary.

EGT1 was targeted to prepare the distyrylbenzene diphosphine **13** by initial lithiation at the brominated sites mediated by *n*-BuLi, followed by reaction with chlorodiphenylphosphine (Scheme 3.11).

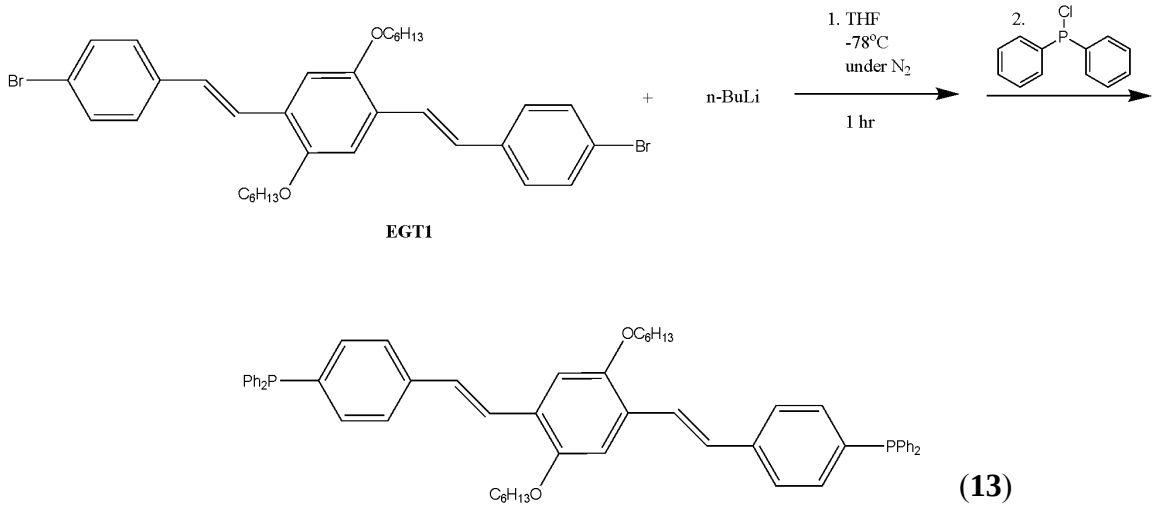

Scheme 3.11. Synthesis of phosphine linker **13**.

The spectral analysis of phosphine **13** indicated that the reaction did not proceed cleanly to a single product; notably, the presence of numerous resonances in the ^{31}P NMR spectrum indicated various products since there only should be two ^{31}P peaks based on the presence of starting material and proposed product **13**. Difficulties have been reported previously in instances where preparation of distyrylbenzene-derivatized phosphines have been attempted by similar routes.[7]

While the synthesis of **EGT1** proceeded readily and without any need for purification as only the desired *E* isomer was present, the subsequent lithiation and reaction with chlorodiphenylphosphine to form the phosphine **13** proved to be much more arduous. The problem seems to arise from the fact that delocalization of the resultant anion after lithiation allows for quenching with the phosphine-derived material at any number of positions along the conjugated chain. Similarly, when **EGT1** is dilithiated, the two anions can delocalize throughout the entire molecule as it is a highly conjugated species. Following this, the addition of chlorodiphenylphosphine will result in

diphenylphosphine addition at whichever point the anion resides—and this is not necessarily the terminal positions as we hope. In turn, phosphine **13** seems implausible to synthesize following lithiation and quenching with chlorodiphenylphosphine since too many side products are possible. As a result, the inability to isolate a pure phosphine **13** precludes the ability to examine polymerization reactions between **13** and any platinum complexes.

3.9 Future Directions for Oligo-PPV Phosphines

While the synthesis of **EGT1** proceeds efficiently in a stereospecific manner (only the *E* isomer is formed), the generation of the analogous phosphine proves to be difficult. Lithiation of the dibrominated **EGT1** affords a dianionic species which appears to delocalize over the entire molecule. As a result, quenching the dianionic **EGT1** with chlorodiphenylphosphine does not yield the desired *para* diphosphine **13**. Instead, because the carbanion can delocalize into the phenyl rings and further onto the vinylene moieties. Thus, when the phosphine quenching reagent is added, the anion is not necessarily at the desired carbon and multiple side products are possible (even probable). Therefore, this synthetic route to phosphines featuring highly conjugated PPV-like linker is not viable for the desired metallopolymer precursor. Future studies could aim at limiting the delocalization of the dianion upon lithiating, but it seems that this phosphine must be obtained via some other route to allow for its use in our proposed platinum-containing OCP. The following describes an alternative synthesis to generating the PPV-like metallopolymer utilizing simple Sonogashira techniques and ligand-exchange at the platinum atom as seen with the **18** spacer (Section 3.5 and 3.6).

Because it is still of interest to examine the effects of platinum in PPV-derived polymers, future studies should be undertaken to design such a metallopolymer without the use of phosphines generated by lithium-halogen exchange. Instead, generation of the phosphine oxide analog (**21**) of the desired phosphine would proceed via simple Heck coupling and this could then be reduced with trichlorosilane to yield phosphine **13** (Scheme 3.12).

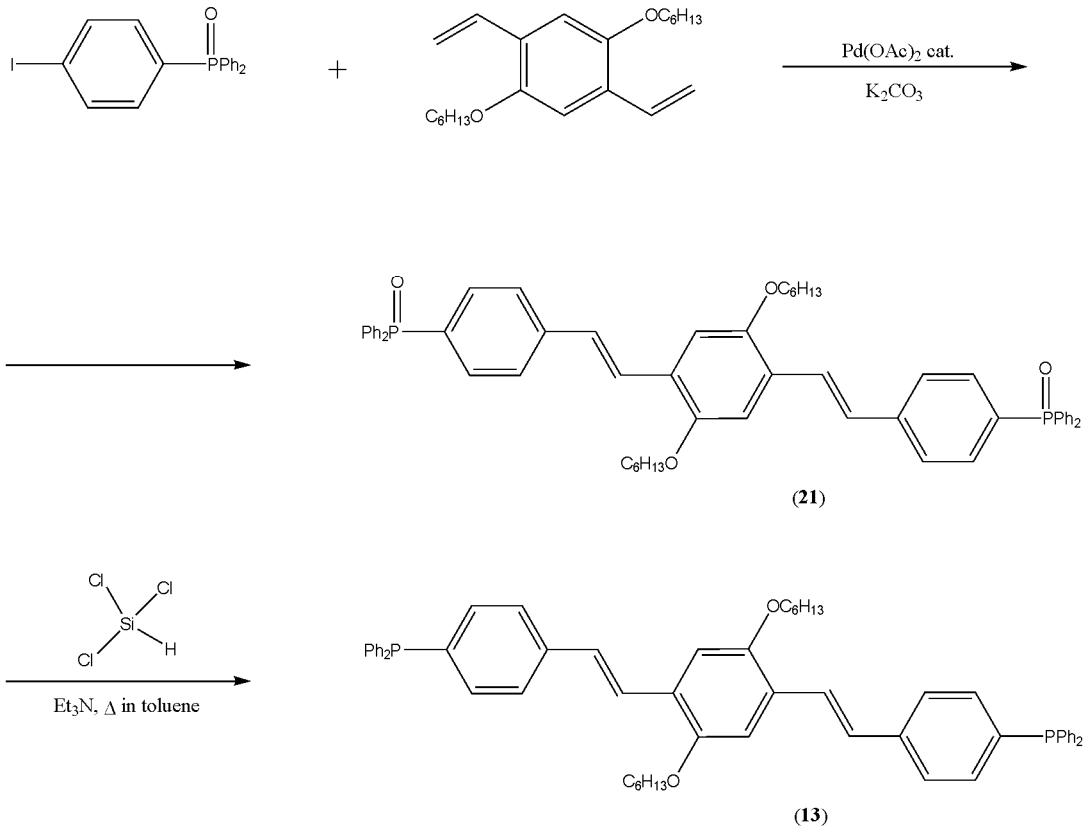

Scheme 3.12. Synthetic route to phosphine **13** via Heck coupling followed by reduction with trichlorosilane.

Once the diphosphine derivative of **EGT1** is isolated and purified, it can then be reacted with dichlorbis(benzonitrile)platinum(II) containing to afford the PPV-like metallopolymer with phosphine connectivity **PStb** as shown previously (Scheme 3.9).

It is reasonable to predict that this polymer would demonstrate enhanced photoluminescence efficiency in terms of radiative emission from the triplet state as compared to other functionalized poly(*p*-phenylene vinylene) polymers lacking heavy atoms. Moreover, the vinylene linkages in addition to the platinum metal may further extend the effective conjugation length to lower the band gap energy even more than seen in other PPV-derivatives as well as tuning electron affinity and ionization potential. As a result, these PPV-like polymers may afford a significant enhancement in conductivity and photophysical parameters than previously studied PPVs. Finally, in an attempt to further functionalize the PPV-like metallopolymer, it would be of particular interest to polymerize the **EGT1**-derived dialkyne with *trans*-[(**1**)$PtCl_2$] (See Chapter 2) to yield a scaffolded PPV-based platinum-containing polymer (Scheme 3.13).

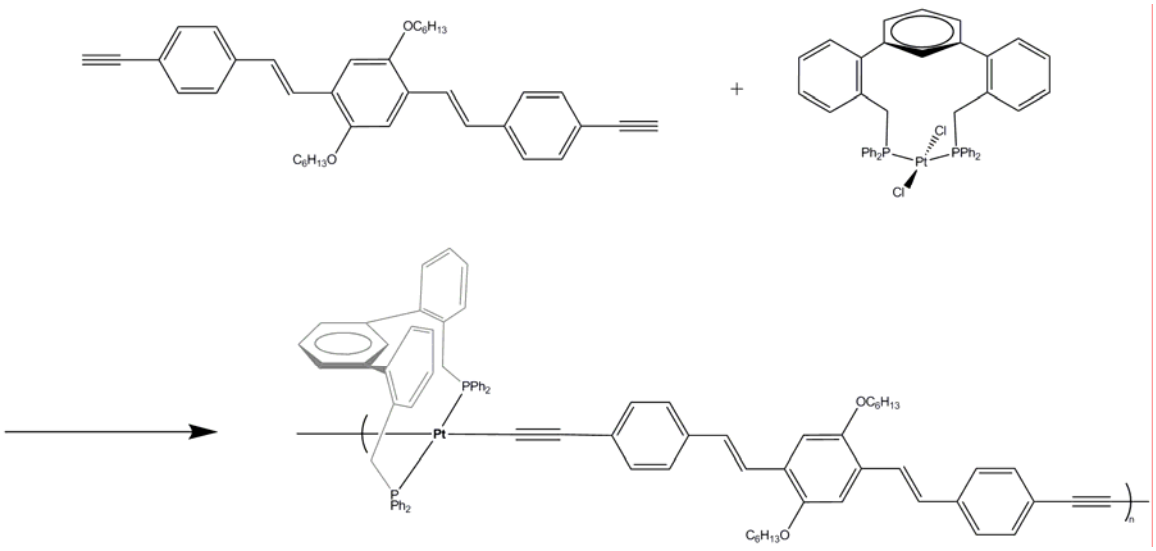

Scheme 3.13. Proposed synthesis of an *m*-terphenylphosphine scaffolded PPV-like metallopolymer.

It would also be of interest to examine a nonmetallated analog of the **PStb** polymer as made with the **EGT1** and some phosphine reagent of interest. Phosphorous-

carbon coupling is a well-documented procedure that can be used to afford PPP-type polymers with phosphorous-carbon connectivity.[17] In this synthetic scheme, phenylphosphine (or a functionalized analog) can be coupled with the dibromo **EGT1** reagent to afford the PPV-like polymer without platinum incorporation into the polymer backbone (Scheme 3.14).

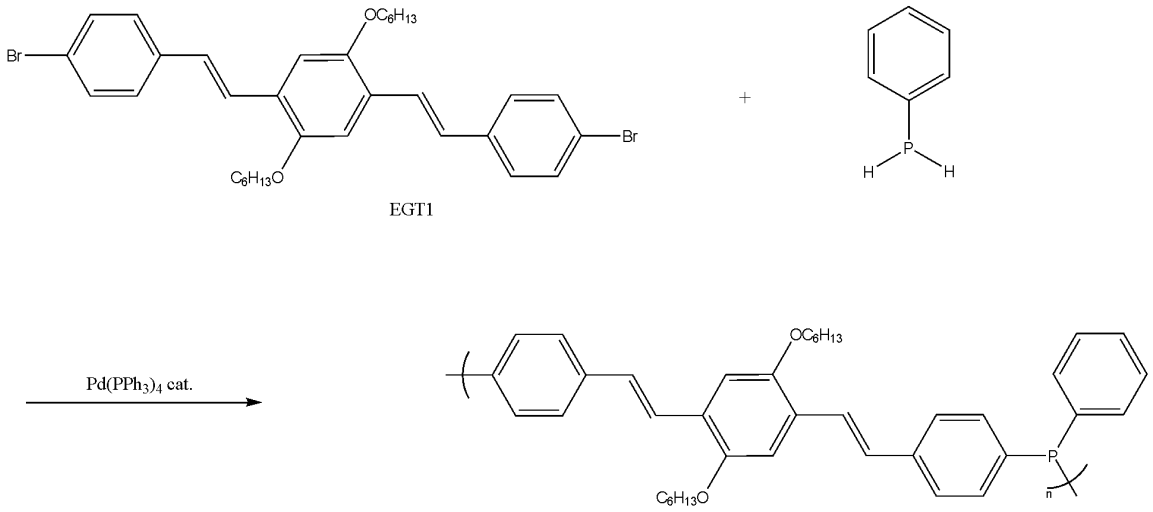

Scheme 3.14. PPV-like polymer based on **EGT1** with phosphine connectivity but lacking the platinum metal.

Depending on the identity of the phosphine used, a myriad of polymers similar in structure could be afforded easily and efficiently from the **EGT1** precursor; this synthetic design is especially interesting because it yields a polymer with phosphorous-carbon connectivity without having to isolate or purify phosphine starting materials. Successful synthesis of this type of polymer would allow direct comparison of photophysical parameters and conductivity to the **PStb** polymer discussed previously. This would allow for a more profound understanding as to the influence of the platinum metal on the polymeric optoelectronics and semiconducting abilities. Moreover, using

diphenylphosphine as the phosphorous source would afford polyelectrolytes as the product of this simple reaction—species which are of particular interest to our current research as discussed in Chapter 4.

While the synthesis of the phosphine analog of **EGT1** was not clean by the route first investigated, there are clearly other avenues to yield interesting platinum-containing PPV-derived polymers. This new class of polymers would likely demonstrate interesting and unique photophysical behavior as a result of the vinylene linkages and the presence of the heavy platinum atom. Moreover, these materials would be highly conjugated species with finely tunable emission wavelengths depending on how the **EGT1**-derived spacer were functionalized. As a result, these polymers promise to be of particular utility in devices that rely on semiconducting materials with specific light-emitting behavior.

Experimental

General Considerations

All air-sensitive reactions were performed using standard Schlenk techniques or in an MBraun UNILab glovebox under nitrogen. Anhydrous solvents were purchased from Fisher Scientific and further dried and degassed using an MBraun solvent purification system. All other reagents were used as received unless otherwise specified. NMR spectra of interest were obtained on a Bruker Avance 300 (operating at 300, 75.4, and 121.4 MHz for ^{1}H, ^{13}C, and ^{31}P nuclei, respectively) or Bruker Avance 500 spectrometer (operating at 500, 125.7, and 202.4 MHz for ^{1}H, ^{13}C, and ^{31}P nuclei, respectively). NMR spectral data are reported in ppm referenced to residual solvent signal (^{1}H and ^{13}C) or 85% phosphoric acid (^{31}P). UV-Vis absorption spectra were

acquired on a Cary 50 Spectrophotometer while photoluminescence (PL) spectra were obtained on a Varian Eclipse fluorimeter.

Synthesis of light-harvesting phosphine oxide (16)

The phosphine oxide **16** was first synthesized using the 4-bromophenyldiphenylphosphine oxide **14**. The ^{31}P NMR of phosphine oxide **14** is provided as reference to discern whether coupling is successful (Fig A-40). ^{31}P NMR (121.4 MHz, $CDCl_3$) δ: 29.5, 25.6, 22.2. In the drybox, phosphine oxide **14** (0.110 g, 0.337 mmol) and $Pd(PPh_3)_4$ (19.45 mg, 5% mol catalyst) were added to a 75 mL pressure flask containing 5 mL of toluene. To the above reaction, a solution of 1,4-diethynyl-2,5-dihexyloxybenzene (0.110 g, 0.337 mmol) and copper iodide (3.21 mg, 5% mol catalyst) in 5 mL of diisopropylamine was added dropwise at a rate of 1 pipet/min while stirring. The reaction flask was brought out of the drybox and stirred at 90 °C for 72 h. At that time, the reaction mixture was diluted to 50 mL with dichloromethane, washed three times with water, dried over anhydrous sodium sulfate and the solvent was removed by rotary evaporation to yield a brick red glassy solid. ^{1}H and ^{31}P analysis of the resultant solid showed one major phosphine oxide species (Fig A-41 and A-42). ^{1}H NMR (300 MHz, $CDCl_3$) δ: 7.8-7.4 (m, 28H), 7.0 (s, 2H), 4.05 (t, 4H), 1.85 (quintet, 4H), 1.6 (quintet, 4H), 1.35 (m, 9H), 0.9 (t, 6H); ^{31}P NMR (121.4 MHz, $CDCl_3$) δ: 29.8, 29.4.

The slight impurity observable in the ^{31}P NMR at 29.8 ppm was attempted to be removed via recrystallization. Phosphine oxide **16** was placed into dichloromethane in a small shell vial and placed into a larger vial containing pentane in hopes of pentane diffusing into the solution of **16** causing precipitation to occur. At this time, solubility tests on the phosphine oxide **16** were performed for future recrystallization attempts.

Compound **16** is soluble in dichloromethane, chloroform, tetrahydrofuran and toluene; it is not soluble in diethyl ether, water or pentane. Recrystallization attempts with dichloromethane/pentane, tetrahydrofuran/pentane and toluene/pentane solvents systems all produced only urchin solids after diffusion of pentane into the solvated phosphine oxide **16**. These methods were unable to produce an X-ray quality crystal so another technique for purifying the crude phosphine oxide **16** was pursued.

Thin-layer chromatography (TLC) analysis showed good separation and resolution of two species in the crude product **16** with a solvent system of 10% methanol in dichloromethane (v/v). Therefore, prep TLC of the crude phosphine oxide was performed with 10% methanol/dichloromethane as the running solvent. The isolated crude phosphine oxide from above was dissolved in about 1 pipetful of dichloromethane and loaded onto a large silica glass-backed TLC plate. About 200 mL of 10% methanol/dichloromethane was added to the prep TLC chamber followed by placement of the TLC plate already loaded with crude phosphine oxide **16**. After 30 minutes, the TLC plate was removed from the running chamber and placed under an ultraviolet lamp to yield three distinct bands—the top was a fluorescent blue, the middle was an orange non-fluorescent layer and the bottom band was a fluorescent light blue. Each of the three layers was isolated from the TLC plate by scraping off the silica and placing it into a separate container. All three prep TLC samples were washed three times with dichloromethane to redissolve the desired compound from the silica, syringe filtered and the solvent removed by rotary evaporation. The top and bottom fluorescent prep TLC fractions did not contain any phosphorous-containing material as indicated by ^{31}P NMR (spectra not shown). The large orange middle fraction from prep TLC yielded a

phosphine oxide product **16** that was no purer than before the purification attempt as determined by ^{31}P NMR (Fig A-43). ^{31}P NMR (121.4 MHz, $CDCl_3$) δ: 34.4, 30.1, 29.5. In fact, the above isolated product had an extra impurity at 34.4 ppm. Thus, the prep TLC did not succeed in purifying the linear phosphine oxide **16** and even appeared to worsen its purity. It seemed possible that the product was still adsorbed to the silica from the TLC plate and so the collected silica was the focus of further product isolation.

The silica from the middle orange prep TLC fraction (*vide supra*) was dissolved in 20 mL of methanol and added to 20 mL of dichloromethane. This mixture was placed into a separatory funnel and washed once with 40 mL of water; at that time, the silica moved into the aqueous layer and settled to the bottom of the separatory funnel. The dichloromethane layer was isolated and the solvent removed by rotary evaporation to yield a red residue that solidified upon resting open to air. ^{31}P NMR of the resultant solid showed improved purity with the desired major peak at 29.4 ppm and only a minor peak at 33.6 ppm. (Fig A-44).

Later syntheses of compound **16** that demonstrated higher degrees of purity were utilized in attempts to grow crystals. One particular solvent system, pentane diffusing into a chlorobenzene solution of **16**, gave urchin-like crystals with excellent purity. The crystallization was set up on 3.08.08 and then analyzed by ^{1}H and ^{31}P NMR (Fig A-45 and A-46). ^{1}H NMR (300 MHz, $CDCl_3$) δ: 7.8-7.4 (m, 28H), 7.0 (s, 2H), 4.05 (t, 4H), 1.85 (quintet, 4H), 1.6 (quintet, 4H), 1.35 (m, 9H), 0.9 (t, 6H); ^{31}P NMR (121.4 MHz, $CDCl_3$) δ: 29.4.

Photophysical characterization of 16

Once an appreciable amount of pure phosphine oxide **16** was obtained from the above synthetic route, it was analyzed via UV-vis and fluorescence spectroscopy. An absorption spectrum of a solution of $4.5*10^{-4}$ M phosphine oxide **16** in dichloromethane was acquired to yield a wavelength of maximum absorbance of 381 nm (Fig B-4). After determining this wavelength, a photoluminescence spectrum of a phosphine oxide solution ($9.8*10^{-7}$ M in dichloromethane) was collected using an excitation wavelength of 381 nm and scanning from 391 to 800 nm (Fig B-5).

Synthesis of fluorene-based phosphine oxide (17)

In the drybox, fluorene-based boronic ester **17** (0.703 g, 1.4 mmol), phosphine oxide **14** (1.0 g, 2.8 mmol) and cesium carbonate (2.27 g, 7.0 mmol) were added to a 75 mL pressure tube followed by addition of $Pd(PPh_3)_4$ (73 mg, 2.5 mol %) and 60 mL of degassed *N,N*-dimethylformamide. (Compound **17** was used as received from Sigma-Aldrich). The reaction vessel was sealed, brought out of the drybox and heated to 95 °C while stirring for 19 h. At that time, the crude reaction mixture was diluted up to 120 mL with dichloromethane, washed five times with water followed by washing with a saturated sodium chloride solution and another portion of water. The dichloromethane was removed by rotary evaporation to yield a deep red crystalline powder presumed to be fluorene-based phosphine oxide **17**; ^{1}H and ^{31}P NMR of the crude solid was acquired to assess its purity (Fig A-47 and A-48). ^{1}H NMR (300 MHz, $CDCl_3$) δ: 8.0-7.2 (m, 7H), 2.3-1.9 (m, 1H), 1.2-0.5 (m, 5H); ^{31}P NMR (121.4 MHz, $CDCl_3$) δ: 33.5, 30.0, 29.9, 29.4. The ^{31}P NMR spectrum shows a sharp peak at the desired 29.6 ppm (reference spectrum from R. Gilliard– *vide infra*) in addition to a number of impurities at 30.2, 30.1 and 29.5

ppm. Representative spectral data for **17** from R. Gilliard: ^{1}H NMR (300 MHz, $CDCl_3$) δ: 7.9-7.5 (m, 33H), 2.1 (m, 4H), 1.9 (m, 2H), 1.3 (m, 2H), 1.1-0.9 (m, 13H), 0.8-0.6 (m, 10H); ^{31}P NMR (121.4 MHz, $CDCl_3$) δ: 29.6. Thus, purification was pursued on this batch of crude phosphine oxide **17** via recrystallization.

Recrystallization attempts for crude product **17** consisted of one of two solvent systems: diffusion of pentane into a solution of **17** in either tetrahydrofuran or dichloromethane. After 24 h, the pentane/tetrahydrofuran setup only yielded a brown residue while the pentane/dichloromethane system afforded a brown residue with some white crystals at the surface. Phosphorous-31 NMR spectral analysis of both the brown oil and the white crystals was performed and showed presence of impurities still (spectra not shown). The recrystallization setups were left for a longer period of time in hopes that more purified product will precipitate out of the dichloromethane. After two weeks, the pentane/tetrahydrofuran setup yielded large white crystals with excellent purity as determined by ^{31}P NMR (Fig A-49). ^{31}P NMR (121.4 MHz, $CDCl_3$) δ: 29.7. All of the white crystals from the recrystallization setups were collected and dried *in vacuo* to yield ~30 mg of pure **17**.

As crystallization of **17** afforded low yields of pure product, TLC was performed to find an optimal solvent system for column chromatography which will be used to purify the next synthetic attempt at **17**. A 50:50 solution of ethyl acetate/hexanes (v/v) showed good separation on alumina TLC plates of the brown residue isolated from one of the above crystallization attempts. Another batch of fluorene-based phosphine oxide **17** was made following the above procedure except that the reaction was heated to 95 °C for 4 d. After the same work-up as detailed before, the resultant deep red solid that was crude

17 was placed in a 50:50 mixture of ethyl acetate/hexanes for column chromatography. As the crude product did not dissolve in this solvent system, the solvent was removed by rotary evaporation and the crude product was then dissolved in a minimum amount of dichloromethane and combined with some chromatographic grade alumina. This suspension was rotovapped to dryness to adsorb the crude product to the alumina which was then loaded onto a 500 mL column filled with about 5 inches of alumina in 50:50 ethyl acetate/hexanes (the running solvent). Using a flow rate of about 2 mL/min, 55 fractions (10 mL) were collected while monitoring the product separation by TLC using the same solvent system as for the column. TLC analysis showed that fractions 27-55 contained pure product so these were combined and the solvent was removed by rotary evaporation. Phosphorous-31 NMR of the resultant beige solid (~80 mg) showed pure fluorene-based phosphine oxide **17** (Fig A-50). ^{31}P NMR (121.4 MHz, $CDCl_3$) δ: 29.6. About 1 gram of crude product was loaded onto the column and only ~80 mg was recovered, about 200 mL of column running solvent was flushed through the column in hopes of isolated more purified product if it were still adsorbed to the alumina. Removal of the solvent afforded another 80 mg of pure phosphine oxide **17**.

Synthesis of 4-iodophenyldiphenylphosphine oxide (15)

In the drybox, 1,4-diiodobenzene (5.0 g, 15.2 mmol) was dissolved into 125 mL of tetrahydrofuran and placed into a 250 mL roundbottom flask equipped with a stirrer bar. The reaction flask was brought out of the drybox and cooled to –78 °C followed by addition of *n*-butyllithium (6.06 mL, 15.2 mmol). After this reaction mixture stirred in the acetone dry ice bath for 1 h, chlorodiphenylphosphine (3.30 g, 15.2 mmol) in about 10 mL of THF was brought out of the drybox and immediately transferred via syringe to the

reaction flask. At that time, the reaction was removed from the dry ice bath and stirred at room temperature for 20 h. The crude reaction mixture was then was then diluted to 250 mL with dichloromethane,[†] washed three times with water and the solvent removed by rotary evaporation to afford a bright yellow viscous liquid. This liquid is then dissolved in 50 mL of dichloromethane and to it is added a 30% solution of hydrogen peroxide (1.2 mL, 152 mmol). This reaction is stirred at room temperature (while vented) for 16 h to yield a light orange solution. After 16 h, the crude reaction mixture is quenched with 5 mL of saturated sodium bicarbonate, washed twice with water and dried over anhydrous sodium sulfate. The dichloromethane is removed by rotary evaporation to leave a pale beige residue. This viscous liquid is then added to about 5 mL of diethyl ether followed by transferal of this solution to 125 mL of pentane. This immediately produces a yellow solid that adheres to the flask and so the ether/pentane mixture is decanted away from the solid into a different 125 mL Erlenmeyer flask and stored in the freezer in order to precipitate the desired phosphine oxide **15**. After thirty minutes, large amounts of white solid are at the bottom of the flask; the solid is isolated by vacuum filtration to afford pure phosphine oxide **15** as shown by ^{1}H and ^{31}P NMR (Fig A-53 and A-54). ^{1}H NMR (300 MHz, $CDCl_3$) δ: 7.7-7.4 (m, 14H); ^{31}P NMR (121.4 MHz, $CDCl_3$) δ: 29.7.

The Sonogashira coupling with 1,4-diethynyl-2,5-dihexyloxybenzene was then attempted with phosphine oxide **15** to determine if the same desired phosphine oxide **16** is synthesized with the iodo analog (Scheme 3.4). The procedure was the same as reported above except that no heating was necessary and the reaction was stirred at room temperature for 16 h. At that time, the workup was the same as detailed before to afford a

[†] While phosphines such as these are sensitive to oxygen, the first step of the reaction is worked up open to air because oxidation is desired and performed in the next step.

clean phosphine oxide **16** (56.5% yield) as shown by ^{1}H and ^{31}P NMR (Fig A-55 and A-56). ^{1}H NMR (300 MHz, $CDCl_3$) δ: 9.4 (br s, 1H, ammonium salt), 7.8-7.4 (m, 28H), 7.0 (s, 2H), 4.05 (t, 4H), 1.85 (quintet, 4H), 1.6 (quintet, 4H), 1.35 (m, 9H), 0.9 (t, 6H); ^{31}P NMR (121.4 MHz, $CDCl_3$) δ: 29.5. The product was dissolved in dichloromethane and passed through silica atop a Buchner funnel to remove the excess ammonium salts. However, this procedure will not and should not be used in the future with phosphine oxides as they adsorb tightly to the silica and much of the product is lost.

Reduction of 16 to afford light-harvesting phosphine 18

The reduction of phosphine oxide **16** follows a similar procedure reported in the literature.[7] In the drybox, phosphine oxide **16** (1.0 g, 1.14 mmol) and 1.59 mL of triethylamine were added to 63 mL of toluene and transferred to a 100 mL roundbottom flask. The reaction flask was attached to a small reflux condenser while still in the drybox, brought out of the drybox and started refluxing. At that time, trichlorosilane (1.2 mL, 11.38 mmol) was added via syringe through the stoppered reflux condenser and the reaction stirred while refluxing for 3 h. After cooling to room temperature, 6.25 mL of degassed sodium bicarbonate was added *very slowly* to the reaction mixture which was then stirred for five minutes. At that time, there was an orange solid suspended in a light orange yellow solution. In order to isolate the solution phase (presumed to contain desired phosphine **18**), an air-free centrifugation was performed. In this vein, six Falcon centrifuge tubes were sealed with small rubber septa and electrical tape; these tubes were then evacuated to leave negative pressure inside. The crude reaction suspension was then drawn up via syringe, taking care not to clog the needle, and placed into the evacuated centrifuge tubes. Once all of the suspension from the reaction flask had been transferred,

the six samples were centrifuged for about 1 min to yield an orange solution above an orange-yellow solid at the bottom of the tube. The solution phase from each centrifuge sample was transferred via syringe into a clean 100 mL roundbottom also under static vacuum (so as to ensure air-free environment but no significant build-up of pressure). The crude solid that still remained in the original reaction flask was washed once with another portion of about 20 mL of anhydrous degassed toluene. The air-free centrifugation was repeated for this suspension as well and the isolated orange solvent combined with the previously collected solution phases. Now all of the desired phosphine was presumed to be in the toluene in the new 100 mL roundbottom flask so it was dried *in vacuo* for 5 h. As there was still a significant amount of solvent left after that amount of time, the roundbottom was left under high N_2 pressure for 40 h in hopes of blowing the toluene off. The next day there was only a red-orange viscous residue left in the roundbottom that was presumed to be the crude phosphine **18**. This sample was pumped into the drybox and analyzed by ^{1}H and ^{31}P NMR spectroscopy (Fig A-57 and A-58). ^{1}H NMR (300 MHz, $CDCl_3$) δ: 7.8-7.4 (m, 28H), 7.0 (s, 2H), 4.05 (t, 4H), 1.85 (quintet, 4H), 1.6 (quintet, 4H), 1.35 (m, 9H), 0.9 (t, 6H); ^{31}P NMR (121.4 MHz, $CDCl_3$) δ: –4.59, –4.84, –5.13. There were some minor impurities at –4.84 ppm and –5.14 ppm in the ^{31}P NMR so further purification was attempted. It should be noted that the orange solid from the centrifugation was analyzed by NMR as well and showed no phosphorous-containing material so was discarded (spectra not shown).

As crude phosphine **18** contained some minor impurities and was a relatively unmanageable viscous residue, it was attempted to be precipitated using dichloromethane and acetonitrile. Thus, in the drybox, the red residue that was the crude phosphine **18** was

dissolved in about 1 pipetful of dichloromethane and then transferred to 5 mL of acetonitrile. Some yellow solid formed upon addition of the concentrated dichloromethane solution to acetonitrile and collected of the solid via a fritted filter was attempted. Unfortunately, filtering through the frit just reproduced the red viscous oil so the dichloromethane, solid and acetonitrile were recombined and placed in the drybox freezer in hopes of precipitation at a lower temperature. After 9 d in the freezer, a solid residue sat at the bottom of the vial containing the acetonitrile and dichloromethane solutions and so the solvent was decanted away and the red residue was dried *in vacuo* for 2 h. Both ^{1}H and ^{31}P NMR spectra of the resultant crystalline solid showed excellent purity for the phosphine **18** (Fig A-59 and A-60). ^{1}H NMR (300 MHz, $CDCl_3$) δ: 7.8-7.4 (m, 28H), 7.0 (s, 2H), 4.05 (t, 4H), 1.85 (quintet, 4H), 1.6 (quintet, 4H), 1.35 (m, 9H), 0.9 (t, 6H); ^{31}P NMR (121.4 MHz, $CDCl_3$) δ: –4.59.

Photophysical characterization of 18

UV-vis and fluorescence spectra were acquired for linear phosphine **18** in dichloromethane as prepared in the drybox. A stock solution of $4.7*10^{-4}$ M (stored in the freezer) of **18** in dichloromethane was diluted to a concentration of $5.0*10^{-5}$ M and analyzed by UV-Vis spectroscopy (Fig B-6). Using an excitation wavelength of 376 nm, a fluorescence emission spectrum was obtained for a $1*10^{-6}$ M solution of **18** in dichloromethane (Fig B-7).

Modifications to the workup of phosphine 18

Future syntheses of phosphine **18** had modified workup procedures owing to the difficulty in performing the above air-free centrifugation. Instead of centrifuging and isolating the toluene portion, all of the solvent was removed *in vacuo* after quenching

with sodium bicarbonate in future batches of **18**. Once all of the solvent is removed, the crude reaction mixture can be brought into the drybox, redissolved in toluene and filtered through celite. The yellow-orange filtrate is collected and dried *in vacuo* to afford the desired phosphine **18**. However, it should be noted that this procedure yields a ^{31}P NMR spectrum that implies some phosphine protonation as evidenced by broadening of the desired peak (Fig A-61). ^{31}P NMR (121.4 MHz, $CDCl_3$) δ: –4.59, –5.13 (br s). This is likely because there is could still be some sodium bicarbonate in the isolated phosphine that when in solution phase (like NMR solvent) can undergo rapid protonation and deprotonation. However, this does not appear to affect that ability of the phosphine to polymerize with the platinum-containing material of interest (*vide supra*). Moreover, the phosphine **18** isolated by the modified workup can still be purified further by dissolving in 1 mL of THF and pipetting into 15 mL of acetonitrile and placing this into the drybox freezer. Ultimately this workup and purification is preferred because evading the air-free centrifugation greatly reduces the likelihood of oxidizing the phosphine accidentally as well as improves the yield of the isolated product after the work-up procedure.

In addition, it is possible to perform a simple open-to-air extraction workup after quenching with sodium bicarbonate so long as it is done expeditiously. Following this route, the reaction mixture is quenched as before and stirred for five minutes. At that time, the reaction mixture is transferred to a separatory funnel and the aqueous layer removed. The remaining organic layer is washed twice with water, dried over anhydrous sodium sulfate and concentrated *in vacuo*. Once all of the toluene is removed, the orange residue is placed under nitrogen or taken into the drybox for any necessary purification.

The light-harvesting phosphine **18** appears to be stable open to air, even when solvated, for at least a couple of hours.

Synthesis of platinum-based polymer 19

In the drybox, phosphine **18** (50 mg, 0.059 mol) was dissolved into about 2 mL of dichloromethane and transferred via pipet to a small shell vial containing dichlorobis(benzonitrile)platinum (27 mg, 0.057 mmol). Upon addition of the solution of **18** to the platinum material an orange gel was formed almost instantly. The solvent was removed *in vacuo* and the presumed polymer **19** was examined by ^{1}H and ^{31}P NMR (Fig A-62 and A-63). ^{1}H NMR (300 MHz, $CDCl_3$) δ: 7.8-7.2 (m, 47H), 7.0 (s, 3H), 4.05 (t, 4H), 1.85 (quintet, 4H), 1.6-0.7 (m, 69H); ^{31}P NMR (121.4 MHz, $CDCl_3$) δ: 15.0 ($^{1}J_{Pt\text{-}P}$ = 3657 Hz), –4.53.

Photophysical characterization of polymer 19

In the drybox, a stock solution of $3.6*10^{-4}$ M polymer **19** in dichloromethane was used as the dilution for UV-vis data acquisition (Fig B-8). The wavelength of maximum absorbance (384 nm) was used as the excitation wavelength in collecting the fluorescence emission spectrum for a $1*10^{-5}$ M solution of **19** in dichloromethane (Fig B-9).

Synthesis of palladium-based polymer 20

In the drybox, phosphine **18** (50 mg, 0.059 mmol) was added to 2 mL of dichloromethane and transferred to a vial containing dichlorobis(benzonitrile)palladium (21.82 mg, 0.0569). Upon addition of the dichloromethane solution of **18** to the palladium-containing reagent, a brown gel was formed instantly. The solvent was then removed *in vacuo* and the resultant brown solid polymer **20** was analyzed by ^{1}H and ^{31}P NMR (Fig A-64 and A-65). ^{1}H NMR (300 MHz, $CDCl_3$) δ: 7.8-7.2 (m, 61H), 7.0 (s, 3H),

4.05 (t, 4H), 1.85 (quintet, 7H), 1.6-0.9 (m, 46), 1.35), 0.9 (t, 22H); ^{31}P NMR (121.4 MHz, $CDCl_3$) δ: 29.1, 24.4, 23.9.

Photophysical characterization of polymer 20

A stock solution of $9.8*10^{-4}$ M of polymer **20** in dichloromethane was diluted to $5*10^{-5}$ M with the same solvent and analyzed by UV-Vis spectroscopy (Fig B-10) to show a wavelength of maximum absorbance of 378 nm. A fluorescence emission spectrum of $1*10^{-6}$ M polymer **20** in dichloromethane was collected with excitation at 378 nm (Fig B-11).

Photoluminescence lifetimes for 16, 18, polymer 19 and polymer 20

Photoluminescence lifetimes were measured using time-correlated single photon counting (TCSPC) method by J. J. Grimland of Dr. J. McNeill's group at Clemson University.

Synthesis of polymer 19b using a 1:1 molar ratio of phosphine to platinum reagent

In the drybox, **18** (144 mg, 0.17 mmol) was dissolved in 6 mL of dichloromethane and transferred to a vial containing dichlorobis(benzonitrile)platinum (80 mg, 0.17 mmol) to afford a bright yellow viscous gel instantly. The solvent was removed *in vacuo* and the resultant orange glassy solid was attempted to be dissolved in chloroform-d_1 to be analyzed by ^{31}P NMR spectroscopy. However, the polymer **19** was now insoluble in this NMR solvent. So the suspension was centrifuged and the chloroform-d_1 decanted away to attempt dissolving the polymer in different solvents. Polymer **19** was not soluble in toluene, DMSO-d_6, benzene-d_6, chlorobenzene or nitrotoluene.

Synthesis of polymer 19c with excess 5% molar excess phosphine 18

In the drybox, phosphine **18** (20 mg, 0.024 mmol) was dissolved in 1 mL of chloroform-d_1 and added to an NMR tube containing dichlorobis(benzonitrile)platinum (11 mg, 0.022 mmol) to afford a yellow gel within the tube. Amidst the yellow gel, there were various orange particles that were suspended. As a short ^{31}P NMR of the resultant gel showed poor signal to noise of a very broad resonance, an overnight ^{31}P NMR was acquired to characterize the afforded product (Fig A-66). ^{31}P NMR (121.4 MHz, $CDCl_3$) δ: 0 to –15 (br s).

Synthesis of platinum-based polymer 19d

In the drybox, phosphine **18** (10 mg, 0.012 mmol) was dissolved in 1 mL of chloroform-d_1 and to it was added an aliquot of 34 μL (0.003 mmol) of a 0.1M trimethylphosphine solution in tetrahydrofuran. The above mixture was transferred via pipet to an NMR tube containing dichlorobis(benzonitrile)platinum (7 mg, 0.013 mmol). After shaking the reaction mixture, a yellow viscous suspension with orange particles was formed. ^{31}P NMR analysis of the resultant reaction liquid showed a broad peak consistent with that seen in previous polymerization attempts yet the trimethyphosphine end-groups were not resolved in the spectrum (Fig A-67). Thus, the NMR-scale reaction was pumped back into the box and 10 μL of a 1.0 M solution of trimethylphosphine in tetrahydrofuran was added to the tube and it sat in the drybox for 12 h. The next day, the reaction mixture was analyzed by ^{31}P NMR which showed a broad resonance for the polymer **19** as well as peaks consistent with end-group trimethylphosphines as well as some oxidized species (Fig A-68). ^{31}P NMR (121.4 MHz, $CDCl_3$) δ: 39.2, 29.5, 12.4, -2.9 (br s), –4.9, –11.6, –23.9.

Synthesis of EGT1

In the drybox, the starting material **11** (1.6 g, 5.22 mmol) and phosphine salt **12** (5.46 g, 10.9 mmol) were added to 100 mL of THF and stirred in a 250 mL roundbottom flask to yield a bright yellow opaque solution. Then a viscous solution of potassium *tert*-butoxide (1.47 g, 13.1 mmol) in ~20 mL of THF was added dropwise to the reaction flask over the course of 35 min. When the base solution entered the mixture of **11** and **12**, a bright orange color appeared and then dissipated. This process continued over the course of addition of base but the color persisted longer as more base was added; upon completion of pipet transferring of the potassium *tert*-butoxide, the solution remained a bright orange color. The reaction mixture was stoppered and stirred in the drybox for 24 h at room temperature. At that time, the solution was brought out of the drybox and 100 mL of 10% HCl in methanol (v/v) was added to the reaction flask. The mixture was diluted with dichloromethane to give a bright yellow/green organic layer which was washed with water (7 x 100 mL), dried over anhydrous sodium sulfate and the solvent removed by rotary evaporation to leave a bright yellow oil. Methanol (~10 mL) was added to the yellow residue and the mixture stirred for ~10 min at room temperature; after 7 min, a yellow precipitate began forming in the reaction flask. The yellow solid was isolated by vacuum filtration and analyzed by ^{1}H and ^{13}C NMR (Fig A-32 and A-33) to show only the *E* isomer formed. ^{1}H NMR (300 MHz, $CDCl_3$) δ: 7.4 (m, 1H), 7.2 (m, 1H), 6.8-6.4 (m, 2H), 3.5 (m, overlapping with THF), 2.0-1.4 (m, 7H), 1.3 (m, 3H), 0.9 (m, 2H); ^{13}C NMR (75.4 MHz, $CDCl_3$) δ: 150, 136, 133, 131, 129, 126, 125, 121, 113, 69,50, 32, 29, 25, 23, 12. Product was subsequently dried *in vacuo* for 4 h to remove residual methanol.

Attempted Preparation of Phosphine 13

Attempted synthesis of **13** was undertaken by first placing **EGT1** (0.200 g, 0.312 mmol) in ~5 mL of THF in a 50 mL roundbottom flask in the drybox. This solution was taken out of the drybox and put under positive N_2 pressure and into an acetone/dry ice bath and *n*-butylllithium (0.275 mL) solution was added via syringe to the roundbottom containing **EGT1** using air-free techniques. The reaction mixture stirred at –78 °C for 1 h at which time chlorodiphenylphosphine (0.158 g, 0.718 mmol) was added via syringe and the mixture stirred under N_2 for ~20 min. After 20 min of stirring still at –78 °C, the acetone/dry ice bath was removed and the light green solution was allowed to warm up to room temperature while turning dark green in color. Stirring at room temperature for another 5 min yielded a orange brown solution and the solvent was then removed by vacuum drying. The crude product **13** was pumped back into the drybox and analyzed by ^{1}H and ^{31}P NMR (Fig A-34 and A-35) to demonstrate numerous phosphorous-containing species present. ^{1}H NMR (300 MHz, $CDCl_3$) δ: 7.8-7.2 (m, 1H), 6.9-6.5 (m, 1H), 4.0-3.5 (m, overlapping with THF), 1.9 (m, 1H), 1.6-1.1 (m, 1H), 0.9 (m, 1H); ^{31}P NMR (121.4 MHz, $CDCl_3$) δ: 39.3, 3.8, –4.9, –14.9, –15.3.

Crude product **13** was stored in the drybox freezer for about 3 wk while other syntheses were pursued. After 3 wk, purification of the phosphine **13** was attempted in the hopes of isolating a clean product that could be used for polymerizations.

The crude phosphine **13** solid was taken in up toluene in the drybox and decanted away from an insoluble solid—presumably lithium salts. ^{31}P NMR showed no improvement in purity of the crude phosphine resulting from this step (spectrum not shown) so the toluene was removed *in vacuo* and the crude solid washed with

acetonitrile. After isolating the insoluble yellow-orange solid (presumably the phosphine **13**), ^{31}P NMR was performed to assess the purity of the phosphine (Fig A-36). ^{31}P NMR (121.4 MHz, $CDCl_3$) δ: 76.1, –4.9, –14.9. There was still a phosphorous-containing impurity at around –15 ppm though the purity of the crude solid improved markedly with the acetonitrile wash. Owing to the small amount of relatively impure phosphine **13** isolated in this particular synthesis, nothing further was done with this compound and another synthesis was undertaken following the same stoichiometry and procedure as detailed before. However, the purification of the crude phosphine **13** is different than reported above so merits attention here.

After removing the THF, ^{1}H and ^{31}P NMR acquired for the crude product assumed to be phosphine **13** (Fig A-37 and A-38). ^{1}H NMR (300 MHz, $CDCl_3$) δ: 7.6-7.2 (m, 1H), 6.8-6.5 (m, 1H), 3.5 (m, overlapping with THF), 1.9 (m, 1H), 1.6-1.1 (m, 1H), 0.9 (m, 1H); ^{31}P NMR (121.4 MHz, $CDCl_3$) δ: 111.3, –4.9, –14.3, –14.9. The ^{31}P NMR showed appreciable impurities at –14, –15 and 111 ppm so purification of this batch was also necessary. The crude product was washed three times with acetonitrile, each time decanting the acetonitrile away from the desired product. ^{31}P NMR showed that the acetonitrile washes removed the impurity at 111 ppm but not those found at –14 and –15 ppm (spectrum not shown). The crude solid that had been washed with acetonitrile was dried *in vacuo* and subsequently dissolved in 25 mL of dichloromethane in a 50 mL roundbottom flask. The crude phosphine **13** in dichloromethane was washed three times with degassed water using air-free techniques. The dichloromethane was then pumped off and the roundbottom flask containing the desired phosphine **13** was left under high N_2 flow overnight in the hopes of evaporating any residual water left from the water wash.

The next day the resultant orange solid was dried *in vacuo* for 1 h and then pumped back in the box for NMR sample preparation; ^{31}P NMR showed the same impurities at –14 and –15 ppm (spectrum not shown) so the air-free water wash did not effectively purify the phosphine **13**.

As solvent washes and water extractions were unsuccessful at purifying the crude phosphine **13**, recrystallization was then attempted in hopes of affording a clean product to be used in polymerization. In the drybox, all of the isolated phosphine **13** from the air-free water wash step was dissolved into about 8 mL of dichloromethane in a 20 mL vial. This vial was placed into a TLC jar which contained about 7 mL of pentane; thus, phosphine **13** was to be purified by pentane diffusing into a dichloromethane solution of the crude product. After 6 d, the dichloromethane was decanted away from a bright orange solid; ^{31}P NMR of this solid showed almost no phosphorous-containing species present in the isolated solid (spectrum not shown). Thus, the dichloromethane was pumped off the decanted layer and the resultant solid was analyzed by ^{31}P NMR. There were *still* impurities in the spectrum of this phosphine **13** especially a prominent resonance –15 ppm (Fig A-39). ^{31}P NMR (121.4 MHz, $CDCl_3$) δ:–4.9, –14.9. No further purification was attempted.

REFERENCES CITED

(1) Sonogashira, K.; Takahashi, S.; Hagihara, N. "A New Extended Chain Polymer, Poly[*trans*-bis(tri-*n*-butylphosphine)platinum 1,4-butadiynediyl]" *Macromolecules* **1977**, *10*.

(2) Nguyen, P.; Gmez-Elipe, P.; Manners, I. "Organometallic Polymers with Transition Metals in the Main Chain" *Chem. Rev.* **1999**, *99*, 1515-1548.

(3) Chiang, C. K.; Heeger, A. J.; MacDiarmid, A. G. "Effect of Uniaxial Stress on Electrical Conductivity of Sulphur Nitride Polymer" *Physical Letters A* **1977**, *60*, 375-377.

(4) Dray, A. E.; Wittmann, F.; Friend, R. H.; Donald, A. M.; Khan, M. S.; Lewis, J.; Johnson, B. F. G. "Structure and Electronic Properties of Transition Metal-Containing Poly-ynes" *Synthetic Metals* **1991**, *41*, 871-874.

(5) Khan, M. S.; Kakkar, A. K.; Long, N. J.; Lewis, J.; Raithby, P.; P., N.; Marder, T. B.; Wittmann, F.; Friend, R. H. "Synthesis and Optical Spectroscopy of Linear Long-Chain Di-terminal Alkynes and Their Pt-σ-acetylide Polymeric Complexes" *J. Mater. Chem.* **1994**, *4*, 1227-1232.

(6) Silverman, E. E.; Cardolaccia, T.; Zhao, X.; Kim, K.-Y.; Haskins-Glusac, K.; Schanze, K. S. "The Triplet State in Pt-Acetylide Oligomers, Polymers and Copolymers" *Coord. Chem. Rev.* **2005**, *249*, 1491-1500.

(7) Wang, Y.; Ranasinghe, M. I.; Goodson III, T. "Ultrafast Fluorescence Investigation of Excitation Energy Transfer in Different Dendritic Core Branched Structures" *J. Am. Chem. Soc.* **2003**, *125*, 9562-9563.

(8) Balema, V. P.; Wiench, J. W.; Pruskia, M.; Pecharsky, V. K. "Solvent-Free Mechanochemical Synthesis of Two Pt complexes: *cis*-$(Ph_3P)_2PtCl_2$ and *cis*-$(Ph_3P)_2PtCO_3$" *Chemical Commun.* **2002**, 1606-1607.

(9) Clarke, M. L.; Ellis, D.; Mason, K. L.; Orpen, A. G.; Pringle, P. G.; Wingad, R. L.; Zahera, D. A.; Baker, R. T. "The Electron-Poor Phosphines $(C_6F_5)_3P$ and $(3,5\text{-}(CF_3)_2C_6H_3)_3P$ Do Not mimic Phosphites as Ligands for Hydroformylation. A Comparision of the Coordination Chemistry of $(C_6F_5)_3P$ and $(3,5\text{-}(CF_3)_2C_6H_3)_3P$ and the Low Hydroformylation Activity of Their Rhodium Complexes" *Dalton Trans.* **2005**, 1294-1130.

(10) Smith, R. C.; Protasiewicz, J. D. "A Trans-Spanning Diphosphine Ligand Based on a *m*-Terphenyl Scaffold and Its Palladium and Nickel Complexes" *Organometallics* **2004**, *23*, 4215-4222.

(11) Friend, R. H.; Gymer, R. W.; Holmes, A. B.; Burroughes, J. H.; Marks, R. N.; Taliana, C.; Bradley, D. D. C.; dos Santos, D. A.; Bredas, J. L.; Logdlund, M.; Salaneck, W. R. "Electroluminescence in Conjugated Polymers" *Nature* **1999**, *397*, 121-128.

(12) Grimsdale, A. C.; Chan, K. L.; Martin, R. E.; Jokisz, P. G.; Holmes, A. B. "Synthesis of Light-Emitting Conjugated Polymers for Applications in Electroluminescent Devices" *Chem. Rev.* **2009**, *109*, 897-1091.

(13) Lee, J.-I.; Kang, I.-N.; Hwang, D.-H.; Shim, H.-K.; Jeoung, S. C.; Kim, D. "Energy Transfer in a Blend of Electroluminescent Polymers" *Chem. Mater.* **1996**, *8*, 1925-1929.

(14) Eckhardt, H.; Shacklette, L. W.; Jen, K. Y.; Elsenbaumer, R. L. "The Electronic and Electrochemical Properties of Poly(phenylenevinylene) and Poly(thienylenevinylenes): An Experimental Study" *J. Chem. Phys.* **1989**, *91*, 1303-1315.

(15) Burroughes, J. H.; Bradley, D. D. C.; Brown, A. R.; Marks, R. N.; Mackay, K.; Friend, R. H.; Burns, P. L.; Holmes, A. B. "Light-emitting Diodes Based on Conjugated Polymers" *Nature* **1990**, *347*, 539-541.

(16) Williams, D. H.; Fleming, I. *Spectroscopic Methods in Organic Chemistry*, Fourth ed.; McGraw-Hill Book Company: UK, 1989.

(17) Lucht, B. L.; St. Onge, N. O. "Synthesis and Characterization of Poly(*p*-phenylenephosphine)s" *Chemical Commun.* **2007**, 2097-2098.

CHAPTER FOUR

SYNTHESIS OF LIGHT-HARVESTING PHOSPHONIUM-BASED POLYELECTROLYTES

4.1 Polyelectrolytes in Modern Technological Applications

Charge transport is an integral process in the operation of photovoltaic and light-emitting devices. Whether excited states are generated by absorption of incident light or electrochemically, the movement of electrons through the device ultimately gives rise to the desired function as discussed in Chapter 1. The current work has thus far focused on conjugated platinum-acetylide type polymers and their potential applicability as superior luminescent materials. However, the successful synthesis of the light-harvesting phosphine (**18**) discussed in Chapter 3 in the context of its utility in metallopolymers led to the subsequent investigation into designing polyelectrolytic polymers using **18** that would offer enhanced conductivity for materials-based applications.

Polyelectrolytes, the subject of the current chapter, are polymers that are charged in some manner. The polymer could have charge that is delocalized over the molecule, or charges could be localized on subunits of the polymer backbone. Only recently within the field of photovoltaics and LEDs have polyelectrolytic materials been studied to understand the effects of charged moieties on the efficiency of these devices.[1-4] However, the ionic nature of these polymers seems to imply that under optimal operating conditions, the polyelectrolytes will promise enhanced charge transport since doped polymers (charge added) often experience more efficient charge mobility in LED devices.[5] Moreover, we intend to discern whether the layering of oppositely charged polyionic species can afford additional conductivity.

Recently, the technique of depositing polyionic species by way of solution-driven adsorption has become of great interest.[6] In this method, the polyelectrolytes (often water-soluble) are deposited on a substrate either by simply soaking it in the aqueous polyion or by some electrochemical process. However, the soaking technique is more efficient because there is no need to ensure 100% reaction completion as is the case with electrochemical deposition. In this layer-by-layer (LBL) composite film construction, the substrate is usually a charged species (chemically treated glass or quartz), and the first layer (consisting of the oppositely charged polyion) is adsorbed to it by deposition from an aqueous solution.[7] After an adequate drying period has elapsed, the monolayer can be subjected to conventional analytical techniques (absorption and fluorescence spectroscopy, cyclic voltammetry, etc.) depending on which bilayer properties are of interest to the researcher. The monolayer-coated substrate is rinsed to remove any debris and then soaked in the counterionic polyelectrolyte solution to adsorb the oppositely charged component of the bilayer assembly. Characterization is then performed for the composite film generated by this first LBL deposition and the process is repeated until the desired number of bilayers have been deposited. It is important to note that the layer thickness is not always consistent for the first few (~10) layers owing to imperfections in the substrate. As a result, there can be uneven coating of the first polyelectrolyte film on the substrate, which leads to significant roughness. In addition, inefficient coating of the substrate can occur owing to the less than ideal film-coating properties of the polyelectrolyte; this also results in roughness of the first few layers in the LBL deposition process. This roughness is propagated through the next deposition step because the oppositely charged polyion solution will fill the "holes" with more material than where

the previously-deposited monolayer forms a flat coating of the substrate. As a result, the first ~10 bilayers can be characterized by inconsistent photophysical data. Generally, a $\leq$ 10 bilayer coating effectively smoothes substrate imperfections, so that very uniform, smooth films can be deposited subsequently by the LBL technique.

An early investigation into bilayer construction was focused on adsorbing a polyanionic species to a positively charged substrate (aminopropylsilanized quartz or glass) followed by depositing counterionic polymers.[8] In this study, the bilayers that formed between a polystyrenesulfonate anionic polymer (**P1**) and an ammonium-containing cationic polymer (**P3**) were studied (Figure 4.1). In order to form the counterionic bilayers, quartz or silicon crystals were positively charged and then submersed in a solution of **P1** for initial adsorption. After rinsing with water, the oppositely charged **P3** was deposited and this process was repeated until the desired number of bilayers (~40) had been deposited.

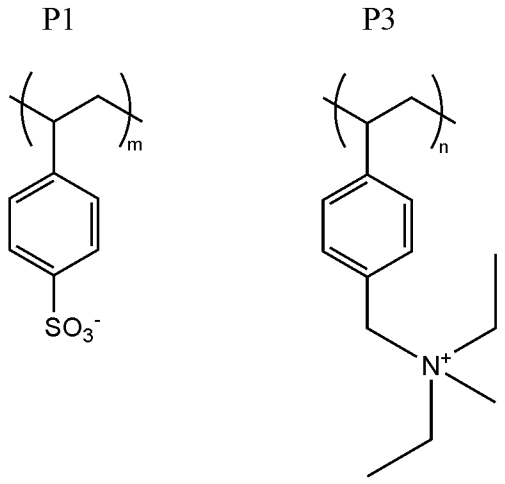

Figure 4.1. Polystrenesulfonate anionic polymer (**P1**) and polystyreneammonium cationic polymer (**P3**) used in one of the initial polyionic bilayer studies.

Absorption spectroscopy and small angle X-ray scattering (SAXS) were the primary methods for tracking bilayer formation of **P1** with **P3**; after each new layer was deposited, an absorption spectrum showed little change in the wavelength of maximum absorbance but an increase in absorbance intensity. More specifically, after 38 layers were deposited in this manner, the absorption data showed an increase in intensity of about 0.005 per layer adsorbed. Moreover, because the absorption spectra for each polyionic species showed similar absorbance maxima (~255 nm), there was no significant shift in the absorbance maximum throughout the layering process. As discussed before, the thickness of the deposited films can vary significantly within the first few bilayer assemblies; therefore, in this study, the composite film thickness was tracked using SAXS to discern whether the LBL deposition yielded bilayer assemblies with consistent thickness. Using this technique, the authors find that each bilayer thickness is roughly 2.27 nm with little variation and the entire 39 layer composite film has a thickness of 43.5 nm. These results demonstrate that oppositely charged polyions can be deposited onto a substrate and stack in such a way that the counterions form bilayers of the same thickness owing to favorable electrostatic interactions between the polyelectrolytes.

While the above study was crucial in demonstrating that polyelectrolytes could be extensively layered after initial deposition on a substrate, it did not address counterionic polymeric species with different photophysical parameters. The novelty in the bilayer formation lies in the fact that polyions with very different absorption and emission behaviors can be layered to effect materials with truly unique photophysical characteristics. Bilayers comprised of two polyelectrolytes having different absorption profiles will serve to broaden the absorption peak of the composite film, a beneficial

property for photovoltaic devices. Moreover, the consequent broadening can also be exploited to produce light-emitting materials with tailored emission profiles, notably for white lighting.

A recent study demonstrated a red-shift of the absorbance properties of an organic conjugated polyelectrolyte (HPURET) upon layering it with a nonconjugated counterionic polymeric material (PDADMAC) (Figure 4.2).[9] The absorption spectra collected throughout the layering process shows a gradual shift in the wavelength of maximum absorbance from about 420 nm to 450 nm as the number of bilayers increases to ten. Not only is the absorbance red-shifted, but it also broadens as more bilayers accumulate. Thus, even addition of a counterionic polymer lacking any significant optical signature of its own can alter the photophysics of an optically active polyelectrolyte by exerting conformational and environmental influences.

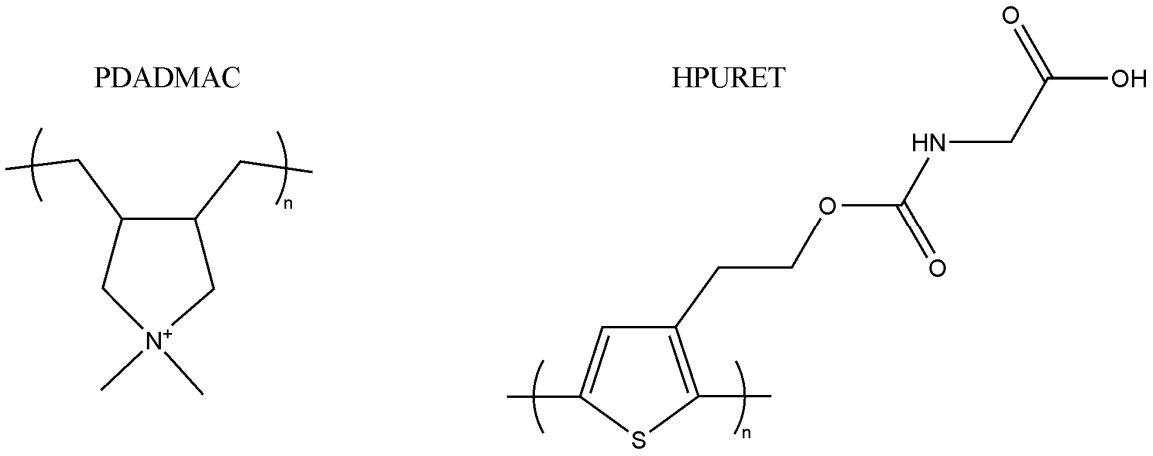

Figure 4.2. Polyelectrolytes PDADMAC and HPURET.

Clearly the formation of bilayers from oppositely charged polyelectrolytes has interesting effects on the photophysical behavior of the material, especially the absorbance. However, counterion interactions can also have profound influences on the

conductivity of the bilayered material. For example, a recent study examined the effects of layering highly-conjugated electrolytes to afford more conductive materials to be used in photovoltaics.[10] In this work, a sulfonate electrolyte (PSO_3^-) was combined with an ammonium-based electrolyte ($PNMe_3^+$) in a bilayer fashion and its photophysical properties and conductivity were studied (Figure 4.3).

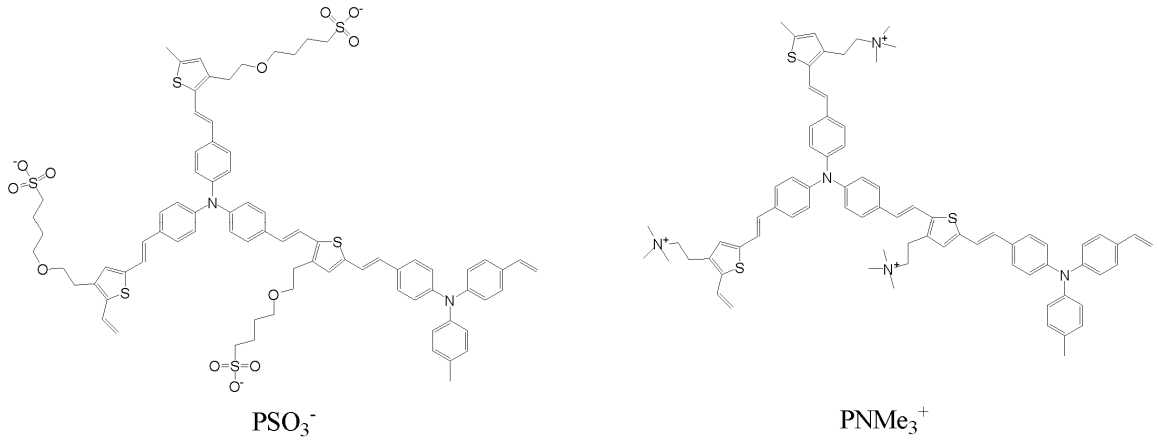

Figure 4.3. Structured for highly-conjugated PSO_3^- and $PNMe_3^+$ electrolytes.

No absorption or emission studies were carried out on PSO_3^- and $PNMe_3^+$ bilayers in this study. However, the photophysical parameters for each molecule were presented in solutions of both methanol (λ_{max} 405 nm for PSO_3^- and 447 nm $PNMe_3^+$) and water (λ_{max} 405 nm for PSO_3^- and 425 nm for $PNMe_3^+$). The emission parameters in the same solvents were also reported but were not of particular interest because these materials are targeted for solar cell applications. The interesting finding of this study is that incident photon to electron conversion efficiencies (IPCE) for each of PSO_3^- and $PNMe_3^+$ were measured separately as well as after they had been assembled in a bilayer. Alone, the polyelectrolytes had IPCE values of 37% and 38% for PSO_3^- and $PNMe_3^+$, respectively. However, after layer by layer deposition starting with a $PNMe_3^+$ base layer,

the IPCE value is 44%. In addition, when the anionic polymer is deposited first to form the bilayer the IPCE further increases up to 55%. Thus, the favorable electrostatic interactions between the polyelectrolyte molecules increase the efficiency with which the device converts harvested incident light into necessary charge transport that will be later used as electricity in a solar cell. Furthermore, the initial layer that forms the direct interface with the electrode also exerts a profound influence on charge injection.

The extensive interest in polyelectrolytes as elements of high performance devices led us to examine the effects of forming similar bilayers with a phosphonium-based polymer derived from phosphine **18** detailed in Chapter 3 (Scheme 4.1). More specifically, employing a simple nucleophilic substitution reaction (S_N2) between the phosphine **18** and a wide variety of primarily alkyl dibromides affords the polyelectrolytic phosphonium polymer.

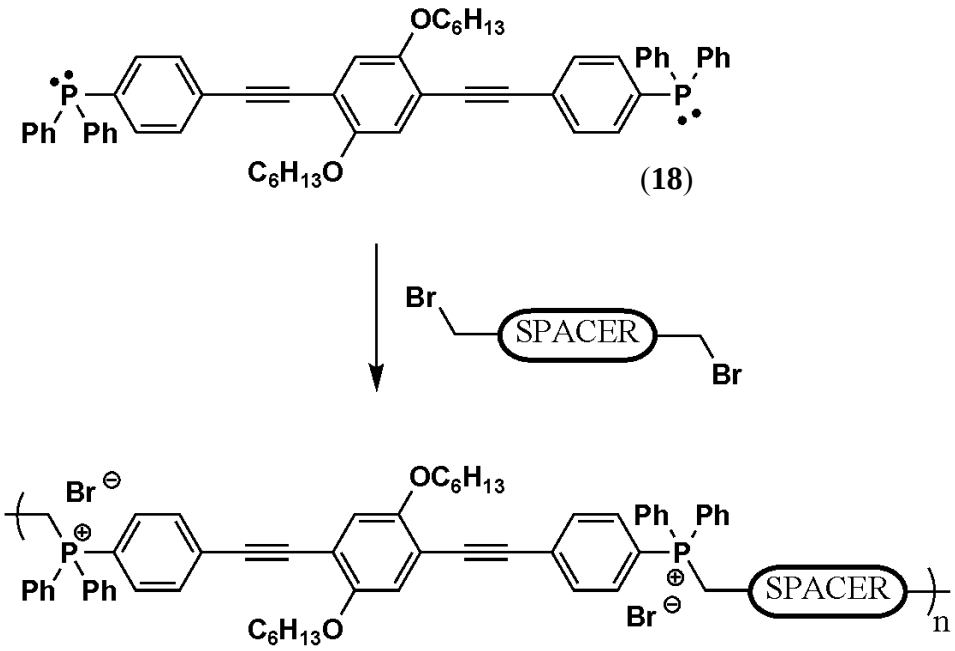

Scheme 4.1. General scheme for synthesis of phosphonium-based polyelectrolyte.

The spacer used in this general polymerization can be chosen based on the desired applications for the synthesized polymer. Because the spacer is not included in the effective conjugation length of the polymer backbone, it may not significantly affect absorption and emission properties of the polyelectrolytes unless it is chromophoric itself. However, the spacer can serve to enhance the solubility of the resultant polycation and may influence morphology, physical strength and film-forming ability. Moreover, long alkyl chains offer the potential to synthesize rod-coil polymers that may have interesting liquid crystalline properties. A wide variety of spacers will be tested to determine the effects of the linker identity on the solubility, photophysical behavior and conductivity of the phosphonium polymer (Scheme 4.2).

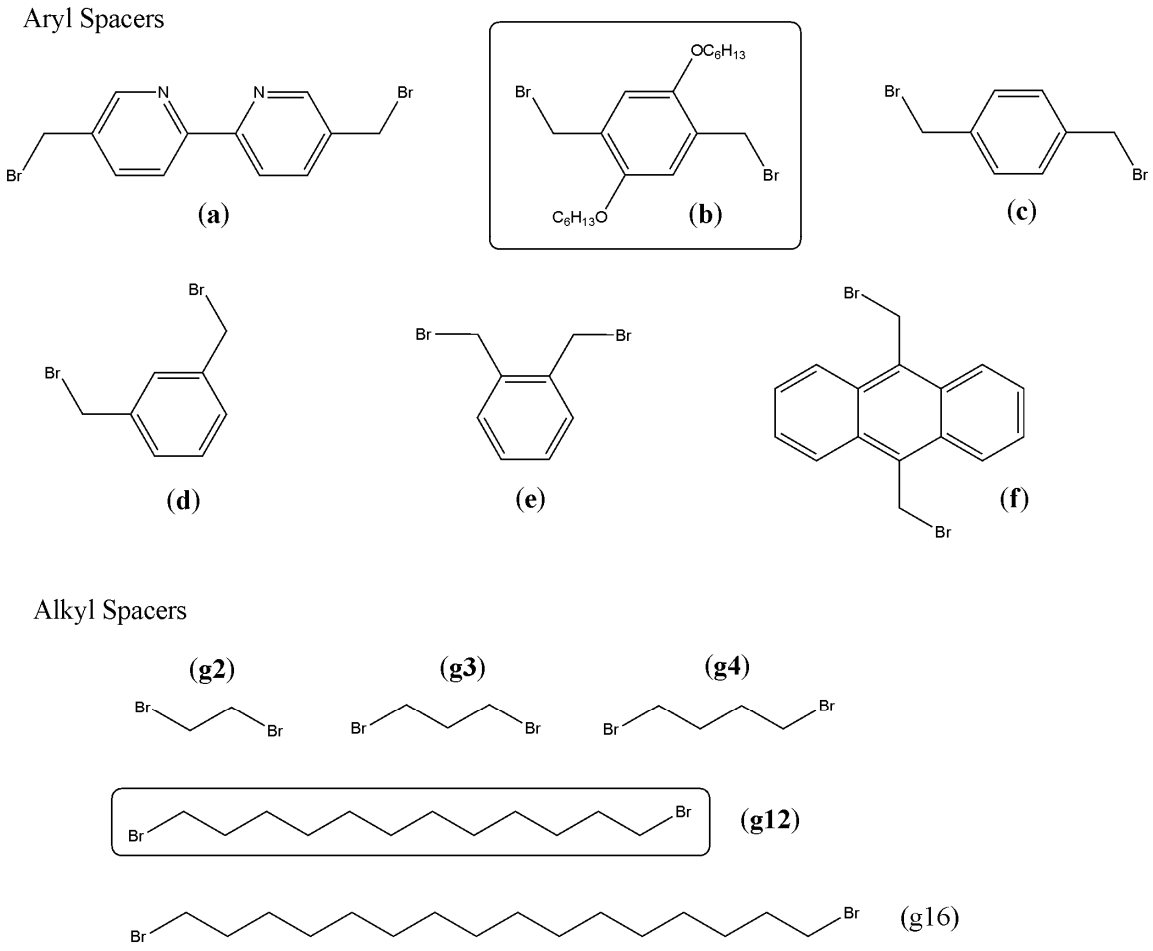

Scheme 4.2. Dibromo materials to be used in the polymerization to afford the analogous phosphonium-based polymers; boxed compounds have been used to generate polyelectrolytes that are specifically discussed in the current work.

It is of particular interest, once the desired polymer has been isolated and purified, to examine its solubility and photophysical characteristics. More importantly, these polycationic molecules will be used in bilayer studies to determine the effect of electrostatic interactions within the layers on absorption and emission maxima and intensities. Two polymers have been targeted for initial synthesis: those using the dihexyloxybenzene (**b**) and dodecyl (**g12**) spacers (Scheme 4.2). Bilayer studies on the

dihexyloxybenzene-based phosphonium polymer with poly(acrylic acid) and sodium poly[2-(3-thienyl)ethyloxy-4-butylsulfonate] will also be detailed.

4.2 Polyelectrolytic Phosphonium-Based Hexyloxybenzene Polymer LHP1-OHx

Synthesis of the phosphonium-based polymer (**LHP1-OHx**) with the dihexyloxybenzene spacer **b** proceeds via an S_N2 reaction at 100 °C in *N*,*N*-dimethylformamide (Scheme 4.3).

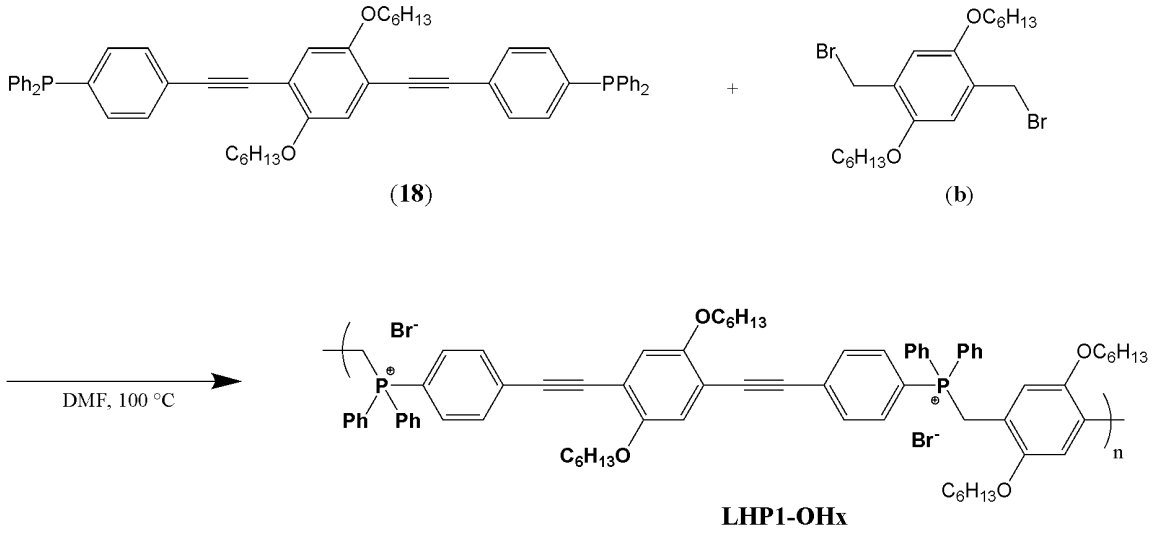

Scheme 4.3. Synthesis of polymer **LHP1-OHx**.

LHP1-OHx is relatively easy to synthesize once phosphine **18** is isolated and purified (see Chapter 3 for details on synthesis of **18**). This polycation is an extremely well-behaved polymer which forms glassy orange free-standing films. **LHP1-OHx** is soluble in a wide variety of organic solvents including acetonitrile, chloroform and dichloromethane and can even be solubilized in water in the presence of an appropriate surfactant, such as sodium dodecyl sulfate (SDS).

The absorption spectrum of **LHP1-OHx** in acetonitrile exhibits two bands at 319.5 and 389.5 nm. The higher energy absorbance likely corresponds to a PAr_3-centered

π→π* transition, while the lower energy absorbance is attributable to the π→π* transition of the **LHP1**-derived mesogen. On the basis of the onset of absorption, the optical band gap of **LHP1-OHx** is estimated at 2.7 eV; this band gap is on the order of many useful OCPs used for light-emitting and conducting devices (Chapter 1) and is slightly lower than the platinum-containing metallopolymer discussed in Chapter 3. Excitation of **LHP1-OHx** at 390 nm yields a broad luminescence peak with a maximum of ~491 nm and a quantum yield of 0.17 in acetonitrile. In dichloromethane, the photoluminescence quantum yield of **LHP1-OHx** is 0.21 after excitation at 390 nm.

Especially interesting is the fact that the **LHP1-OHx** polycation shows significant photoluminescence solvatochromism depending on the solvent used for sample preparation (Figure 4.4).

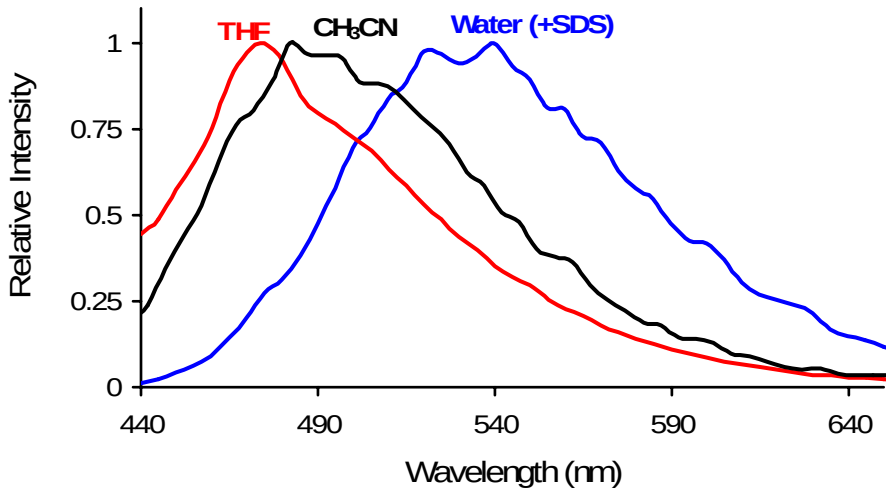

Figure 4.4. Photoluminescence data for **LHP1-OHx** in solvents of increasing polarity.

Figure 4.4 illustrates that as the polarity of the solvent increases, the photoluminescence emission progressively red-shifts. Solvatochromism occurs due to a difference in solvation-mediated stabilization of the ground versus excited state of a

molecule.[11] The extent of the stabilization depends on the dipole moment and polarizability of the chromophore (Figure 4.5).

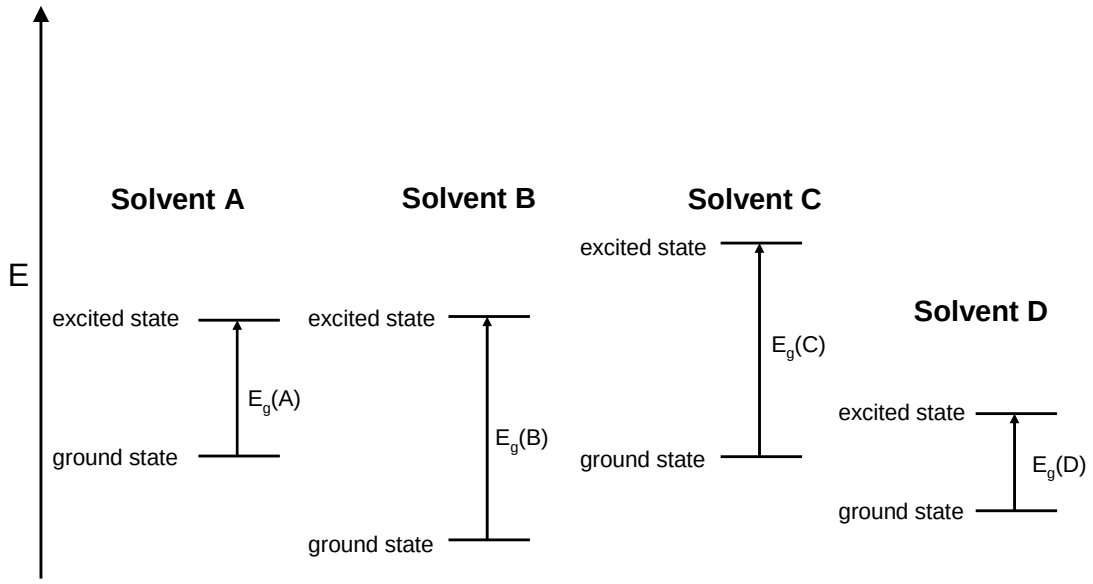

Figure 4.5. Differing energy levels for ground and excited state of a molecule depending on the solvent; note that the solvent can preferentially stabilize the ground or excited state relative to each other or can stabilize both.

Solvatochromic effects can thus elucidate some important information about the nature of the excited state of **LHP1-OHx**. The red-shifting implies that the excited state becomes increasingly more stabilized *relative* to the ground state. Moreover, that the quantum yield decreases (Φ = 17% in acetonitrile versus Φ = 21% in dichloromethane) as the solvent polarity increases is expected because solvent-mediated excited state stabilization leads to more viable nonradiative decay pathways. Therefore, it appears that the excited state of **LHP1-OHx** is more polar and/or polarizable than the ground state since increasing the solvent polarity red-shifts the photoluminescence emission and decreases the overall photoluminescence quantum yield.

The fact that **LHP1-OHx** was soluble in water with SDS prompted an interest to investigate its ability to form aggregates in solvated form. Thus, the photoluminescence of **LHP1-OHx** was examined in environments with 0, 0.5, 1 and 2 times the critical micelle concentration (cmc) of SDS (cmc = 8 mM) (Figure 4.6).

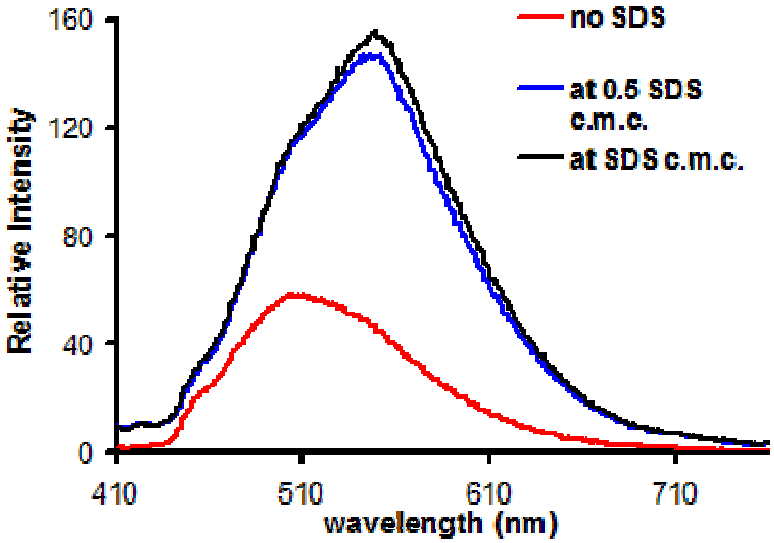

Figure 4.6. Critical micelle concentration study of **LHP1-OHx** with SDS as followed by fluorescence spectroscopy; traces shown do not include that for twice the cmc of SDS.

The above figure demonstrates that increasing [SDS] from 0 to 0.5 cmc causes a red-shift in the photoluminescence of **LHP1-OHx** from 510 to 550 nm with a concomitant and significant increase in intensity. However, no additional notable change results when [SDS] is increased from 0.5 cmc to the cmc of SDS. These results suggest that the change in photophysical behavior is not a result of SDS micelle formation, but rather due to the ionic strength of the solution, a hypothesis consistent with the observation that λ_{em} progressively red-shifts as solvent polarity increases (Figure 4.4).

4.3 Utility of Light-Harvesting Phosphonium Polyelectrolytes in Layer-by-Layer Film Deposition

The charged nature of **LHP1-OHx** suggests its potential for favorable intermolecular interactions with other polyelectrolytes to affect the photophysical behavior of the resultant multicomponent materials. We envisioned, for example, that composite films could be cast in which **LHP1-OHx** would engage in intermolecular excited state energy transfer (fluorescence resonance energy transfer—FRET) to afford unique and efficient light-harvesting and light-emitting materials. Our initial studies on **LHP1-OHx** for bilayer assemblies involved alternate coating of a glass substrate with **LHP1-OHx** from acetonitrile and poly(acrylic acid) (PAA) from water maintained at pH = 4 (Figure 4.7). The **LHP1-OHx** layer was first deposited followed by the PAA in the bilayer assembly construction process.

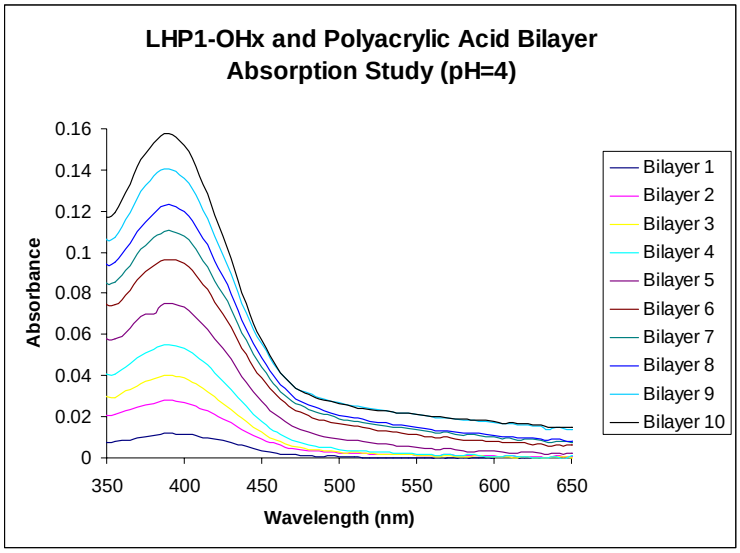

Figure 4.7. Bilayer study of **LHP1-OHx** and poly(acrylic acid) as followed by absorption spectroscopy.

The layering process between the cationic **LHP1-OHx** and (protonated) poly(acrylic acid) did not yield any changes in the wavelength of maximum absorbance with bilayers one and ten both exhibiting an absorption maximum of 390 nm. As expected, though, there is an increase in absorbance as the number of layers is increased. A plot of the maximum absorbance intensity versus number of layers reveals a linear relationship (Figure 4.8). The magnitude of the absorbance increase with each bilayer was as expected on the basis of related bilayer assemblies.[9] Specifically, each bilayer leads to an increase in absorbance intensity of 0.008 units, similar to the absorbance increase of 0.005 units per bilayer observed for **P1**/**P3** bilayer assemblies discussed in Section 4.1.[8]

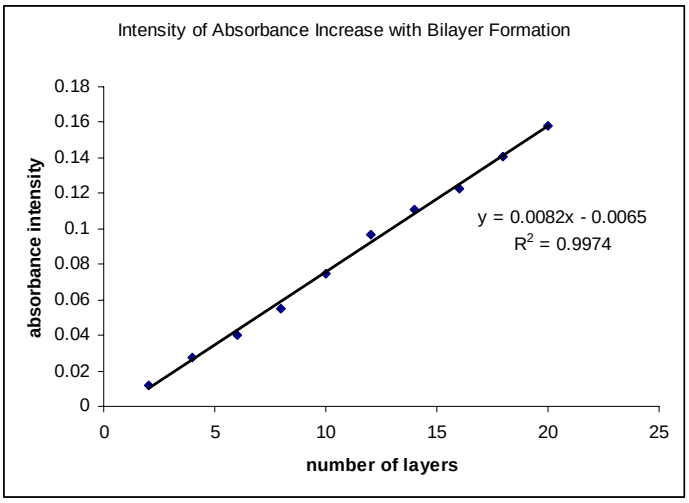

Figure 4.8. Plot of number of layers versus intensity of absorbance maximum from the **LHP1-OHx**/PAA bilayer study at pH = 4.

Many layer-by-layer (LBL) studies do not show a linear relationship between absorbance and layer number over the first ~10 layers due to imperfections in these first few bilayer coating steps.[7] That our system is linear over the entire range indicates

outstanding LBL deposition behavior and efficiency. These results also imply that each additional monolayer, whether it is **LHP1-OHx** or PAA, interacts with the previously deposited top layer in the same way for every deposition step. As a result, the conformational changes that occur upon bilayer assembly between **LHP1-OHx** and PAA at pH = 4 are consistent and seemingly irreversible even upon exposure to solvents of very different dielectric constants (in this case, water and acetonitrile).

Since the initial **LHP1-OHx**/PAA bilayer study was conducted at a pH of 4, the carboxylic acid moieties of PAA remained protonated. It was of interest to examine how the LBL process would change when the same bilayer assembly was carried out between PAA and **LHP1-OHx** at pH = 13, where PAA would be deprotonated to an anionic species (Figure 4.9).

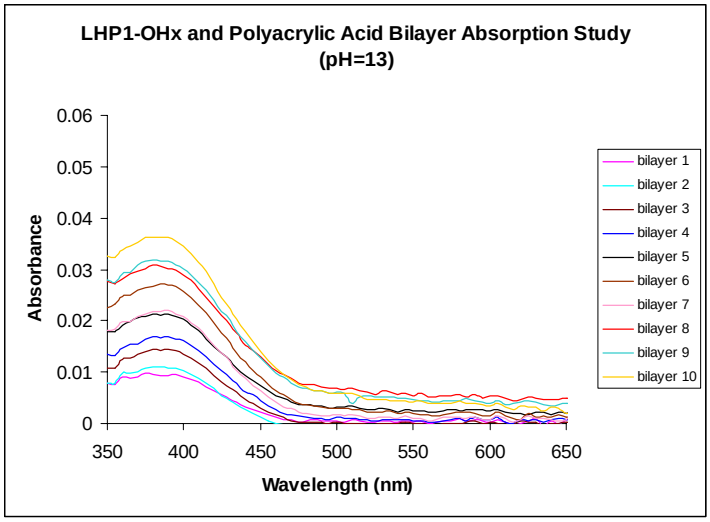

Figure 4.9. Bilayer study of **LHP1-OHx** and poly(acrylic acid) as followed by absorption spectroscopy at pH = 13.

The absorption maxima of bilayers formed between deprotonated PAA and **LHP1-OHx** exhibited the same λ_{max} as those cast at pH = 4, and again there was no

significant shift in the wavelength of maximum absorbance from the first bilayer to the tenth bilayer. Again, a relatively linear relationship was observed between the number of bilayers and the absorbance (Figure 4.10).

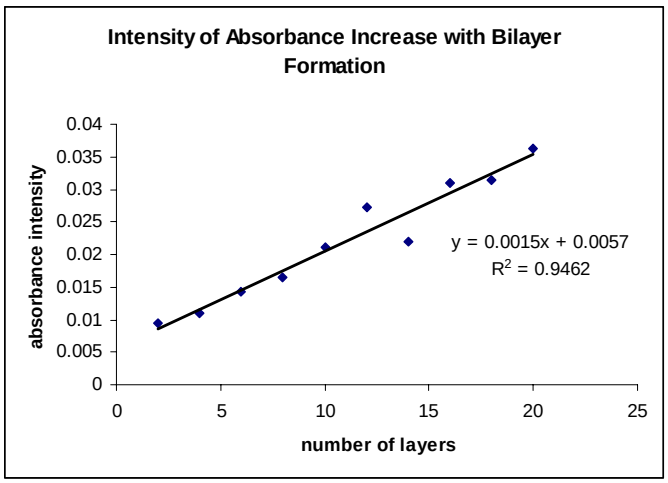

Figure 4.10. Plot of number of layers versus intensity of absorbance maximum from the **LHP1-OHx**/PAA bilayer study at pH = 13.

One difference observed between the pH = 4 and pH = 13 studies was that the absorbance intensity increase per layer was much lower in the pH = 13 **LHP1-OHx**/PAA bilayer study (Figure 4.10). There was also some inconsistency in the absorbance intensity throughout the study, possibly due to salt deposition on the substrate from the NaOH that was added to the PAA solution to bring it to a pH of 13. Moreover, because it has been shown that **LHP1-OHx** is soluble in basic water (with added SDS), it is possible that the basic PAA solution could erode some of the previously-deposited **LHP1-OHx** layers.

Because the absorption data for the **LHP1-OHx**/PAA indicated well-behaved, uniform film-forming qualities, the photoluminescence of the bilayer assemblies was also examined using the pH = 4 PAA solution (Figure 4.11).

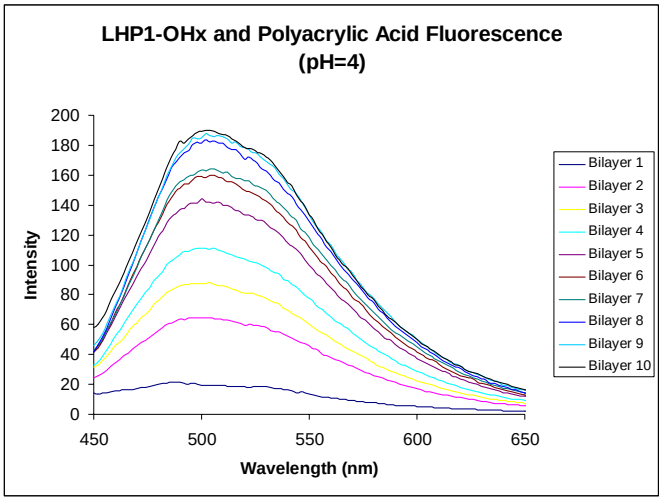

Figure 4.11. Bilayer study of **LHP1-OHx** and PAA as followed by fluorescence spectroscopy.

The photoluminescence data show only a negligible red-shifting of about 10 nm between bilayers one and twenty. This result seems promising for light-emitting devices that require a green emission wavelength. Examination of the photoluminescence intensity increase as the number of layers increase shows a leveling off of intensity enhancement (Figure 4.12). This could be due to an internal quenching of films with increased thickness because, above bilayer 12, the absorbance is greater than 0.1 (Figure 4.7).

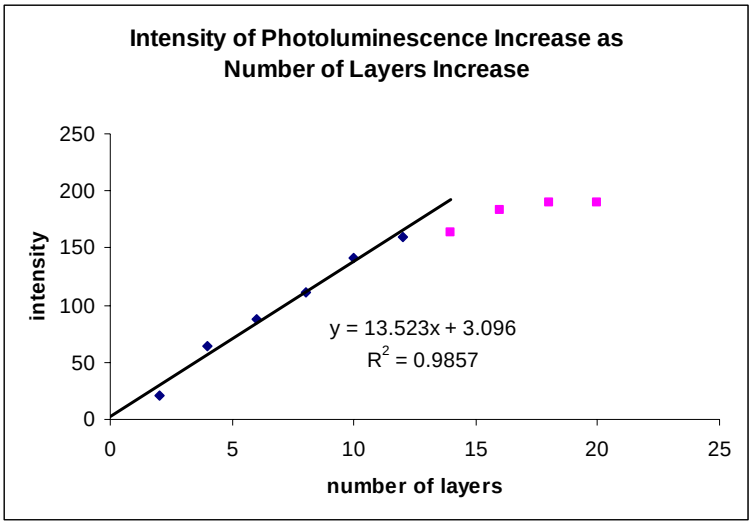

Figure 4.12. Plot of number of layers versus intensity of photoluminescence maximum from the **LHP1-OHx**/PAA bilayer study at pH = 4.

This data treatment demonstrates that with each additional layer deposited, the photoluminescence intensity increases by about 9.2; however, the data series does not follow a linear trend. However, linear regression through twelve bilayers shows a much better fit ($R^2 = 0.986$). It should be noted that a sample with absorbance ≥ 0.1 is subject to internal quenching (*vide supra*) or inner filter effects from the fluorimeter. Examination of the above bilayer assembly photoluminescence data in Figure 4.12 shows that at about the twelfth bilayer, the intensity begins to level off to yield a hyperbolic plot. This is to be expected because the absorbance of the composite film at bilayer twelve is around 0.1 and so any additional bilayer depositions are subject to the aforementioned internal quenching. The data also shows a red-shifting in the photoluminescence as the number of bilayer assemblies accumulates.

Having demonstrated that **LHP1-OHx** is a superior participant in LBL film assembly, it was of interest to probe bilayer formation between **LHP1-OHx** and an

optically active anionic polyelectrolyte. Thus, under basic conditions, bilayer assemblies were constructed in the same manner as before between **LHP1-OHx** and sodium poly[2-(3-thienyl)ethyloxy-4-butylsulfonate] (PTP), a commercially available anionic organic conjugated polymer (Figure 4.13).

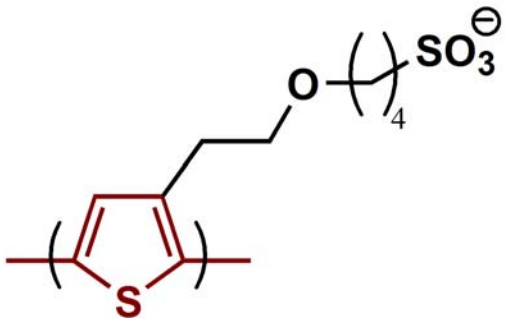

Figure 4.13. Structure of optically active anionic PTP polyelectrolyte to be used in bilayer formation with **LHP1-OHx**.

Absorption data for the **LHP1-OHx** and PTP bilayers show a moderate shift in the wavelength of maximum absorbance as the number of layers increases (Fig 4.14).

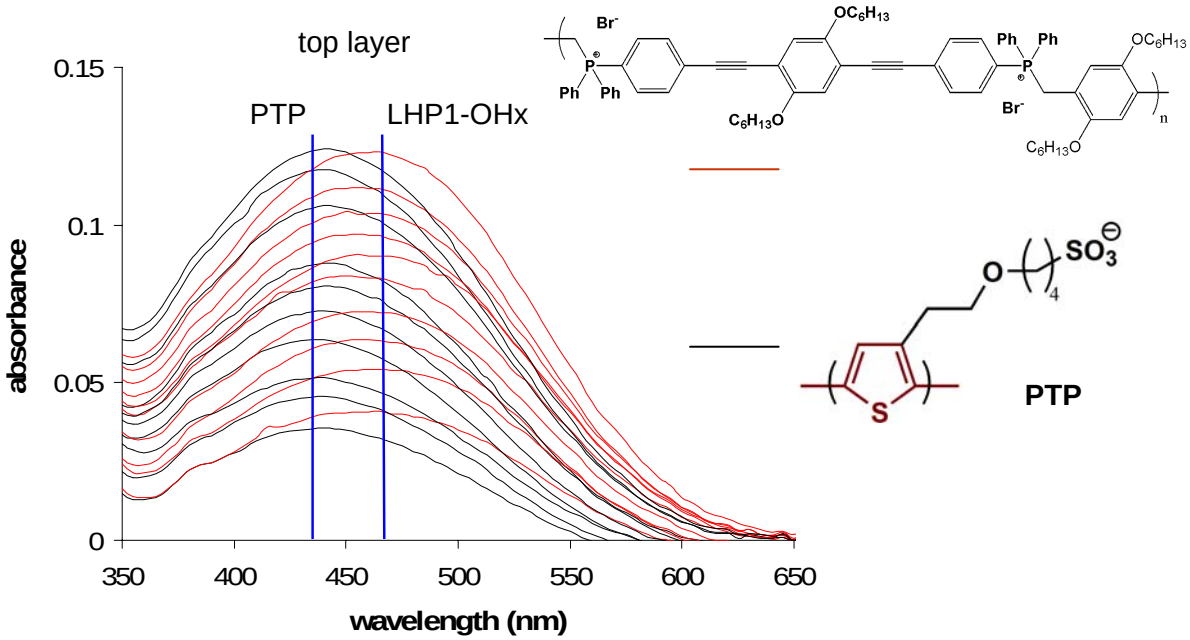

Figure 4.14. Bilayer assemblies of **LHP1-OHx** and PAA as followed by absorption spectroscopy with annotation to show which polelectrolyte is the top layer.

The striking inconsistency in the absorbance intensity as the number of bilayers deposited increases is not that unusual since there can be imperfections in the monolayer thickness and morphology for the first several deposition steps (*vide supra*). These results may also suggest that the PTP is not as ideal of a colayer component with **LHP1-OHx** as was PAA. The most interesting observation, however, is that the layer deposition appears to effect conformational changes in the assemblies depending on which polyelectrolyte is the top layer.

Figure 4.14 shows that when the PTP is the top layer in the assembly, the wavelength of maximum absorbance (434 nm) is significantly blue-shifted by 30 nm as

compared to when the **LHP1-OHx** is on top (λ_{max} = 464 nm). These results imply that there is a reversible conformational change in one of the polyelectrolytes (likely the PTP) that occurs when the other polyion is deposited, and that these conformational changes are propagated through all previously-deposited layers. This could be due to the different solvent systems (**LHP1-OHx** layer casted from acetonitrile while PTP is casted from water) forcing the PTP to assume different conformations depending on whether the **LHP1-OHx** is present on top. Future studies are needed to fully characterize and rationalize the conformational changes occurring during the deposition process. Tunneling electron or atomic force microscopy are potential methods to discern the morphology of these polyions in film form.

4.4 Other Polyelectrolytic Phosphonium-Based Polymers with Aromatic Spacers

The initial synthesis of **LHP1-OHx** was promising in that it showed that a polyelectrolytic phosphonium-based polymer could be made easily via a simple S_N2 between a primary alkyl bromide and phosphine **18**. Other aryl and aromatic spacers were then attempted to be incorporated into the polymer backbone; more specifically, phosphonium based polymers were synthesized using *o*-xylyl (Scheme 4.4) and bipyridine (Scheme 4.5) spacers.

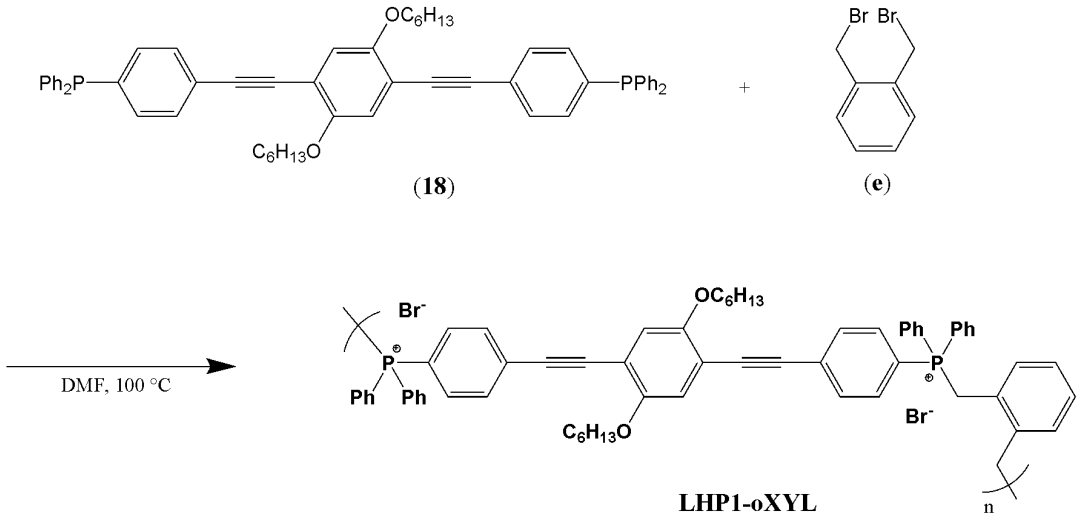

Scheme 4.4. Synthesis of **LHP1-oXYL**.

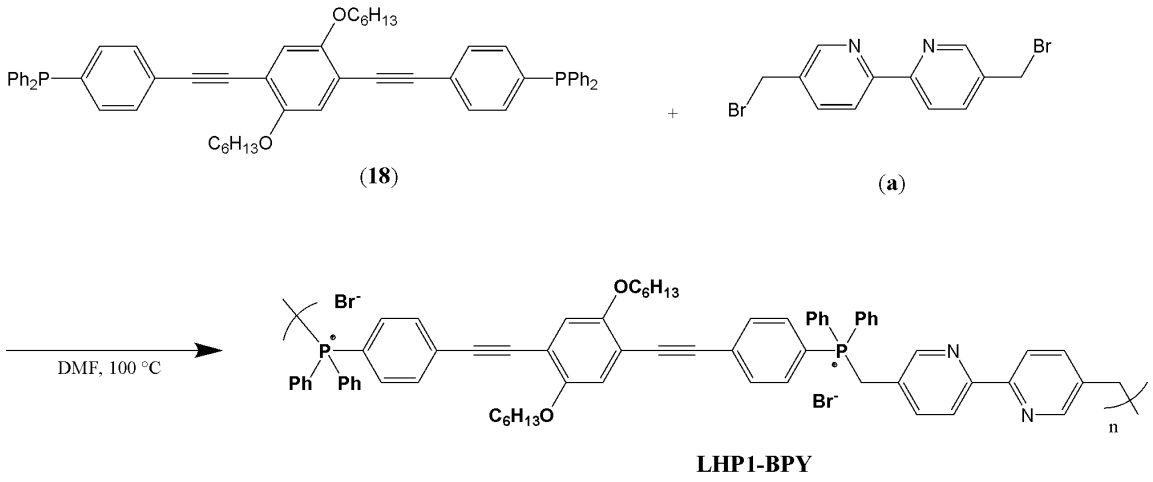

Scheme 4.5. Synthesis of **LHP1-BPY**.

The incorporation of xylyl and bipyridine spacers into the phosphonium-based polyelectrolyte is aimed at determining the effects of the linker on the photophysical and morphological properties of the polymer.

Results and Discussion

Currently, little characterization of the **LHP1-oXYL** and **LHP1-BPY** polymers has been performed owing to their limited solubility in a variety of organic solvents and less than well defined NMR spectra. The **LHP1-BPY** polyelectrolyte was completely insoluble in chloroform, diethyl ether and only slightly soluble in dimethylsulfoxide while the **LHP1-oXYL** was soluble in chloroform; however, both polymers demonstrated ^{31}P NMR spectra other than expected. Ideally, the ^{31}P NMR should show one broad resonance with perhaps a very small peak correlated with end group phosphorous atoms. Broadening in NMR can be indicative of slow tumbling motion (true for large molecules such as polymers) or of closely related chemical shifts grouped together to give the appearance of one broad peak (also true for atoms within a polymeric backbone). The ^{31}P NMR for the **LHP1-oXYL** shows five sharp peaks, one of which corresponding to oxidized phosphine **18**. It is possible that the polymerization did not proceed to completion due to solubility issues. However, the ^{31}P NMR spectrum of the **LHP1-BPY** polymer is promising (Figure 4.15); this spectrum shows a somewhat broad resonance at 24.0 ppm and a much smaller peak at 25.8 ppm.

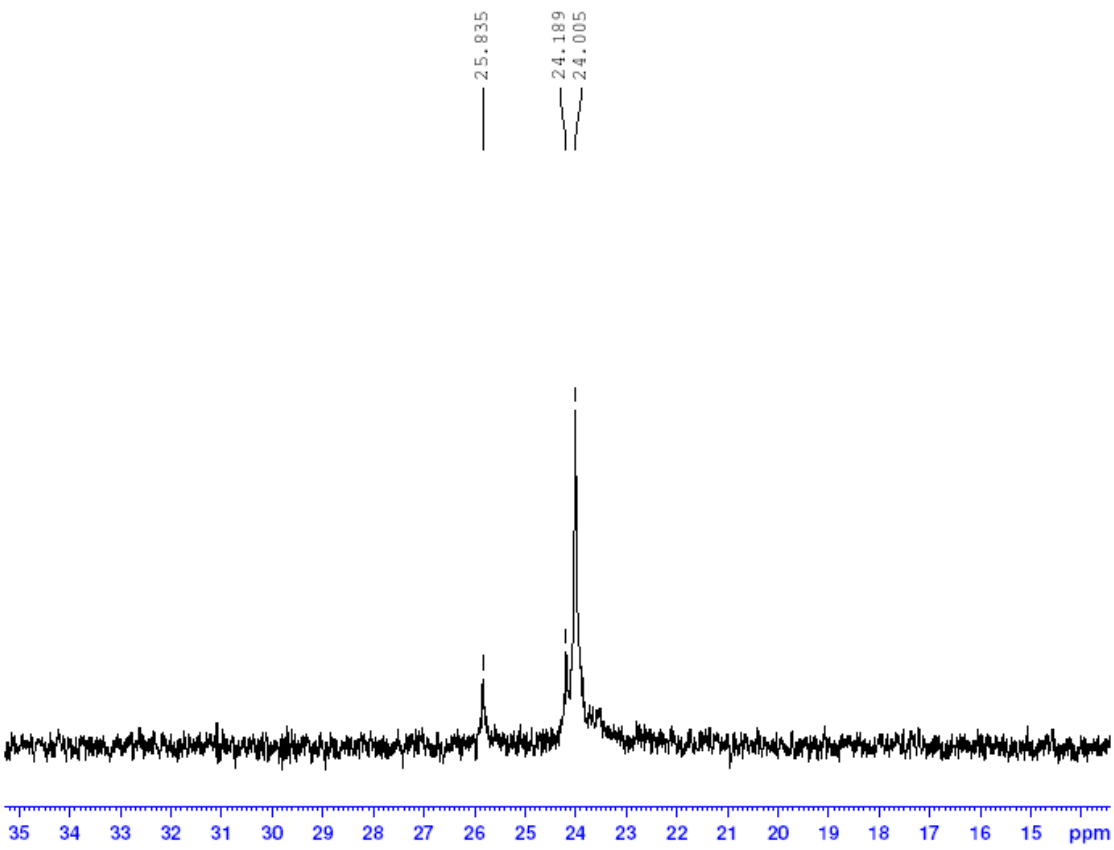

Figure 4.15. Phosphorous-31 NMR spectrum of **LHP1-BPY**.

The smaller, more upfield peak is attributable to end-group phosphorous atoms. However, the fact that the **LHP1-BPY** is insoluble in most organic solvents and water makes it difficult to carry out photophysical studies similar to those performed on **LHP1-OHx**.

4.5 Polyelectrolytic Phosphonium-Based Dodecyl Polymer LHP1-DOD

Having demonstrated that a phosphonium-based polyelectrolyte could be made with aryl-type spacers but that some significant solubility issues arise in the absence of solubilizing units on the spacers, it became of interest to make phosphonium polyelectrolyes with alkyl-type spacers to afford enhanced solubility. The cationic

polymer (**LHP1-DOD**) was thus made using 1,12-dibromododecane (**g12**) as the dibromide monomer to incorporate the dodecyl group in the polymeric backbone (Scheme 4.6).

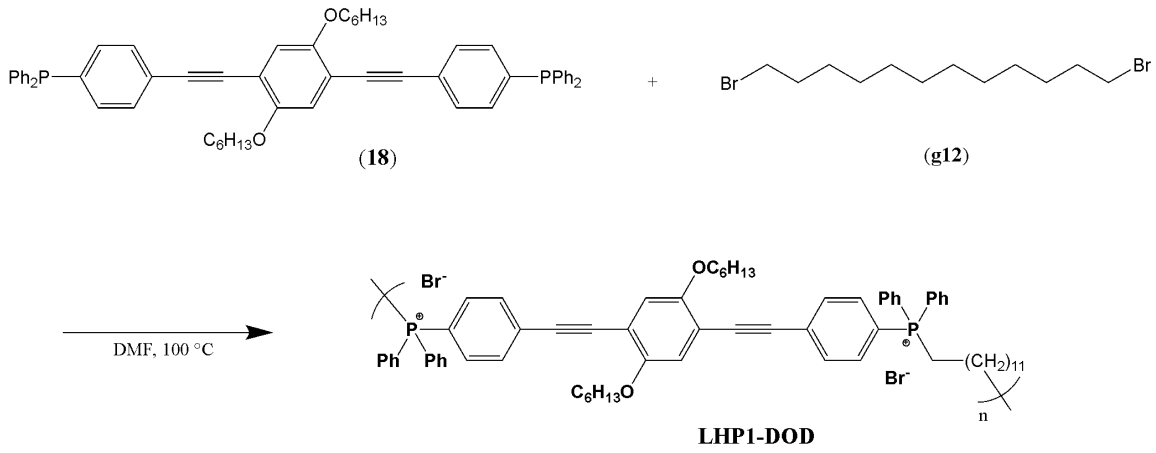

Scheme 4.6. Synthesis of **LHP1-DOD**.

Results and Discussion

Initial synthetic attempts at **LHP1-DOD** employed the use of 2.1 equiv of 1,12-dibromododecane to drive the reaction towards completion at 80 °C. This was performed because NMR spectral data indicated no polymerization had proceeded after 3 d heating with 1.1 equiv of the alkyl dibromide. Even after the second equiv of 1,12-dibromododecane, ^{1}H and ^{31}P NMR demonstrated that polymerization had not yet occurred and so the reaction mixture was taken up again in DMF and heated to 100 °C. The ^{1}H and ^{31}P NMR analysis of the **LHP1-DOD** product reveals that dimerization is achieved under the current reaction conditions, as expected from the stoichiometry. Especially telling are the relative integrations of the aromatic to aliphatic resonances for **LHP1-DOD**; this would be 30:48, aromatic to aliphatic respectively, if the polymer were

the isolated product. However, the relative integrations seen in the ^{1}H NMR are roughly 30:70, which is consistent with formation of the **LHP1-DOD** dimer (Figure 4.15).

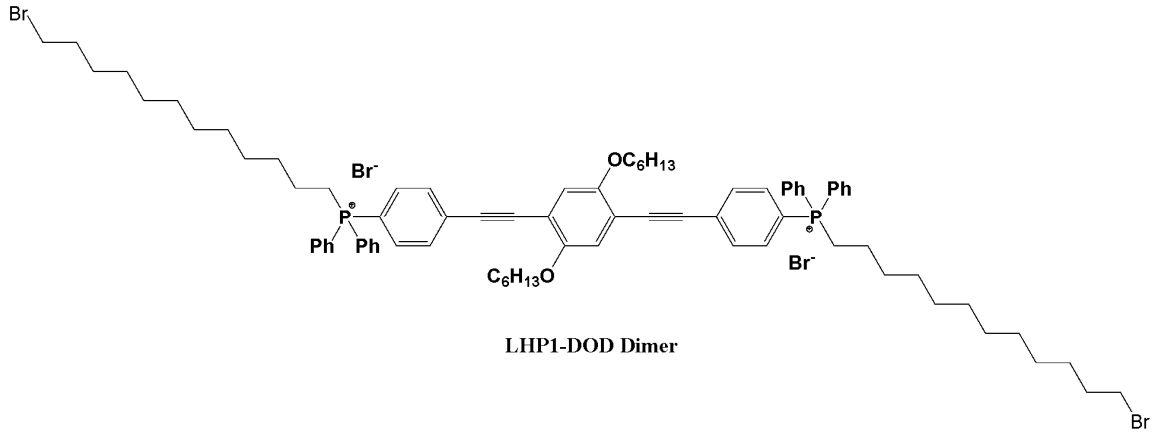

Figure 4.15. **LHP1-DOD** dimer isolated from the polymerization reaction between phosphine **18** and 1,12-dibromododecane (**g12**).

The facile formation of the **LHP1-DOD** dimer suggests that the synthesis could be easily altered to afford the desired polymer. It appears that if the reaction is performed at 100 °C, polymerization should proceed readily. Future studies, therefore, should be aimed at isolating the **LHP1-DOD** polyelectrolyte in this manner.

However, the dimer obtained from the initial investigations of **LHP1-DOD** is an outstanding telechelic monomer with envisioned utility to form different types of polymers (Scheme 4.7).

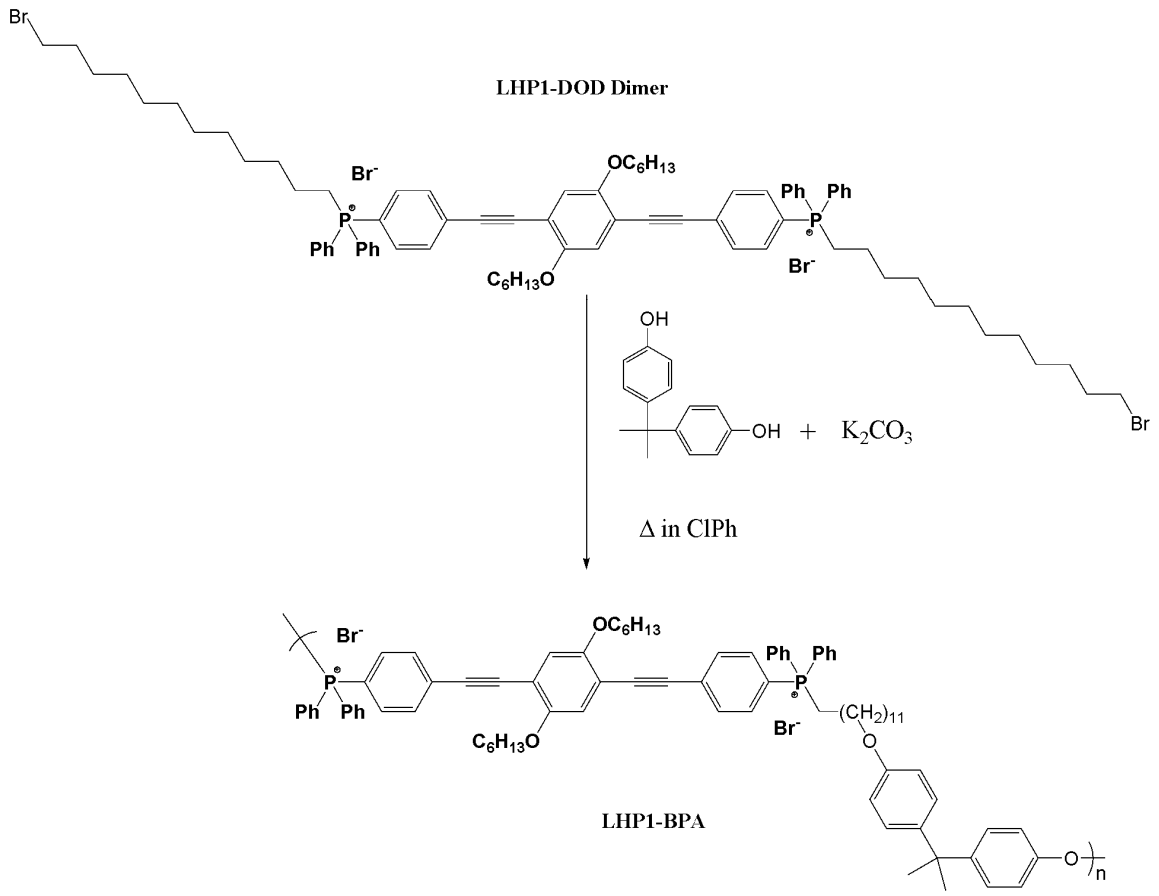

Scheme 4.7. Synthesis of **LHP1-BPA** polyelectrolyte using the **LHP1-DOD** dimer.

The initial polymerization planned relies on the simple S_N2 reaction between the terminal alkyl bromides of the **LHP1-DOD** dimer and bisphenol A for form the **LHP1**-containing polyether, **LHP1-BPA** (Scheme 4.7). Future studies should examine the viability of this reaction to isolate the **LHP1-BPA** polymer; if these results are promising, other diol variants can be used to generate a wide variety of **LHP1-DOD** dimer derived polymers. Ester, amide and amine-containing polymers are also obvious targets upon extension of the **LHP1-DOD** dimer.

4.6 Conclusions

The synthesis of phosphonium-based polyelectrolytes proceeds readily and easily via a simple S_N2 reaction between the previously isolated phosphine **18** and a variety of primary alkyl dibromides. It is important to note that a temperature of at least 100 °C is necessary to drive the polymerization towards completion.

The isolated **LHP1-OHx** polymer forms high quality, translucent bright orange films by simple drop-casting. Initial investigations into its photophysical properties show a significant solvatochromic effect; increasing the polarity of the solvent used for this type of characterization has a profound influence on the photoluminescence emission and quantum yield. More interesting, though, is the different nature of interactions between the **LHP1-OHx** and other anionic or neutral polymers as demonstrated by the bilayer assembly investigations. With poly(acrylic acid), deposition of each individual monolayer results in a consistent interaction between the **LHP1-OHx** and PAA polymers at a pH = 4 as evidenced by linear increase of absorbance with each bilayer formation. However, bilayer assemblies between **LHP1-OHx** and PTP show conformational changes of the entire composite film with each added monolayer. This is likely due to different intermolecular interactions between the polyions depending on which polymer has just been deposited and from which solvent (either acetonitrile or water). While this investigation is only in its nascent stages, future studies should be concerned with examining bilayer assemblies between **LHP1-OHx** and other polyions to see how sensitive the layering process is to the counterionic polymer structure. Moreover, the results from the PTP bilayer assembly study can be better understood once the morphology of the two polyelectrolytes is characterized during the layering process.

Either tunneling electron microscopy or atomic force microscopy would be potential techniques to assess the polyelectrolyte conformation before and after deposition.

It is also worth mentioning the high photoluminescence quantum yield (Φ = 17% in acetonitrile and Φ = 21% in dichloromethane) for **LHP1-OHx**; only measurements utilizing the same solvents can be used to compare the photoluminescence quantum yield of **LHP1-OHx** to the neutral coordination polymers (**P19** and **P20**) discussed extensively in Chapter 3. In general, if the **LHP1-OHx** is more rigid than the neutral coordination polymers, less excited state energy will be lost via nonradiative decay processes such as vibrational relaxation and an enhanced photoluminescence quantum yield should be observed. Thus, the significant enhancement of the quantum yield of the charged **LHP1-OHx** compared to both neutral coordination polymers (in dichloromethane) suggests that the polyelectrolyte is inherently more rigid. Future studies should carry out quantum yield measurements in solvents of varying polarity to discern the extent of quantum yield enhancement due to solvatochromic effects or inherent conformational properties of the **LHP1-OHx** polymer. In addition, because it is of interest to fully characterize the photophysical and semiconducting properties of the polyelectrolyte, it is necessary to obtain the photoluminescence lifetime of **LHP1-OHx**. Finally, cyclic voltammetry should be performed to discern the HOMO and LUMO energy level to definitively assess the quality of **LHP1-OHx** as a semiconducting material.

Because the synthetic route to afford the phosphonium-based polymer is a simple S_N2, a wide range of polyelectrolytes should be synthetically accessible. Only a few primary alkyl dibromides have been used thus far to yield the corresponding polymer, but future studies should aim to isolate more polyelectrolytes using different spacers (Scheme

4.2). Moreover, if a functionalized dibromide were to be used in the polymerization, the resultant polyelectrolyte could further be reacted to yield a phosphonium-based polymer capable of undergoing additional chromophore or fluorophore appending. These polyelectrolytes would have interesting and tunable optical properties depending on the spacer incorporated within the polymeric backbone.

Experimental

General Considerations

All air-sensitive reactions were performed using standard Schlenk techniques or in an MBraun UNILab glovebox under nitrogen. Anhydrous solvents were purchased from Fisher Scientific and further dried and degassed using an MBraun solvent purification system. All other reagents were used as received unless otherwise specified. NMR spectra of interest were obtained on a Bruker Avance 300 (operating at 300, 75.4, and 121.4 MHz for ^{1}H, ^{13}C, and ^{31}P nuclei, respectively) or Bruker Avance 500 spectrometer (operating at 500, 125.7, and 202.4 MHz for ^{1}H, ^{13}C, and ^{31}P nuclei, respectively). NMR spectral data are reported in ppm referenced to residual solvent signal (^{1}H and ^{13}C) or 85% phosphoric acid (^{31}P). UV-Vis absorption spectra were acquired on a Cary 50 Spectrophotometer while photoluminescence (PL) spectra were obtained on a Varian Eclipse fluorimeter.

Synthesis of phosphonium-based hexyloxybenzene polymer (LHP1-OHx)

Phosphine **18** (85.0 mg, 0.1 mmol) and 1,4-bis(bromomethyl)-2,5-dihexyloxybenzene (**b**) (51.3 mg, 0.11 mmol) were added to a 5 mL conical vial followed by addition of *N*, *N*-dimethylformamide (~3 mL). The reaction mixture was heated to 100 °C for 72 h while stirring (not under positive nitrogen pressure). At that time, the crude

reaction mixture was added to 15 mL of diethyl ether to afford a yellow-orange precipitate. This suspension was centrifuged for 30 s and the light yellow clear diethyl ether was discarded to leave an orange oil that was presumed to be **LHP1-OHx**. After drying *in vacuo*, the sticky residue still remained and so the crude polymer was combined with acetonitrile (~2 mL) and the solvent removed by rotary evaporation to yield an orange glass film that was **LHP1-OHx** (82 mg, 63%). The resultant product was analyzed by ^{1}H and ^{31}P NMR (Fig A-69 and A-70). ^{1}H NMR (300 MHz, $CDCl_3$) δ: 8.0-7.2 (br m, 47H), 6.7 (br s, 6H), 6.4 (br s, 4H),4.8 (br s, 3H), 4.0 (br s, 4H), 3.6-3.4 (br m, 2H), 3.1 (s, 2H), 2.4 (s, 12 H), 2.0-0.6 (overlapping m, 122H); ^{31}P NMR (121.4 MHz, $CDCl_3$) δ: 26.9 (br), 22.4, 22.2, 22.0, 21.7.

Photophysical characterization of LHP1-OHx

UV-vis of a solution of **LHP1-OHx** in acetonitrile ($4.7*10^{-5}$ M) showed two wavelengths of maximum absorbance at 319.5 nm and 389.5 nm (Fig B-12). Photoluminescence for **LHP1-OHx** ($4.7*10^{-7}$ M in acetonitrile) occurred at 488.1 nm after excitation at 320 nm (figure not shown); excitation at 390 nm produced an emission spectrum with a maximum at 491.9 nm (Fig B-13).

Critical micelle concentration study with LHP1-OHx

Solutions of 0, 0.5, 1 and 2 times the critical micelle concentration (cmc) of sodium dodecyl sulfate were prepared in HPLC-grade water. These solutions corresponded to 0 M, 4.1 mM, 8.2 mM and 16.4 mM SDS in water, respectively. An aliquot of **LHP1-OHx** in acetonitrile (3.4 μL of a $4.7*10^{-5}$ M stock solution) was added to each of these and the fluorescence spectra were acquired after exciting at 390 nm (Fig B-14 through B-17).

LHP1-OHx and poly(acrylic acid) bilayer study

The counterionic polymer solutions used for the bilayer study were as follows: $1.7*10^{-4}$ M solution of the cationic polymer **LHP1-OHx** in acetonitrile and a 0.1% wt% solution of poly(acrylic acid) (PAA) in water. A pH = 4 for the PAA solution was maintained so that the carboxylic acid moieties remained protonated.

Glass microscope slides (Fisher Brand) were first cleaned with tetrahydrofuran and then sonicated in HPLC grade water for 10 min. At that time, the glass slide was air-dried and then placed into a Cary 50 UV-vis Spectrometer for blanking purposes. Subsequent experiments were performed by scanning 285 to 800 nm.

LHP1-OHx was first deposited on the glass by dipping the microscope slide into a beaker containing the $1.7*10^{-4}$ M cationic solution. The duration of the dipping process was only for long enough to coat both sides of the glass. After air drying, the absorption spectrum was obtained. The glass slide was then dipped in the 0.1% PAA solution, again long enough only to coat both sides of the glass and the slide was air-dried. Once dry, the absorption spectrum was obtained as before. This process was repeated until an adequate number of bilayers accumulated on the slide for the UV-vis study (Fig B-17).

The **LHP1-OHx** and poly(acrylic acid) bilayer assembly was also studied by fluorescence spectroscopy using the same solutions prepared previously. The bilayers were deposited on the glass microscope slide in the same manner and the fluorescence spectra were acquired by exciting the bilayer films at 395 nm and scanning from 405 to 680 nm (slit width for these experiments were 5 cm) (Fig B-18).

Bilayer assemblies were also constructed between **LHP1-OHx** ($7.3*10^{-5}$ M in acetonitrile) and PAA (0.1% wt% in water) at a pH = 13. Absorption and

photoluminescence data was acquired as before (Fig B-19) but the fluorescence study yielded inconsistent results so as not to merit providing.

LHP1-OHx and Poly[2-(3-thienyl)ethyloxy-4-butylsulfonate] (PTP) Bilayer Study

The counterionic polymer solutions used for the bilayer study were as follows: $1.3*10^{-5}$ M solution of the cationic polymer **LHP1-OHx** in acetonitrile and a 0.1% wt% solution of poly[2-(3-thienyl)ethyloxy-4-butylsulfonate] (PTP) in water. A pH = 8 for the PTP solution was maintained.

Bilayer assemblies were formed in the same depositing manner as detailed previously and the photophysical characteristics were followed by UV-vis spectroscopy (Fig B-20).

Synthesis of phosphonium-based polymer with o-xylyl spacer (LHP1-oXYL)

Phosphine **18** (42.0 mg, 0.050 mmol) and 1,2-bis(bromomethyl)benzene (**e**) (14.4 mg, 0.545 mmol) were added to a 5 mL conical vial followed by addition of ~3 mL DMF. The reaction was stirred at 100 °C for 72 h (not under nitrogen). At that time, the crude reaction mixture was transferred into ~15 mL of diethyl ether to afford a cloudy yellow solution. This solution was centrifuged to leave an orange residue beneath a light yellow solution phase. The ether was decanted away and the orange residue dried *in vacuo* to hopefully afford a solid **LHP1-oXYL**. However, after 3 h of drying *in vacuo*, the residue still remained and so was washed with acetonitrile (not soluble) and any residual solvent removed by rotary evaporation. At this time, a yellowish orange glassy residue remained (53 mg, 96%) that was presumed to be the desired polymer, **LHP1-oXYL**. The polymer was then analyzed by ^{1}H and ^{31}P NMR (Fig A-71 and A-72). ^{1}H NMR (300 MHz, $CDCl_3$) δ: 8.1-7.1 (br m, 18H), 6.9 (m, 4H), 4.0 (m, 4H), 1.8 (br s, 1H),

2.6-1.1 (m, 4H), 1.8 (br m, 2H); ^{31}P NMR (121.4 MHz, $CDCl_3$) δ: 29.4, 23.9, 23.6, 23.3, 22.9, 22.1.

Synthesis of phosphonium-based polymer with bipyridine spacer (LHP1-BPY)

Phosphine **18** (85.0 mg, 0.10 mmol) and 5,5'-bis(bromomethyl)-2,2'-bipyridine (**a**) (37.8 mg, 0.11 mmol) were added to a 5 mL conical vial followed by addition of ~3 mL DMF and the reaction mixture was stirred at 100 °C for 72 h (not under nitrogen). At that time, the crude orange reaction mixture was added to ~15 mL of diethyl ether to produce a cloudy yellow solution as seen with the **LHP1-oXYL**. Again, centrifugation separated the phases into an orange residue at the bottom and a light yellow solution phase at the top. The ether was decanted away and the orange residue was washed with acetonitrile and any remaining solvent was removed by rotary evaporation to yield a yellow glassy solid that was likely the crude **LHP1-BPY** (65 mg, 55%). The polymer was then analyzed by ^{1}H and ^{31}P NMR (Fig A-73 and A-74) but was insoluble in chloroform-d_1 and only modestly soluble in dimethylsulfoxide-d_6. ^{1}H NMR (300 MHz, $CDCl_3$) δ: 8.8-7.9 (br m, 13H), 7.9-7.3 (br m, 5H), 4.0-3.2 (br overlapping m, 10H), 1.6-0.5 (br overlapping m, 4H); ^{31}P NMR (121.4 MHz, $CDCl_3$) δ: 25.8, 24.2, 24.0.

Synthesis of phosphonium-based dodecyl polyelectrolyte (LHP1-DOD)

Phosphine **18** (43 mg, 0.051 mmol) and 1,12-dibromododecane (**g12**) (17 mg, 0.051 mmol) were each dissolved in ~1.5 mL of DMF in separate vials. The solvated species were transferred back and forth to ensure that equimolar amounts of starting materials were present in the reaction vessel. Once the reaction mixture was transferred to a 25 mL round bottom flask, the vials were rinsed with another 1.5 mL of DMF each and this was combined with the crude reaction mixture. The reaction was then stirred under

nitrogen while heating to 80 °C for 72 h. At that time, another 0.1 equivalents of the 1,12-dibromododecane (2 mg, 0.006 mmol) for end-capping purposes. After stirring under nitrogen at 80 °C for another 3 h, the DMF was removed by rotary evaporation and any residual DMF was removed by azeotrope formation between acetonitrile and DMF. ^{31}P NMR was acquired for the crude product (Fig A-75) but showed a significant amount of starting phosphine **18** still present.

The crude reaction product was redissolved in ~1.5 mL DMF and was combined with another equivalent of 1,12-dibromododecane (17 mg, 0.051 mmol) and diluted up to 8 mL with DMF in a 25 mL round bottom flask. The reaction mixture was then heated under nitrogen to 100 °C for 5 d. At that time, the DMF was removed by rotary evaporation to afford a bright orange glassy solid that was the crude **LHP1-DOD**. Phosphorous-31 NMR of the afforded product was acquired (Fig A-76) and showed almost no starting material. The crude **LHP1-DOD** was washed with hexane to remove any unreacted 1,12-dibromododecane and ^{1}H and ^{31}P NMR were acquired (Fig A-77 and A-78). ^{1}H NMR (300 MHz, $CDCl_3$) δ: 9.4 (br s, 4H), 8.0-7.3 (br overlapping m, 56H), 7.0 (m, 4H), 4.1 (q, 1H), 4.0 (m, 4H), 3.8-3.5 (br m, 8H), 3.4 (q, 4H), 2.6 (t, 2H), 2.1-1.9 (br s, 2H), 1.8 (br m, 8H), 1.6-1.0 (br overlapping m, 96H), 0.8 (br m, 12H); ^{31}P NMR (121.4 MHz, $CDCl_3$) δ: 29.5, 25.5, 25.0-24.9 (br m), 23.7. In addition, a ^{1}H-^{1}H COSY spectrum was acquired to determine the nature of an impurity with an aldehyde-type chemical shift (Fig A-79).

The crude **LHP1-DOD** was dissolved in dichloromethane, washed three times with water, dried *in vacuo* to afford a pure product[†] (60 mg, 78%) as demonstrated by ^{1}H and ^{31}P NMR (Fig A-80 and A-81). ^{1}H NMR (300 MHz, $CDCl_3$) δ: 8.0-7.4 (br

[†] Percent yield calculated based on the isolated product being the dimer (*vide supra*).

overlapping m, 38H), 7.0 (s, 2H), 4.1 (q, 1H), 4.0 (m, 4H), 3.8-3.6 (br m, 5H), 3.5 (q, 1H), 3.4 (q, 3H), 1.8-1.6-1.0 (br overlapping m, 73H), 0.8 (br m, 10H); ^{31}P NMR (121.4 MHz, $CDCl_3$) δ: 29.5, 25.5, 25.0-24.9 (br m), 23.7.

REFERENCES CITED

(1) Ho, P. K. H.; Kim, J.-S.; Burroughes, J. H.; Becker, H.; Li, S. F. Y.; Brown, T. M.; Cacialli, F.; Friend, R. H. "Molecular-Scale Interface Engineering for Polymer Light-Emitting Diodes" *Nature* **2000**, *404*, 481-484.

(2) Cimrova, V.; Schmidt, W.; Rulkens, R.; Schulze, M.; Meyer, W.; Neher, D. "Efficient Blue Light Emitting Devices Based on Rigid-Rod Polyelectrolytes" *Adv. Mater.* **1996**, *8*, 585-588.

(3) Lee, H.; Lee, Y.; Statz, A. R.; Rho, J.; Park, T. G.; Messersmith, P. B. "Substrate-Independent Layer-by-Layer Assembly by Using Mussel-Adhesive-Inspired Polymers" *Adv. Mater.* **2008**, *20*, 1619-1623.

(4) Thnemann, A. F.; Ruppelt, D. "Electroluminescent Polyelectrolyte-Surfactant Complexes" *Langmuir* **2001**, *17*, 5098-5102.

(5) Blochwitz, J.; Pfeiffer, M.; Fritz, T.; Leo, K. "Low Voltage Organic Light Emitting Diodes Featuring Doped Phthalocyanine as Hole Transport Material" *Appl. Phys. Lett.* **1998**, *73*, 729-731.

(6) Decher, G. "Fuzzy Nanoassemblies: Toward Layered Polymeric Multicomposites" *Science* **1997**, *227*, 1232-1237.

(7) Tipathy, S. K.; Kumar, J.; Nalwa, H. S. *Handbook of Polyelectrolytes and Their Applications*, First ed.; American Scientific Publishers: Stevenson Ranch, CA, 2002.

(8) Decher, G.; Hong, J. D. "Buildup of Ultrathin Multilayer Films by a Self-Assembly Process: III. Consecutively Alternating Adsorption of Anionic and Cationic Polyelectrolytes on Charged Surfaces" *Thin Solid Films* **1992**, *210-211*, 831-835.

(9) Kim, M.; Sandman, D. J. "Polycation Effects on Electronic Spectra of Conjugated Poymers in Programmed Electrostatic Assemblies" *J. Macromol. Sci. A* **2001**, *38*, 1291-1304.

(10) Taranekar, P.; Qiao, Q.; Jiang, H.; Ghiviriga, I.; Schanze, K. S.; Reynolds, J. R. "Hyperbranched Conjugated Polyelectrolyte Bilayers for Solar-Cell Applications" *J. Am. Chem. Soc.* **2007**, *129*, 8958-8959.

(11) Hiriyama, S.; Steer, R. P. "Solvatochromism and Barochromism Revisited and Revealed" *J. Chem. Educ.* **2008**, *85*, 317-319.

APPENDICES

Appendix A

NMR SPECTRA

Terphenylphosphine (**1**); EGT-1-4; 08/29/07

Structure:

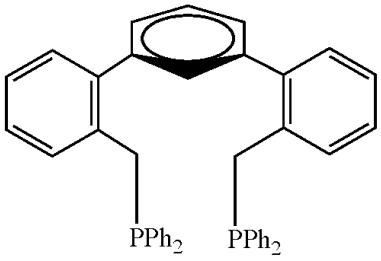

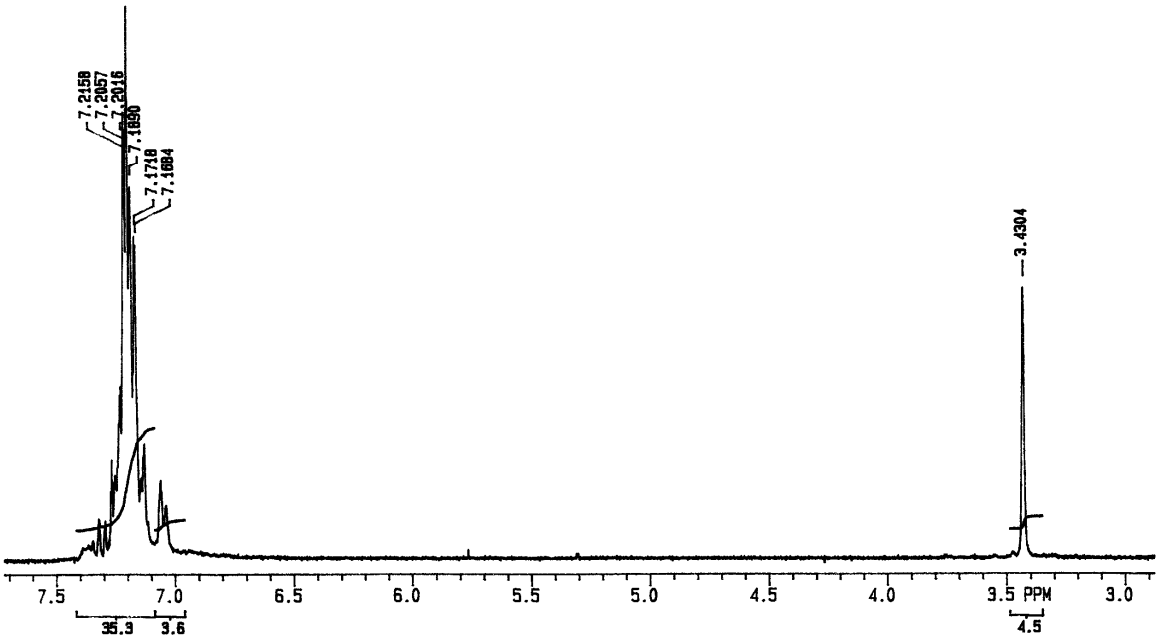

Figure A-1: ^{1}H NMR (300 MHz, $CDCl_3$) of **1**.

Terphenylphosphine (**1**); EGT-1-4; 08/29/07

Structure:

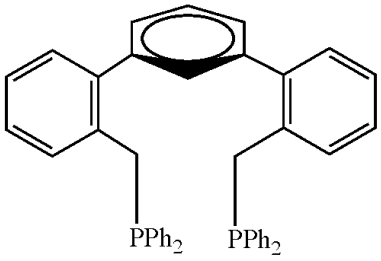

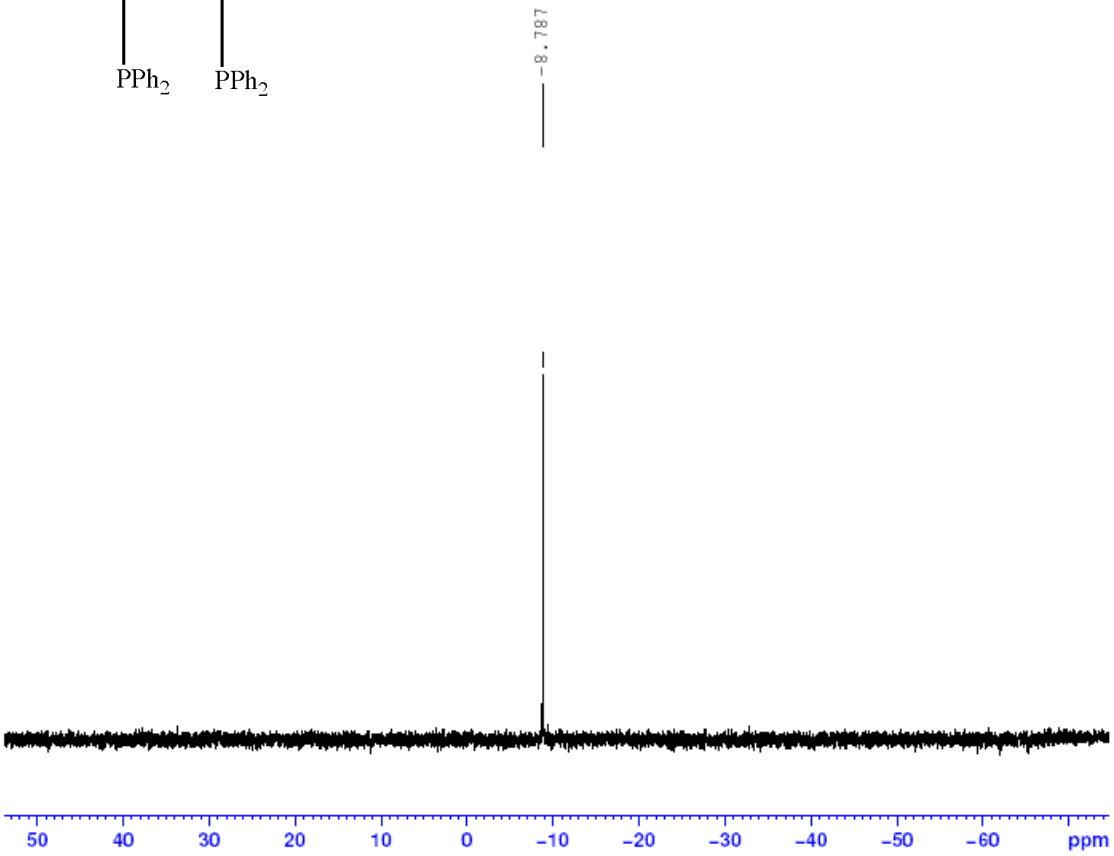

Figure A-2: ^{31}P NMR (121.4 MHz, $CDCl_3$) of **1**.

Platinum-based starting material (**2**); EGT-1-1; 08/29/07

Structure:

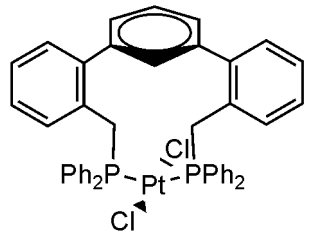

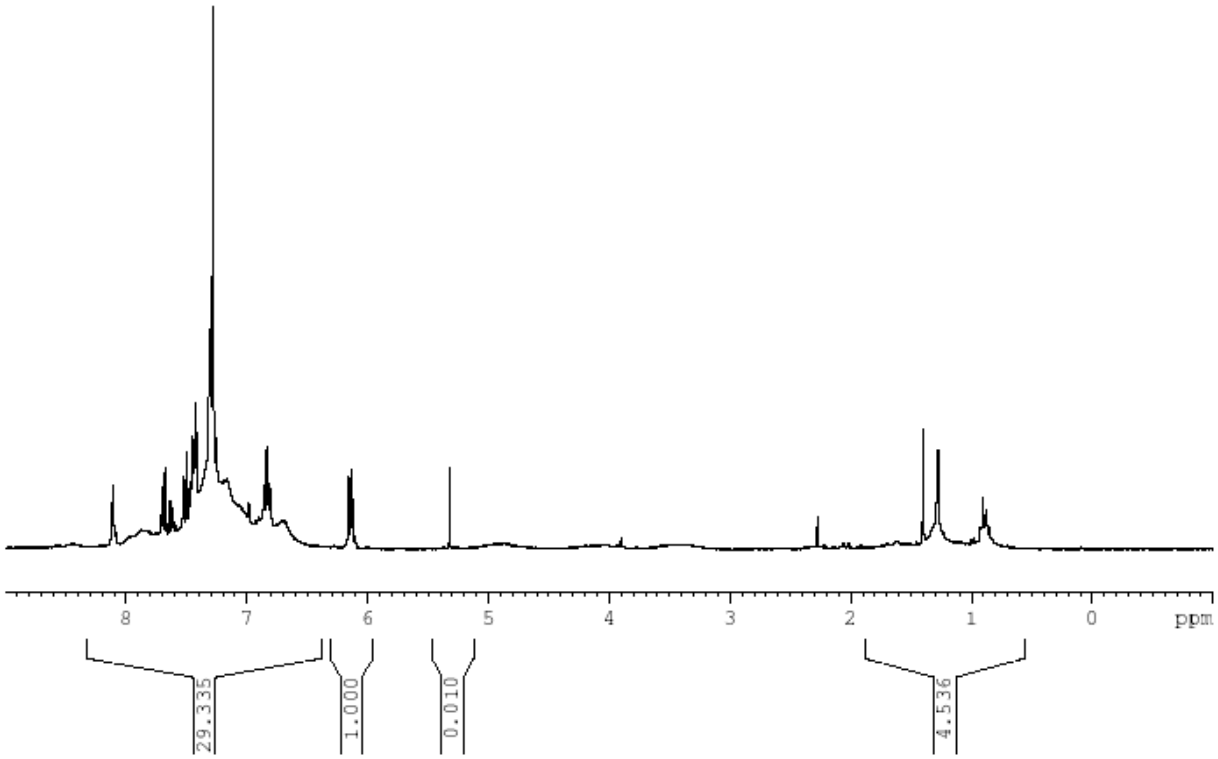

Figure A-3: ^{1}H NMR (300 MHz, $CDCl_3$) of **2**.

Platinum-based starting material (**2**); EGT-1-1; 08/29/07

Structure:

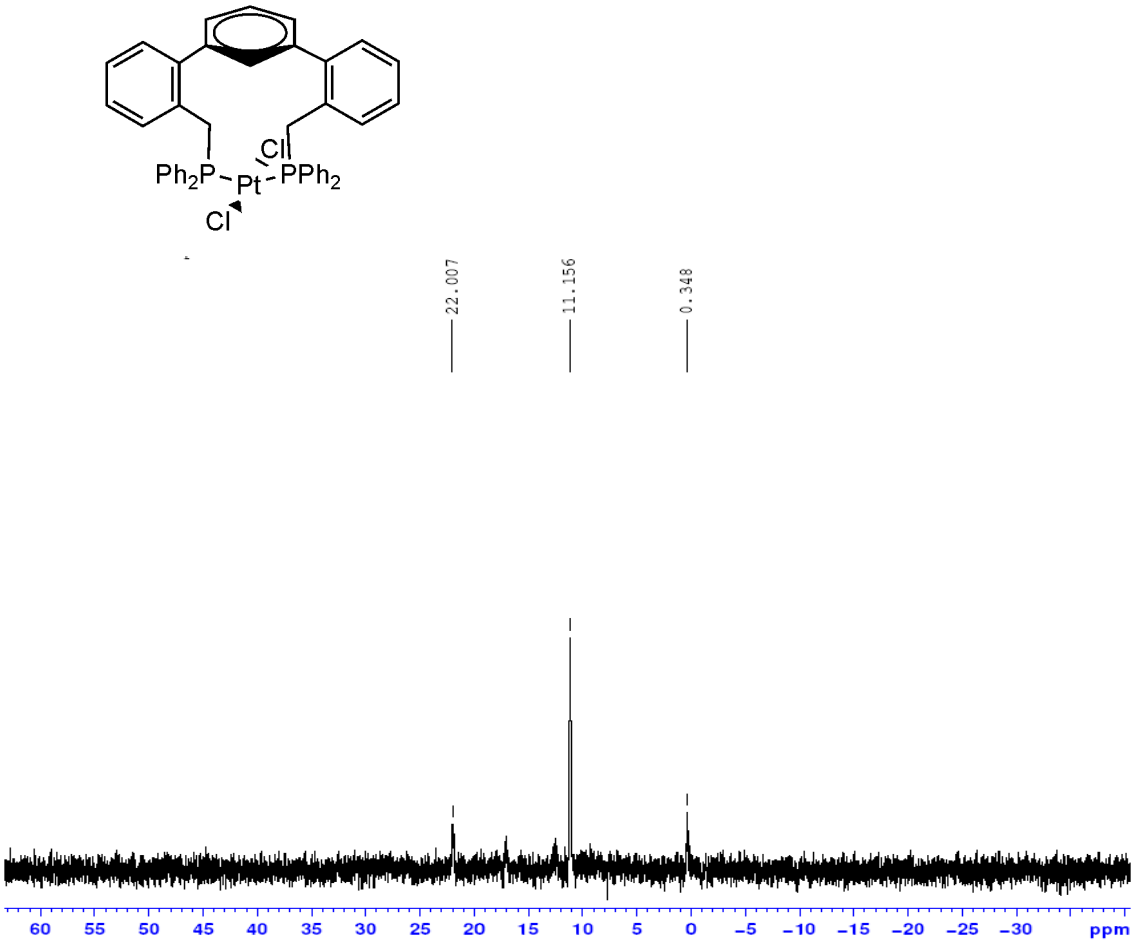

Figure A-4: ^{31}P NMR (121.4 MHz, $CDCl_3$) of **2**.

Platinum alkynyl model compound (**3**); EGT-1-7; 09/14/07

Structure:

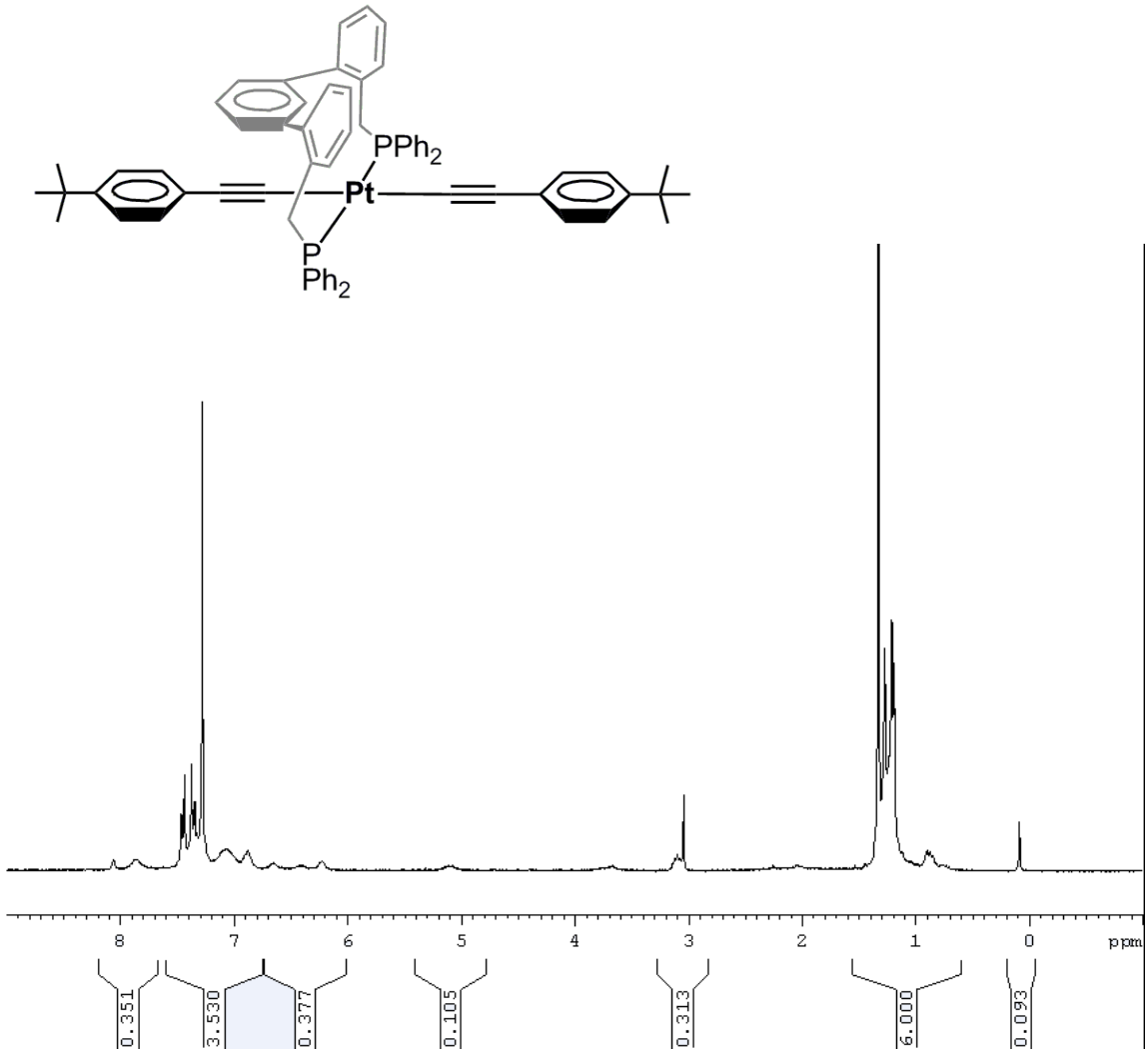

Figure A-5: ^{1}H NMR (300 MHz, $CDCl_3$) of **3**.

Platinum alkynyl model compound (**3**); EGT-1-7; 09/14/07

Structure:

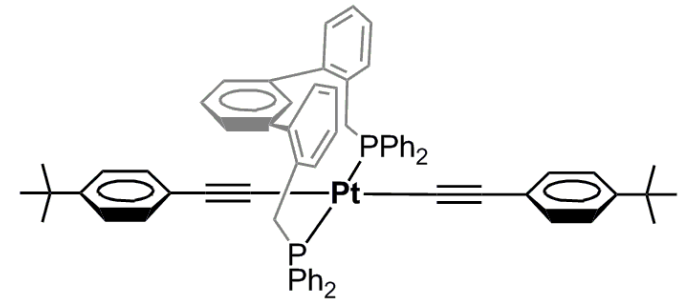

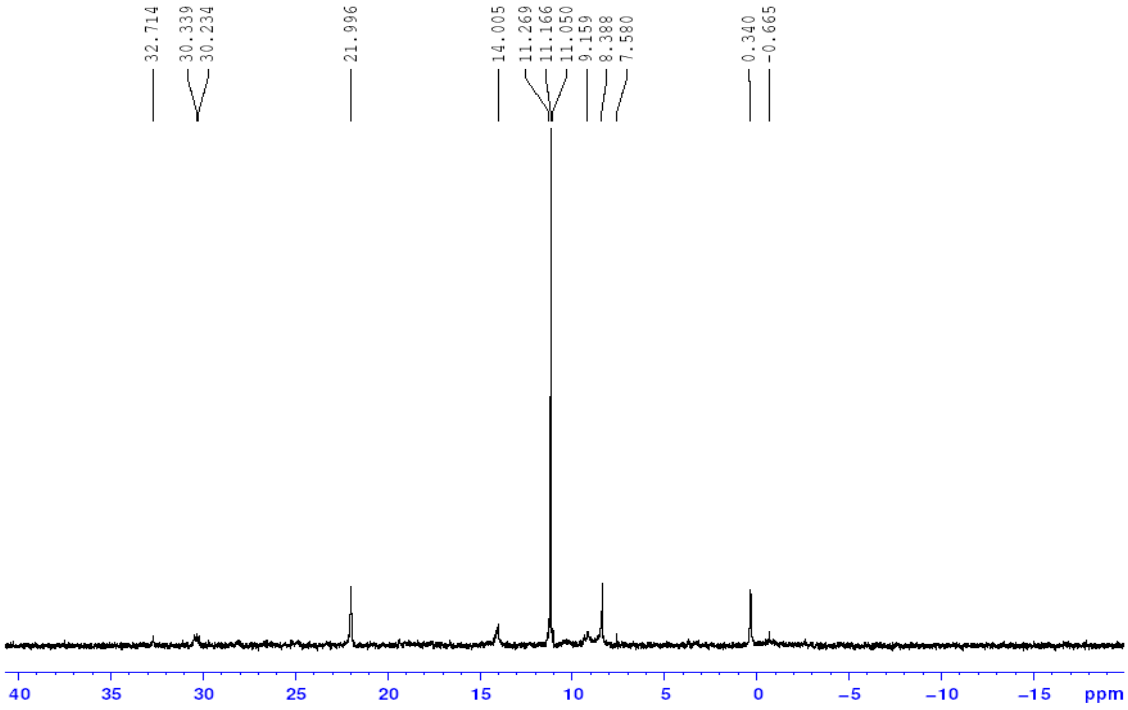

Figure A-6: ^{31}P NMR (121.4 MHz, $CDCl_3$) of **3**.

Platinum alkynyl model compound (**3**); EGT-1-7; 09/14/07

Structure:

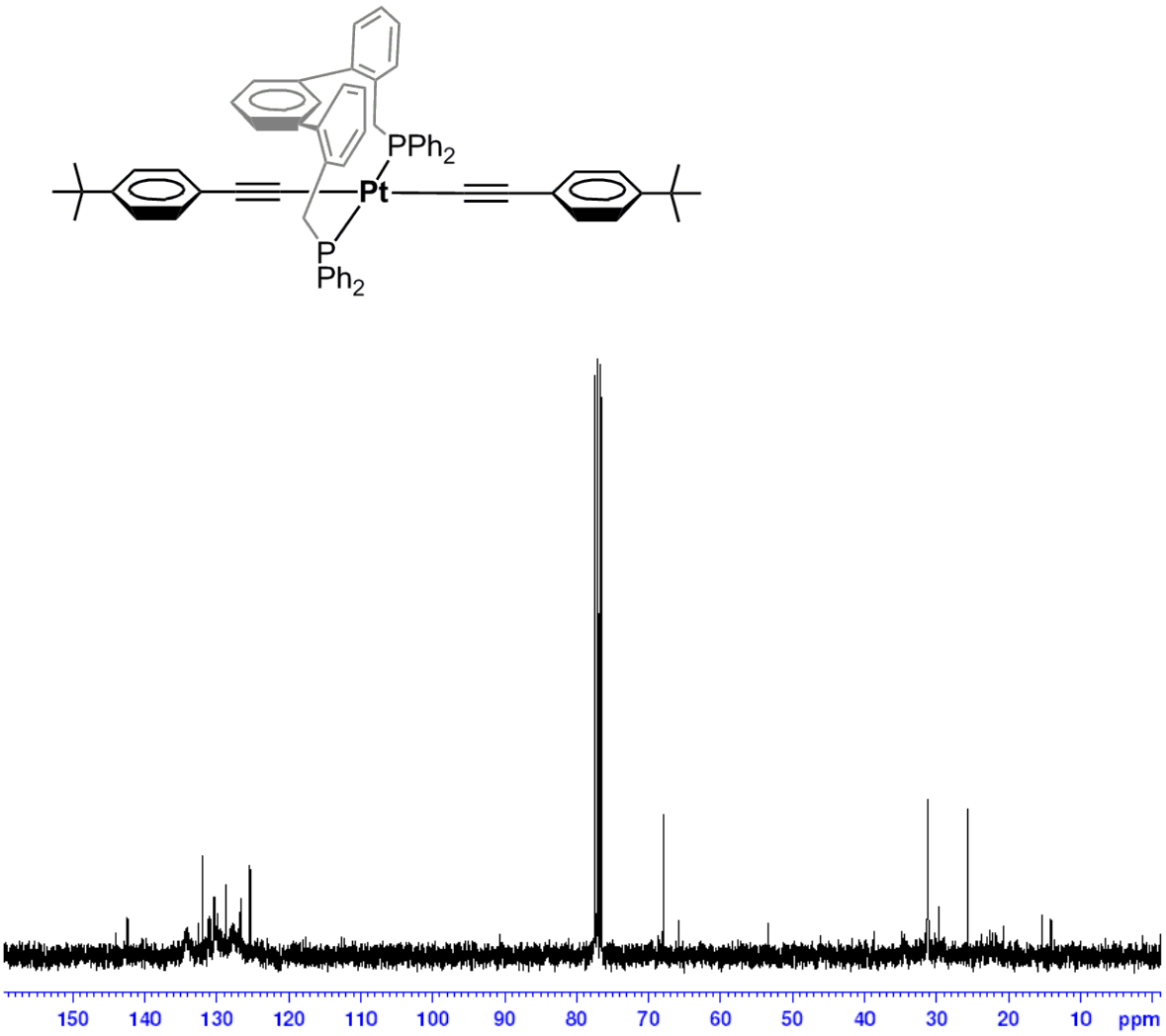

Figure A-7: ^{13}C NMR (75.4 MHz, $CDCl_3$) of **3**.

TMS-protected 1,4-diethynyl-2,5-dihexyloxybenzene; EGT-1-43; 2/22/08

Structure:

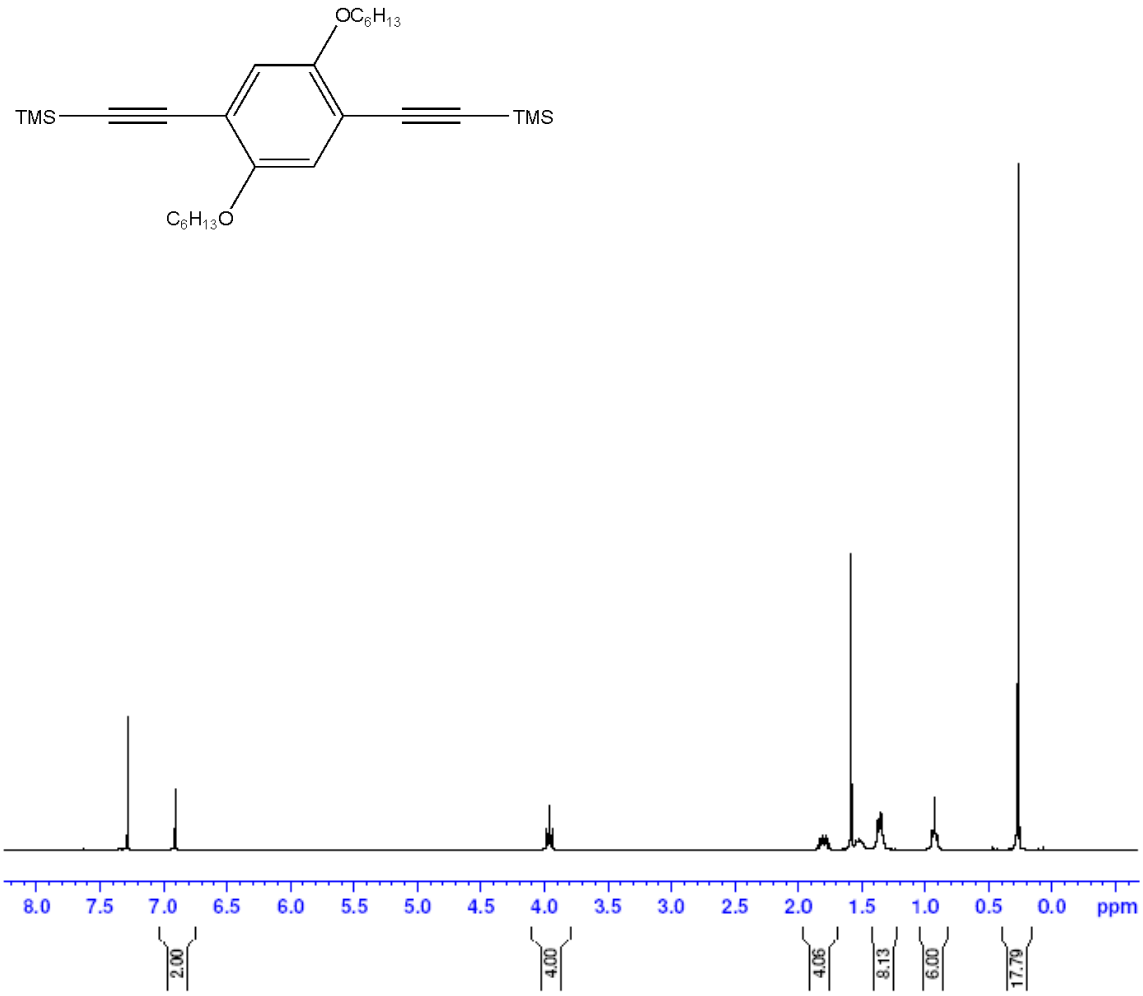

Figure A-8: ^{1}H NMR (300 MHz, $CDCl_3$) of 1,4-diethynyl-2,5-dihexyloxybenzene after deprotection of the TMS groups previously present on the acetylenes.

1,4-diethynyl-2,5-dihexyloxybenzene (**B**); EGT-1-16; 10/17/07

Structure:

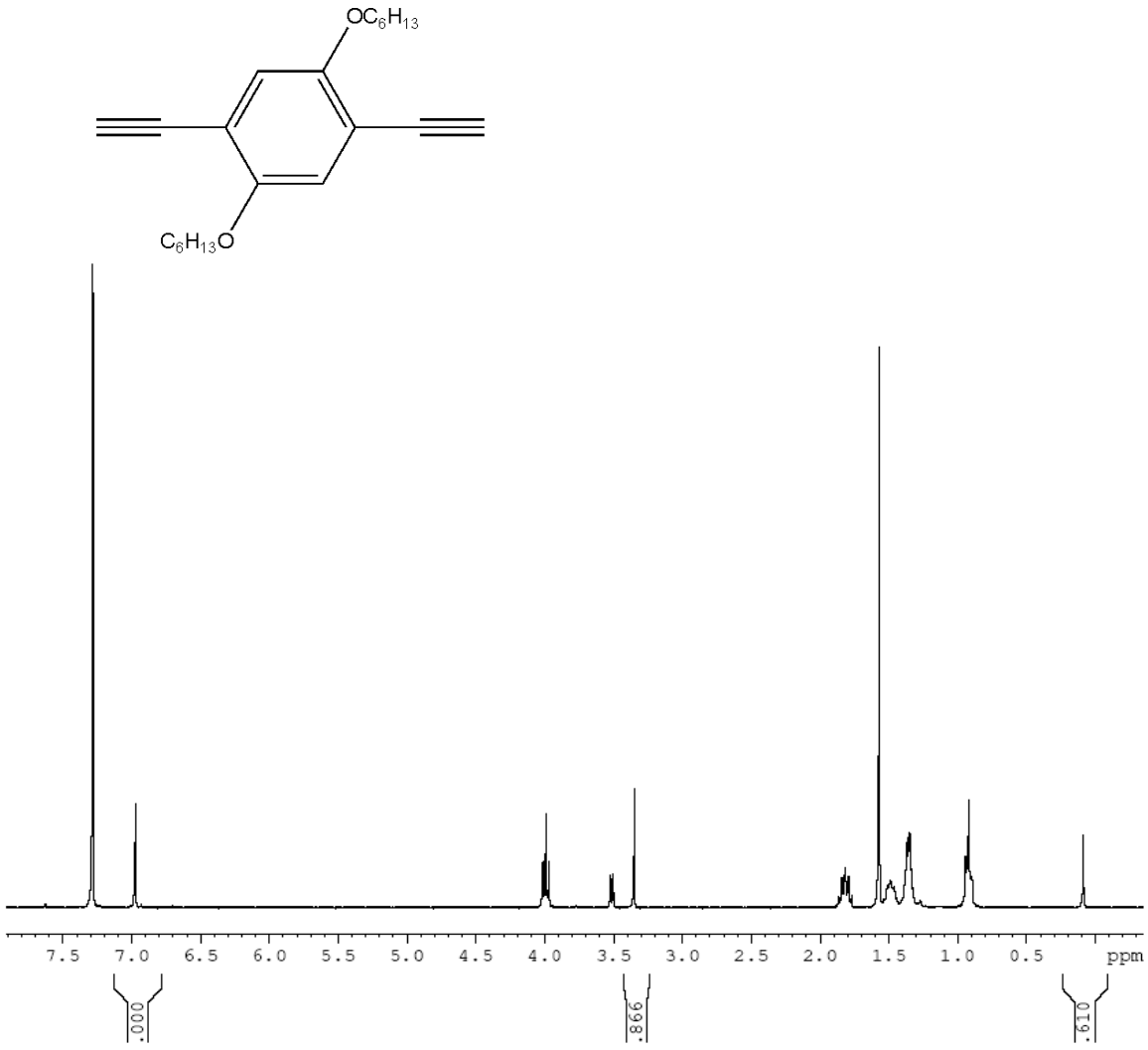

Figure A-9: ^{1}H NMR (300 MHz, $CDCl_3$) of 1,4-diethynyl-2,5-dihexyloxybenzene (**B**) after deprotection of the TMS groups previously present on the acetylenes.

Alkoxy Functionalized Platinum-based Polymer (**4**); EGT-1-20; 11/02/07

Structure:

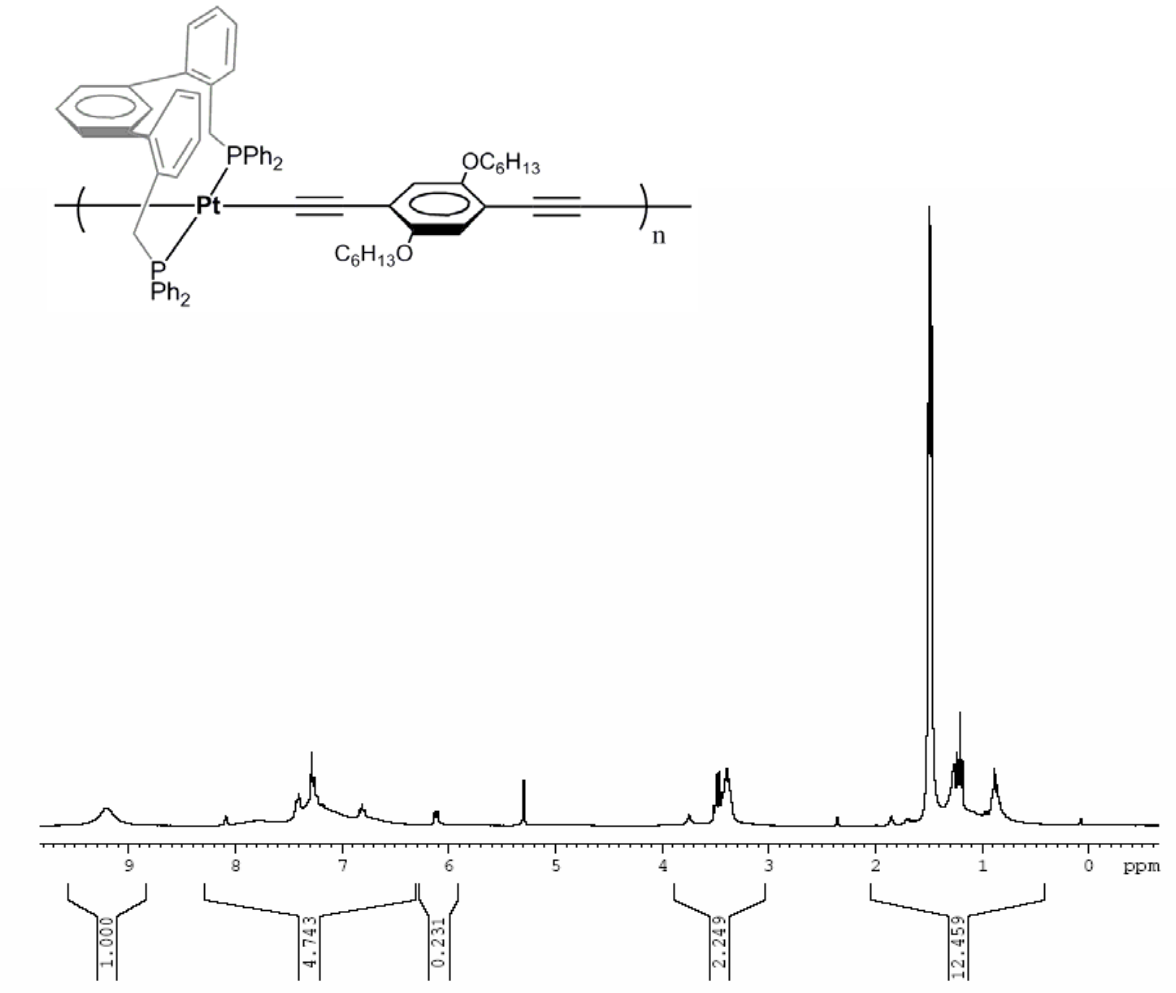

Figure A-10: ^{1}H NMR (300 MHz, $CDCl_3$) of alkoxy substituted ethynylbenzene platinum polymer.

Alkoxy Functionalized Platinum-based Polymer (**4**); EGT-1-20; 11/02/07

Structure:

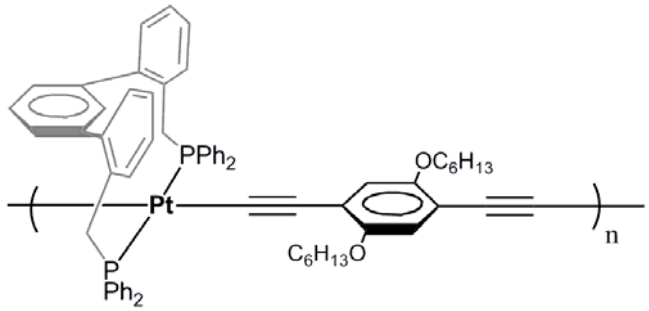

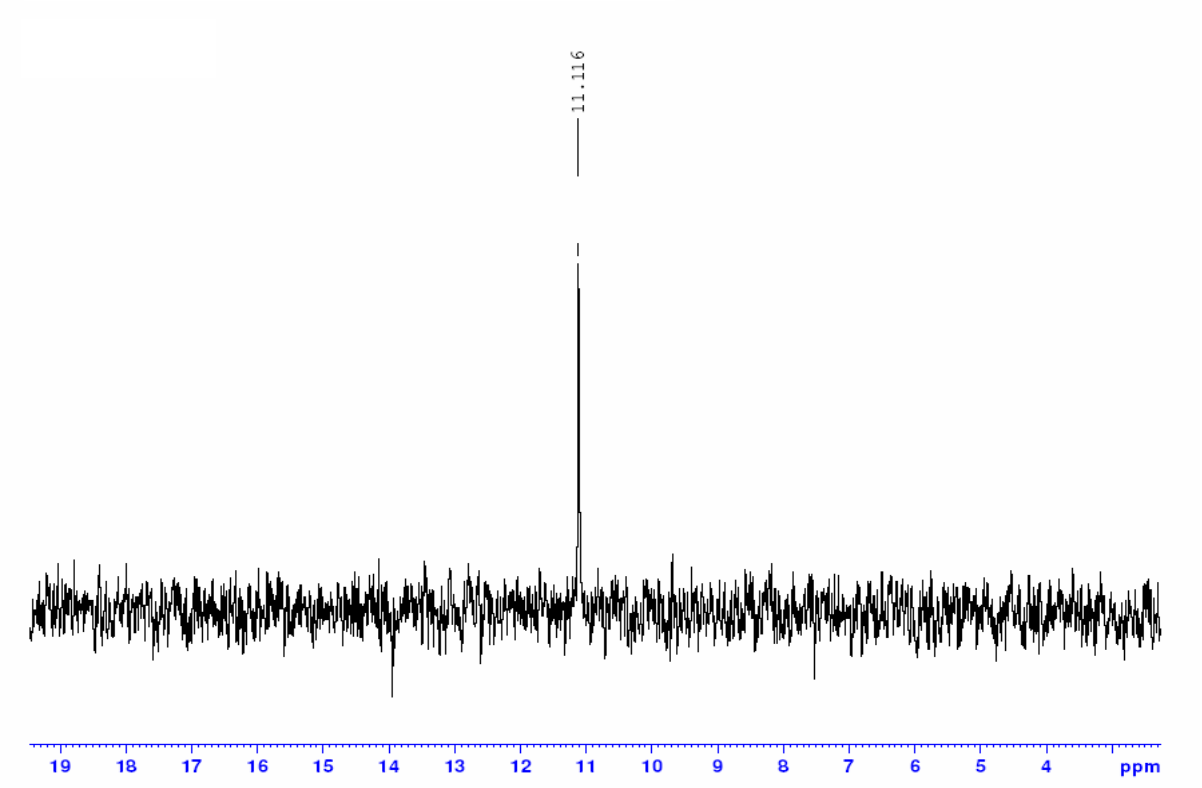

Figure A-11: ^{31}P NMR (121.4 MHz, $CDCl_3$) of alkoxy substituted ethynylbenzene platinum polymer.

Alkoxy Functionalized Platinum-based Polymer (**4**); EGT-1-20; 11/02/07

Structure:

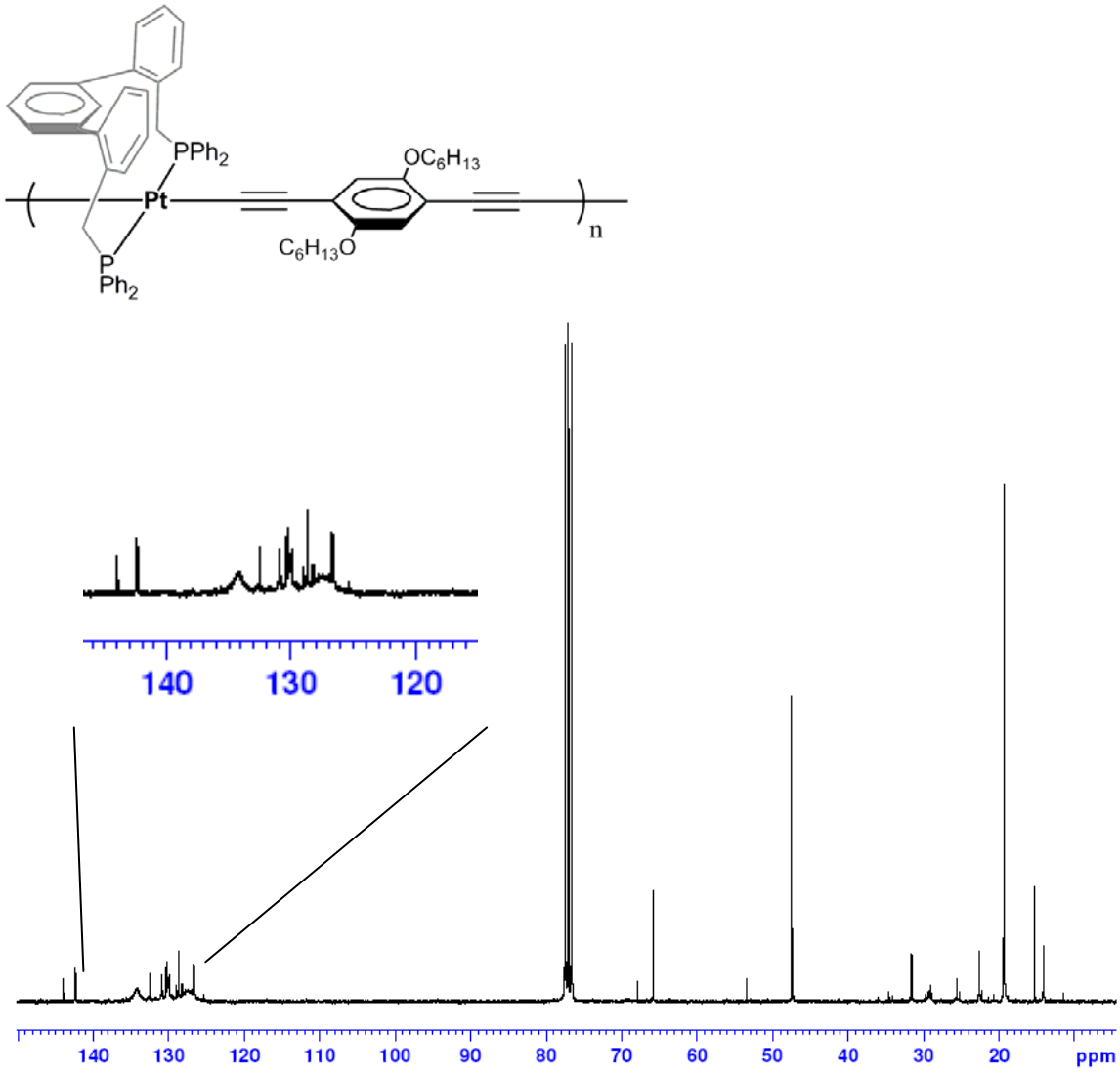

Figure A-12: ^{13}C NMR (75.4 MHz, $CDCl_3$) of alkoxy substituted ethynylbenzene platinum polymer.

Platinum-based starting material (**2**); EGT-1-20; 11/02/07

Structure:

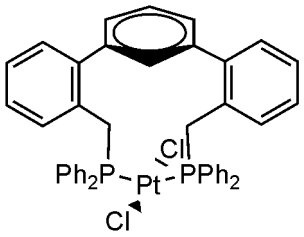

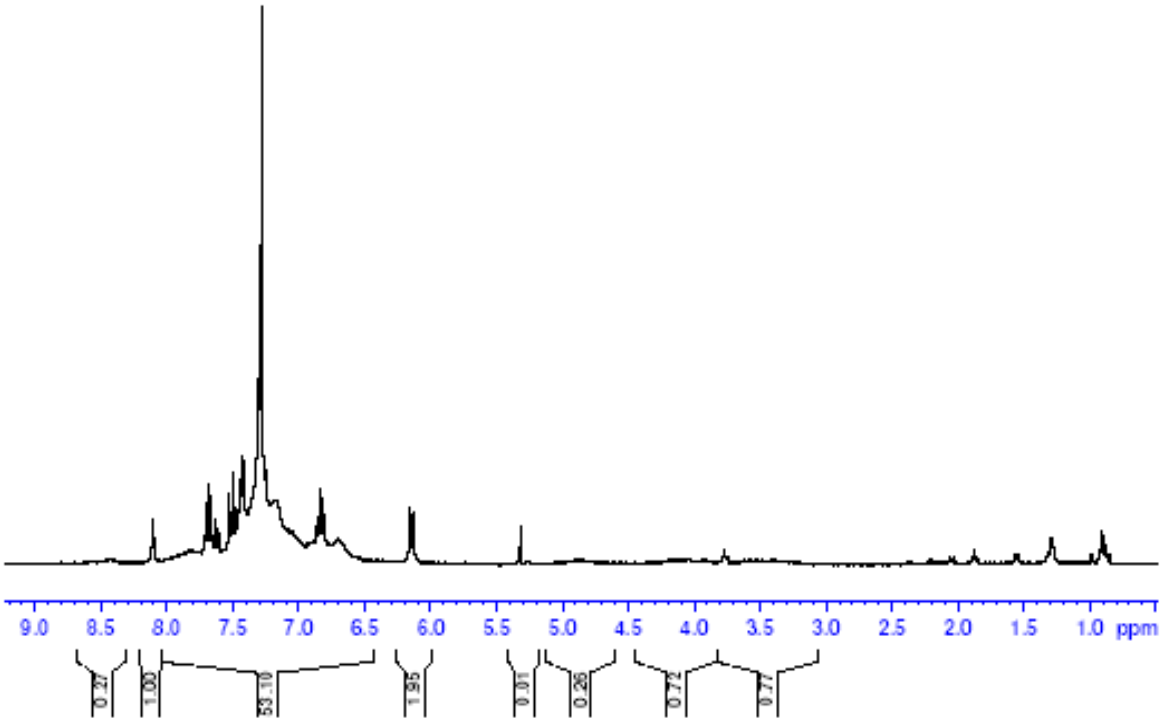

Figure A-13: ^{1}H NMR (300 MHz, $CDCl_3$) of new batch of dichloroplatinum **2**.

Platinum-based starting material (**2**); EGT-1-20; 11/02/07

Structure:

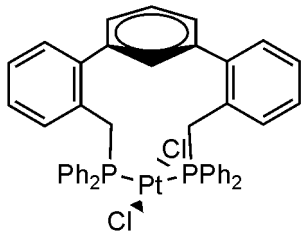

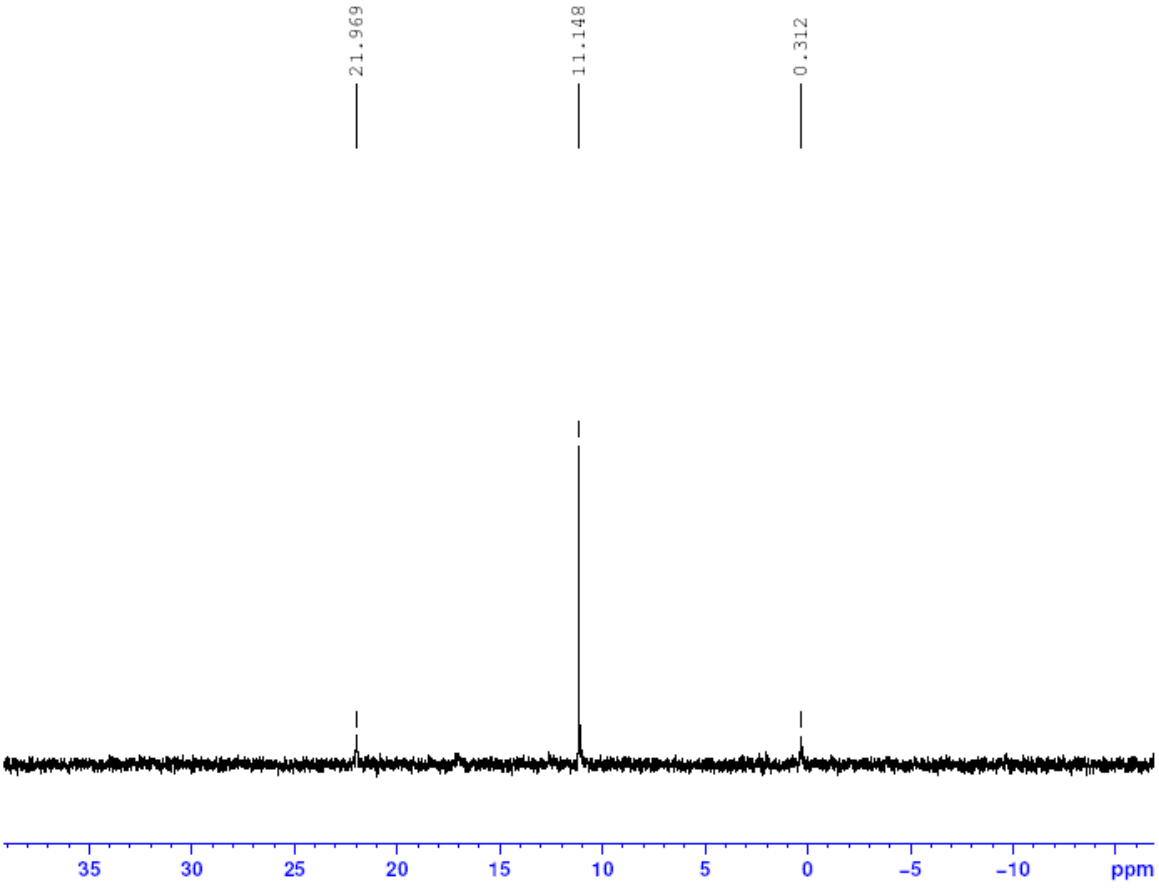

Figure A-14: ^{31}P NMR (121.4 MHz, $CDCl_3$) of new batch of dichloroplatinum **2**.

Platinum-based starting material (**2**); EGT-1-21; 11/09/07

Structure:

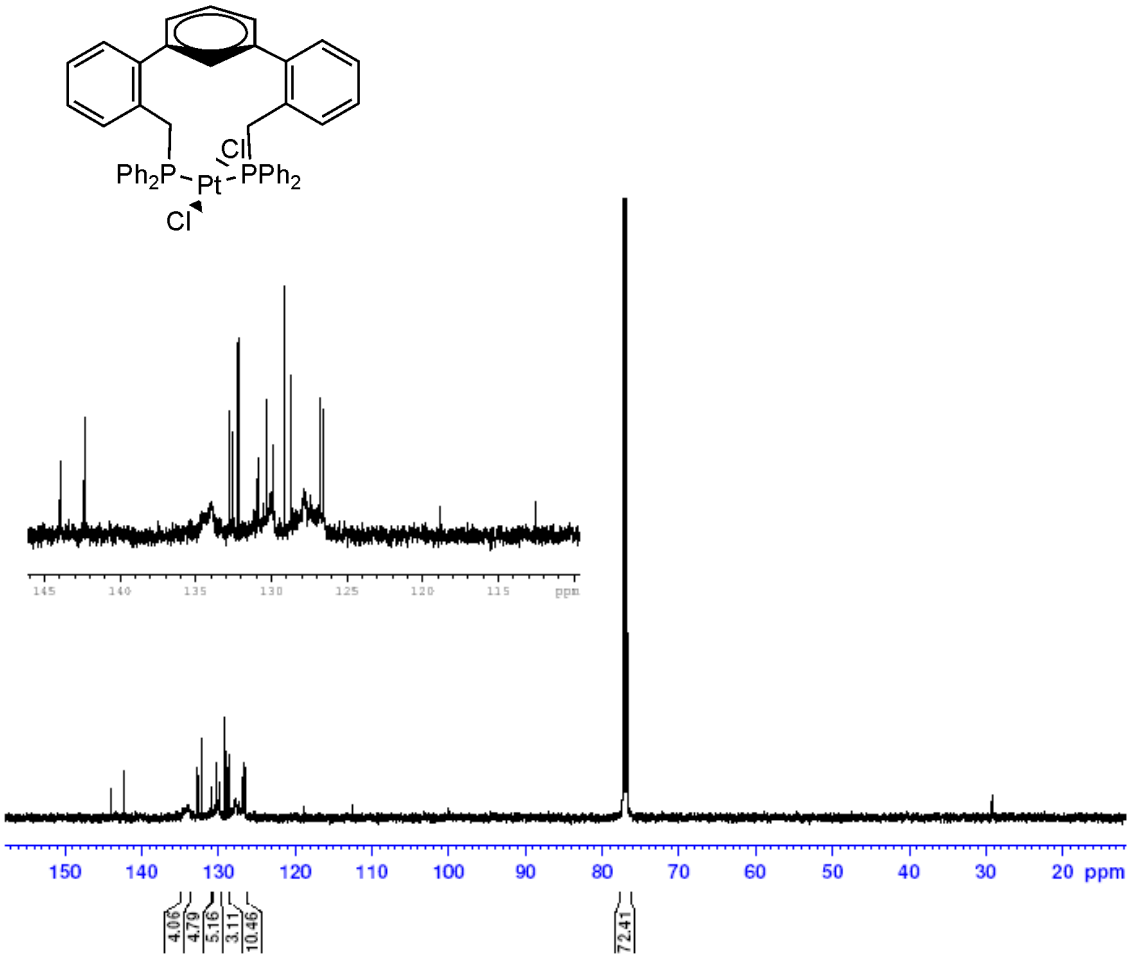

Figure A-15: ^{13}C NMR (125 MHz, $CDCl_3$) of new batch of dichloroplatinum **2**.

Alkoxy Functionalized Platinum-based Polymer (**4**); EGT-1-84; 9/02/07

Structure:

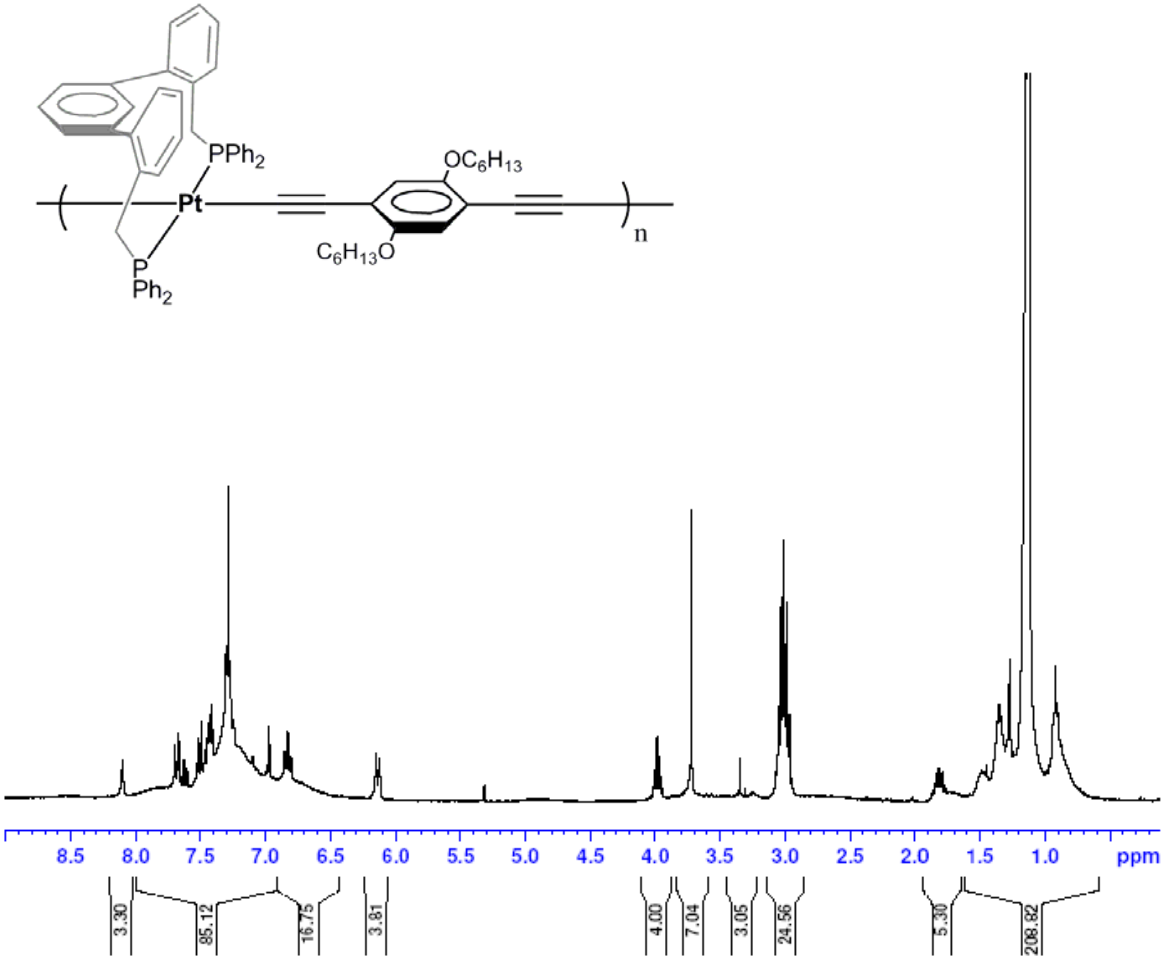

Figure A-16: ^{1}H NMR (300 MHz, $CDCl_3$) of alkoxy substituted ethynylbenzene platinum polymer.

Alkoxy Functionalized Platinum-based Polymer (**4**); EGT-1-84; 9/02/08

Structure:

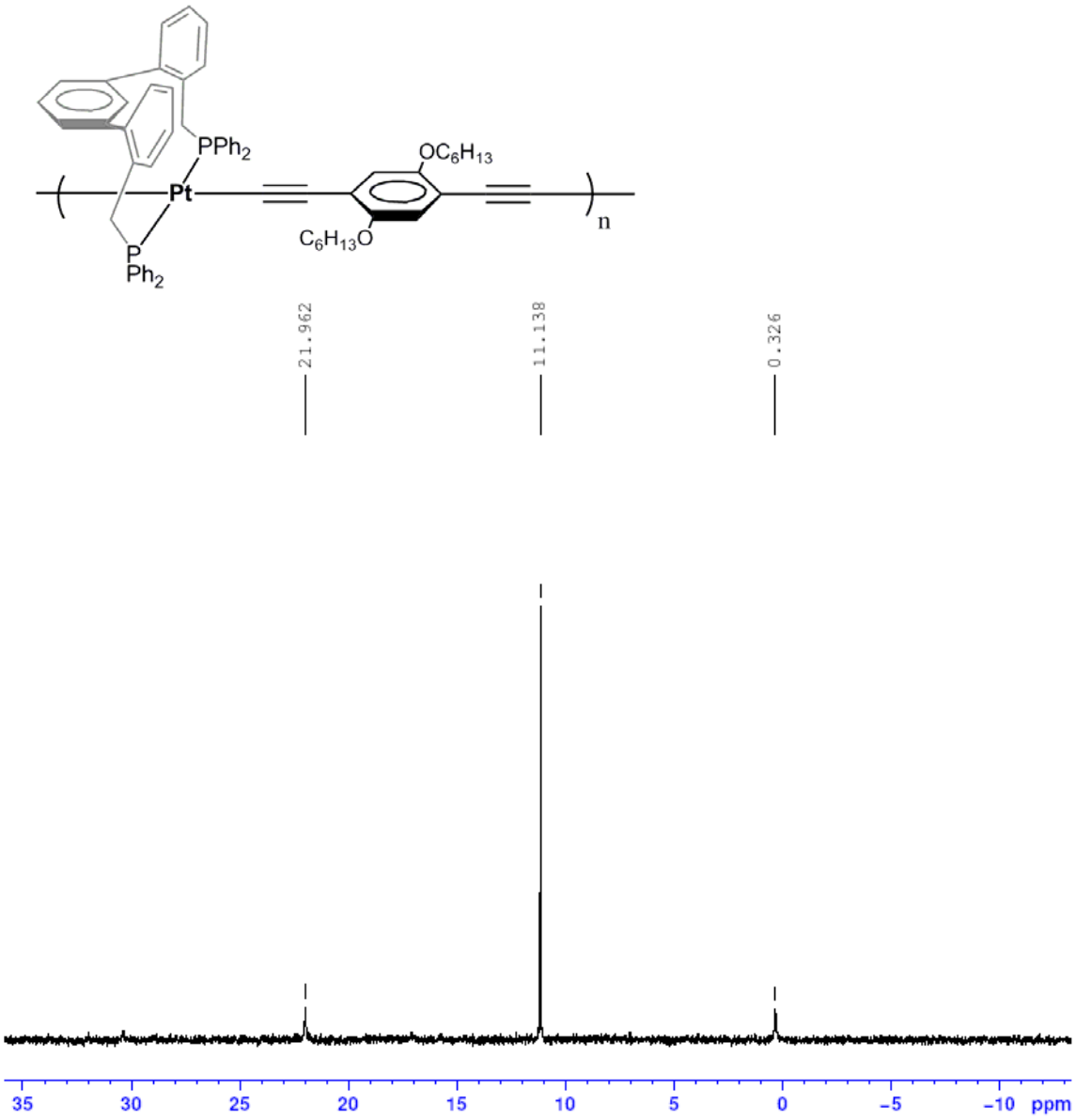

Figure A-17: ^{31}P NMR (121.4 MHz, $CDCl_3$) of alkoxy substituted ethynylbenzene platinum polymer.

Alkoxy Functionalized Platinum-based Polymer (**4**); EGT-1-84; 9/02/08

Structure:

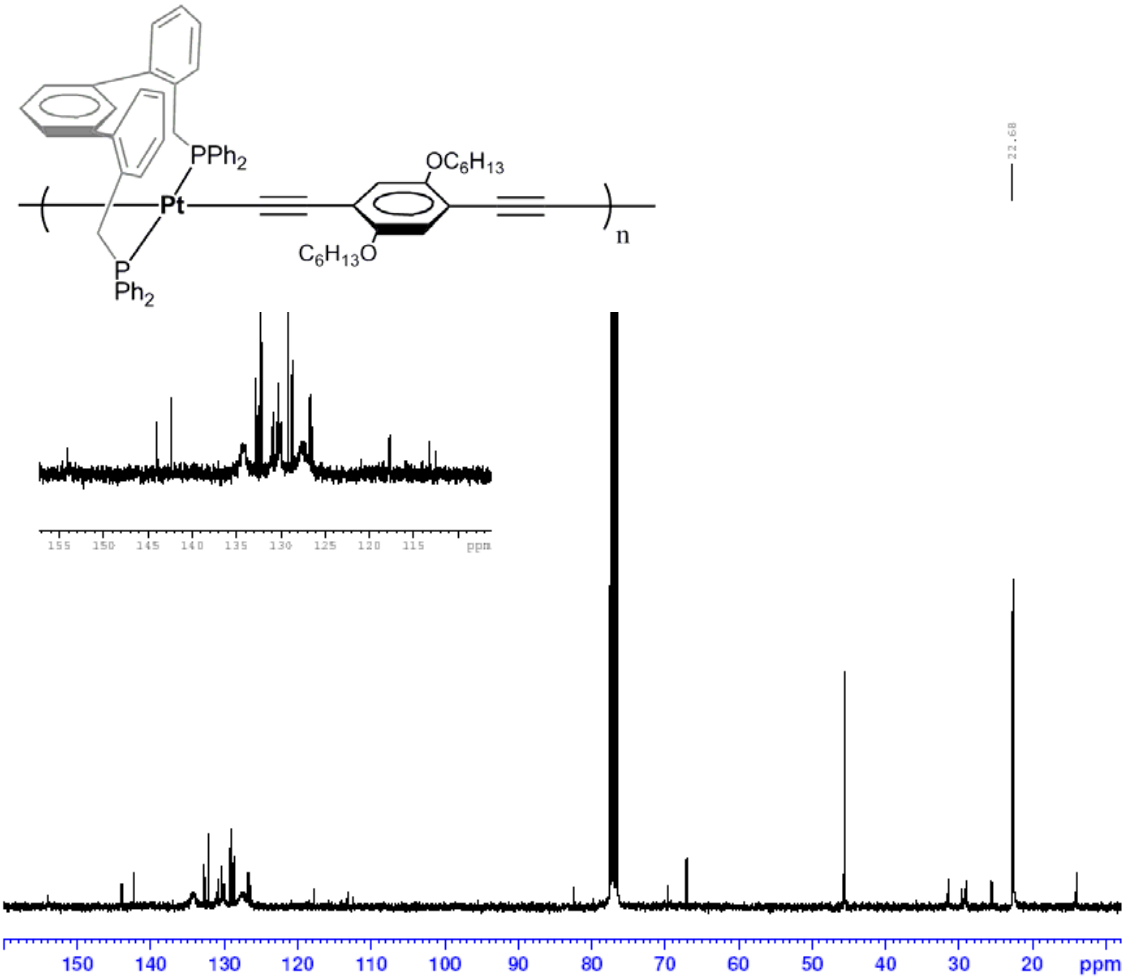

Figure A-18: ^{13}C NMR (75.4 MHz, $CDCl_3$) of alkoxy substituted ethynylbenzene platinum polymer.

Trimethyl((4-nitrophenyl)ethynyl)silane; EGT-1-27; 11/26/07

Structure:

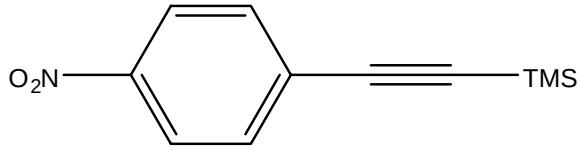

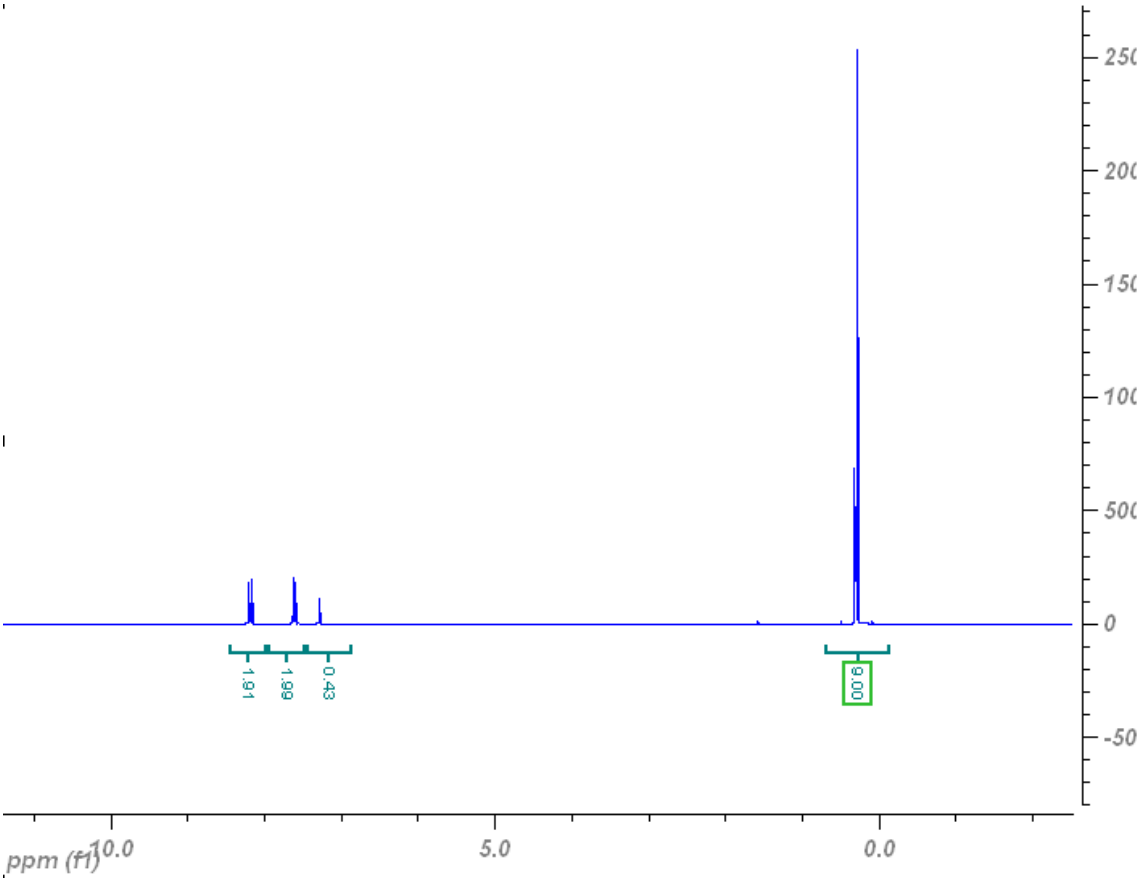

Figure A-19: ^{1}H NMR (300 MHz, $CDCl_3$) of trimethyl((4-nitrophenyl)ethynyl)silane.

Complex **6**; EGT-1-12; 10/01/07

Structure:

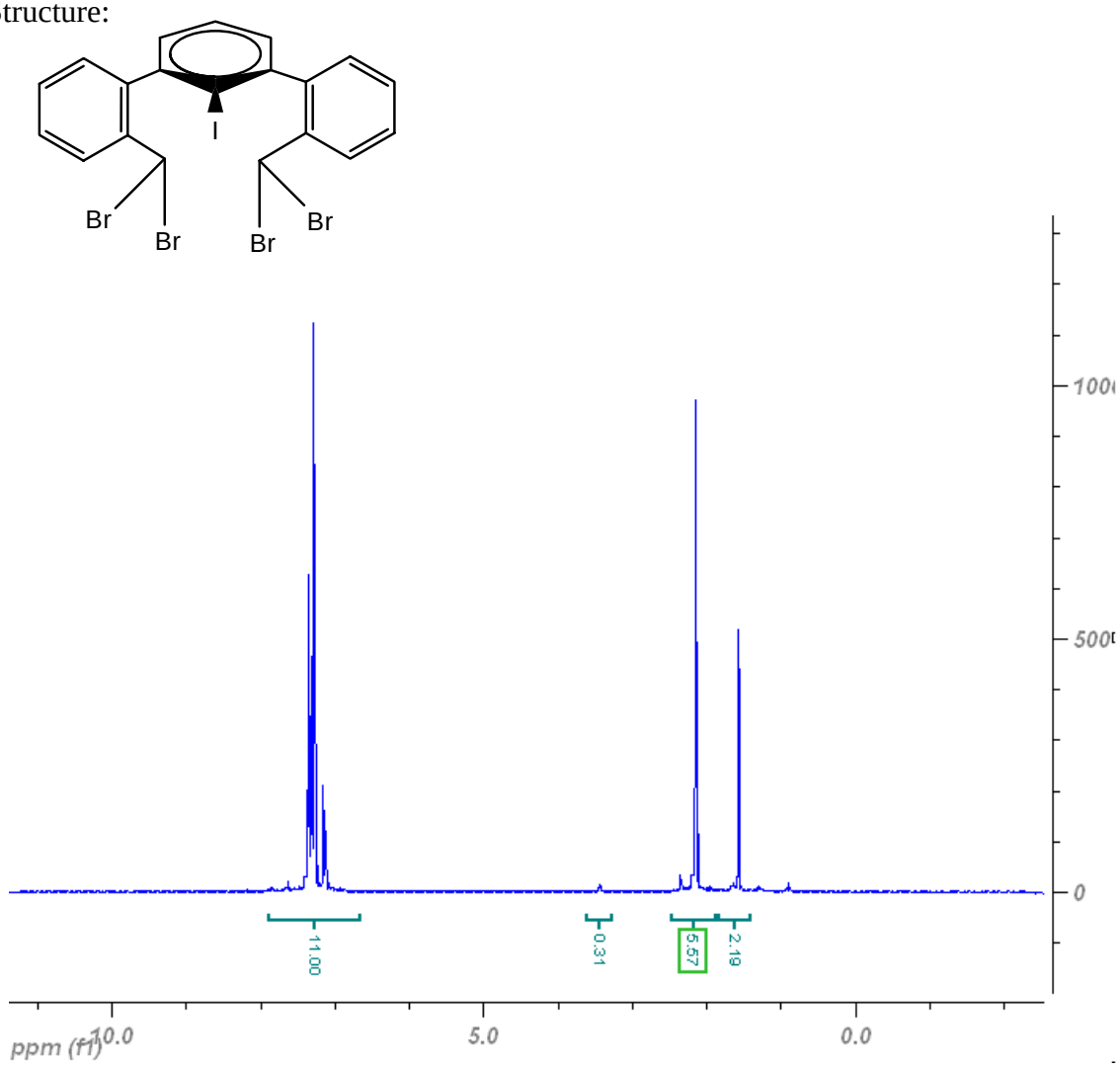

Figure A-20: ^{1}H NMR (300 MHz, $CDCl_3$) of tetrabrominated terphenyl with an iodide on the central phenyl ring.

Complex **7**; EGT-1-12; 10/01/07

Structure:

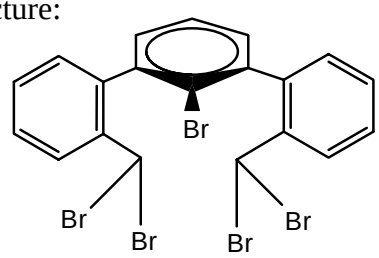

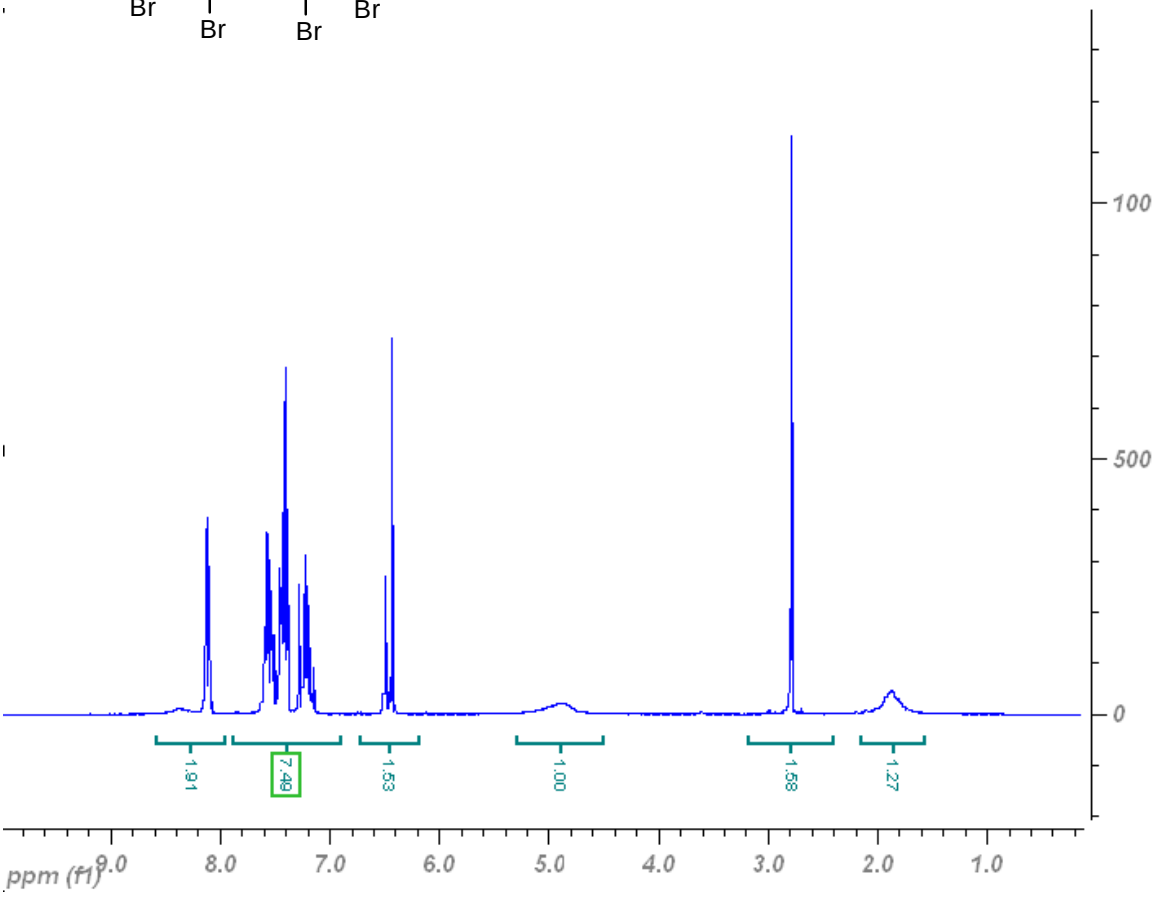

Figure A-21: ^{1}H NMR (300 MHz, $CDCl_3$) of tetrabrominated terphenyl with a bromide on the central phenyl ring.

Complex **8**; EGT-1-13; 10/05/07

Structure:

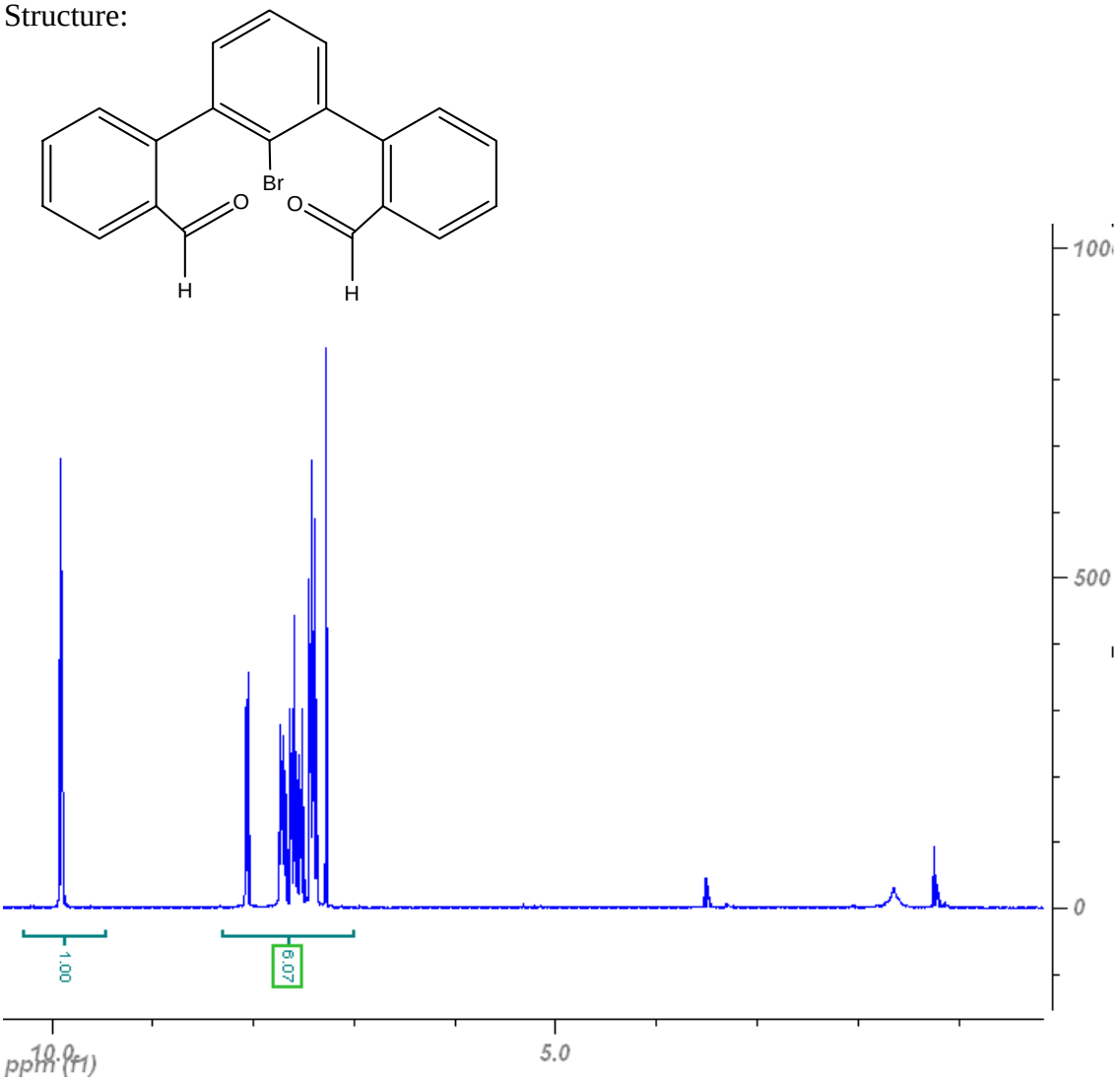

Figure A-22: ^{1}H NMR (300 MHz, $CDCl_3$) of terphenyldialdehyde with a bromide on the central phenyl ring.

Functionalized terphenylphosphine **9**; EGT-1-70; 07/20/08

Structure:

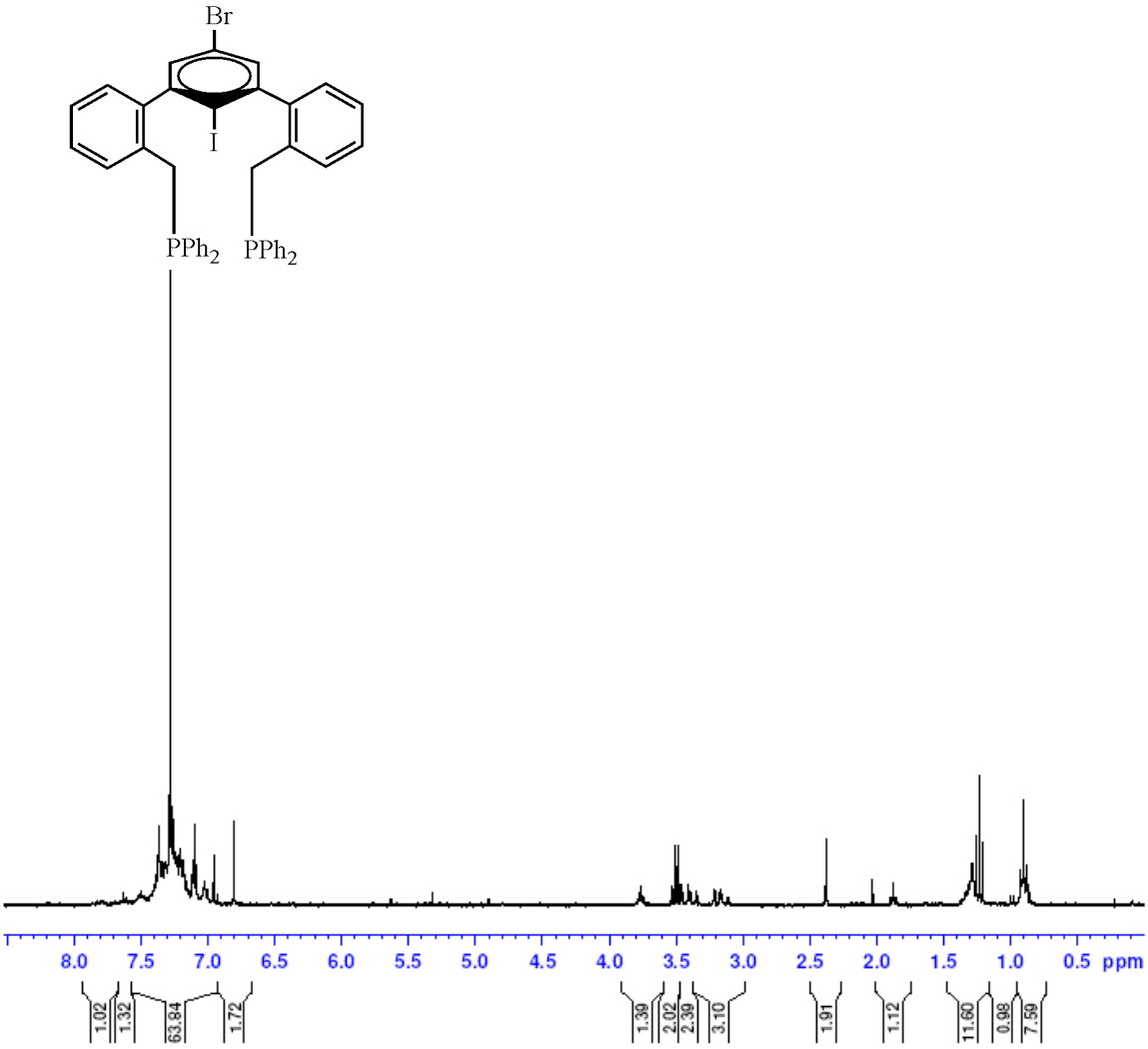

Figure A-23: ^{1}H NMR (300 MHz, $CDCl_3$) of functionalized terphenylphosphine with a bromide and iodide on the central phenyl ring.

Functionalized terphenylphosphine **9**; EGT-1-70; 07/18/08

Structure:

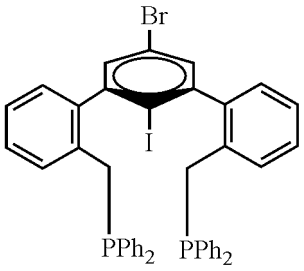

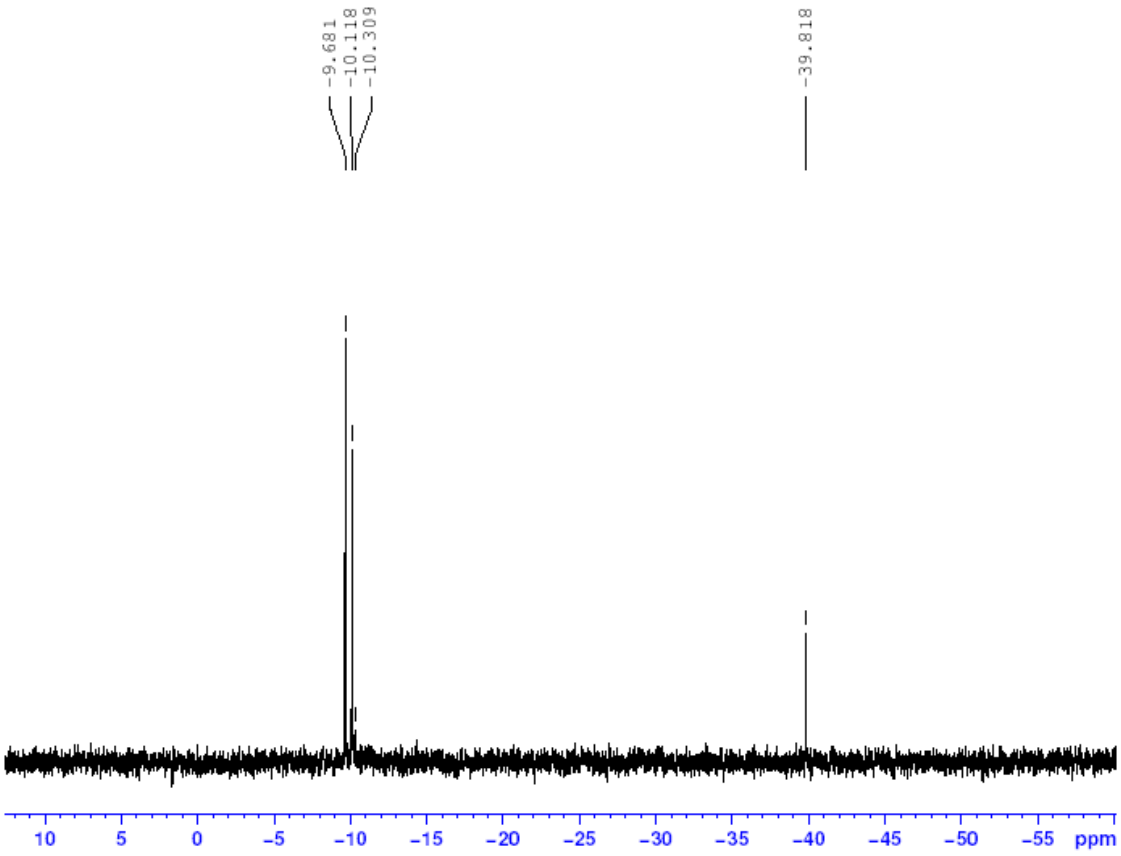

Figure A-24: ^{31}P NMR (121.4 MHz, $CDCl_3$) of functionalized terphenylphosphine with a bromide and iodide on the central phenyl ring.

Functionalized terphenylphosphine **9**; EGT-1-71; 07/21/08

Structure:

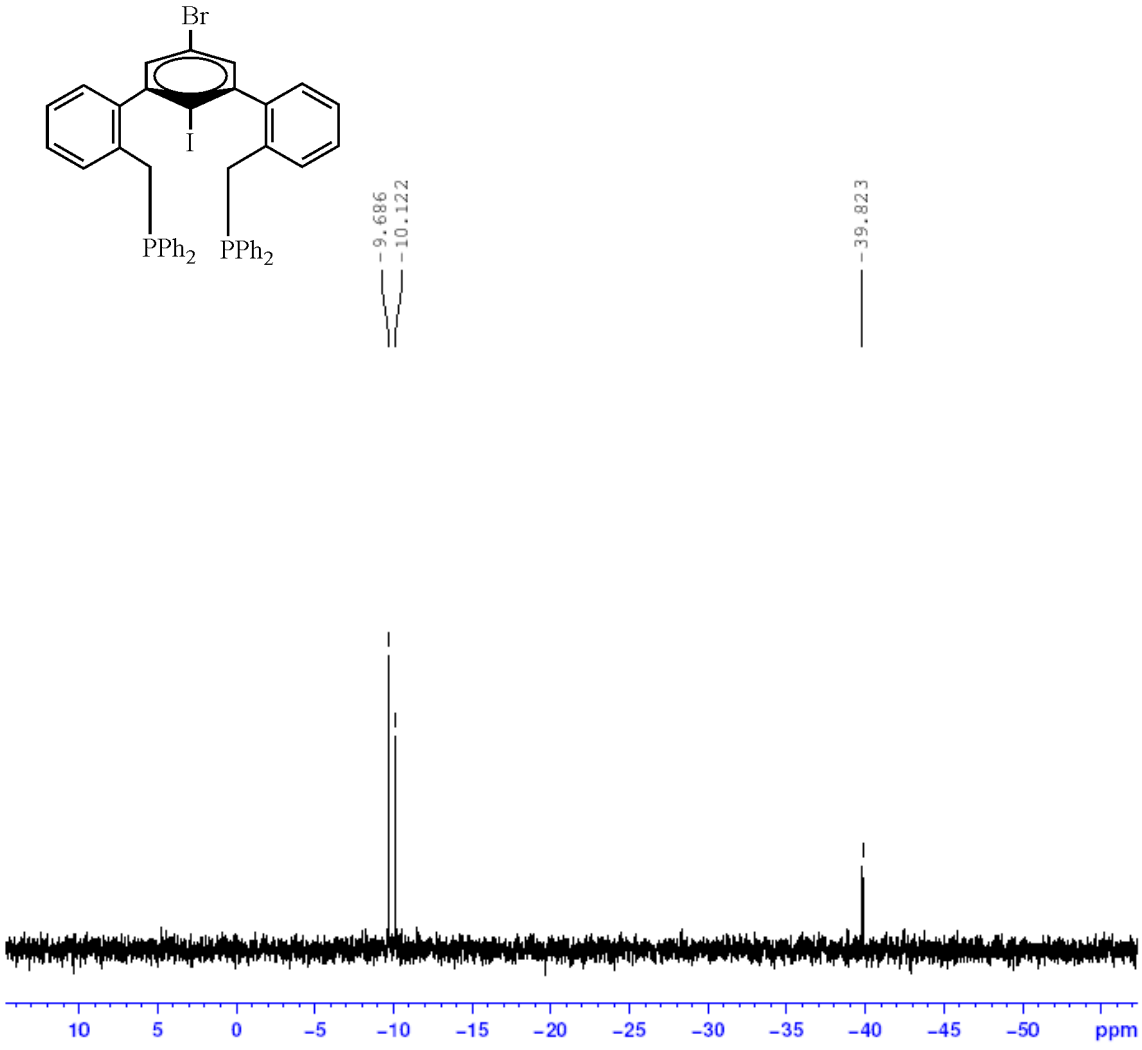

Figure A-25: ^{31}P NMR (121.4 MHz, $CDCl_3$) of functionalized terphenylphosphine with a bromide and iodide on the central phenyl ring after air-free water wash.

Functionalized terphenylphosphine **9**; EGT-1-72; 07/22/08

Structure:

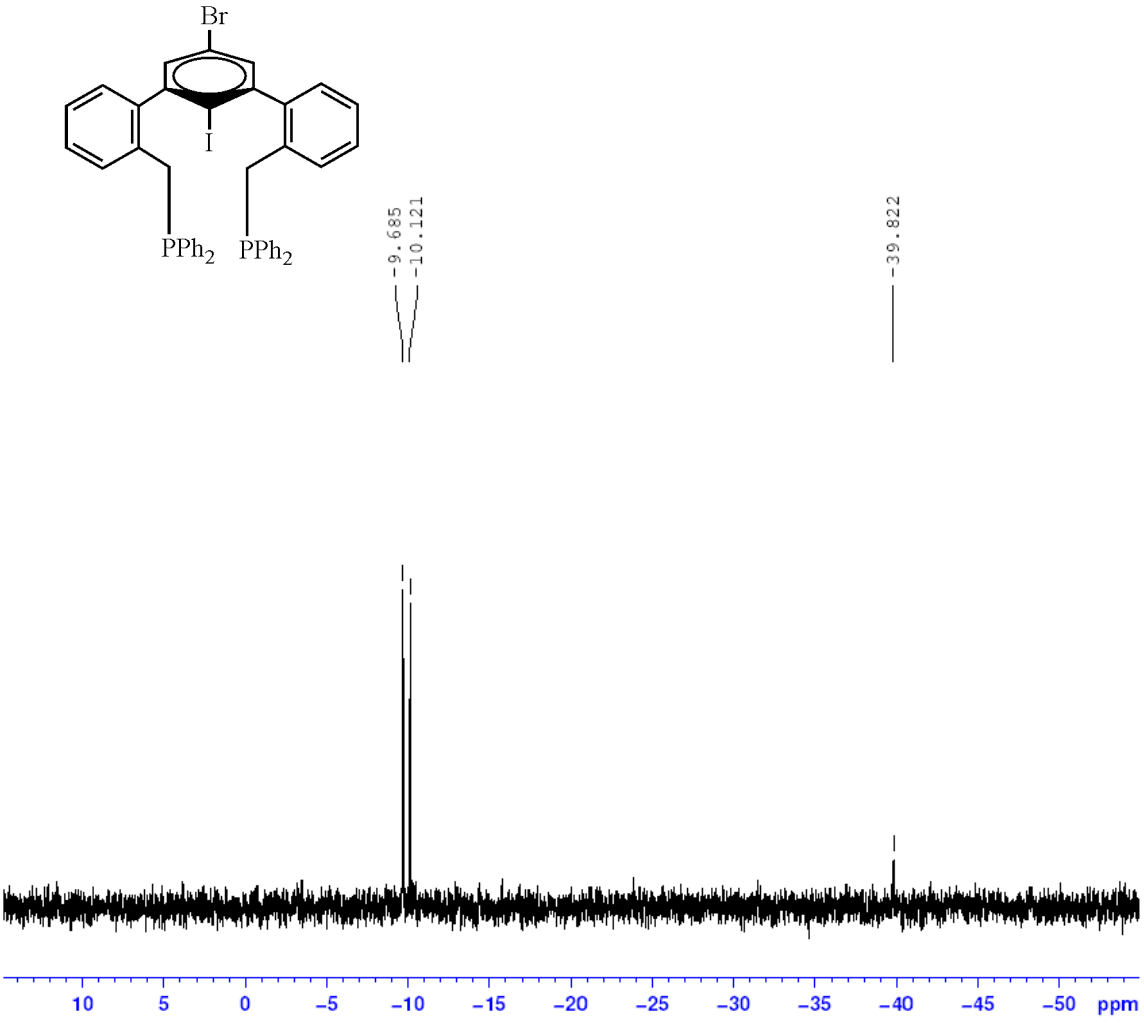

Figure A-26: ^{31}P NMR (121.4 MHz, $CDCl_3$) of functionalized terphenylphosphine **9** as made with only 2.1 equiv of chlorodiphenylphosphine.

Functionalized terphenyl-scaffolded platinum complex **10**; EGT-1-73; 07/23/08

Structure:

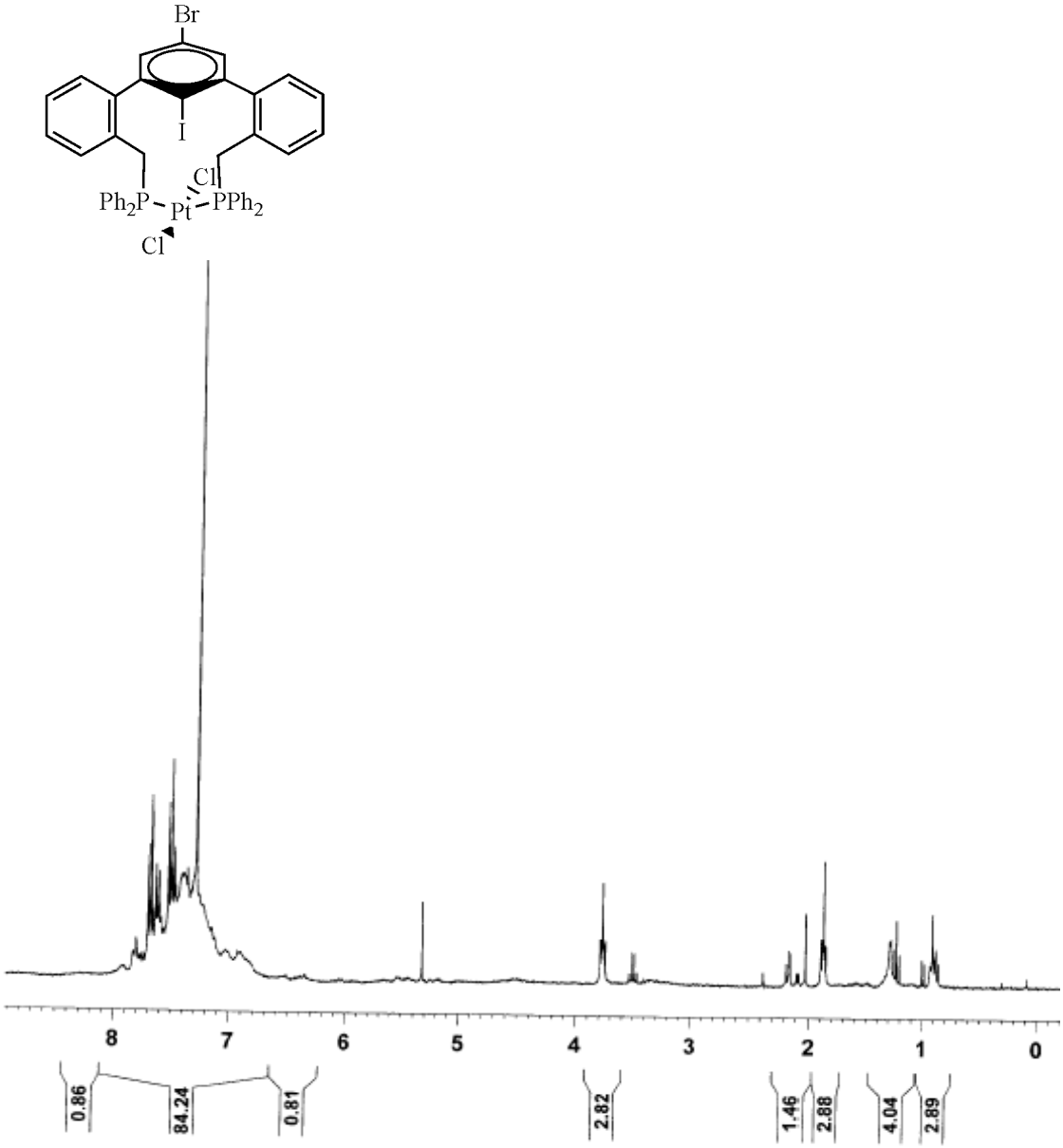

Figure A-27: ^{1}H NMR (121.4 MHz, $CDCl_3$) of functionalized terphenyl-scaffolded platinum species **10**.

Functionalized terphenyl-scaffolded platinum complex **10**; EGT-1-73; 07/23/08

Structure:

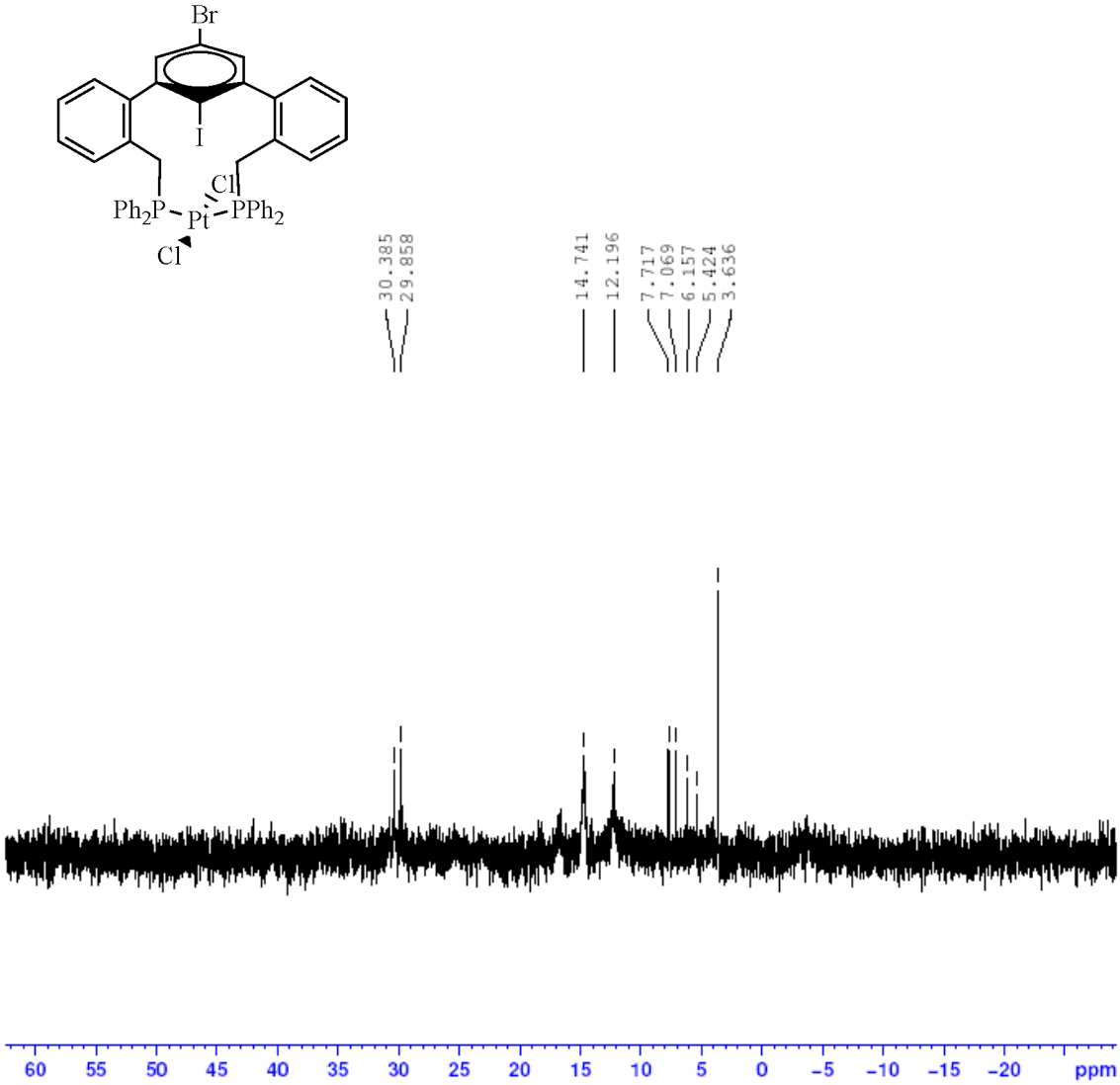

Figure A-28: ^{31}P NMR (121.4 MHz, $CDCl_3$) of functionalized terphenyl-scaffolded platinum species **10**.

Functionalized terphenyl-scaffolded platinum complex **10**; EGT-1-73; 07/25/08

Structure:

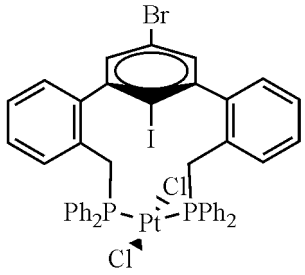

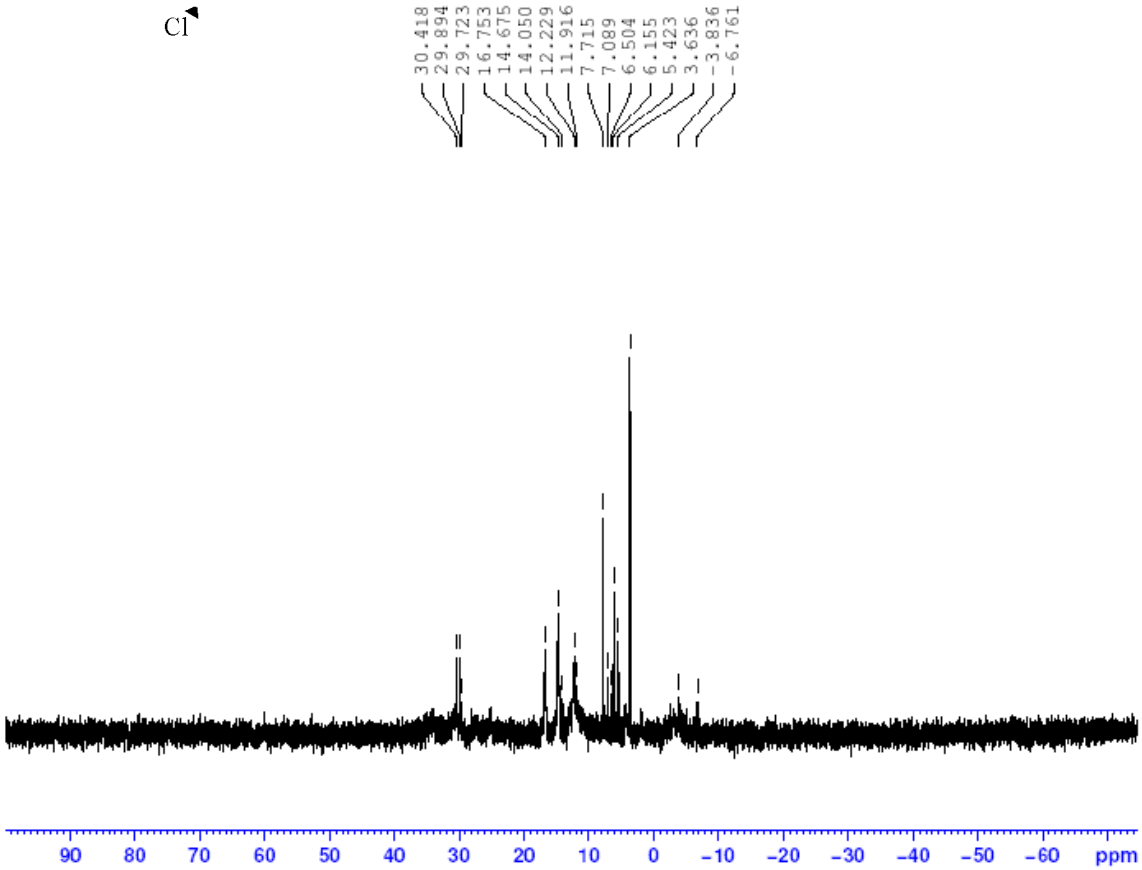

Figure A-29: ^{31}P NMR (121.4 MHz, $CDCl_3$) of functionalized terphenyl-scaffolded platinum species **10** after heating to 60°C for 2 h.

Functionalized terphenyl-scaffolded platinum complex **9**; EGT-1-73; 07/25/08

Structure:

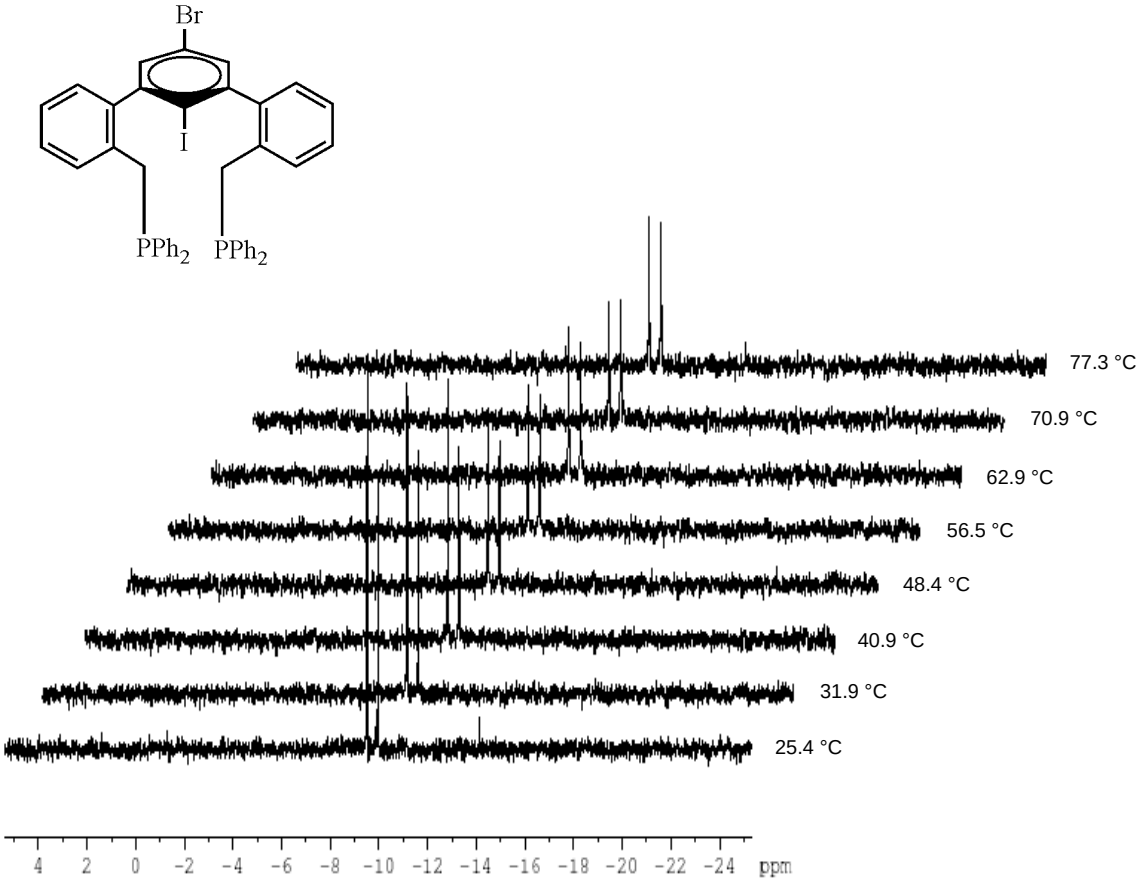

Figure A-30: VT-^{31}P NMR (121.4 MHz, $CDCl_3$) of functionalized terphenylphosphine **9** showing no coalescence or change in relative amounts of *syn* and *anti* isomer.

Functionalized phenyldialdehyde **11**; EGT-1-29; 12/01/07

Structure:

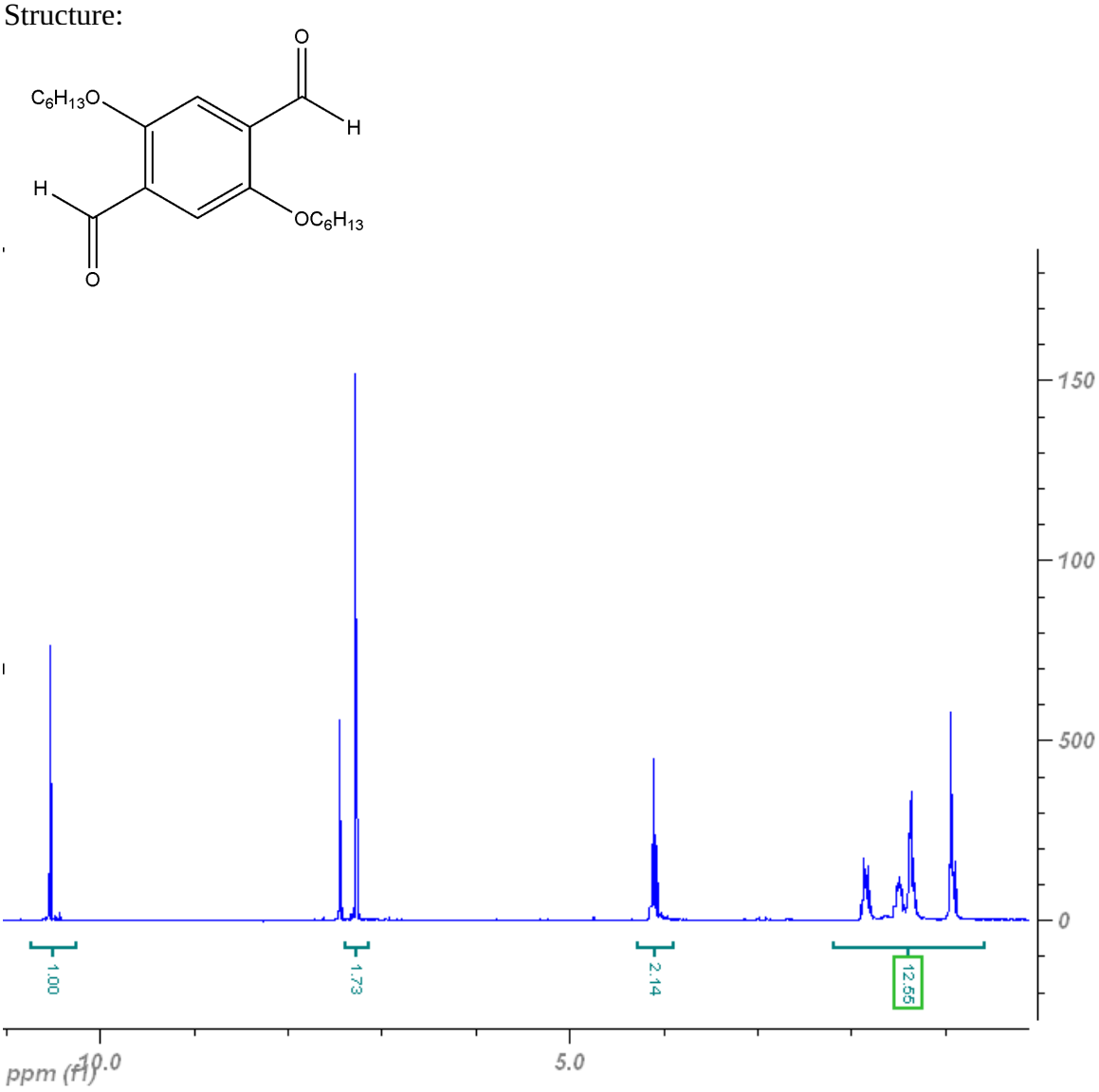

Figure A-31: ^{1}H NMR (300 MHz, $CDCl_3$) functionalized phenyldialdehyde **11**.

EGT1; EGT-1-30; 12/03/07

Structure:

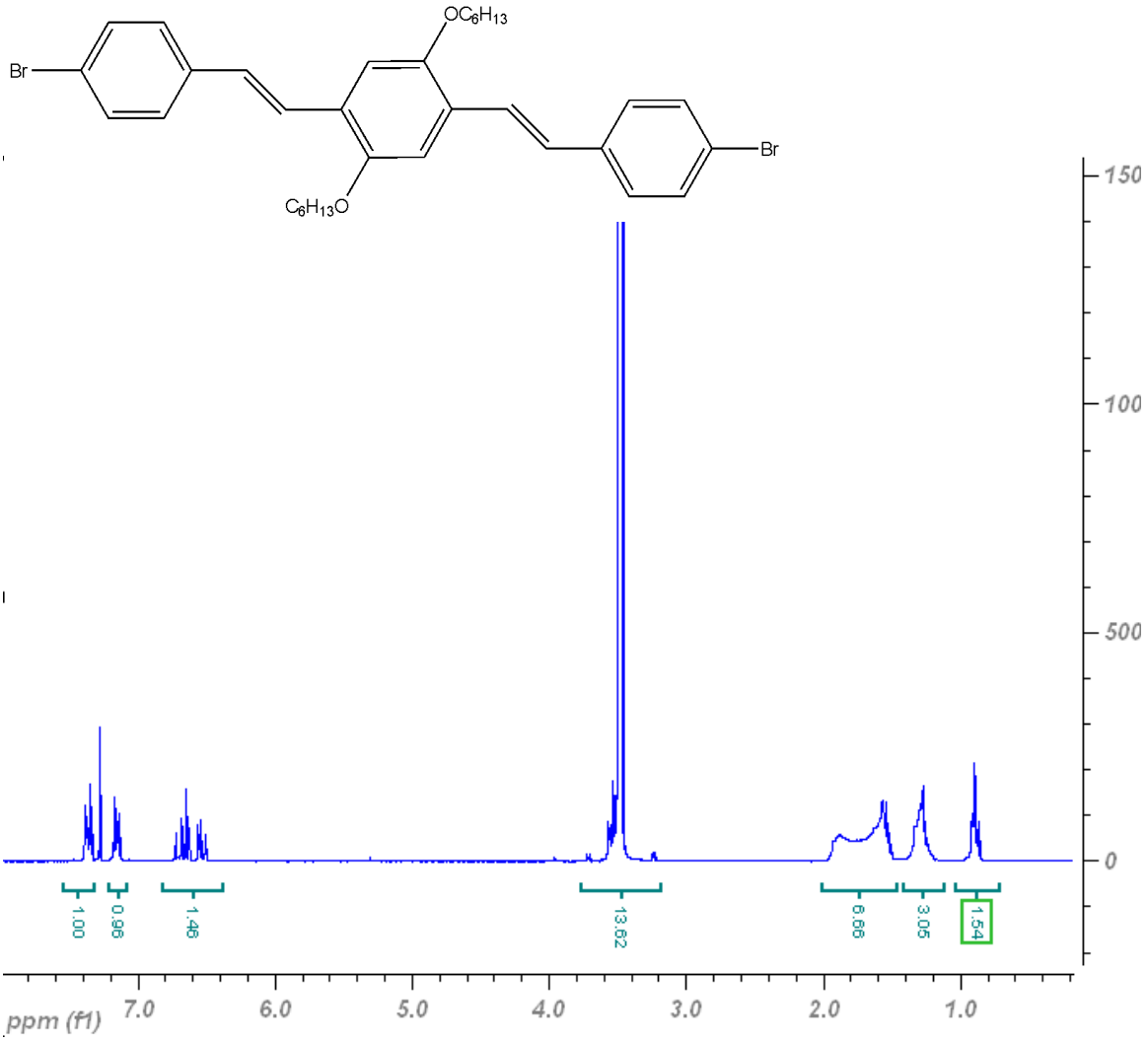

Figure A-32: ^{1}H NMR (300 MHz, $CDCl_3$) of **EGT1**.

EGT1; EGT-1-30; 12/03/07

Structure:

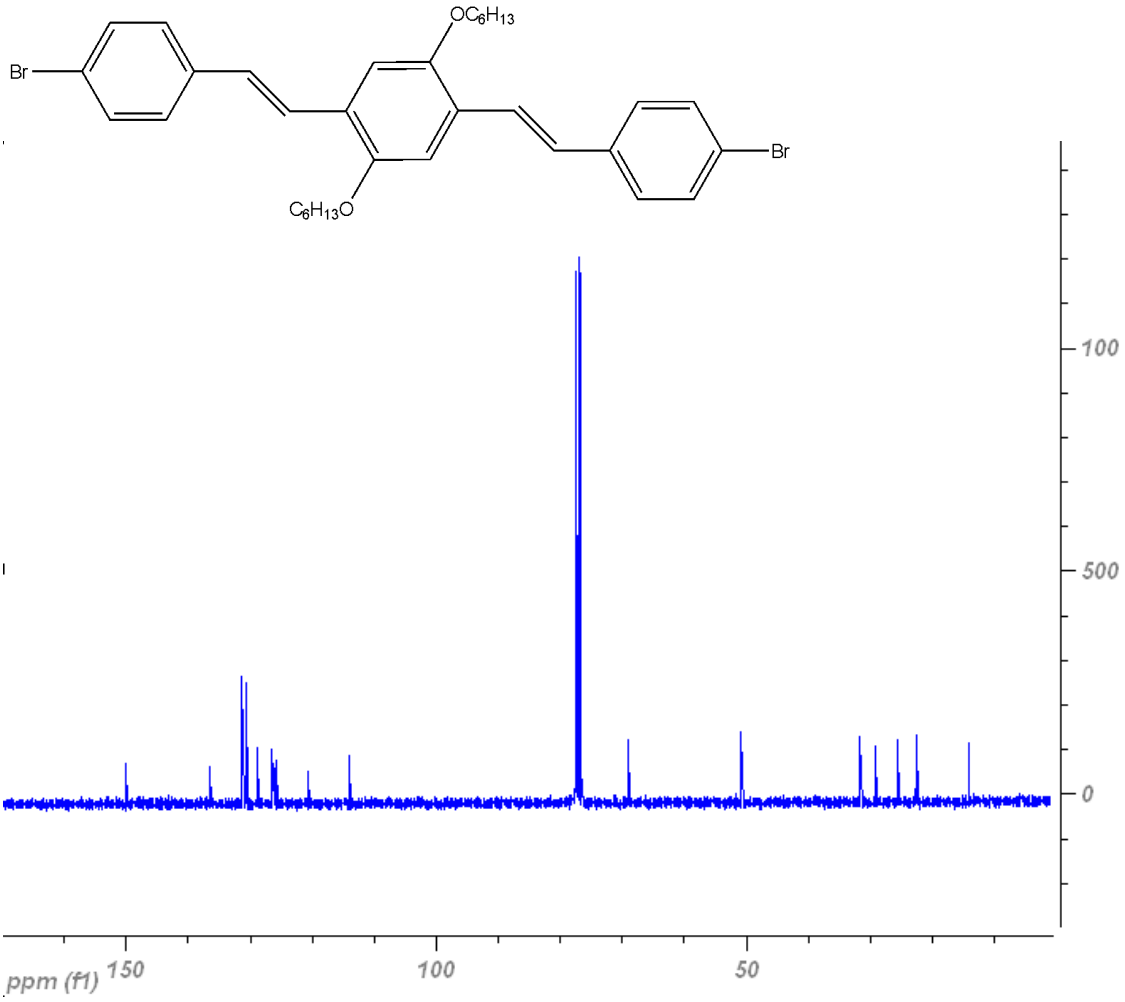

Figure A-33: ^{13}C NMR (75.4 MHz, $CDCl_3$) of **EGT1**.

Phosphine scaffold **13**; EGT-1-31; 12/05/07

Structure:

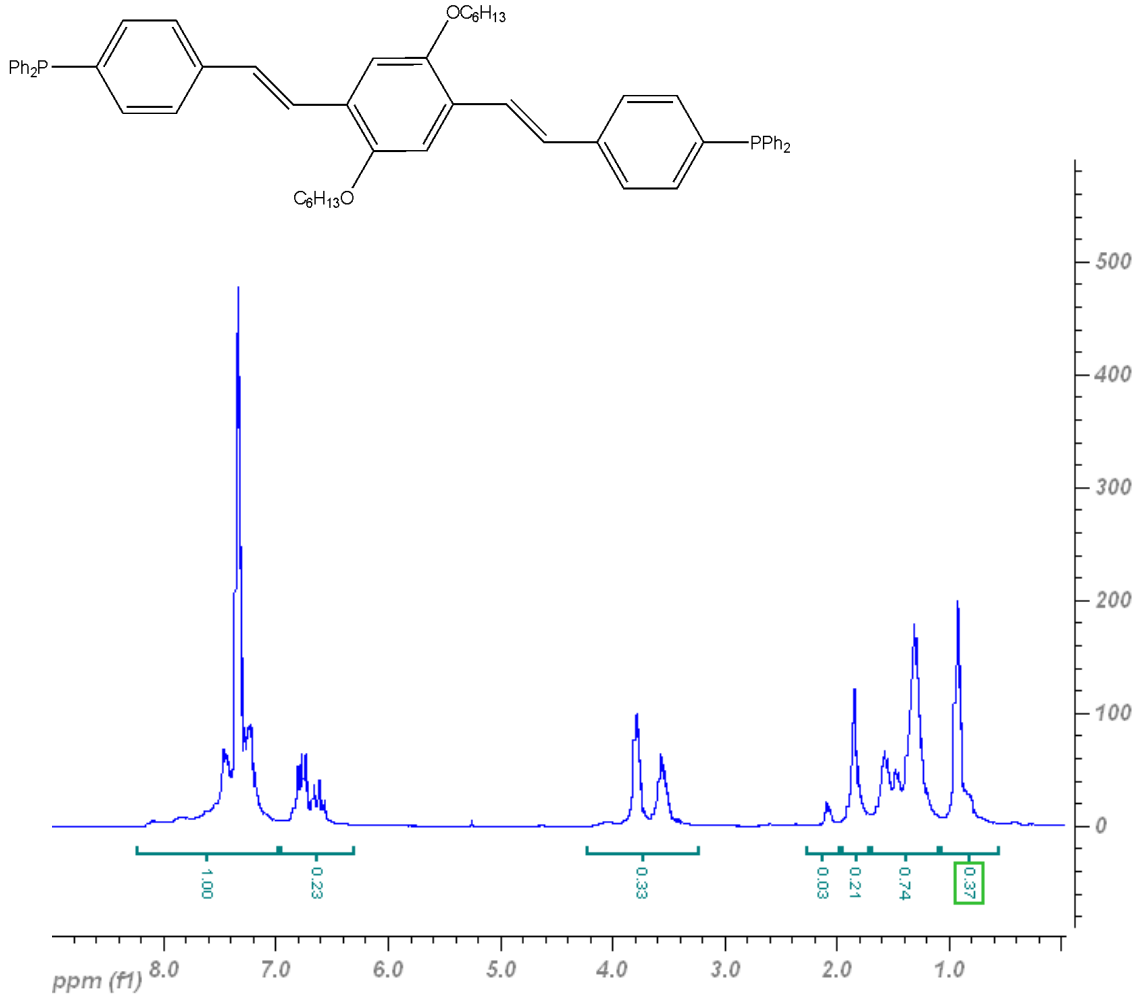

Figure A-34: ^{1}H NMR (300 MHz, $CDCl_3$) of unique phosphine scaffold **13**.

Phosphine scaffold **13**; EGT-1-31; 12/05/07

Structure:

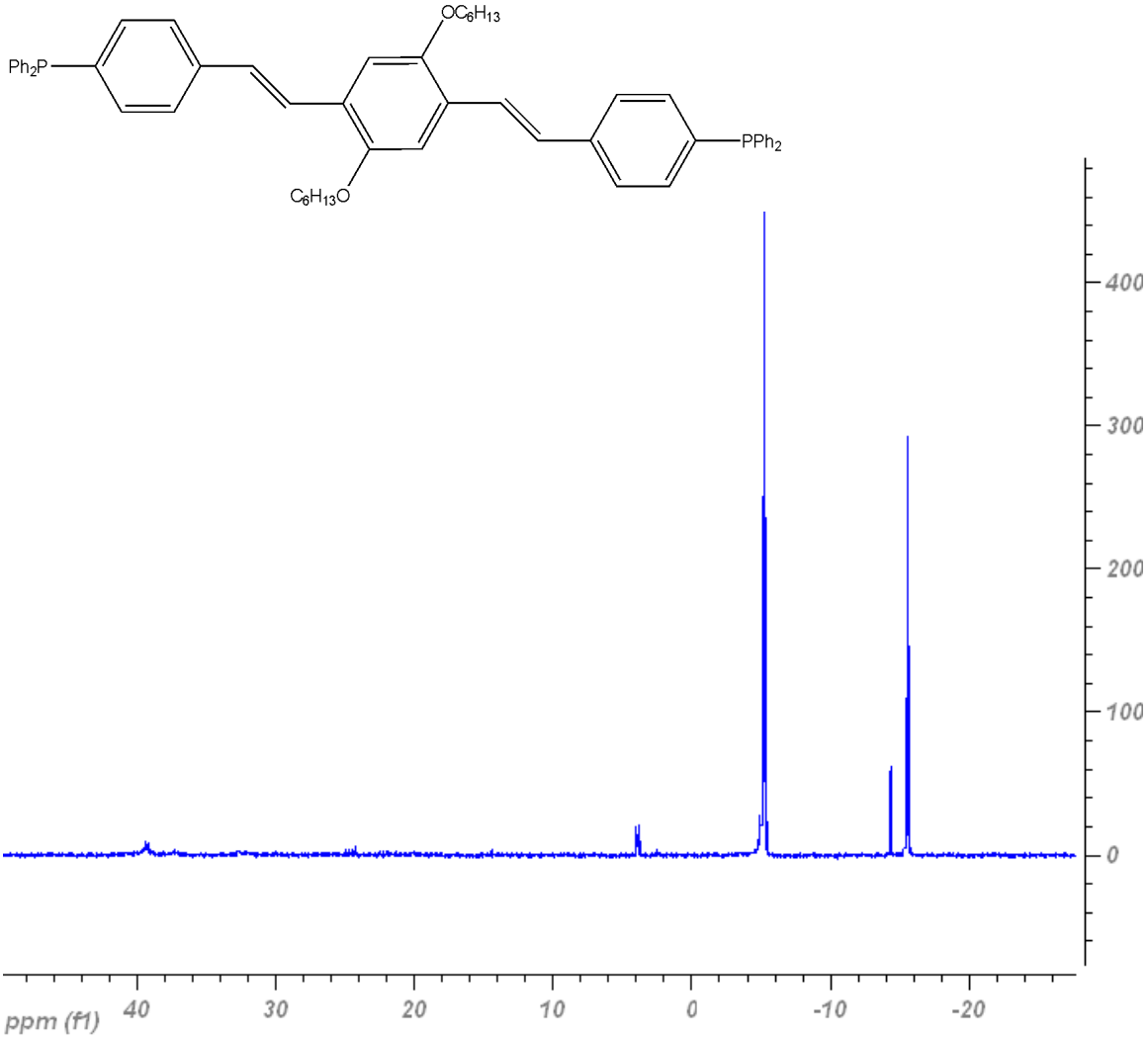

Figure A-35: ^{31}P NMR (121.4 MHz, $CDCl_3$) of unique phosphine scaffold **13**.

Phosphine scaffold **13**; EGT-1-32; 01/10/08

Structure:

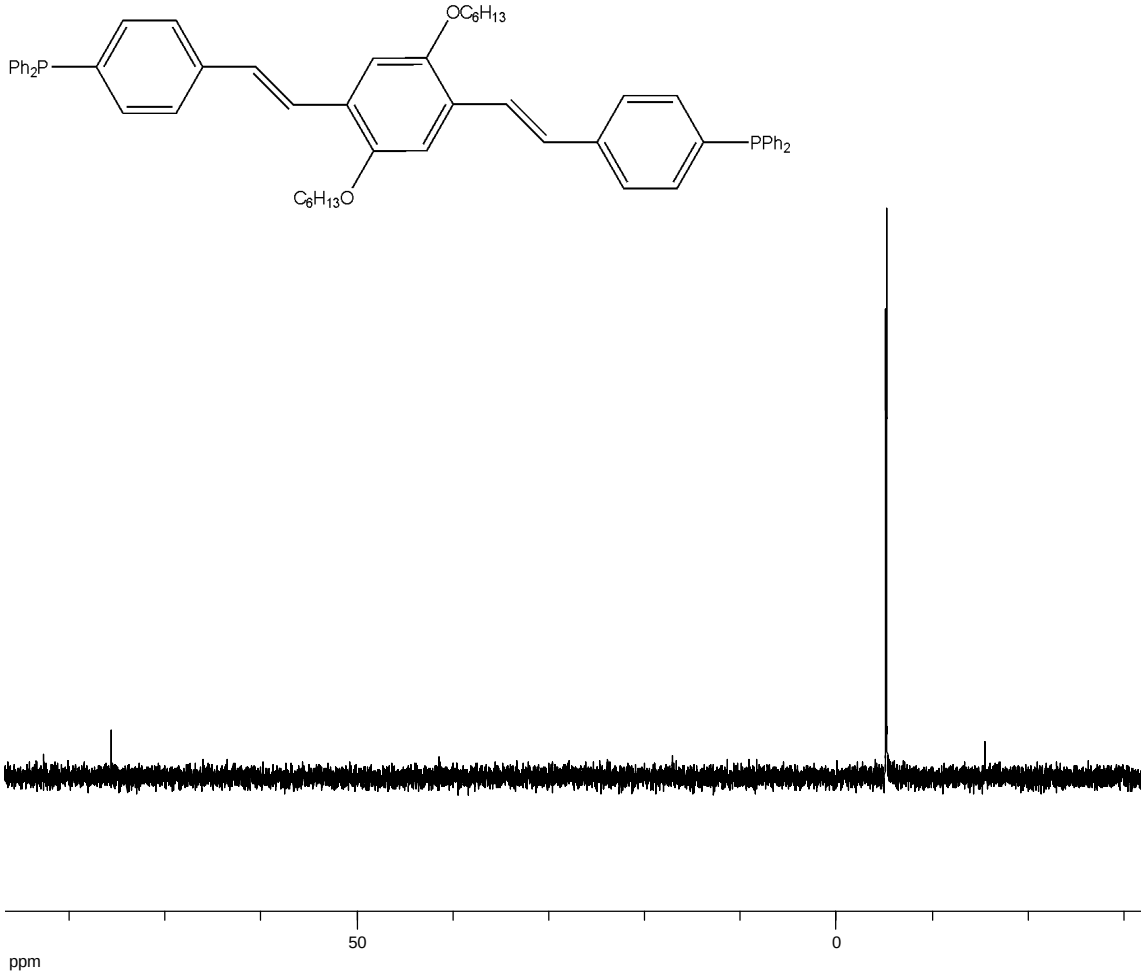

Figure A-36: ^{31}P NMR (121.4 MHz, $CDCl_3$) of phosphine **13** after washing with acetonitrile.

Phosphine scaffold **13**; EGT-1-34; 01/24/08

Structure:

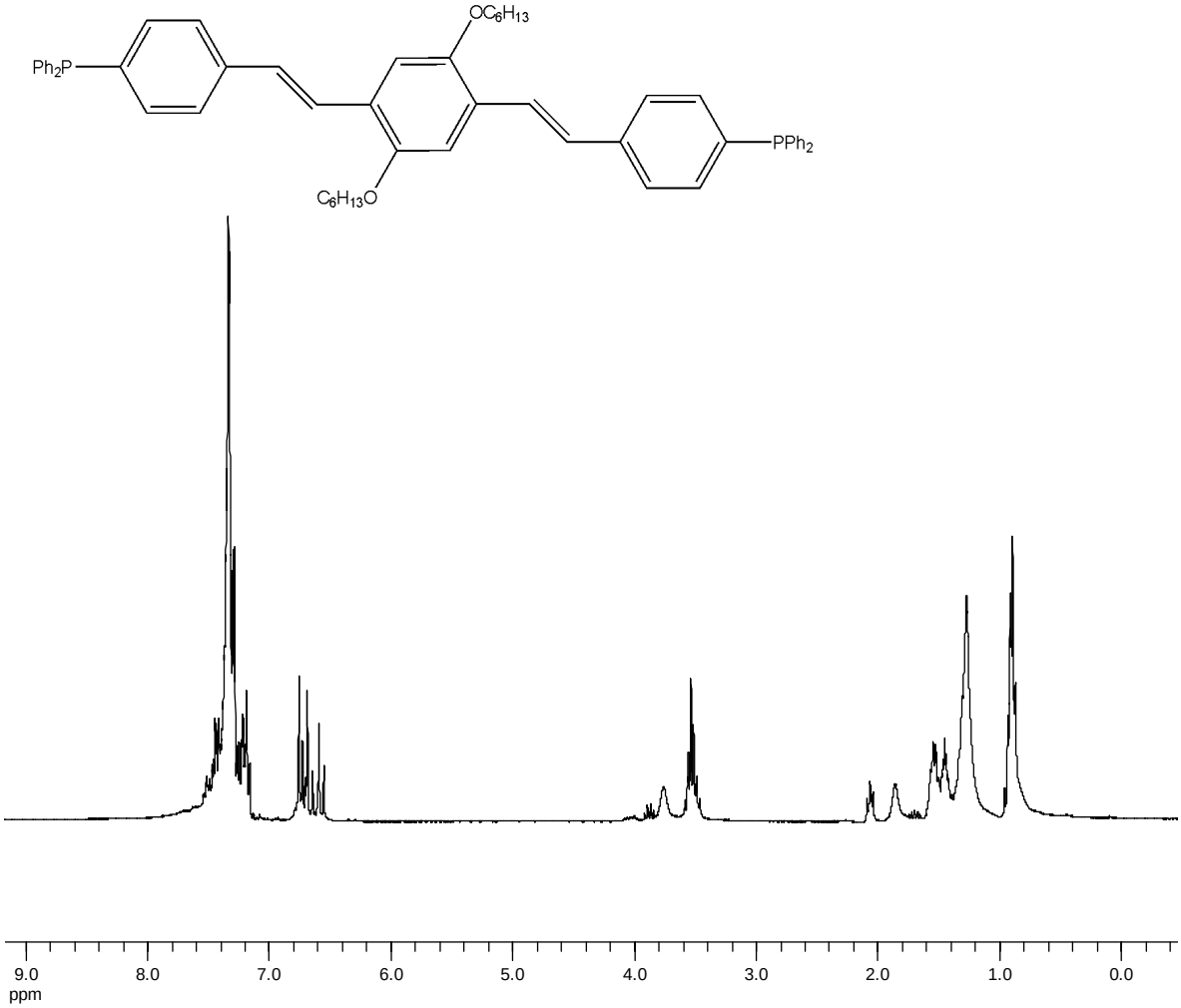

Figure A-37: ^{1}H NMR (300 MHz, $CDCl_3$) of later batch of phosphine **13**.

Phosphine scaffold **13**; EGT-1-34; 01/24/08

Structure:

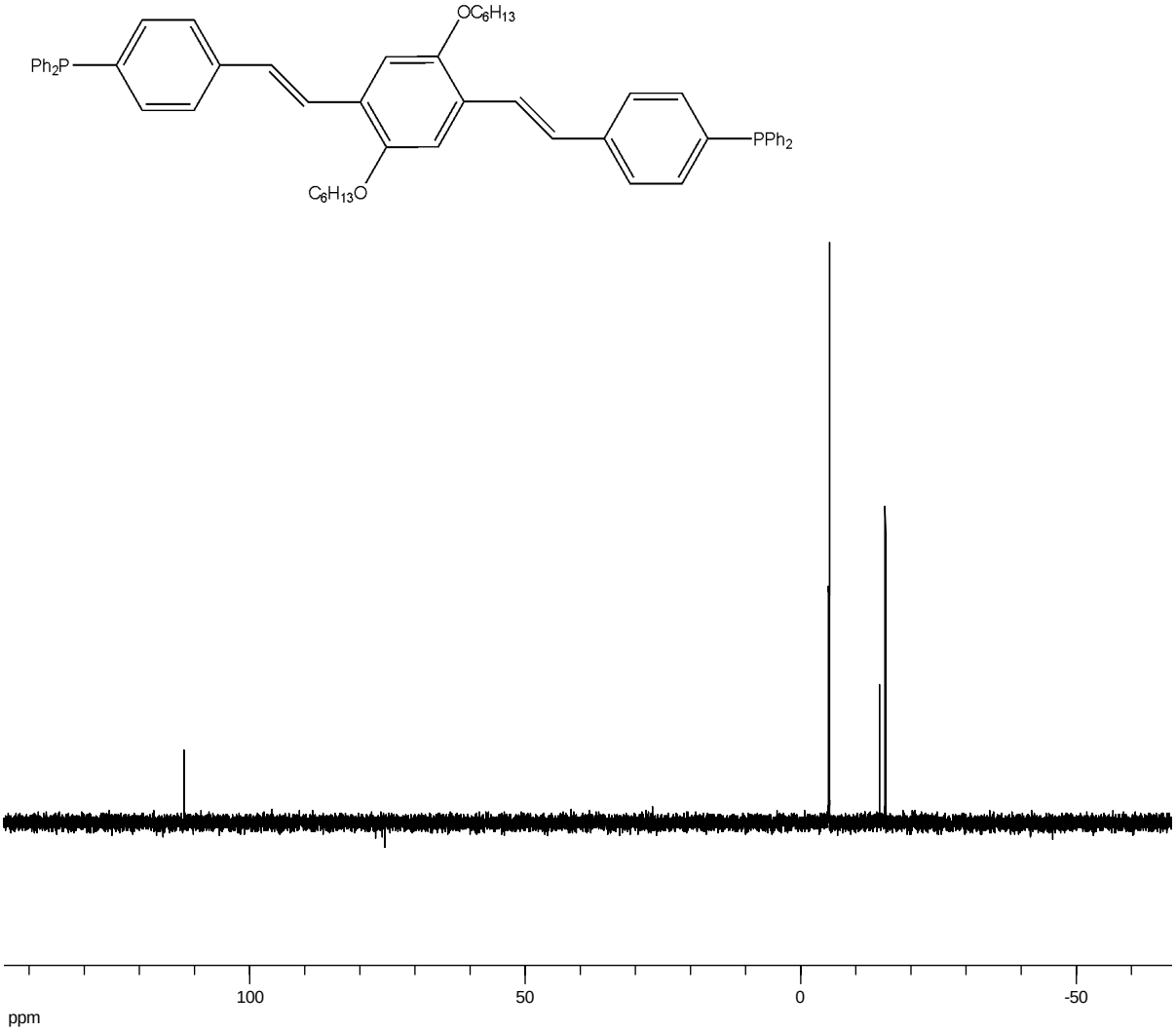

Figure A-38: ^{31}P NMR (121.4 MHz, $CDCl_3$) of later batch of phosphine **13**.

Phosphine scaffold **13**; EGT-1-36; 01/30/08

Structure:

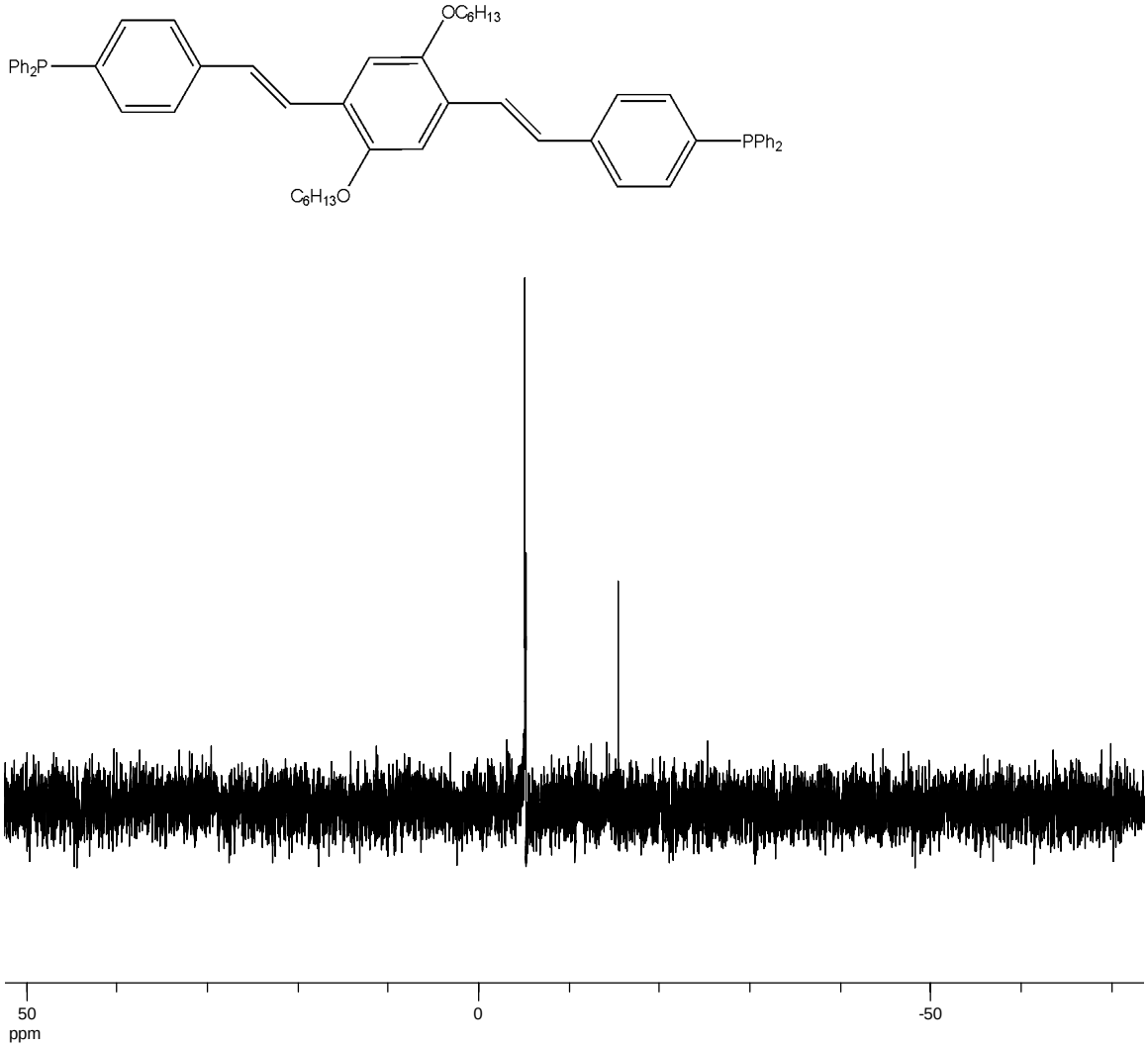

Figure A-39: ^{31}P NMR (121.4 MHz, $CDCl_3$) of phosphine **13** attempt at recrystallizing by diffusion of pentane into a solution of **13** in dichloromethane.

4-bromophenyldiphenylphosphine oxide **14**; EGT-1-37; 02/08/08

Structure:

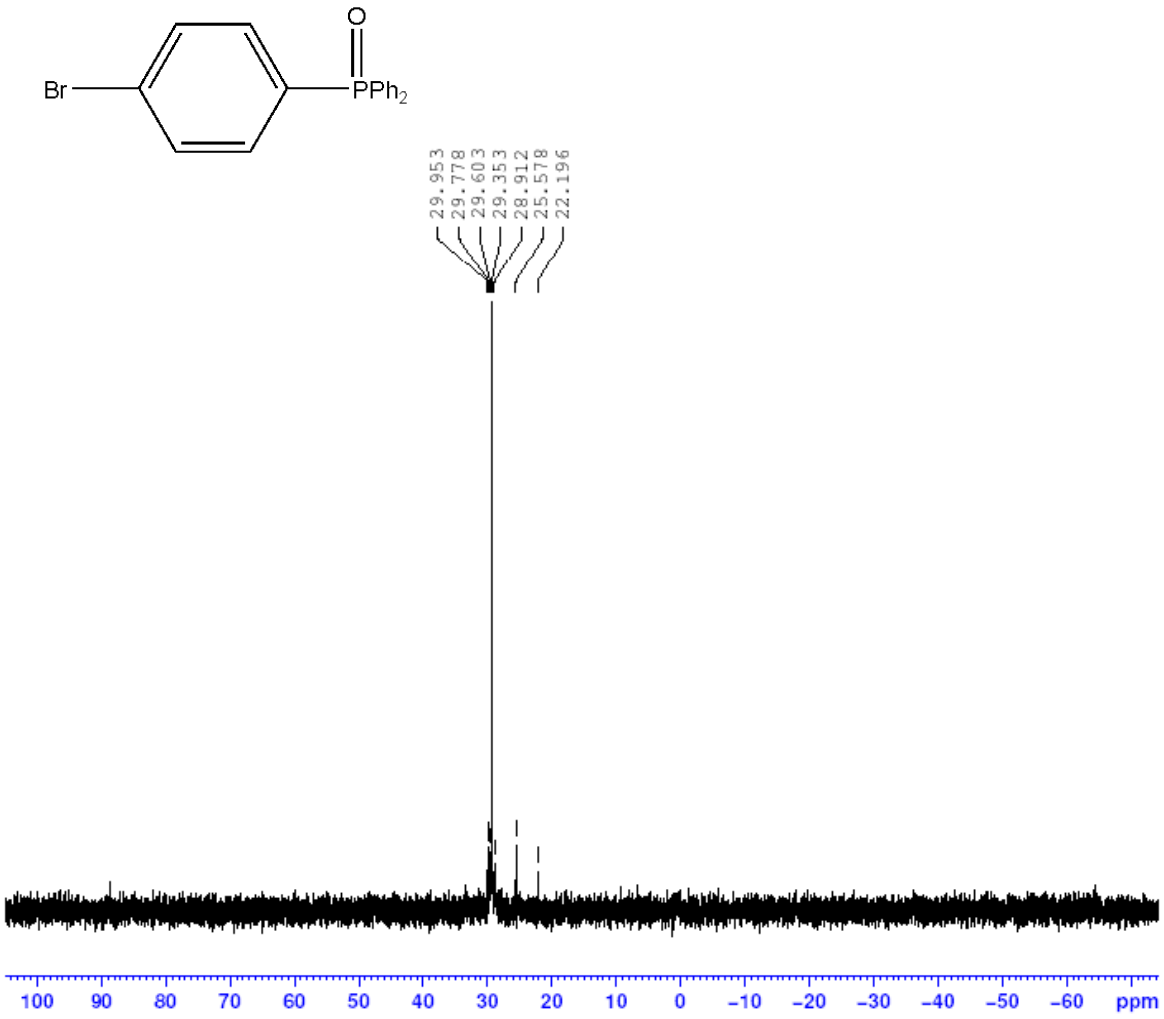

Figure A-40: ^{31}P NMR (121.4 MHz, $CDCl_3$) of phosphine oxide **14** starting material to be used in Sonogashira coupling to afford desired linear phosphine oxide.

Linear phosphine oxide **16**; EGT-1-37; 02/12/08

Structure:

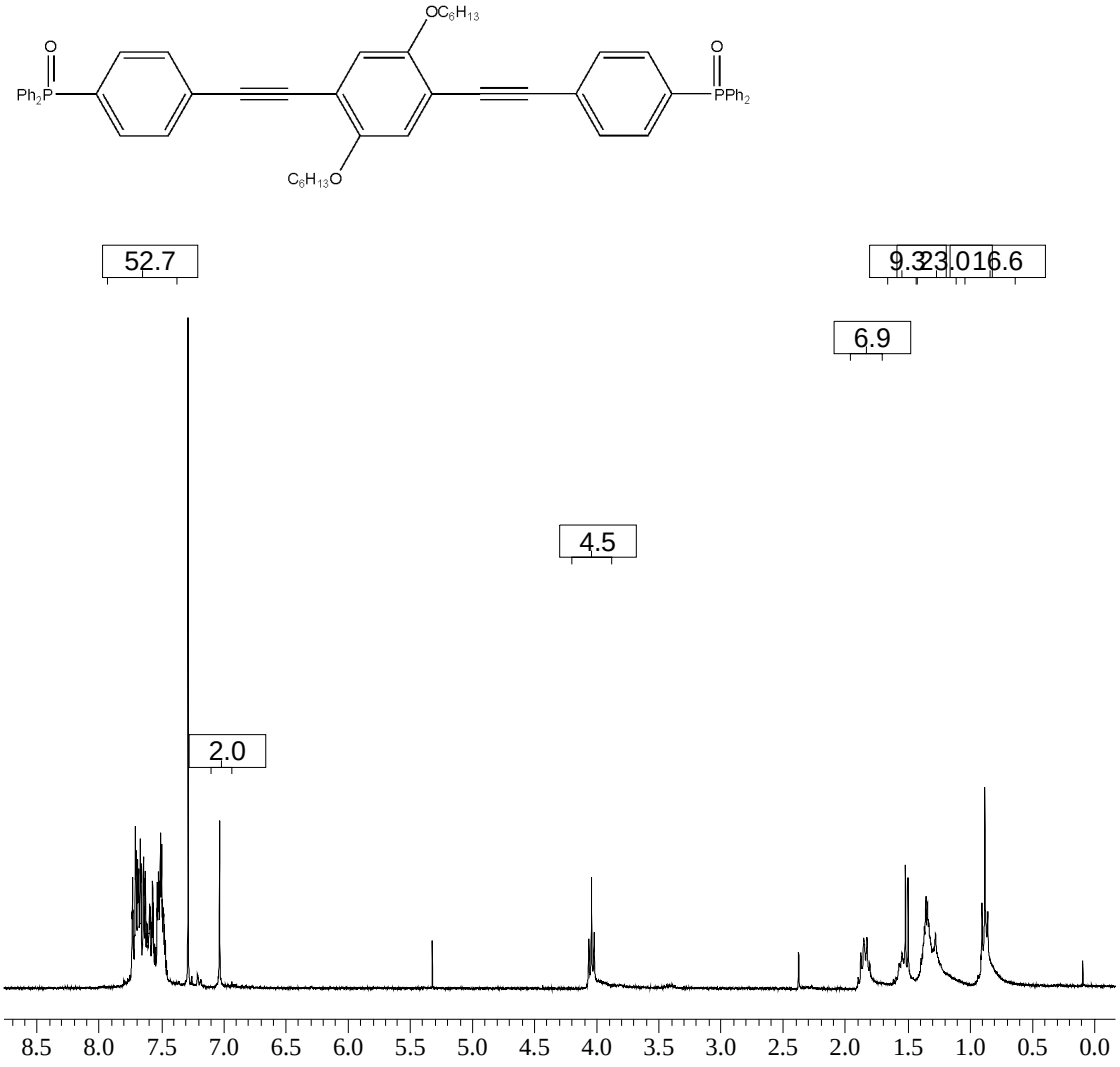

Figure A-41: ^{1}H NMR (300 MHz, $CDCl_3$) of linear phosphine oxide **16** from Sonogashira coupling between compound **14** and 1,4-diethynyl-2,5-dihexyloxybenzene.

Linear phosphine oxide **16**; EGT-1-37; 02/12/08

Structure:

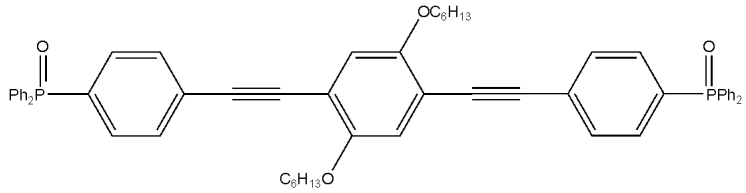

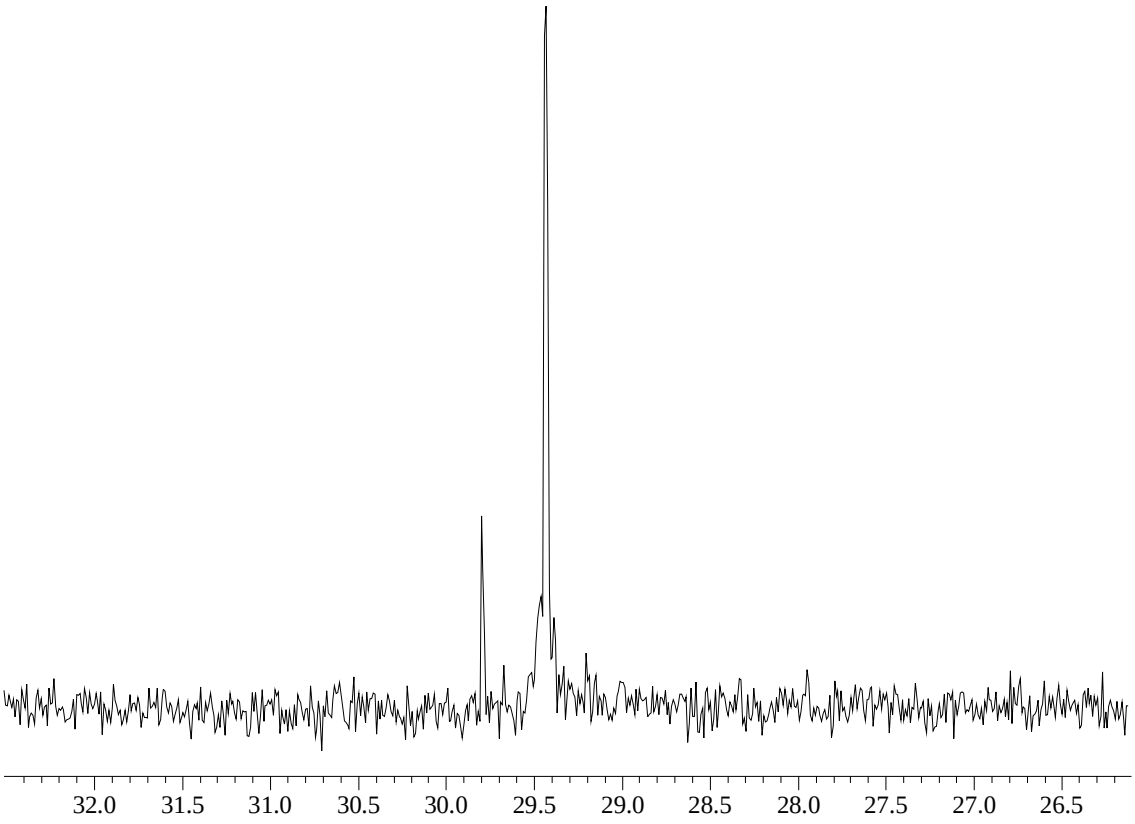

Figure A-42: ^{31}P NMR (121.4 MHz, $CDCl_3$) of linear phosphine oxide **16** from Sonogashira coupling between compound **14** and 1,4-diethynyl-2,5-dihexyloxybenzene.

Linear phosphine oxide **16**; EGT-1-41; 02/18/08

Structure:

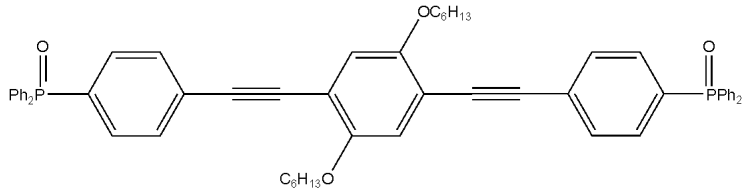

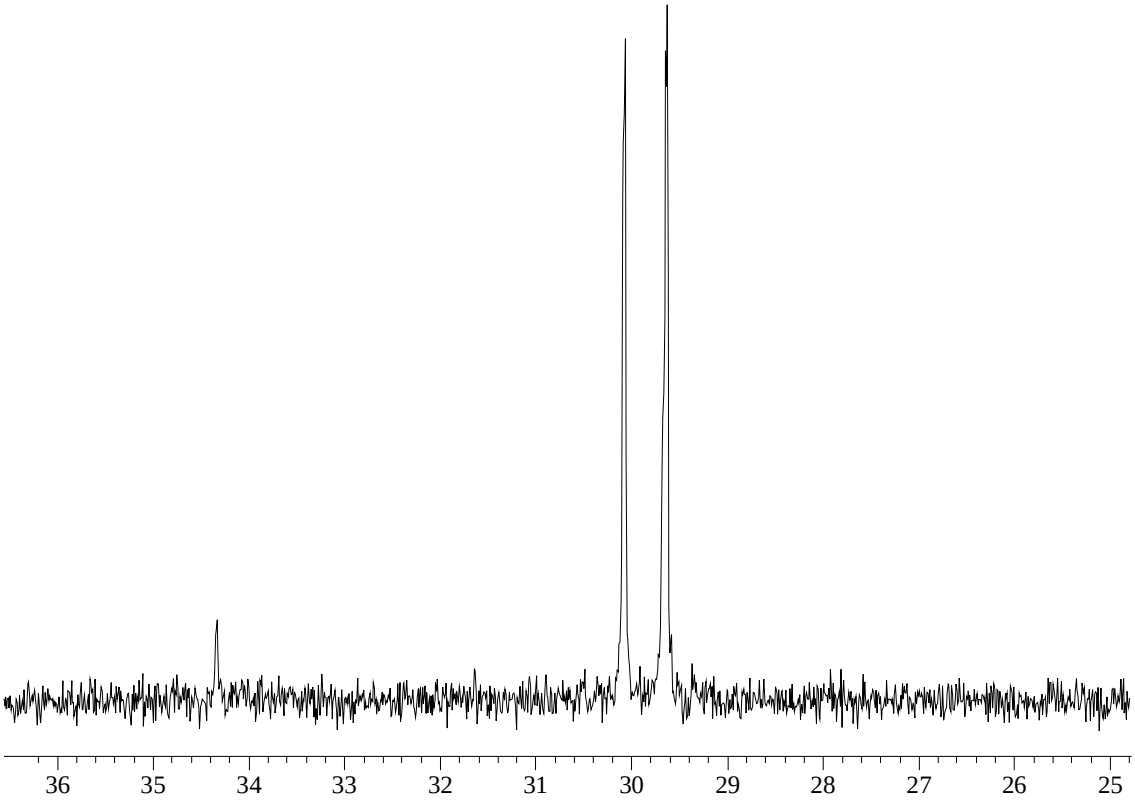

Figure A-43: ^{31}P NMR (121.4 MHz, $CDCl_3$) of linear phosphine oxide **16** from middle fraction of prep TLC.

Linear phosphine oxide **16**; EGT-1-41; 02/19/08

Structure:

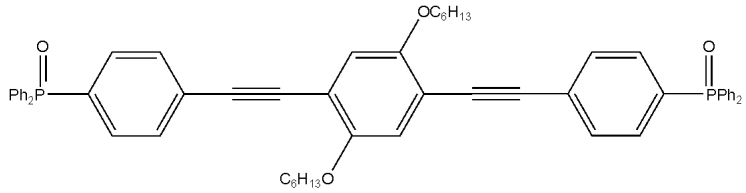

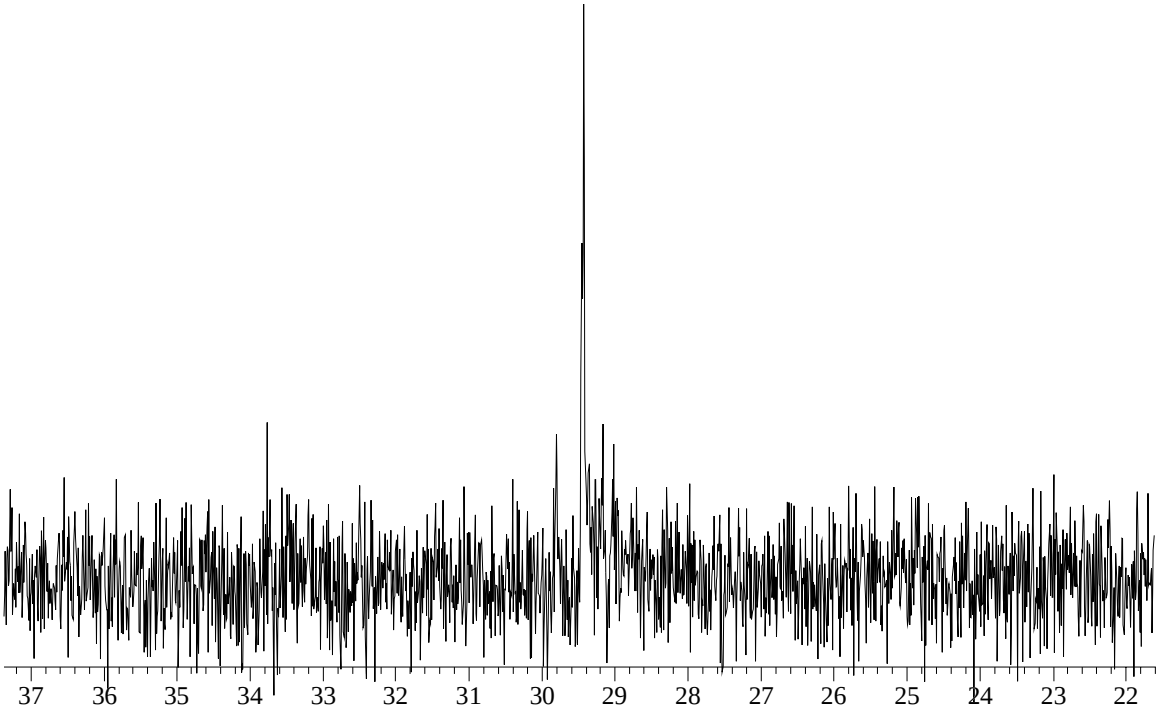

Figure A-44: ^{31}P NMR (121.4 MHz, $CDCl_3$) of linear phosphine oxide **16** from middle fraction of prep TLC after redissolving the silica in methanol and performing a DCM/water extraction to isolate the organic layer.

Linear phosphine oxide **16**; EGT-1-44; 03/08/08

Structure:

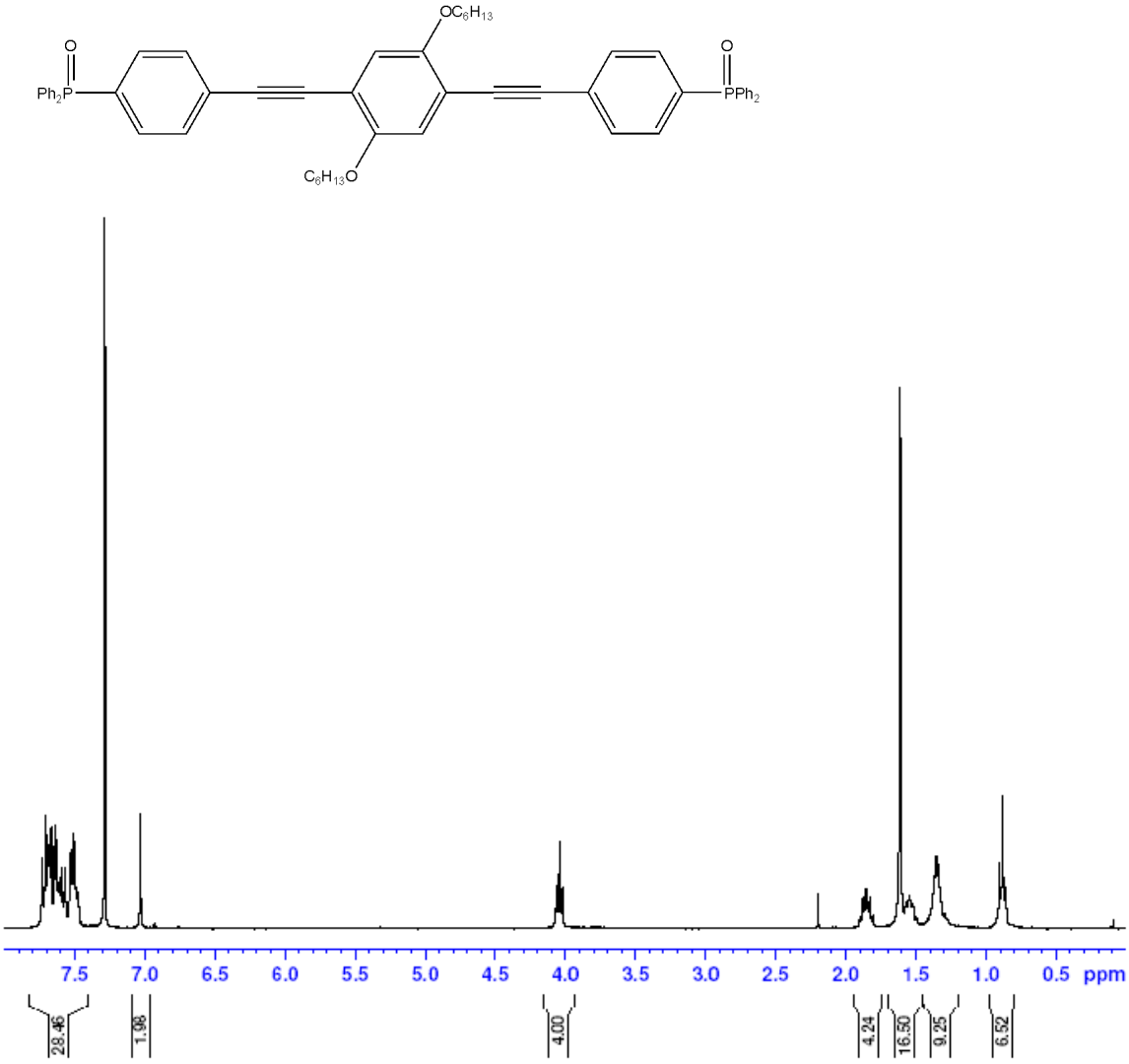

Figure A-45: ^{1}H NMR (300 MHz, $CDCl_3$) of linear phosphine oxide **16** as purified by recrystallization from diffusion of pentane into a chlorobenzene solution of **16**.

Linear phosphine oxide **16**; EGT-1-44; 03/08/08

Structure:

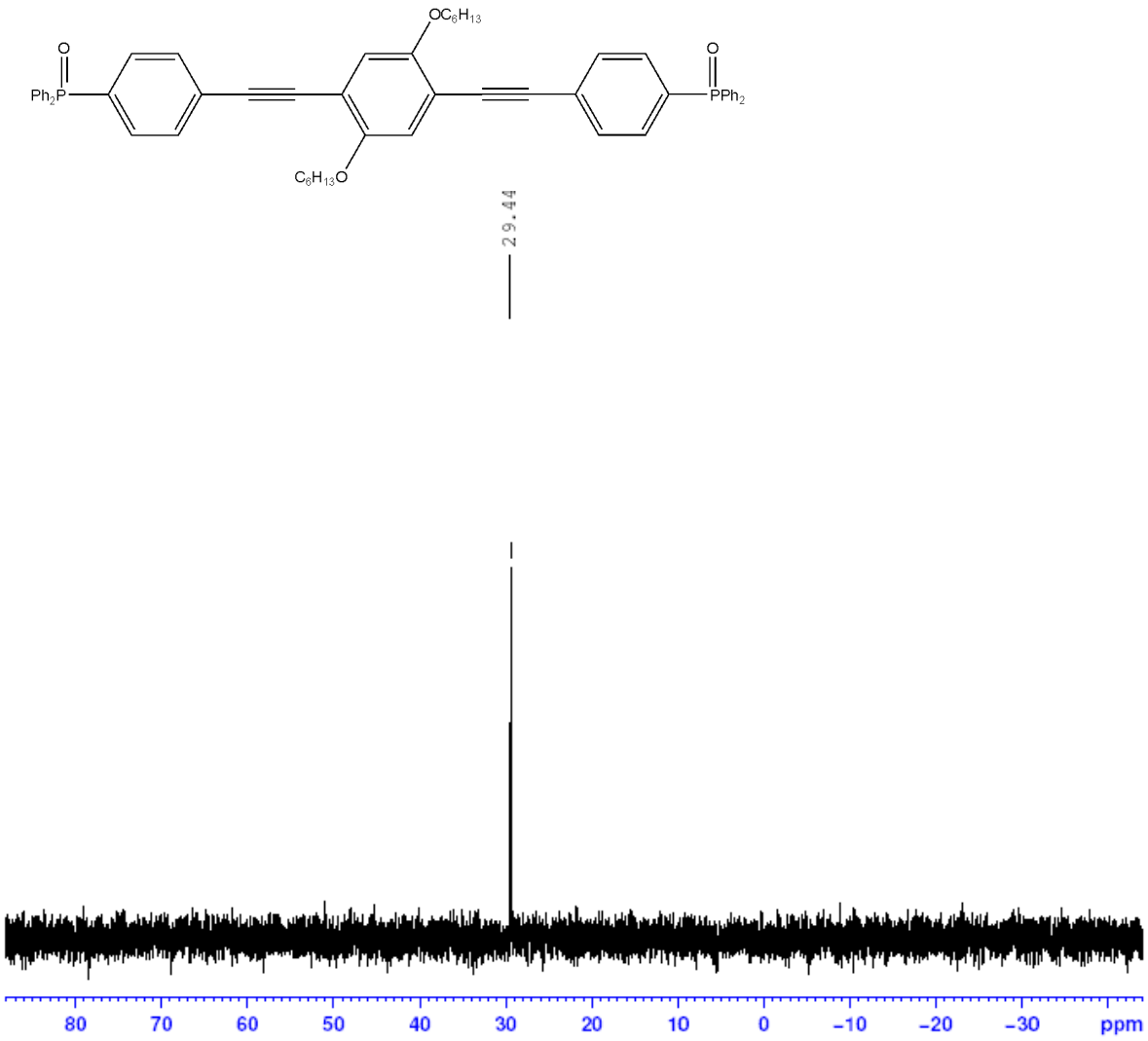

Figure A-46: ^{31}P NMR (121.4 MHz, $CDCl_3$) of linear phosphine oxide **16** as purified by recrystallization from diffusion of pentane into a chlorobenzene solution of **16**.

Fluorene-based phosphine oxide **17**; EGT-1-53; 05/06/08

Structure:

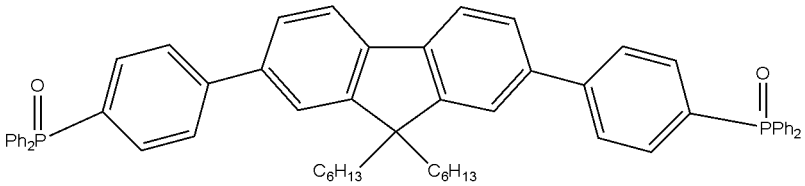

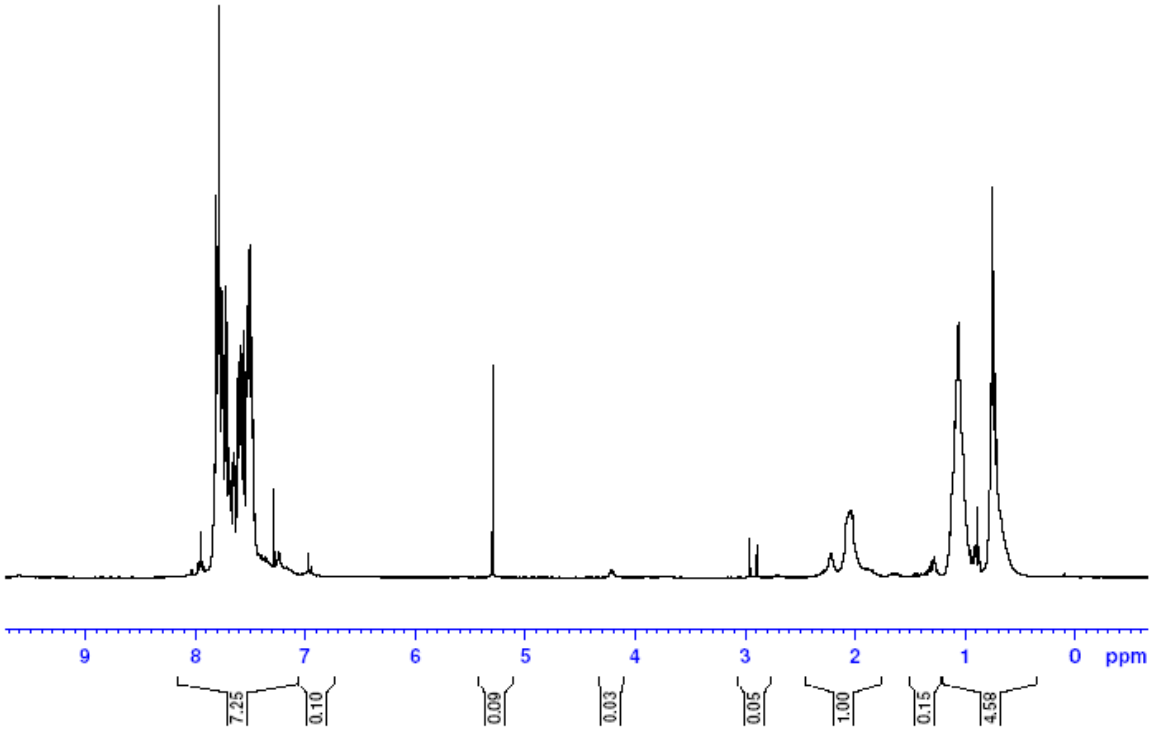

Figure A-47: ^{1}H NMR (300 MHz, $CDCl_3$) of fluorene-based phosphine oxide **17**.

Fluorene-based phosphine oxide **17**; EGT-1-53; 05/06/08

Structure:

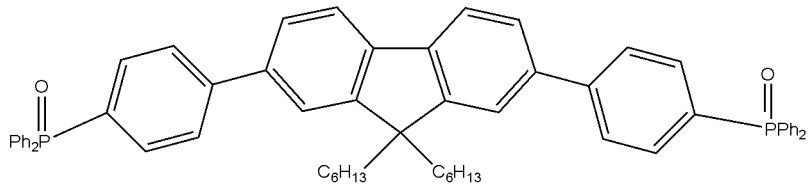

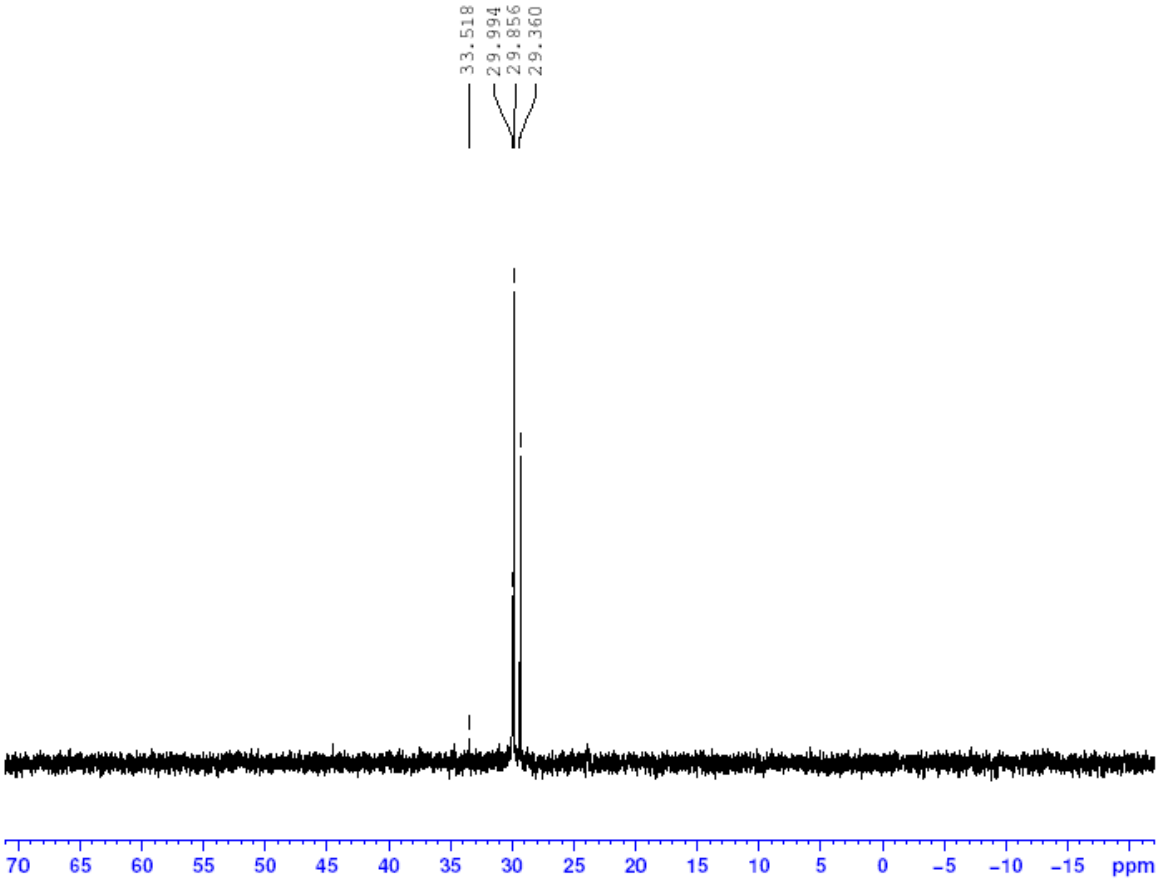

Figure A-48: ^{31}P NMR (121.4 MHz, $CDCl_3$) of fluorene-based phosphine oxide **17**.

Fluorene-based phosphine oxide **17**; EGT-1-57; 05/26/08

Structure:

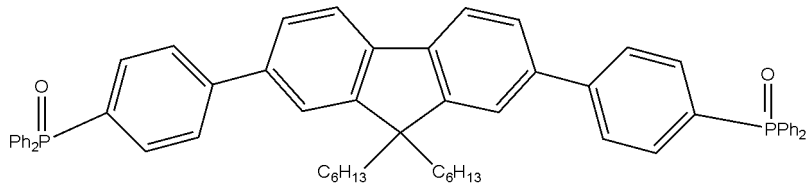

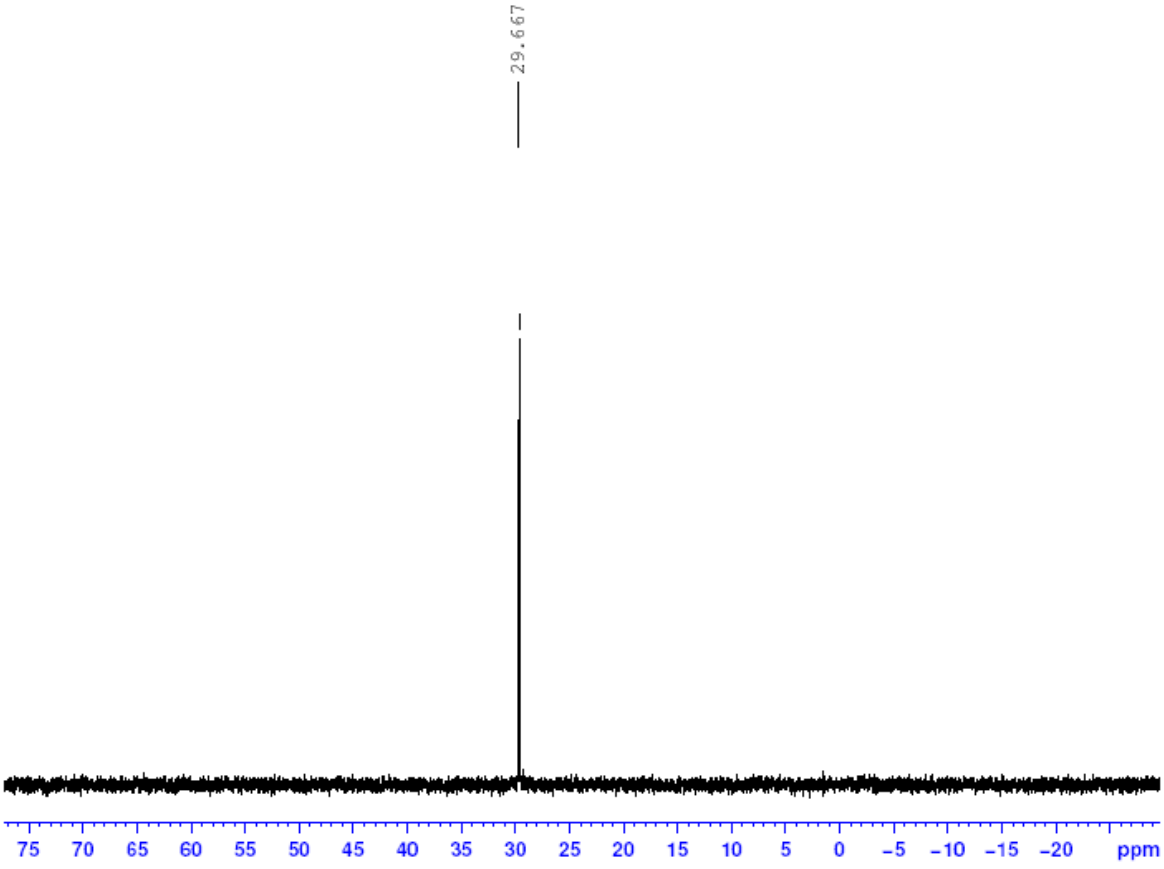

Figure A-49: ^{31}P NMR (121.4 MHz, $CDCl_3$) of white solid formed after two weeks of diffusion of pentane into a concentrated tetrahydrofuran solution of **17**.

Fluorene-based phosphine oxide **17**; EGT-1-58; 05/29/08

Structure:

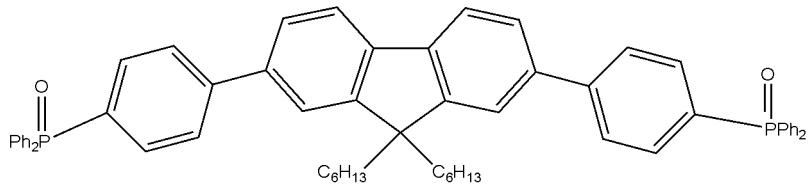

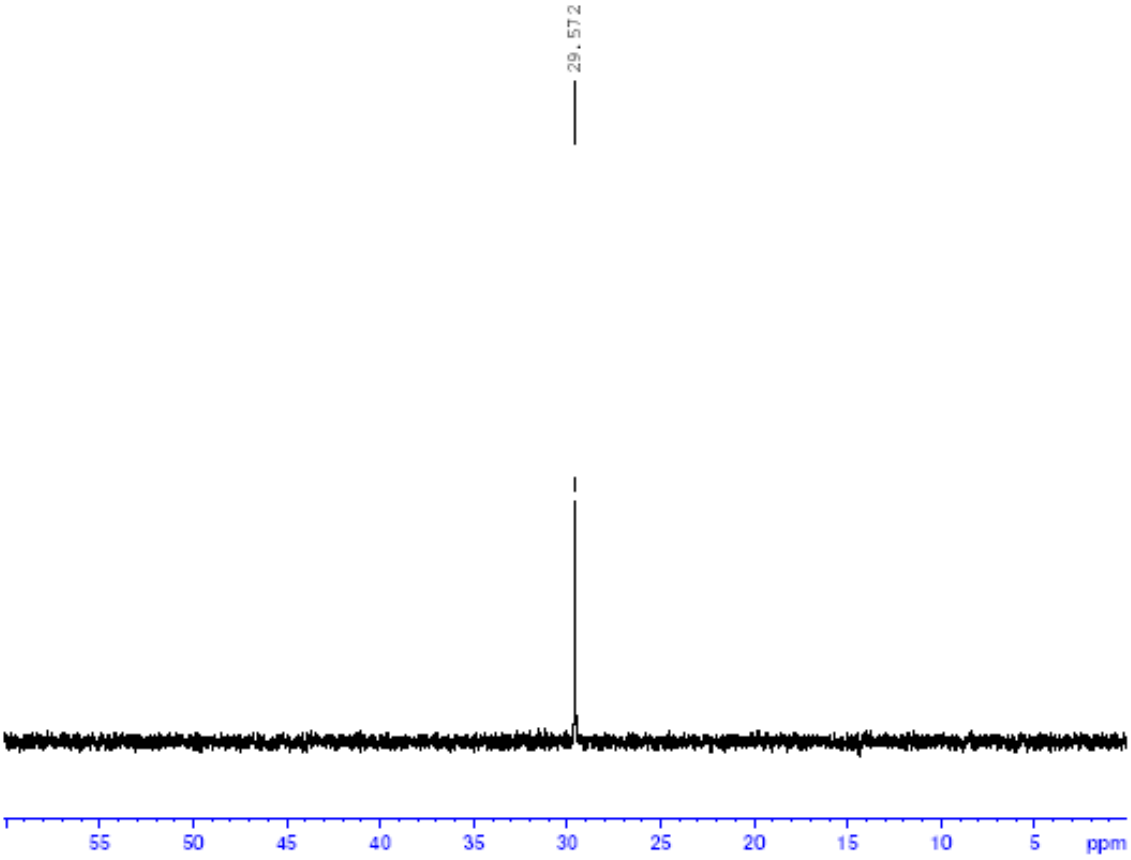

Figure A-50: ^{31}P NMR (121.4 MHz, $CDCl_3$) of fractions 27-55 from alumina column chromatography of **17**.

Fluorene-based phosphine oxide **17**; EGT-1-53; 05/06/08

Structure:

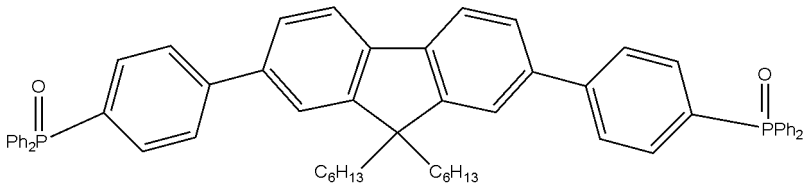

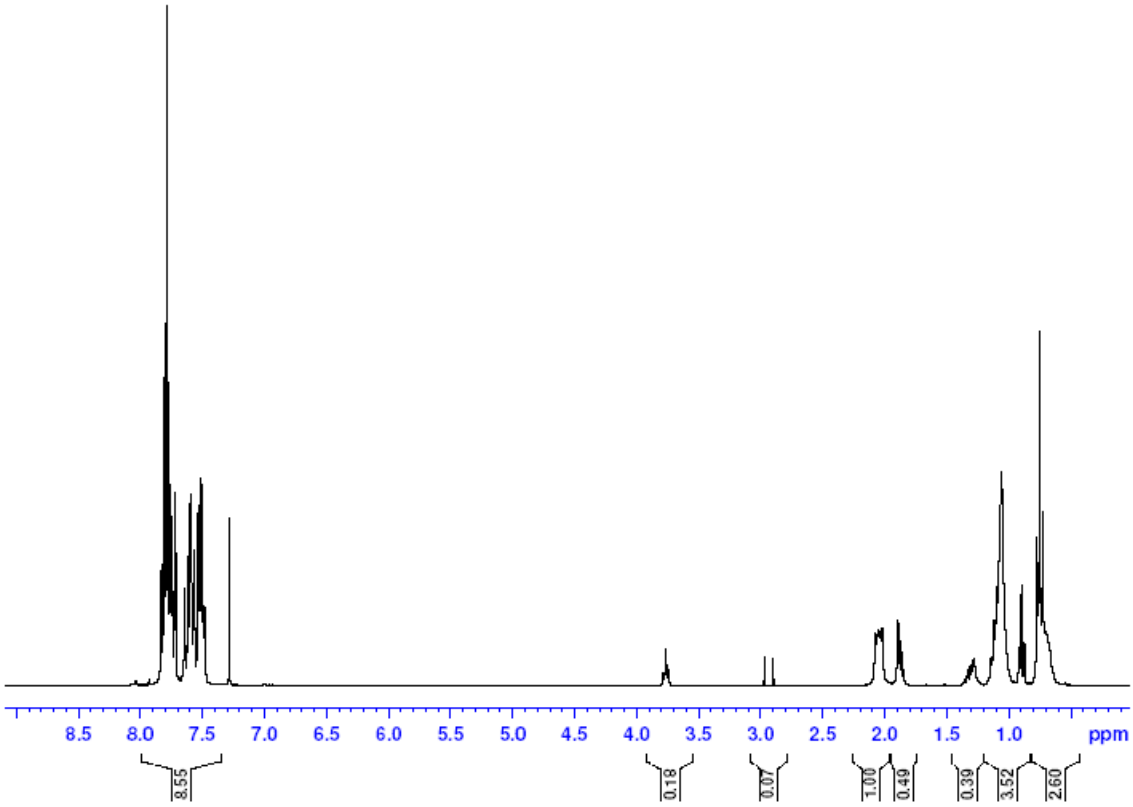

Figure A-51: ^{1}H NMR (300 MHz, $CDCl_3$) of phosphine oxide **17** as synthesized by R. Gilliard.

Fluorene-based phosphine oxide **17**; EGT-1-53; 05/06/08

Structure:

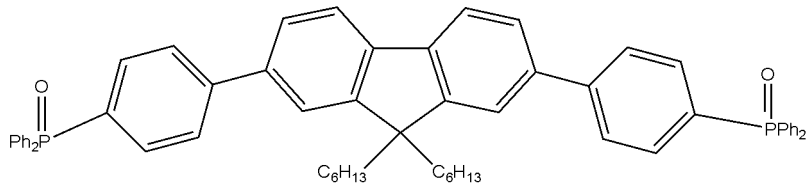

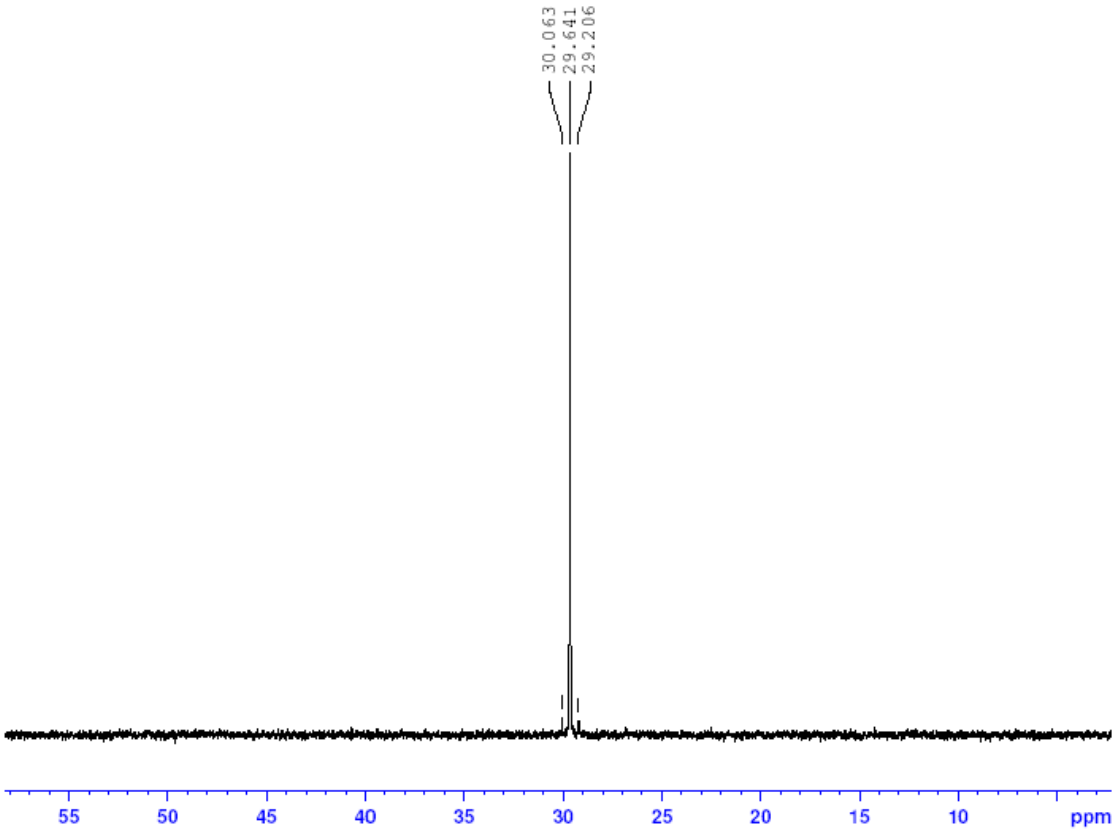

Figure A-52: ^{31}P NMR (121.4 MHz, $CDCl_3$) of phosphine oxide **17** as synthesized by R. Gilliard.

Phosphine oxide **15**; EGT-1-78; 08/15/08

Structure:

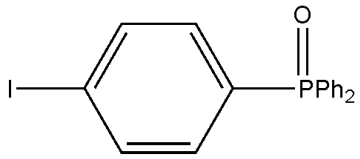

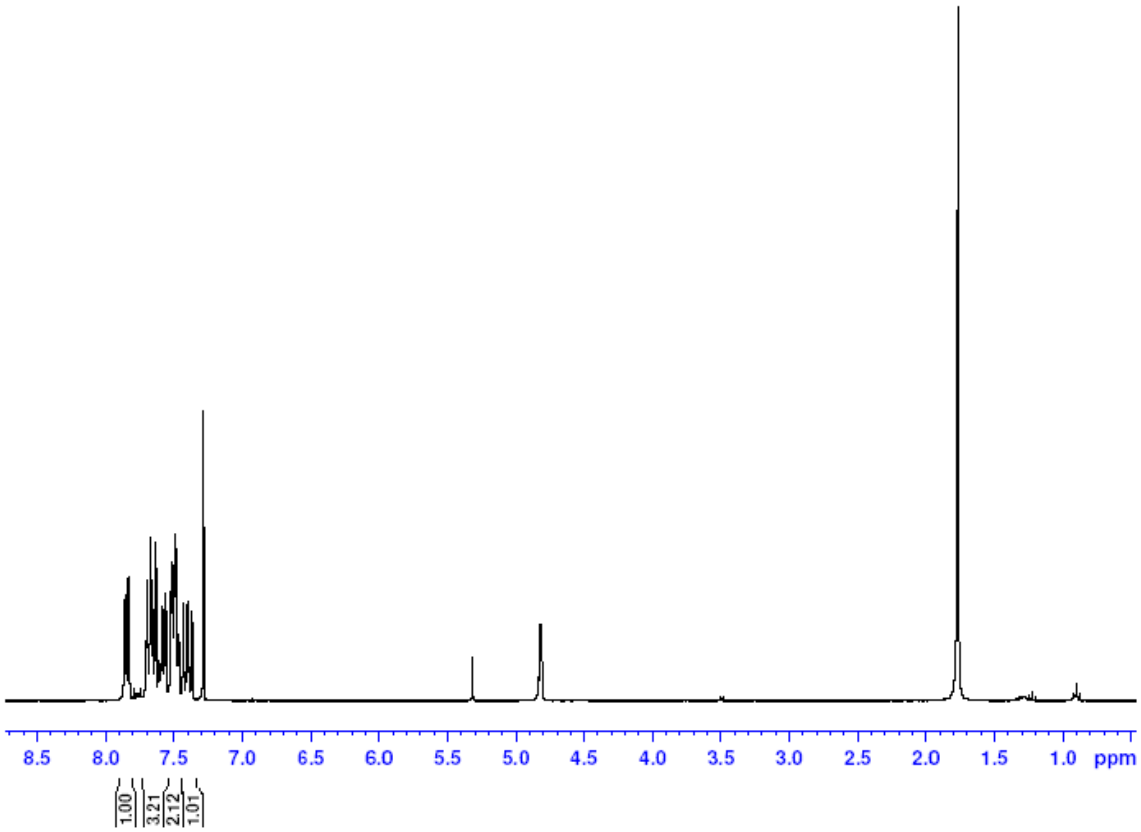

Figure A-53: ^{1}H NMR (300 MHz, $CDCl_3$) of phosphine oxide **15**.

Phosphine oxide **15**; EGT-1-78; 08/15/08

Structure:

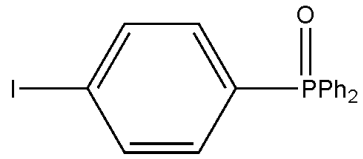

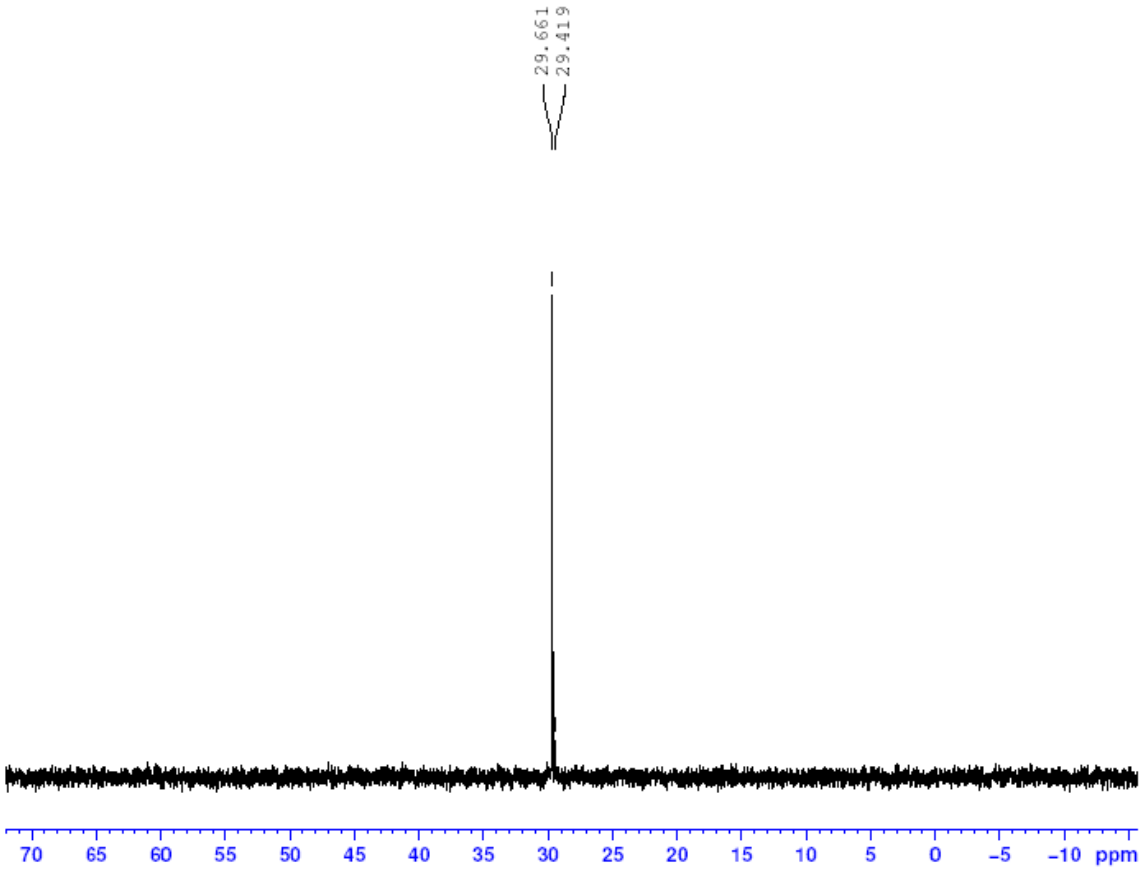

Figure A-54: ^{31}P NMR (121.4 MHz, $CDCl_3$) of phosphine oxide **15**.

Phosphine oxide **16**; EGT-1-79; 08/19/08

Structure:

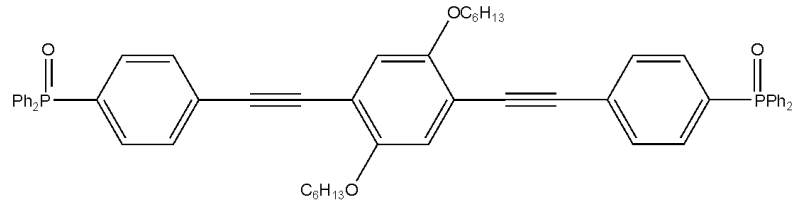

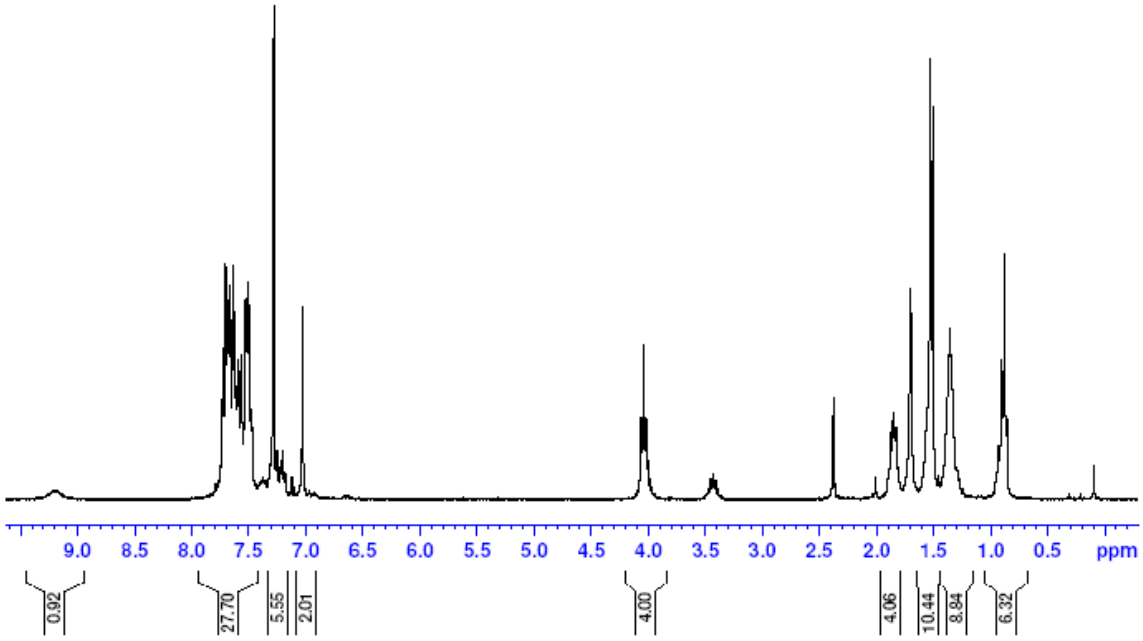

Figure A-55: ^{1}H NMR (300 MHz, $CDCl_3$) of phosphine oxide **16** as made by Sonogashira coupling of phosphine oxide **15** and 1,4-diethynyl-2,5-dihexyloxybenzene.

Phosphine oxide **16**; EGT-1-79; 08/19/08

Structure:

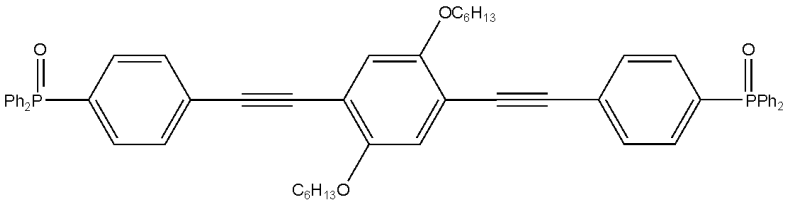

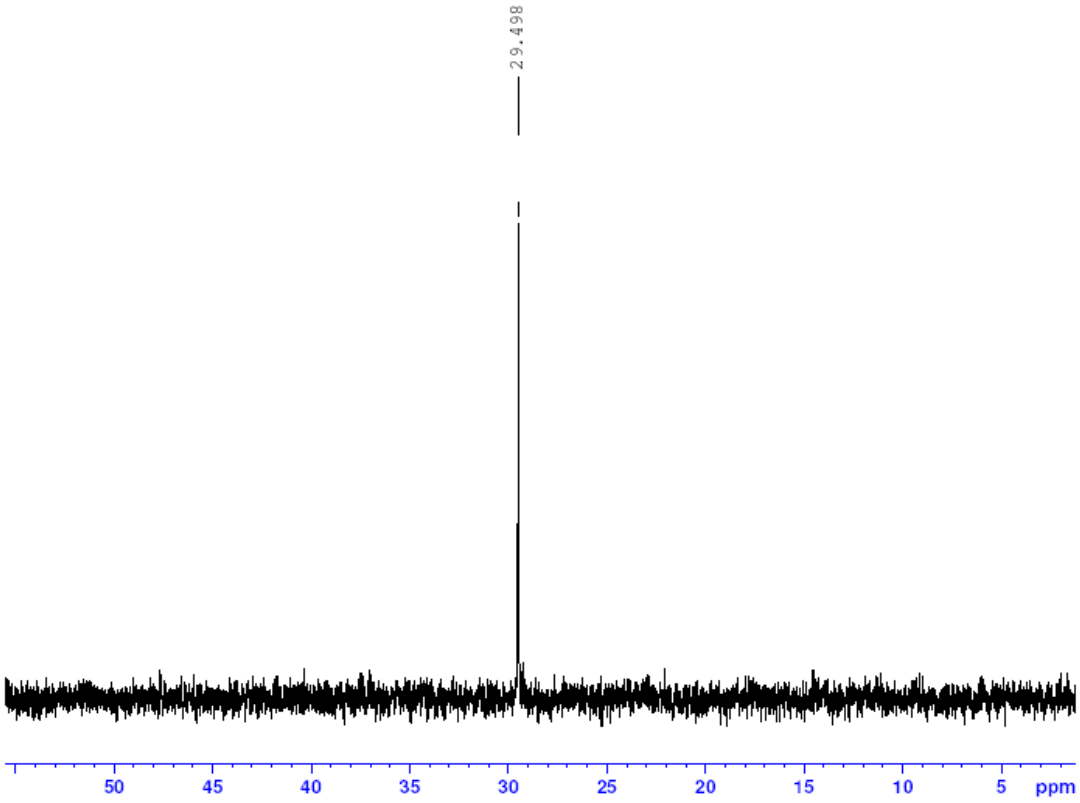

Figure A-56: ^{31}P NMR (121.4 MHz, $CDCl_3$) of phosphine oxide **16** as made by Sonogashira coupling of phosphine oxide **15** and 1,4-diethynyl-2,5-dihexyloxybenzene.

Phosphine **18**; EGT-1-46; 03/15/08

Structure:

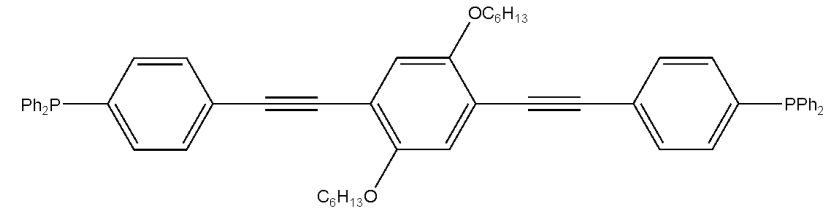

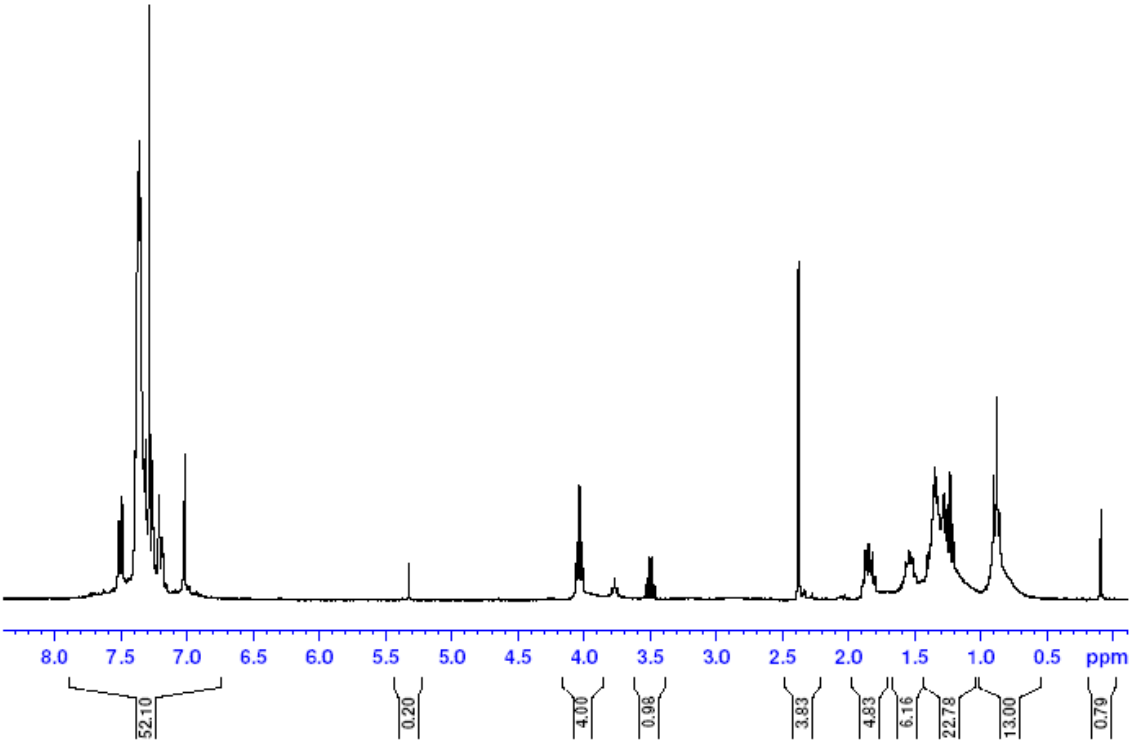

Figure A-57: ^{1}H NMR (300 MHz, $CDCl_3$) of crude phosphine **18**.

Phosphine **18**; EGT-1-46; 03/15/08

Structure:

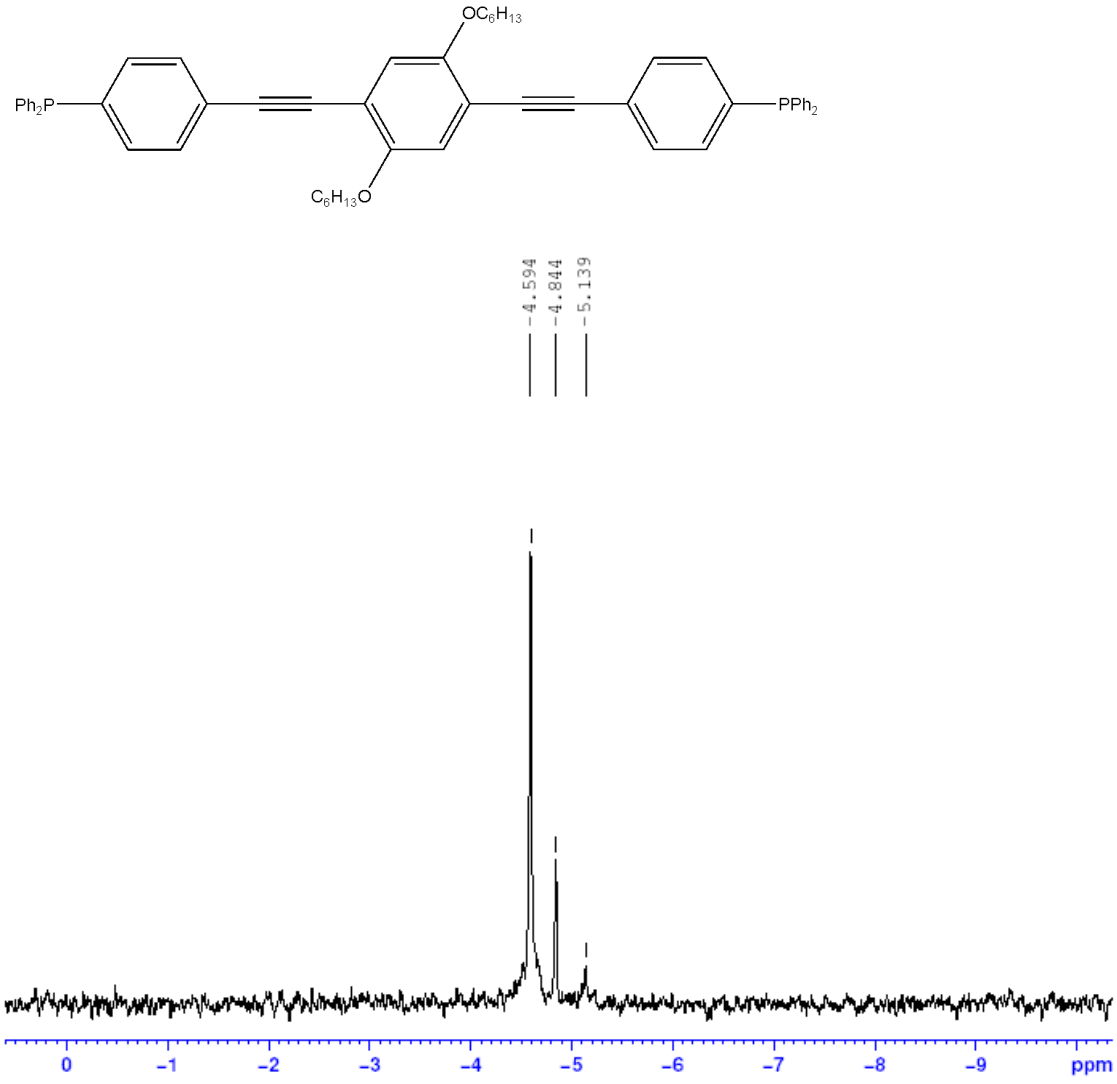

Figure A-58: ^{31}P NMR (121.4 MHz, $CDCl_3$) of crude phosphine **18**.

Phosphine **18**; EGT-1-47; 03/27/08

Structure:

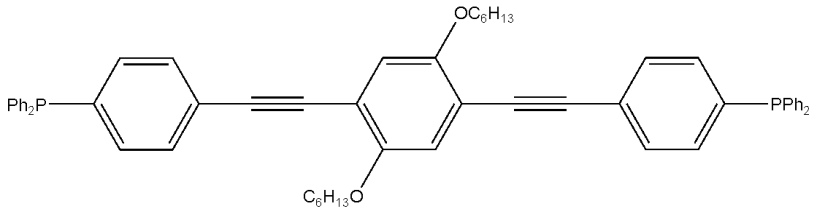

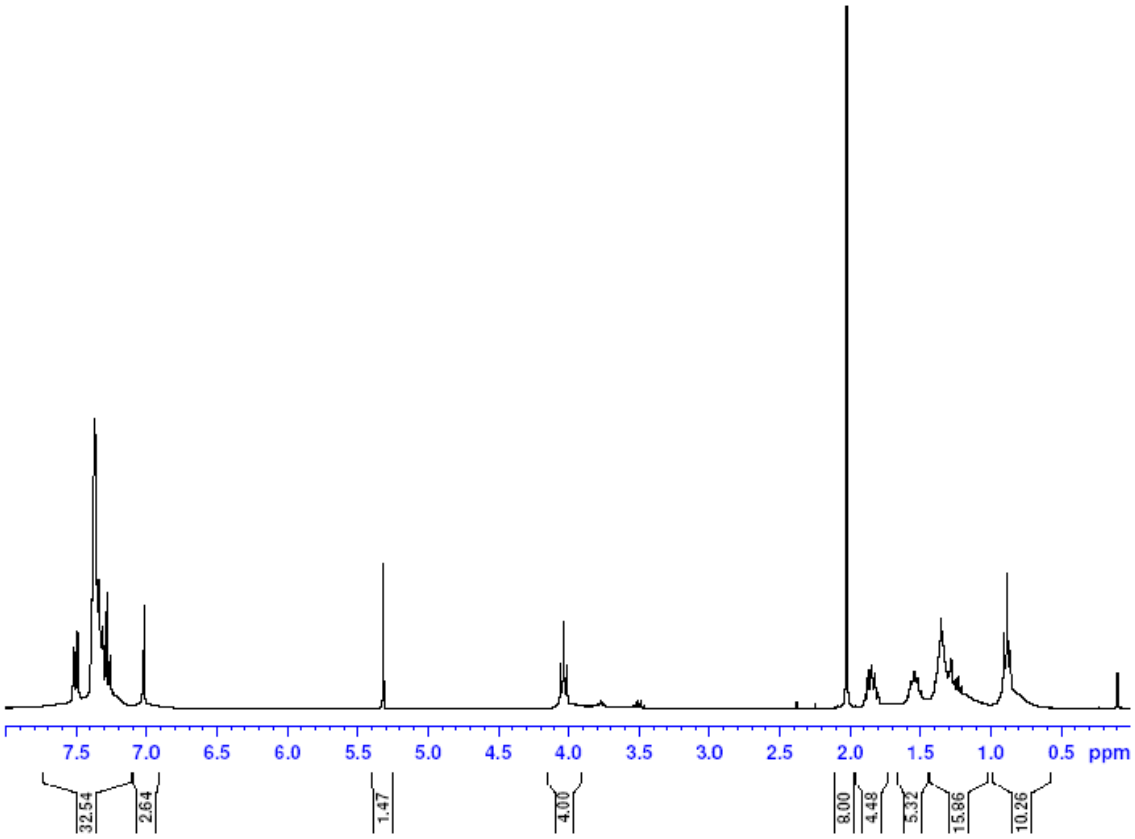

Figure A-59: ^{1}H NMR (300 MHz, $CDCl_3$) of phosphine **18** as purified by dissolving in dichloromethane and precipitating in acetonitrile in the freezer.

Phosphine **18**; EGT-1-47; 03/27/08

Structure:

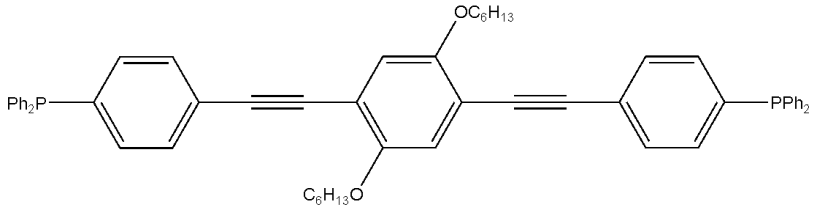

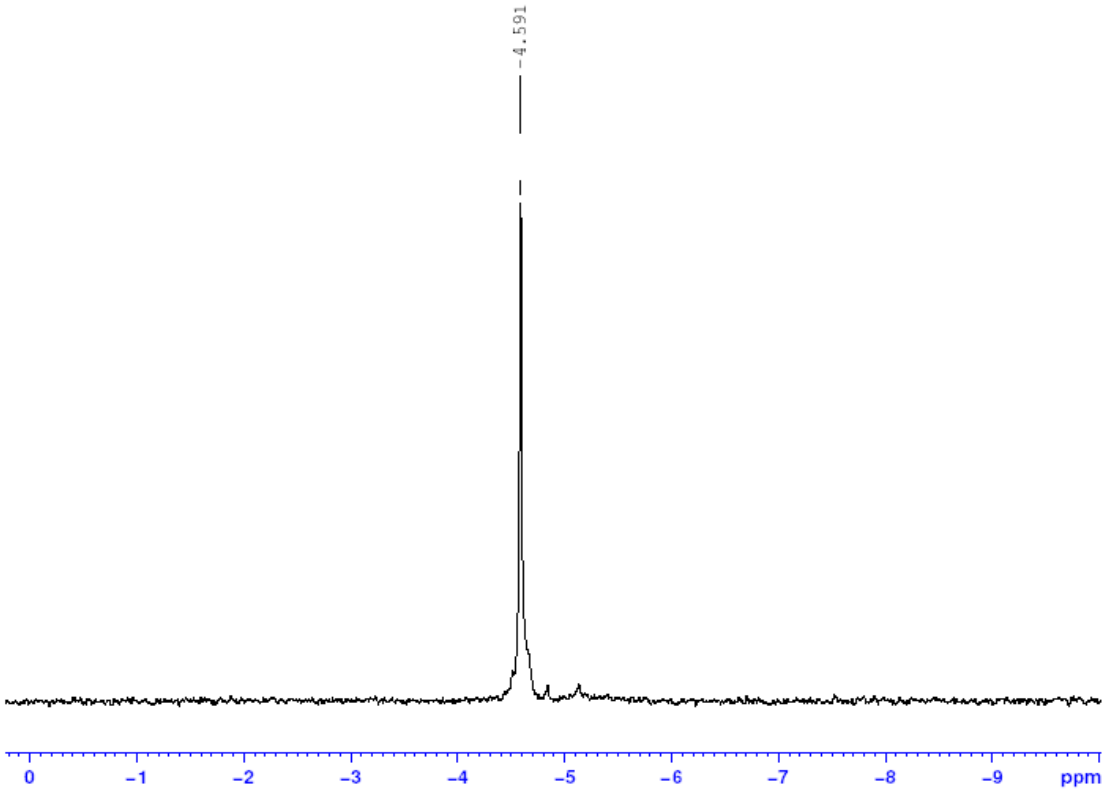

Figure A-60: ^{31}P NMR (121.4 MHz, $CDCl_3$) of phosphine **18** as purified by dissolving in dichloromethane and precipitating in acetonitrile in the freezer.

Phosphine **18**; EGT-1-47; 08/25/08

Structure:

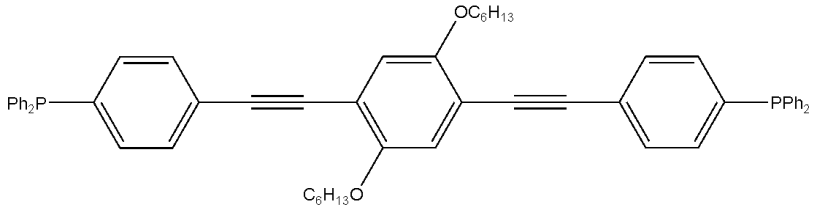

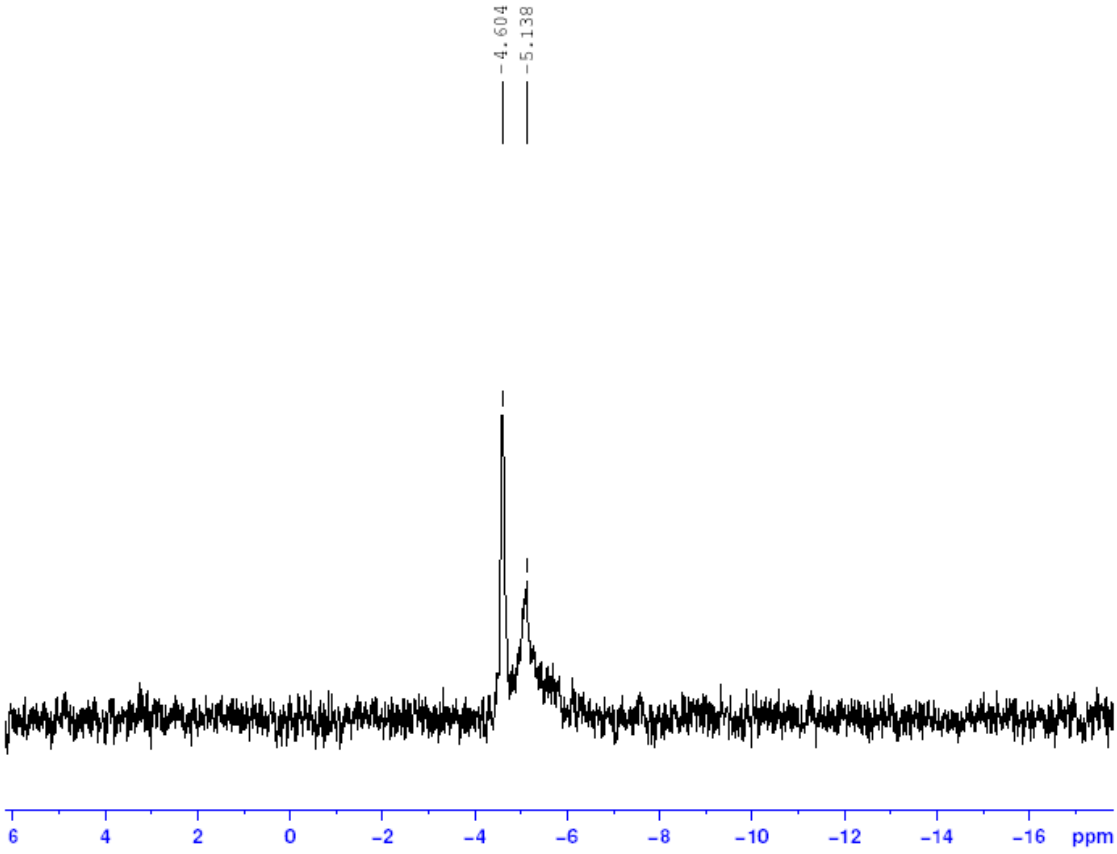

Figure A-61: ^{31}P NMR (121.4 MHz, $CDCl_3$) of phosphine **18** from modified workup with a broadened signal that seems to imply proton exchange at the phosphorous atom.

Polymer **19**; EGT-1-48; 03/28/08

Structure:

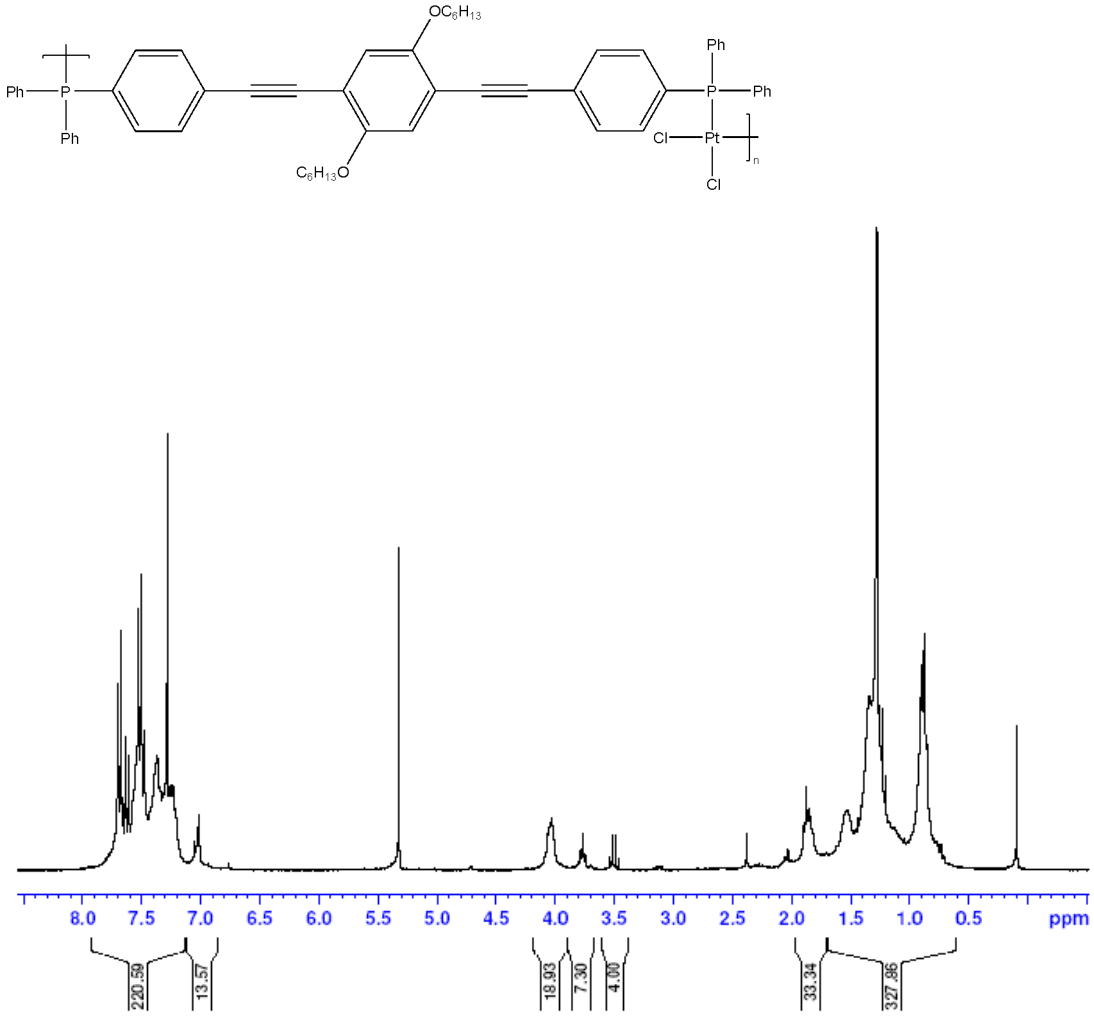

Figure A-62: ^{1}H NMR (300 MHz, $CDCl_3$) of polymer **19**.

Polymer **19**; EGT-1-48; 03/28/08

Structure:

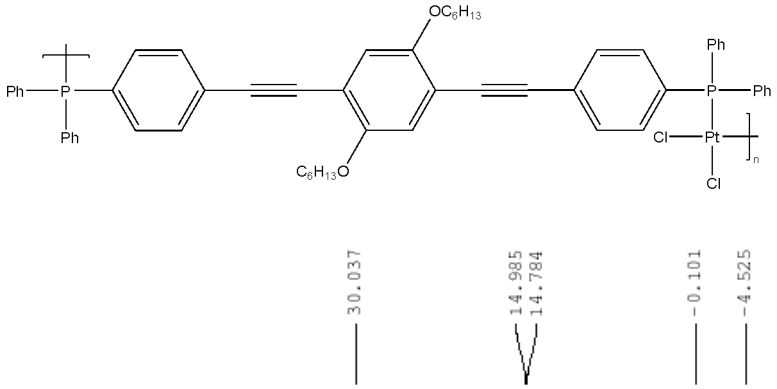

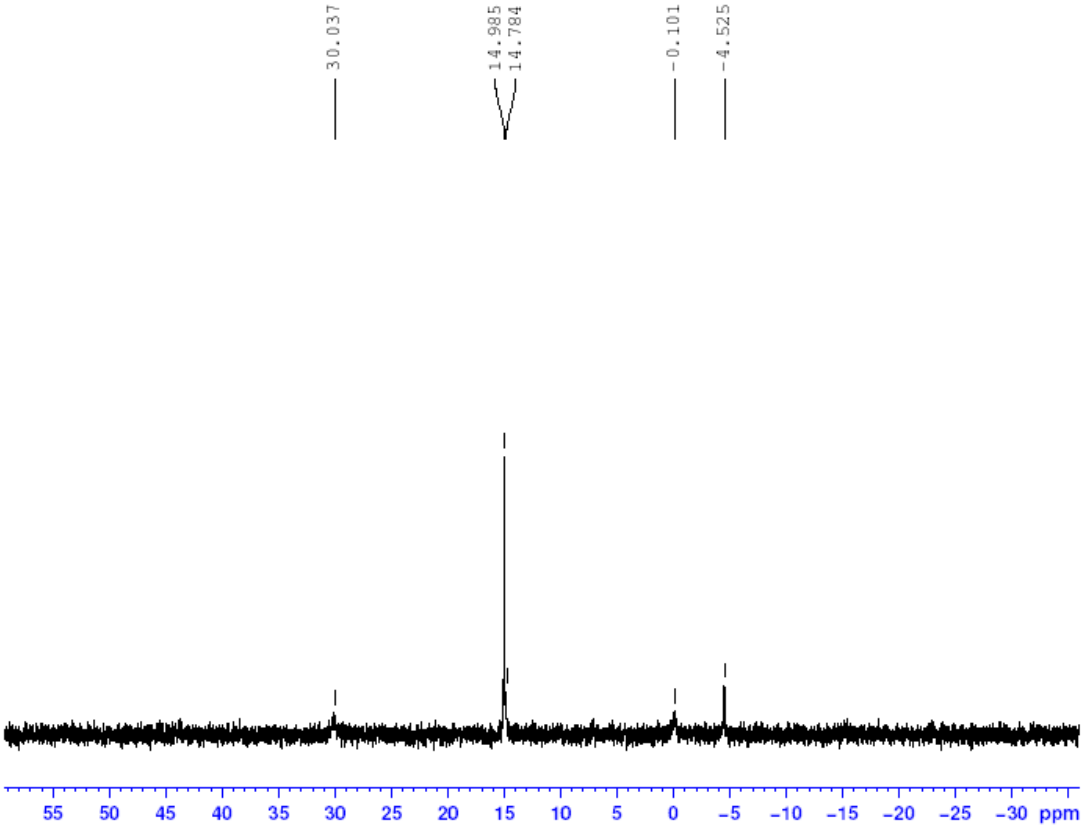

Figure A-63: ^{31}P NMR (121.4 MHz, $CDCl_3$) of polymer **19**.

Polymer **20**; EGT-1-49; 03/28/08

Structure:

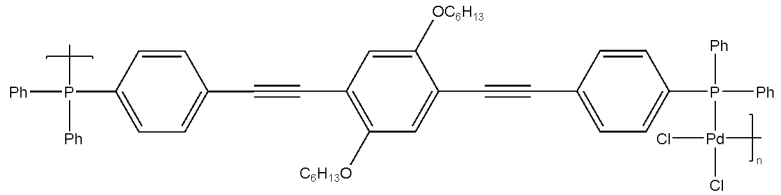

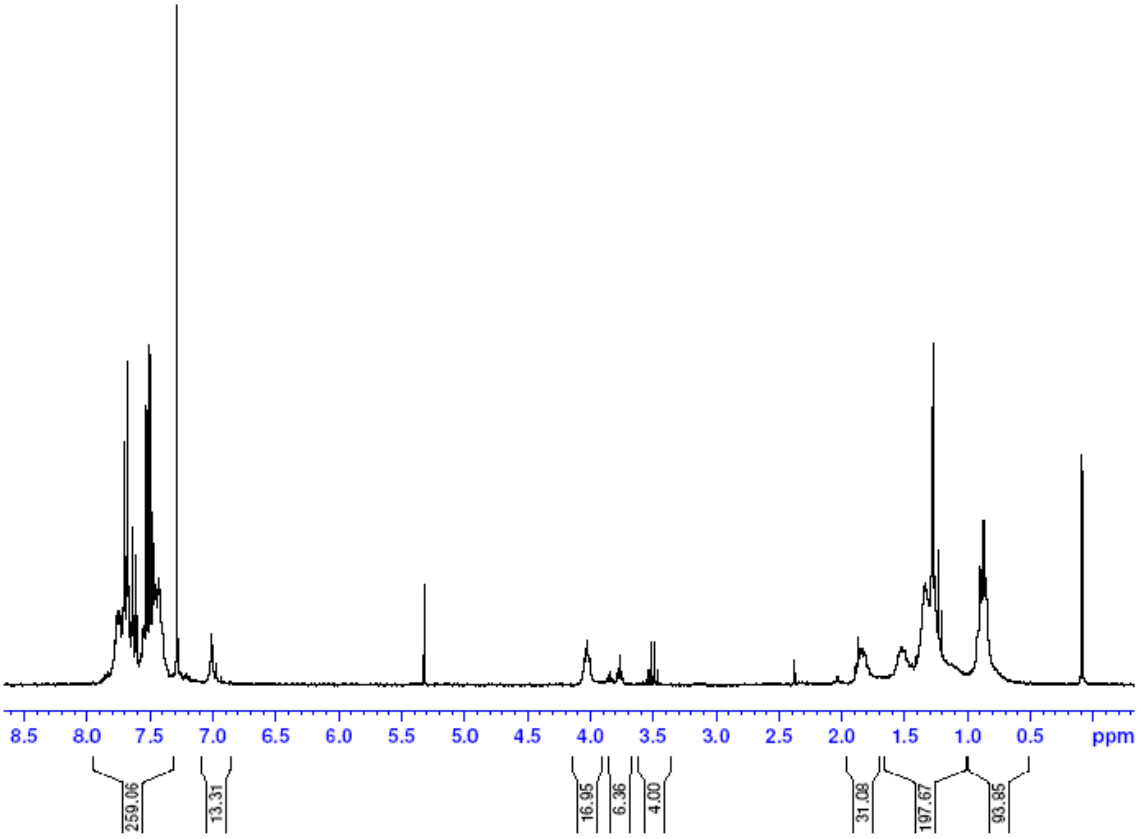

Figure A-64: ^{1}H NMR (300 MHz, $CDCl_3$) of polymer **20**.

Polymer **20**; EGT-1-49; 03/28/08

Structure:

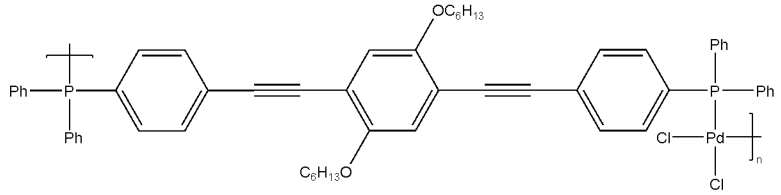

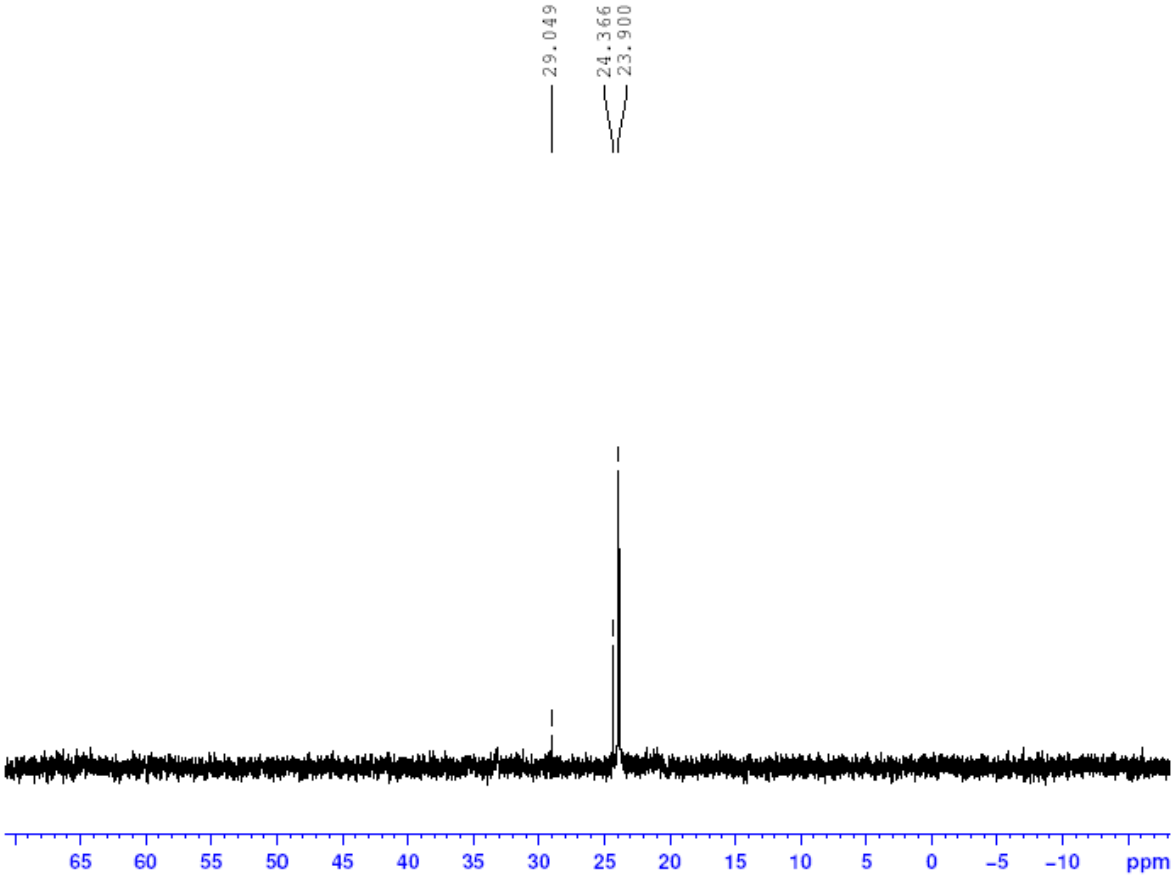

Figure A-65: ^{31}P NMR (121.4 MHz, $CDCl_3$) of polymer **20**.

Polymer **19c**; EGT-1-83; 09/01/08

Structure:

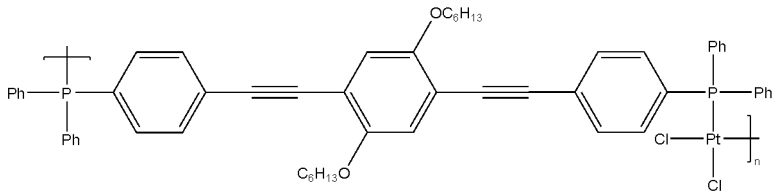

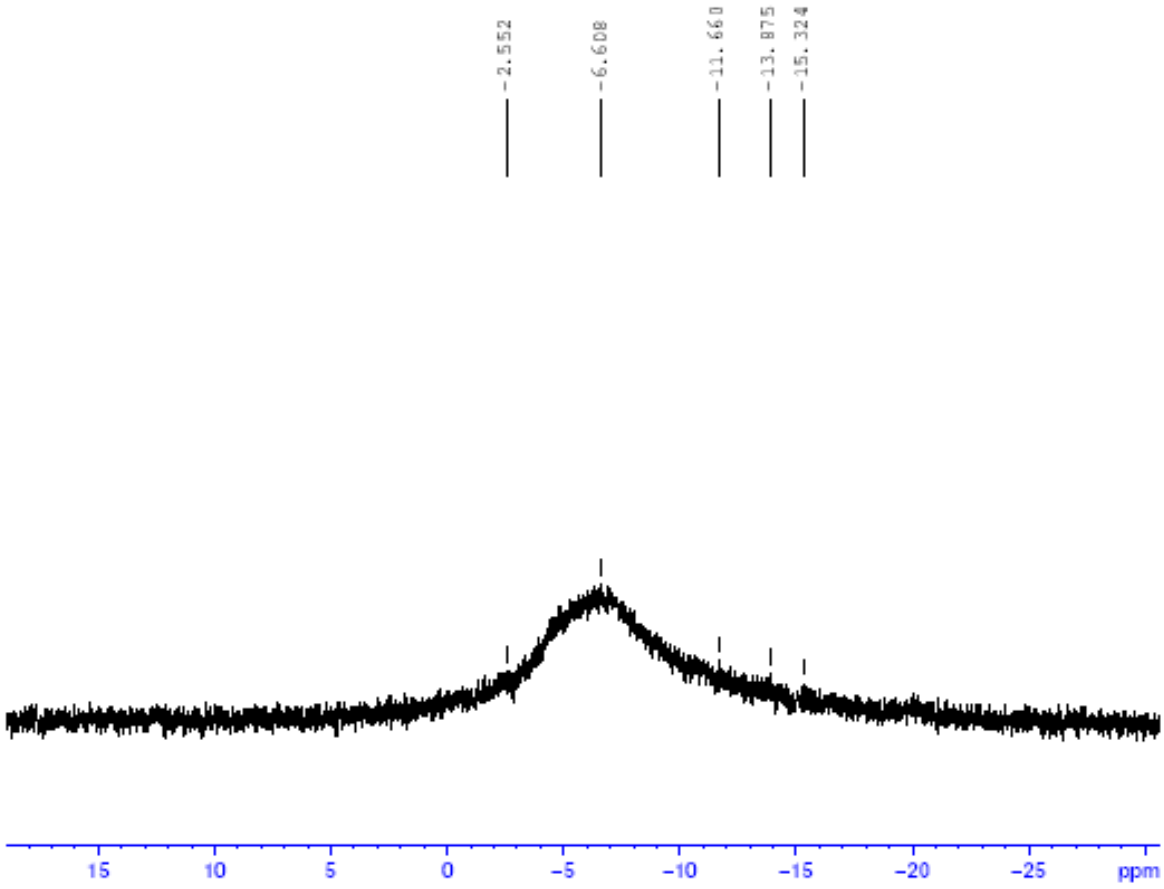

Figure A-66: ^{31}P NMR (121.4 MHz, $CDCl_3$) of polymer **19** as made with 5% excess phosphine **18**.

Polymer **19d**; EGT-1-86; 09/08/08

Structure:

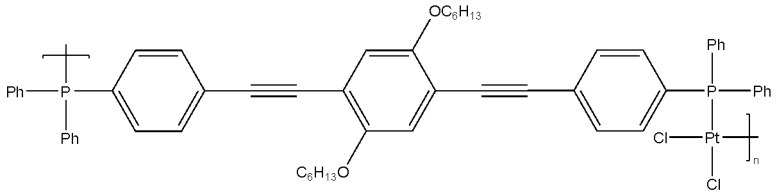

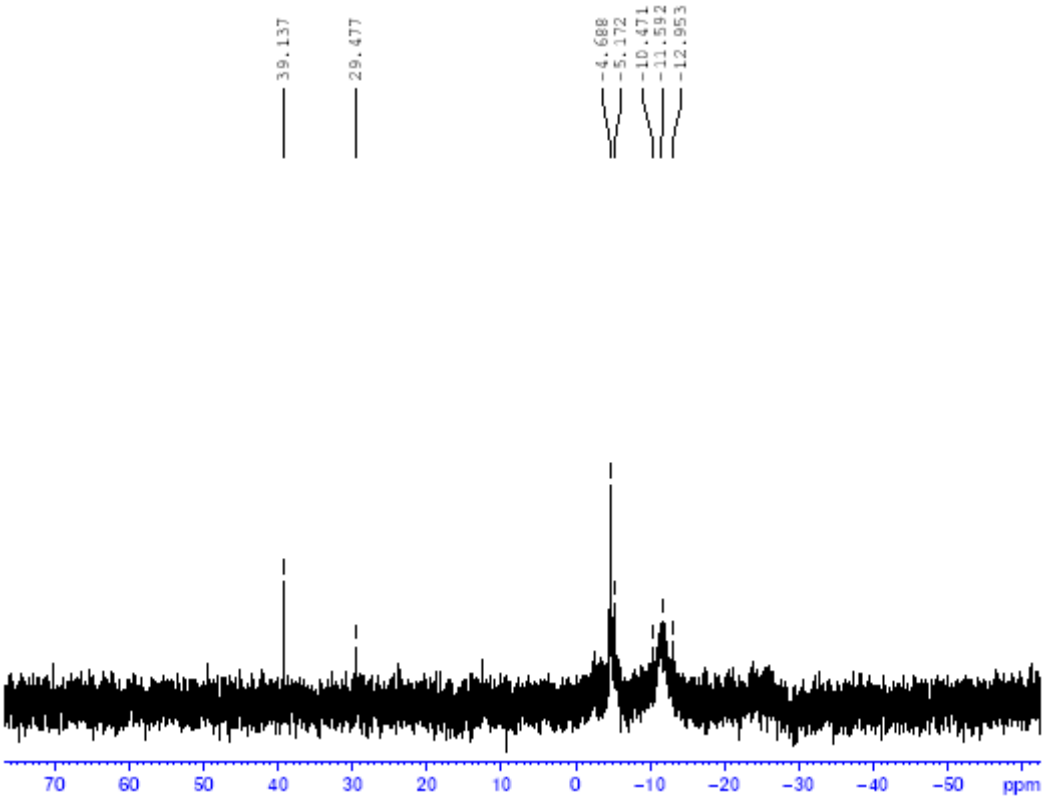

Figure A-67: ^{31}P NMR (121.4 MHz, $CDCl_3$) of polymer **19** as made with added trimethylphosphine to reduce polymer length.

Polymer **19d**; EGT-1-86; 09/08/08

Structure:

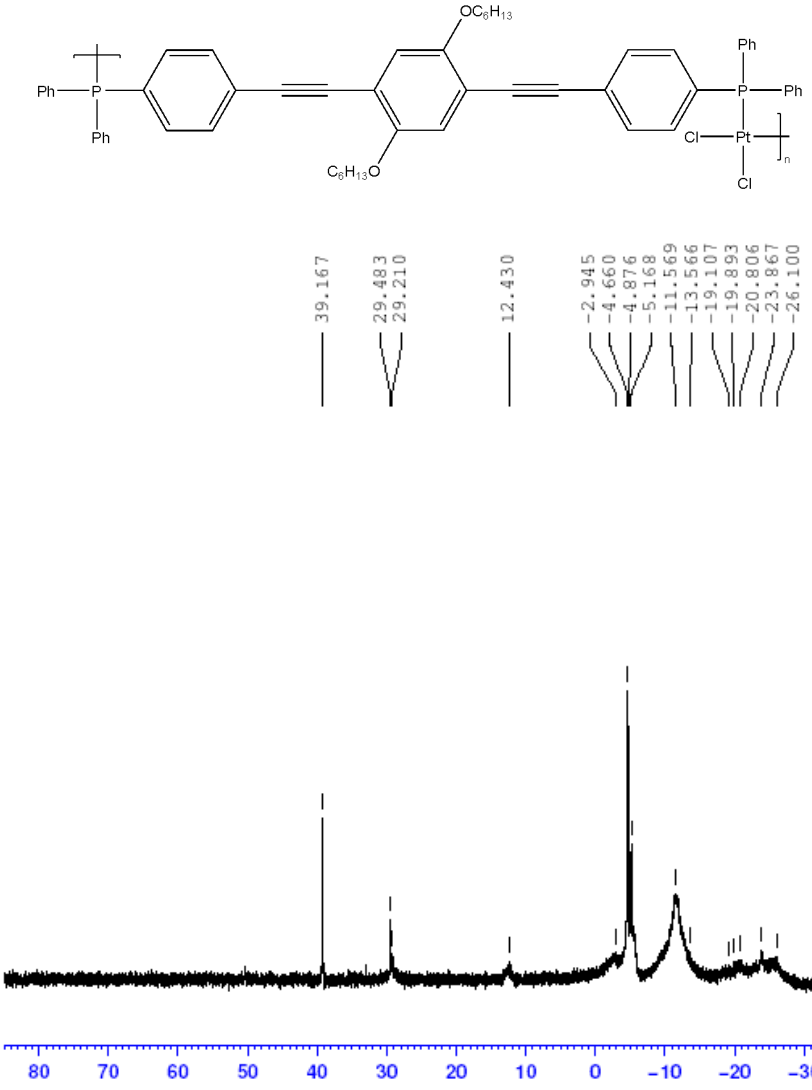

Figure A-68: ^{31}P NMR (121.4 MHz, $CDCl_3$) of polymer **19** with an extra aliquot of trimethylphosphine.

LHP1-OHx; EGT-1-93; 09/22/08

Structure:

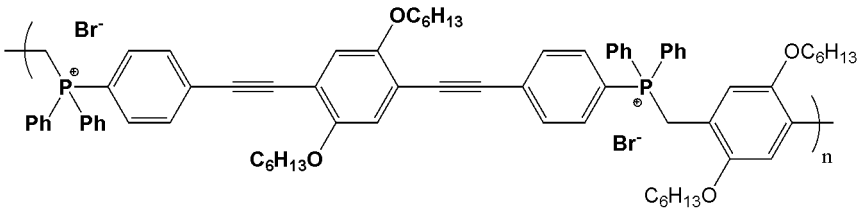

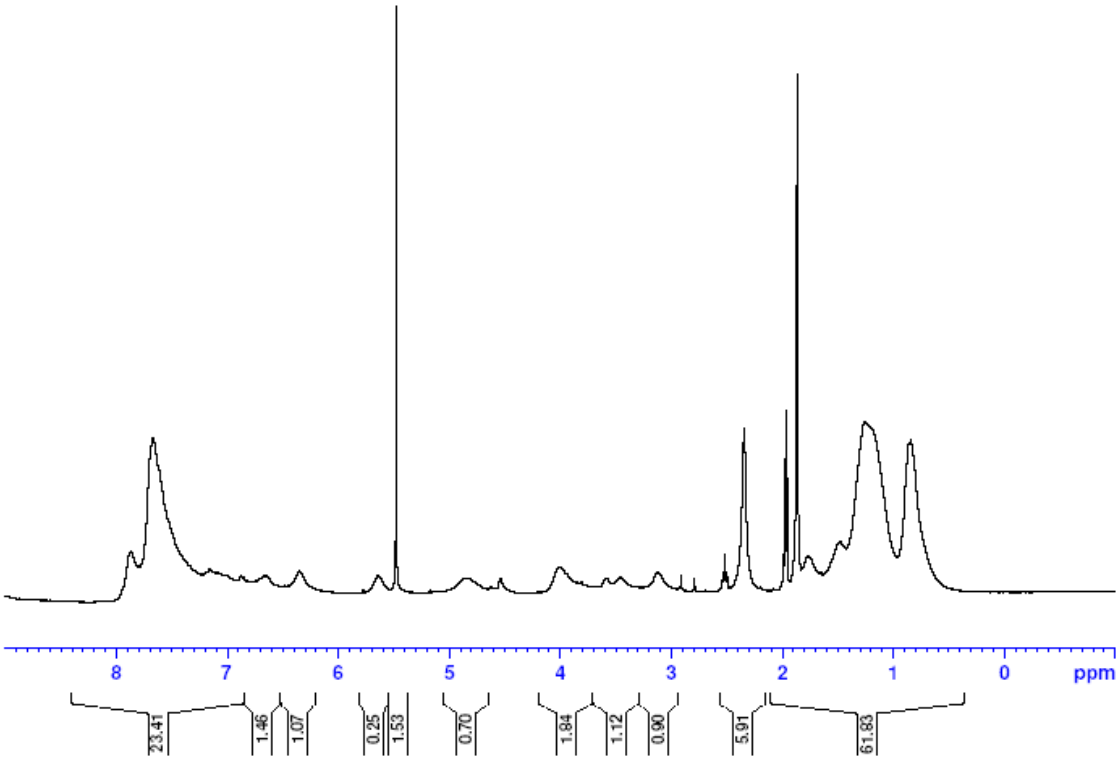

Figure A-69: ^{1}H NMR (300 MHz, $CDCl_3$) of **LHP1-OHx**.

LHP1-OHx; EGT-1-93; 09/22/08

Structure:

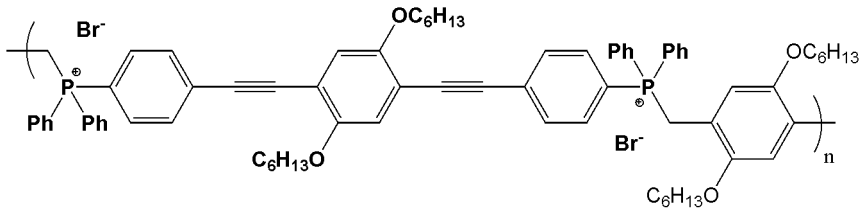

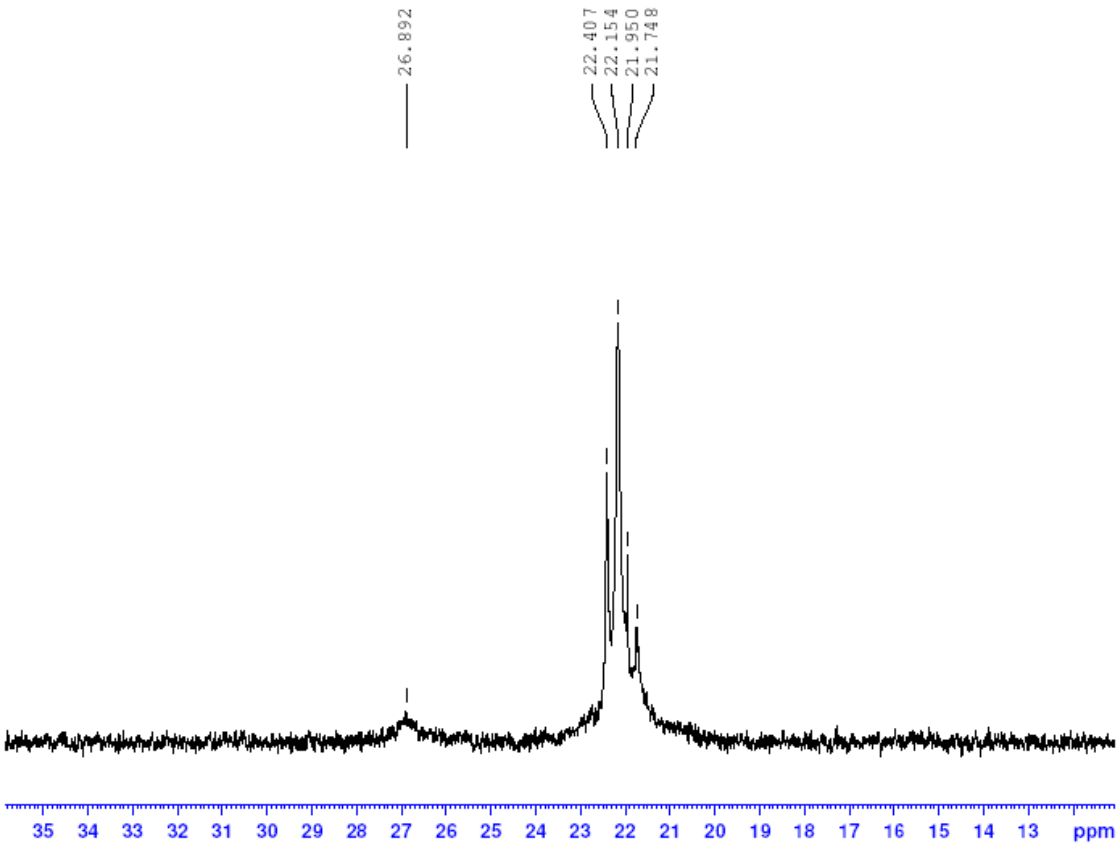

Figure A-70: ^{31}P NMR (121.4 MHz, $CDCl_3$) of **LHP1-OHx**.

LHP1-oXYL; EGT-1-94; 09/22/09

Structure:

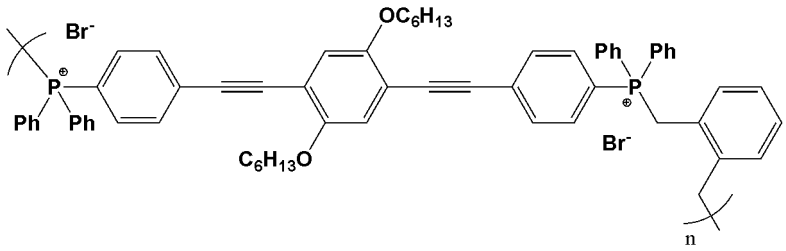

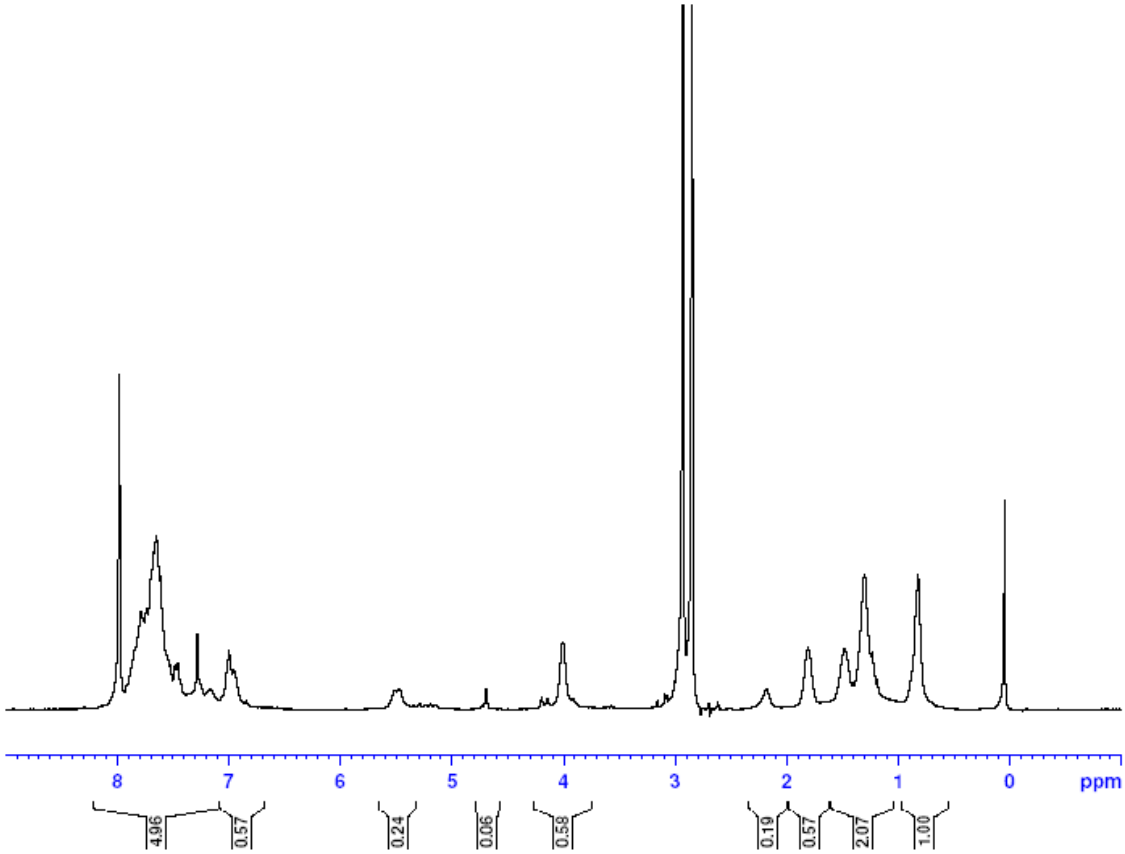

Figure A-71: ^{1}H NMR (300 MHz, $CDCl_3$) of **LHP1-oXYL**.

LHP1-oXYL; EGT-1-94; 09/22/08

Structure:

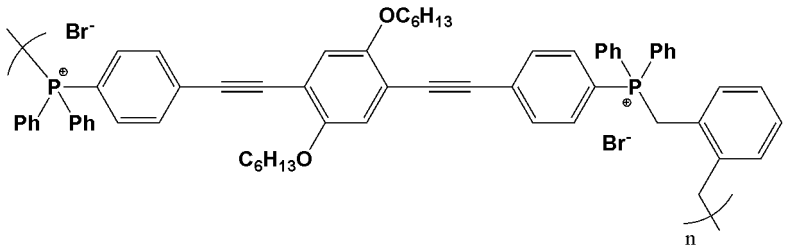

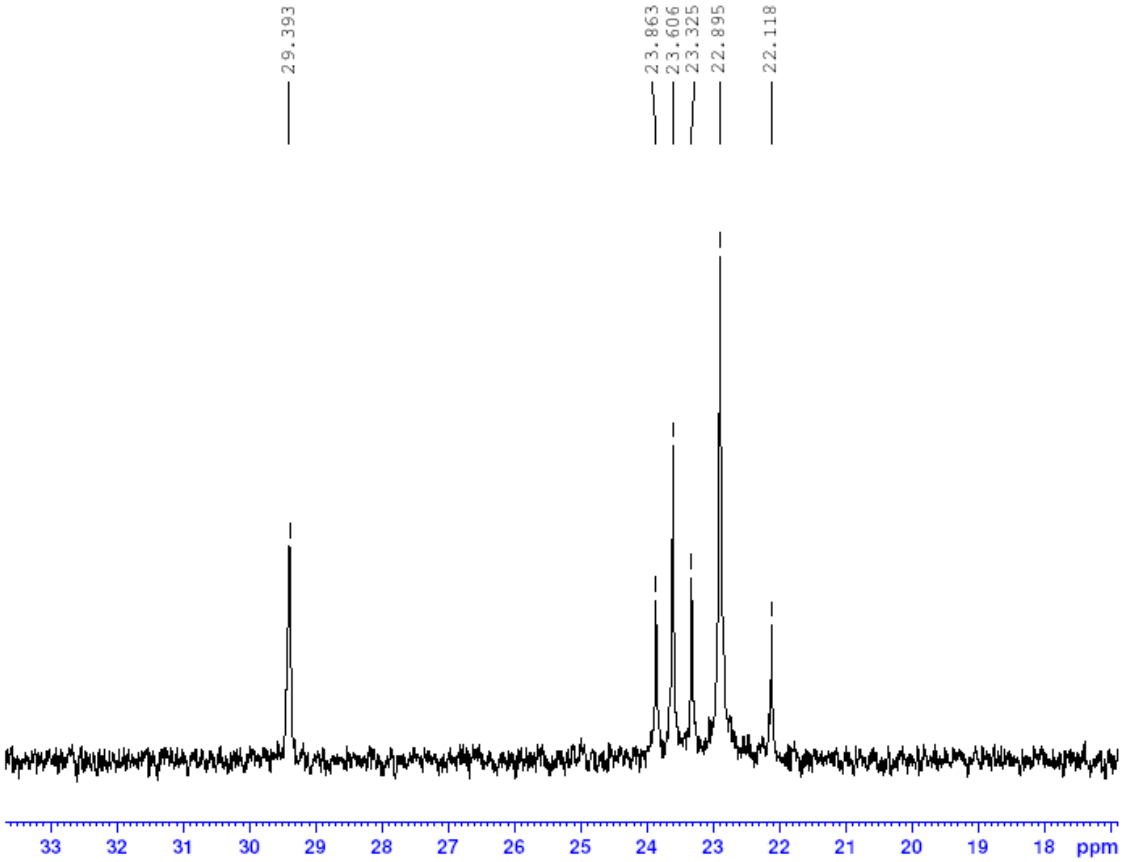

Figure A-72: ^{31}P NMR (121.4 MHz, $CDCl_3$) of **LHP1-oXYL**.

LHP1-BPY; EGT-1-92; 09/22/08

Structure:

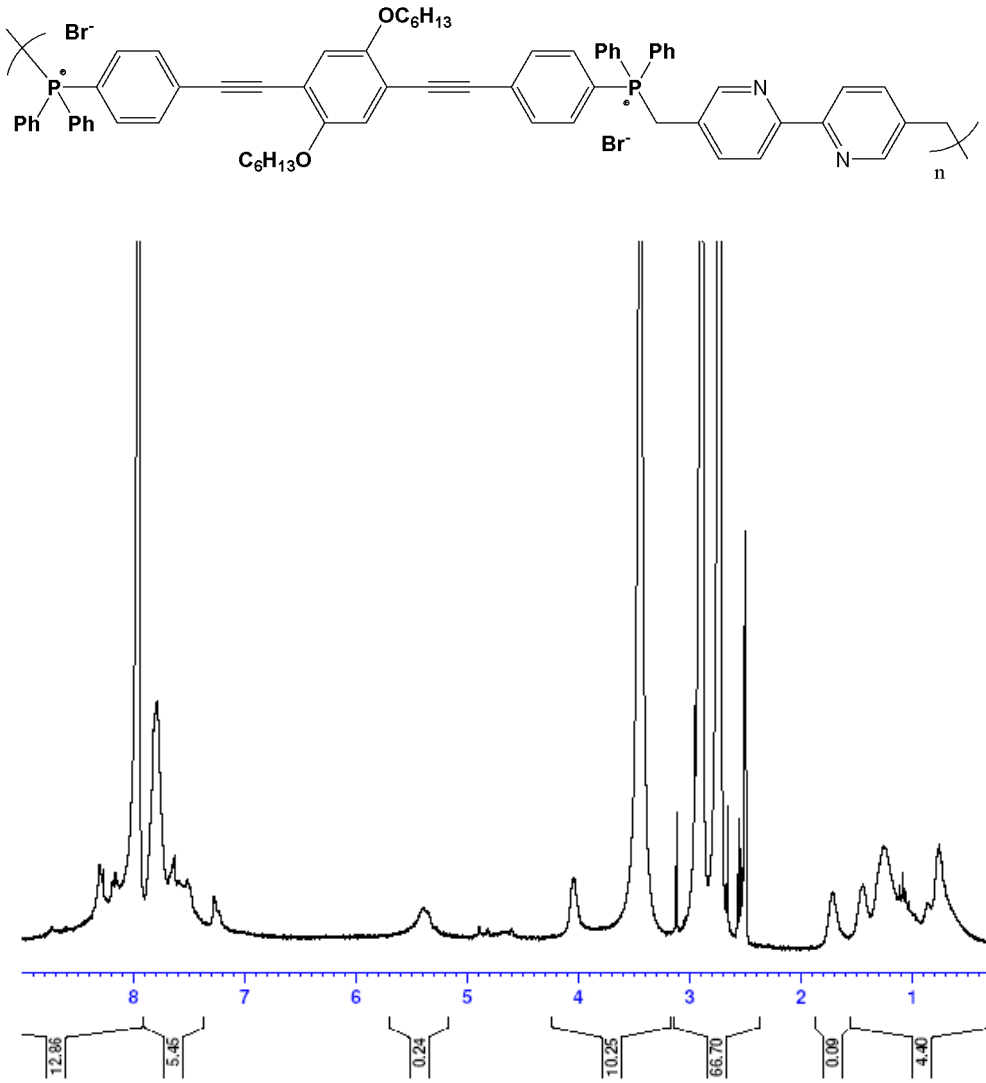

Figure A-73: ^{1}H NMR (300 MHz, DMSO-d_6) of **LHP1-BPY**.

LHP1-BPY; EGT-1-92; 09/22/08

Structure:

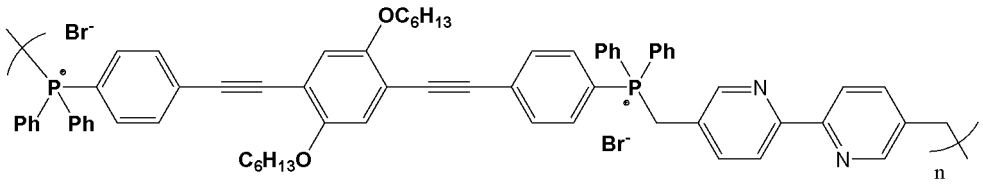

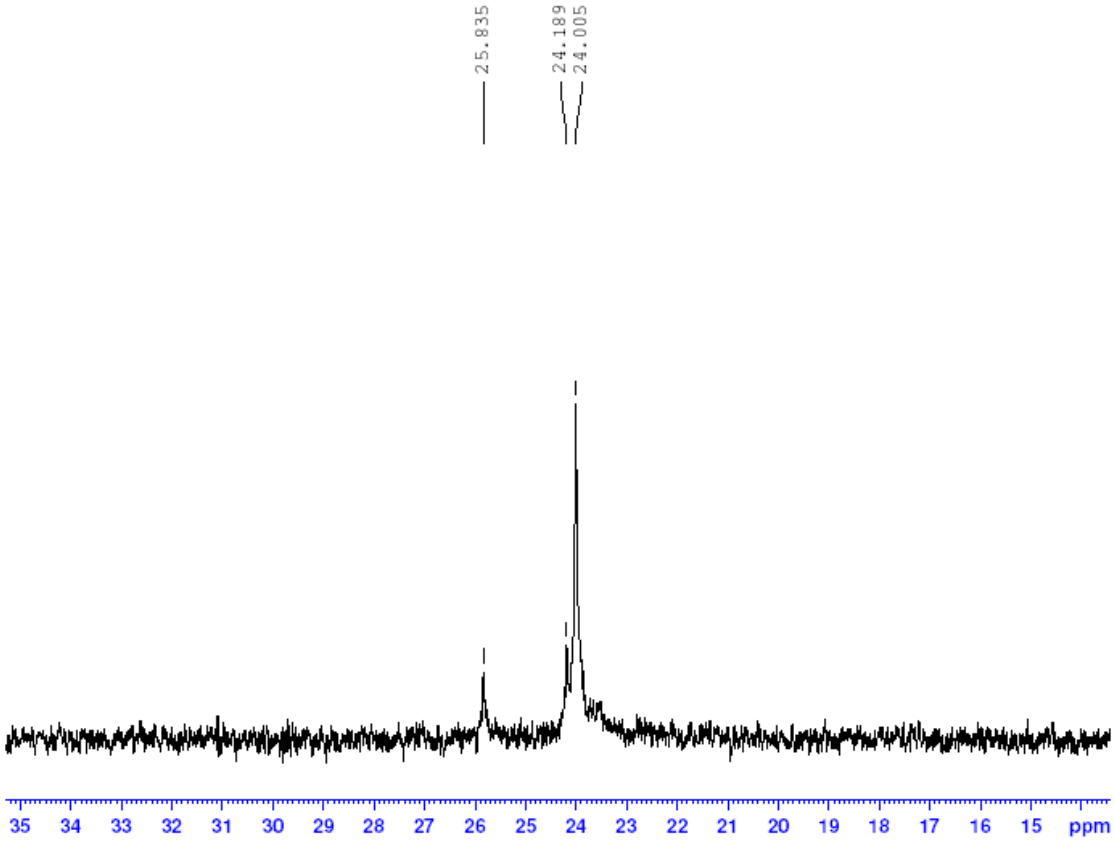

Figure A-74: ^{31}P NMR (121.4 MHz, DMSO-d_6) of **LHP1-BPY**.

LHP1-DOD; EGT-2-7; 03/09/09

Structure:

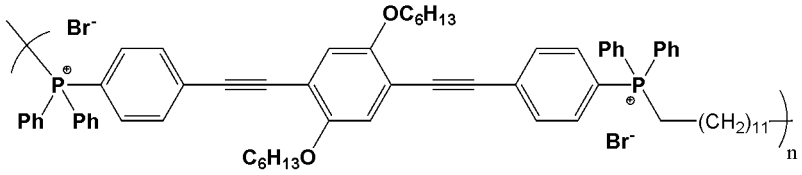

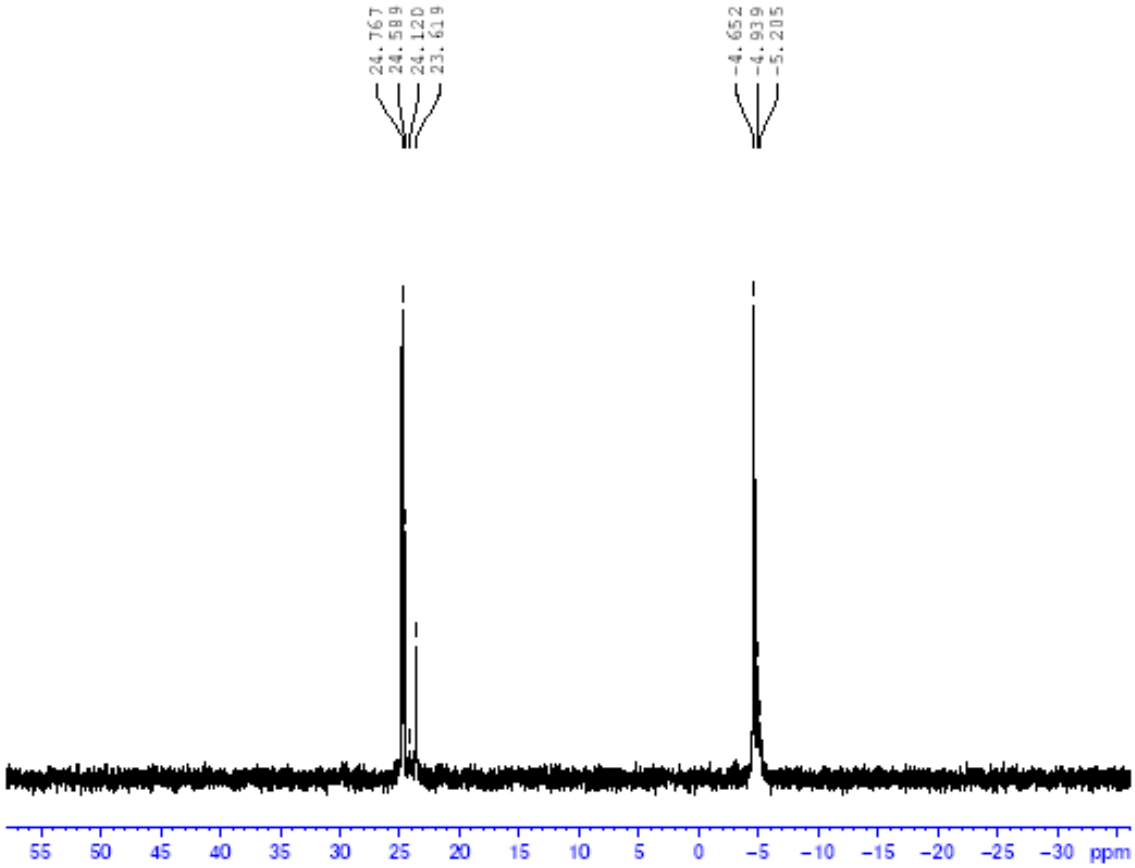

Figure A-75: ^{31}P NMR (121.4 MHz, $CDCl_3$) of **LHP1-DOD**.

LHP1-DOD; EGT-2-8; 03/09/09

Structure:

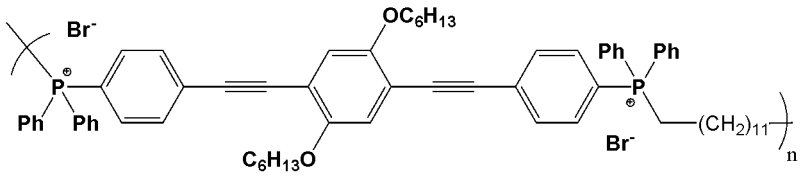

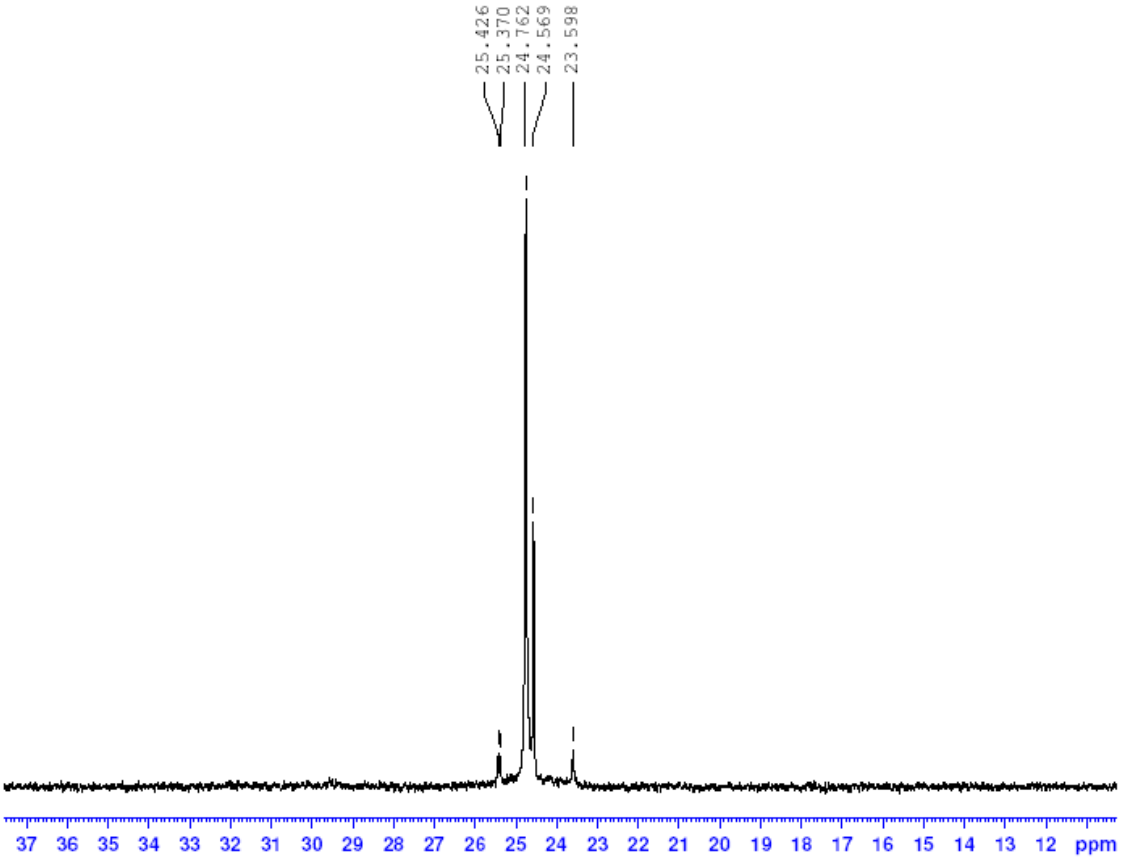

Figure A-76: ^{31}P NMR (121.4 MHz, $CDCl_3$) of **LHP1-DOD** after another equiv of 1,12-dibromododecane added to the reaction mixture.

LHP1-DOD; EGT-2-8; 03/09/09

Structure:

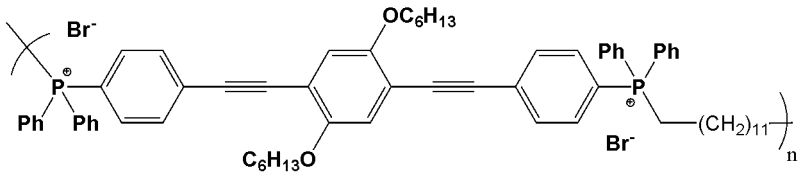

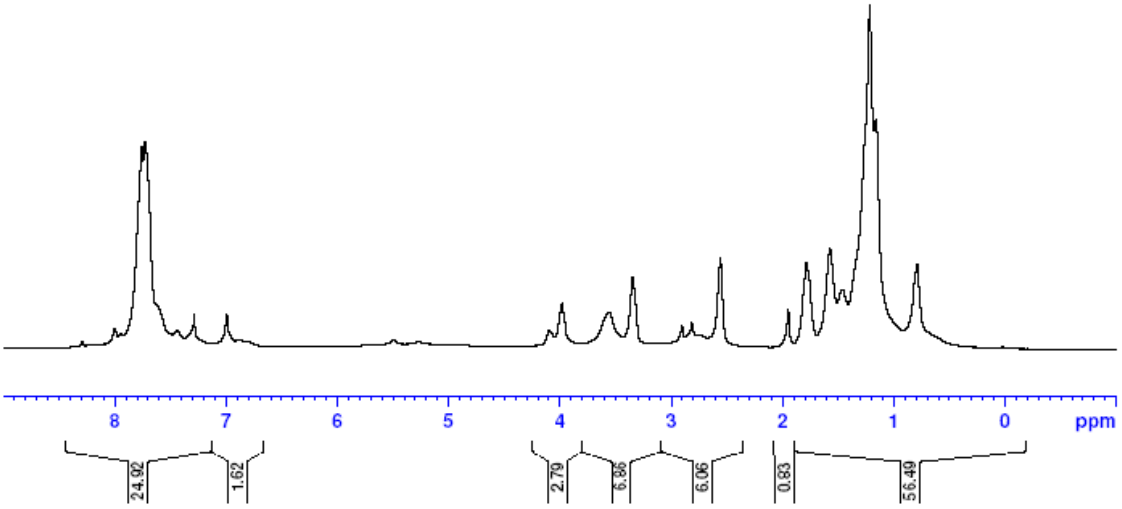

Figure A-77: ^{1}H NMR (300 MHz, $CDCl_3$) of **LHP1-DOD** after washing with hexanes.

LHP1-DOD; EGT-2-8; 03/09/09

Structure:

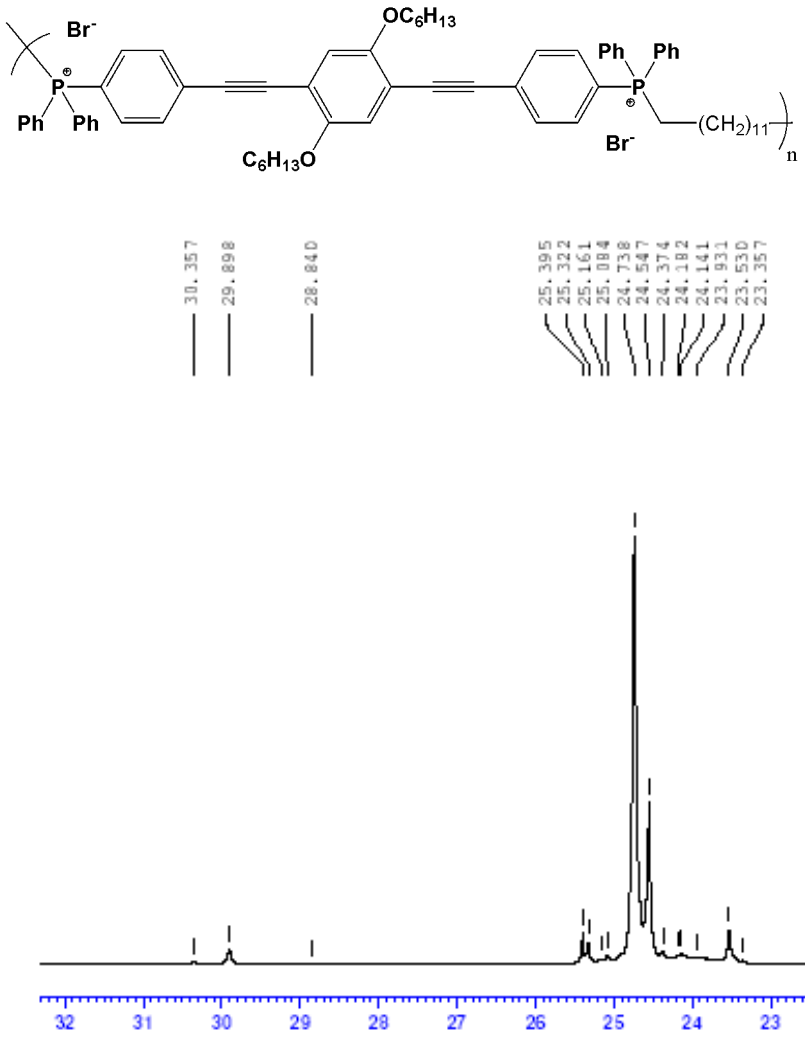

Figure A-78: ^{31}P NMR (121.4 MHz, $CDCl_3$) of **LHP1-DOD** after washing with hexanes.

LHP1-DOD; EGT-2-8; 03/09/09

Structure:

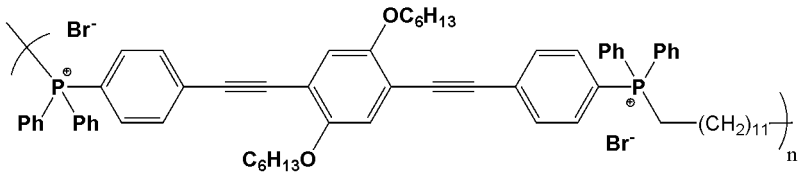

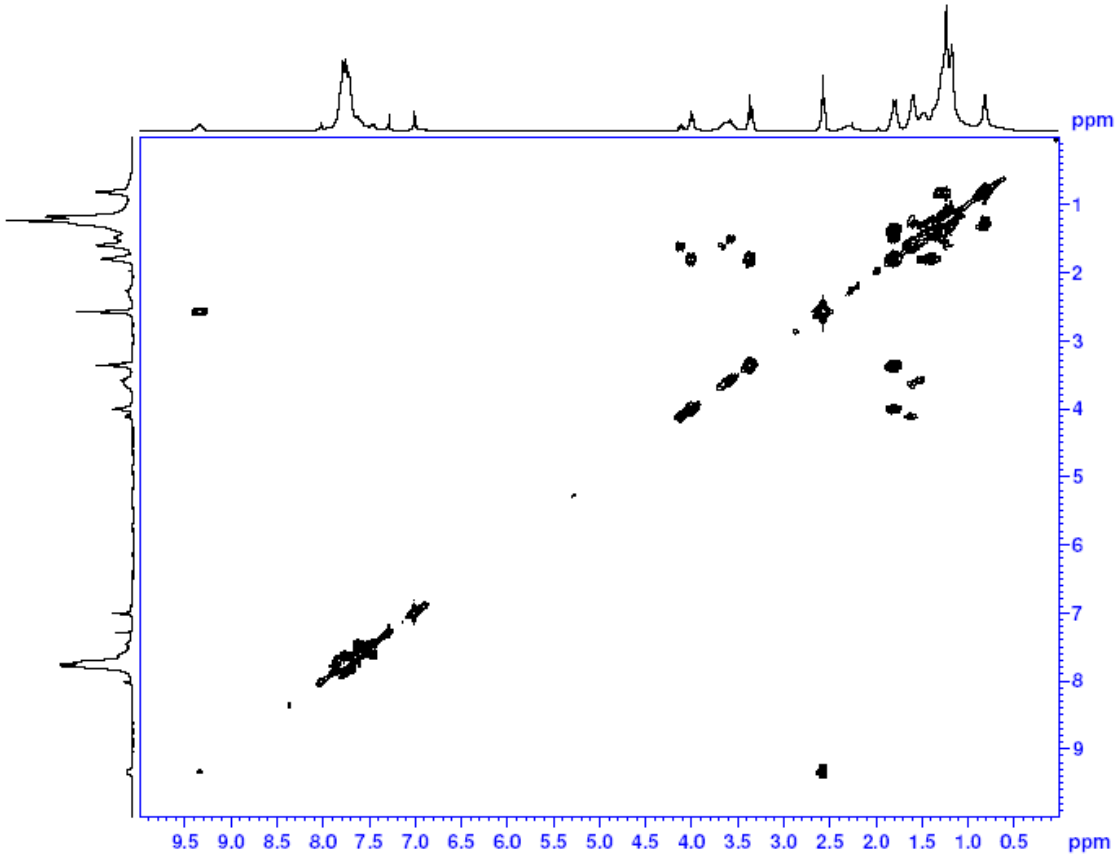

Figure A-79: ^{1}H-^{1}H COSY (300 MHz, $CDCl_3$) of **LHP1-DOD**.

LHP1-DOD; EGT-2-8; 03/09/09

Structure:

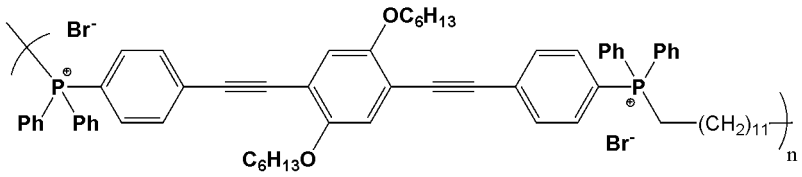

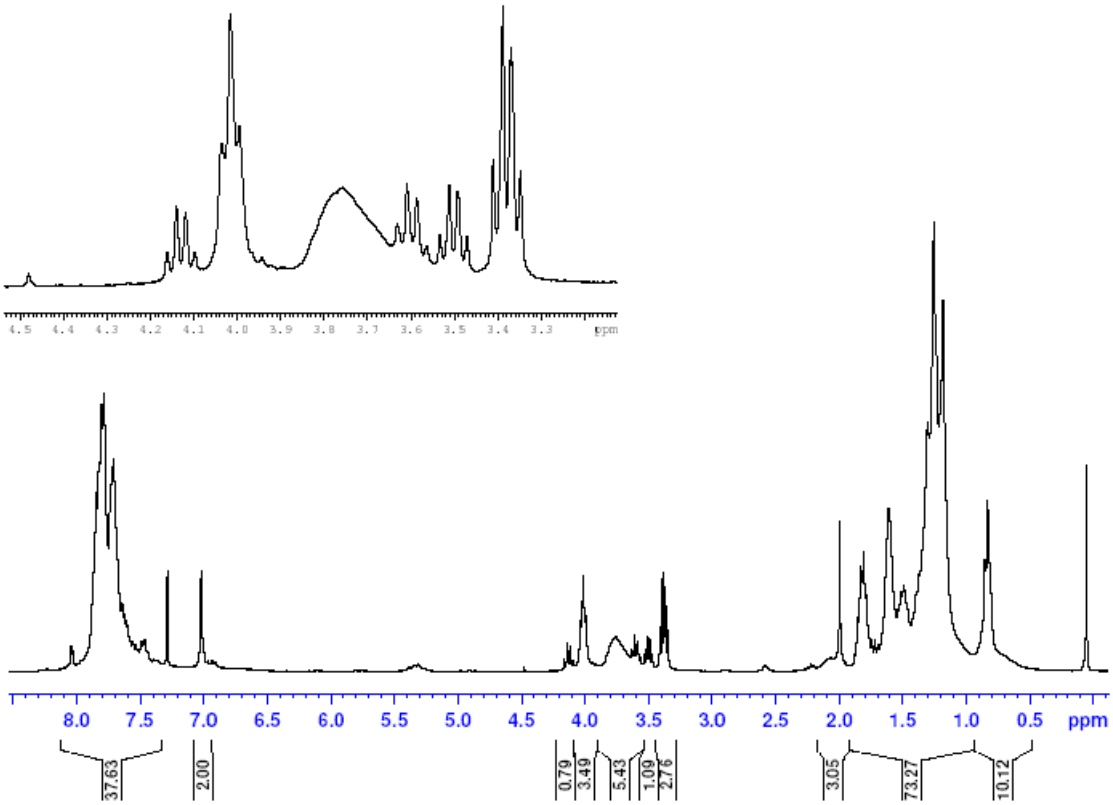

Figure A-80: ^{1}H NMR (300 MHz, $CDCl_3$) of **LHP1-DOD** after dichloromethane/water extraction.

LHP1-DOD; EGT-2-8; 03/09/09

Structure:

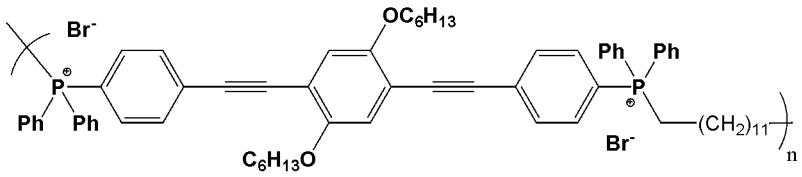

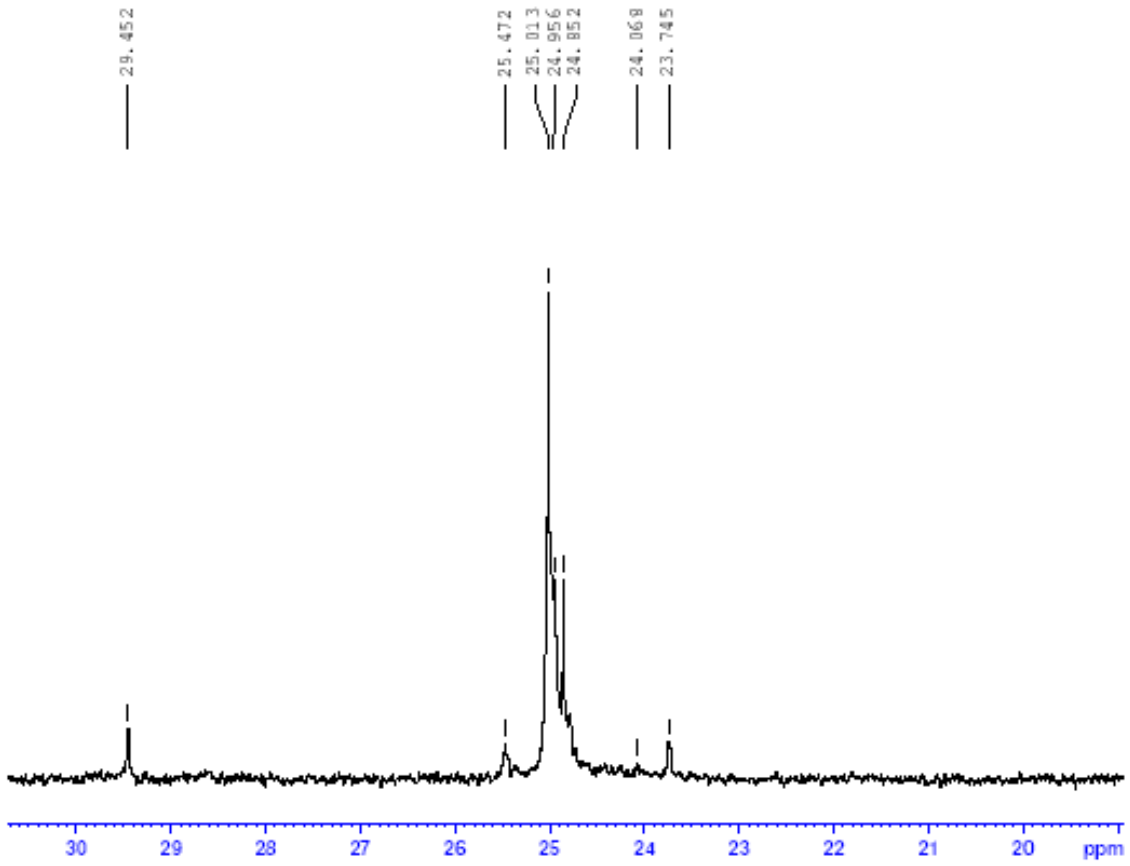

Figure A-81: ^{31}P NMR (121.4 MHz, $CDCl_3$) of **LHP1-DOD** after dichloromethane/water extraction.

Appendix B

UV-vis and Photoluminescence Spectra

Alkoxy Functionalized Platinum-based Polymer **4**; EGT-1-20; 11/02/07

Structure:

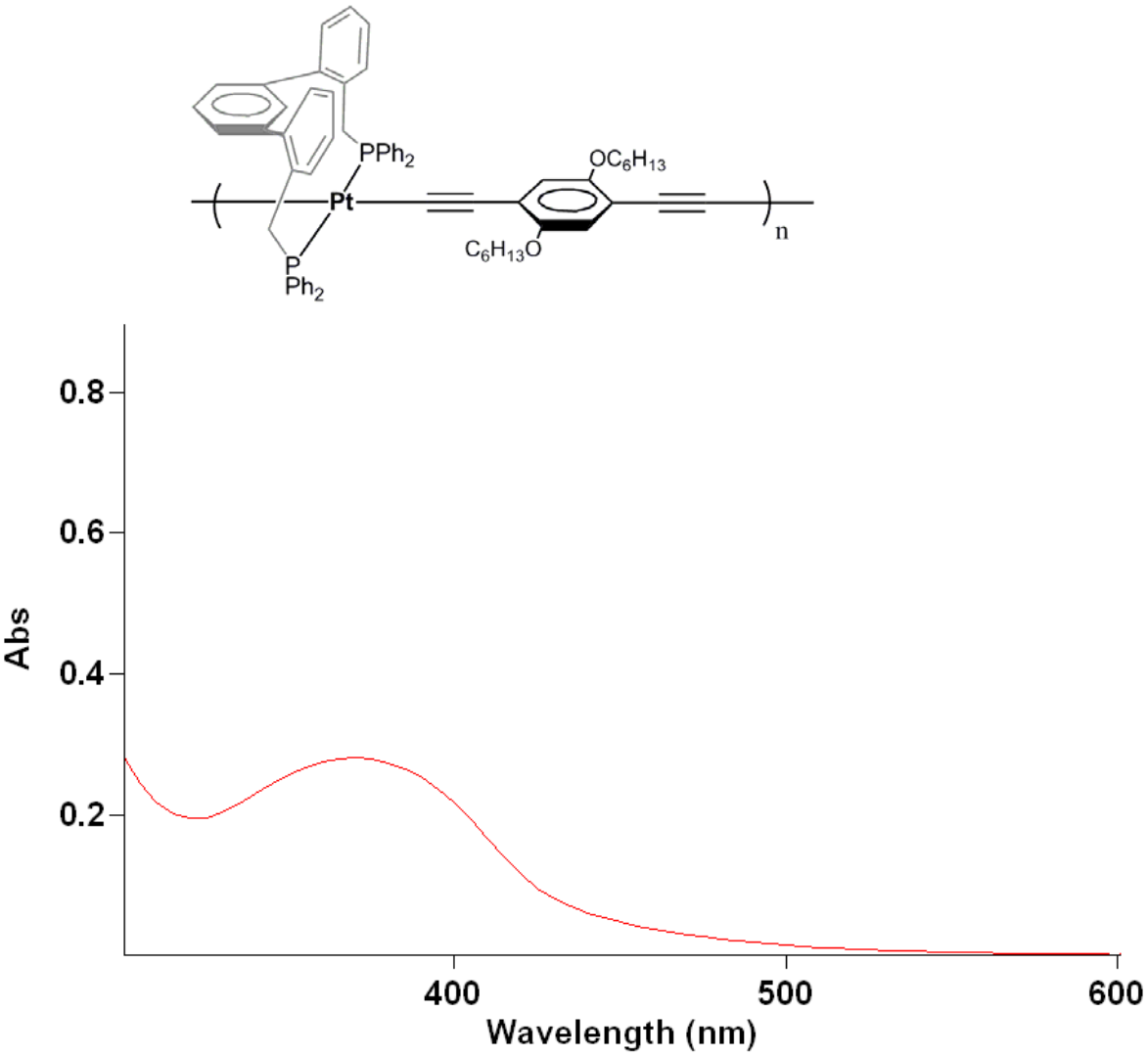

Figure B-1: Absorption spectrum for alkoxy metallopolymer **4** showing a maximum absorbance of ~370 nm.

Alkoxy Functionalized Platinum-based Polymer **4**; EGT-1-88; 09/10/08

Structure:

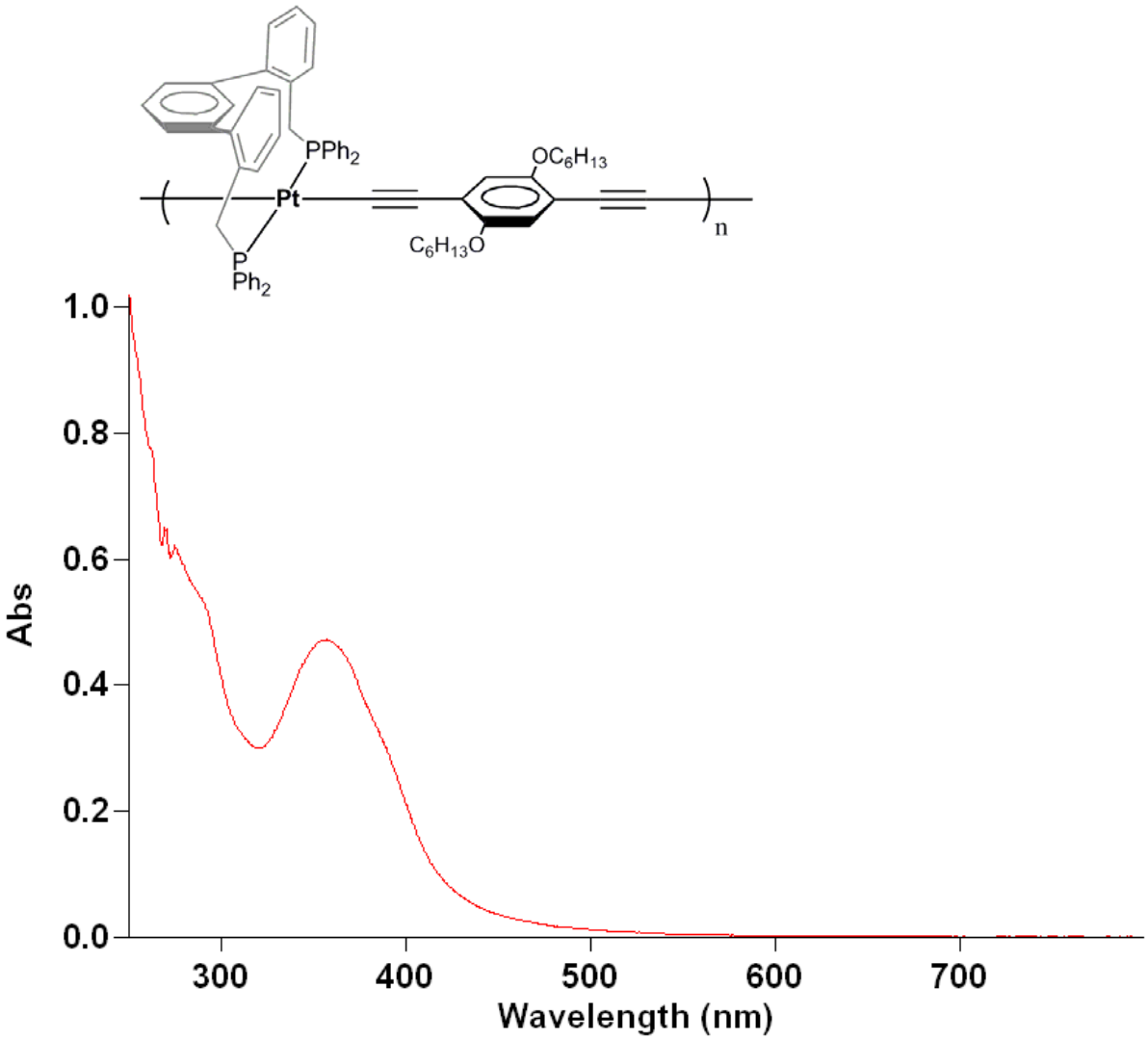

Figure B-2: Absorption spectrum for alkoxy metallopolymer **4** synthesized on 9/02/08 showing a maximum absorbance of ~357 nm.

Alkoxy Functionalized Platinum-based Polymer **4**; EGT-1-88; 09/10/08

Structure:

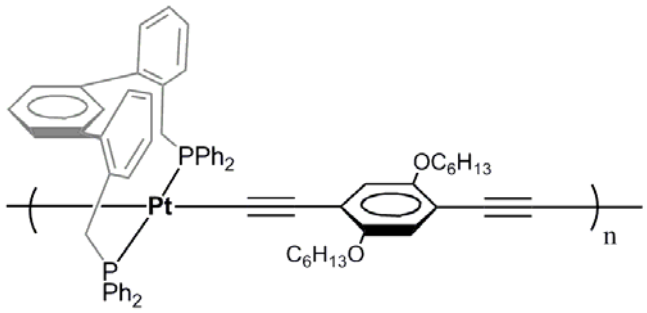

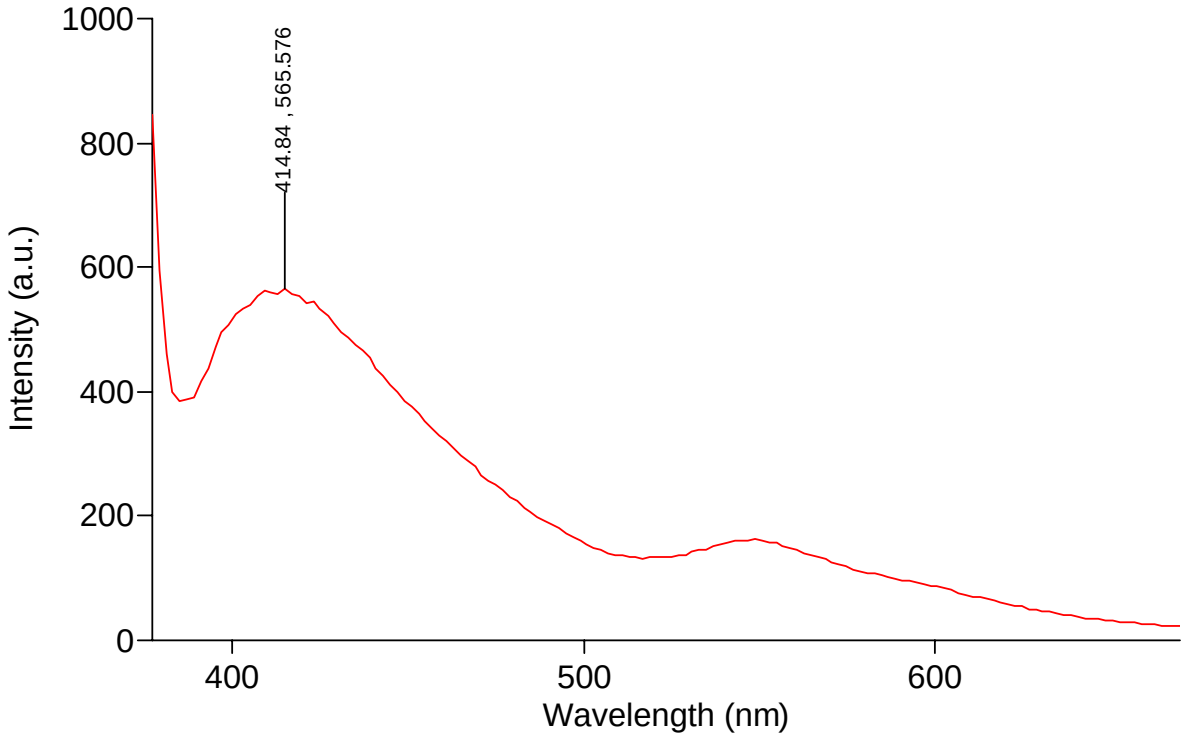

Figure B-3: Photoluminescence spectrum for alkoxy metallopolymer **4** synthesized on 9.02.08 using an excitation wavelength of 357 nm.

Linear phosphine oxide **16**; EGT-1-50; 04/03/08

Structure:

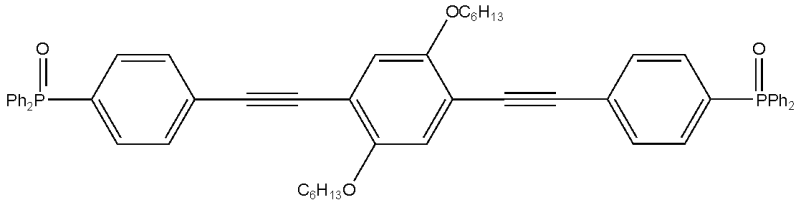

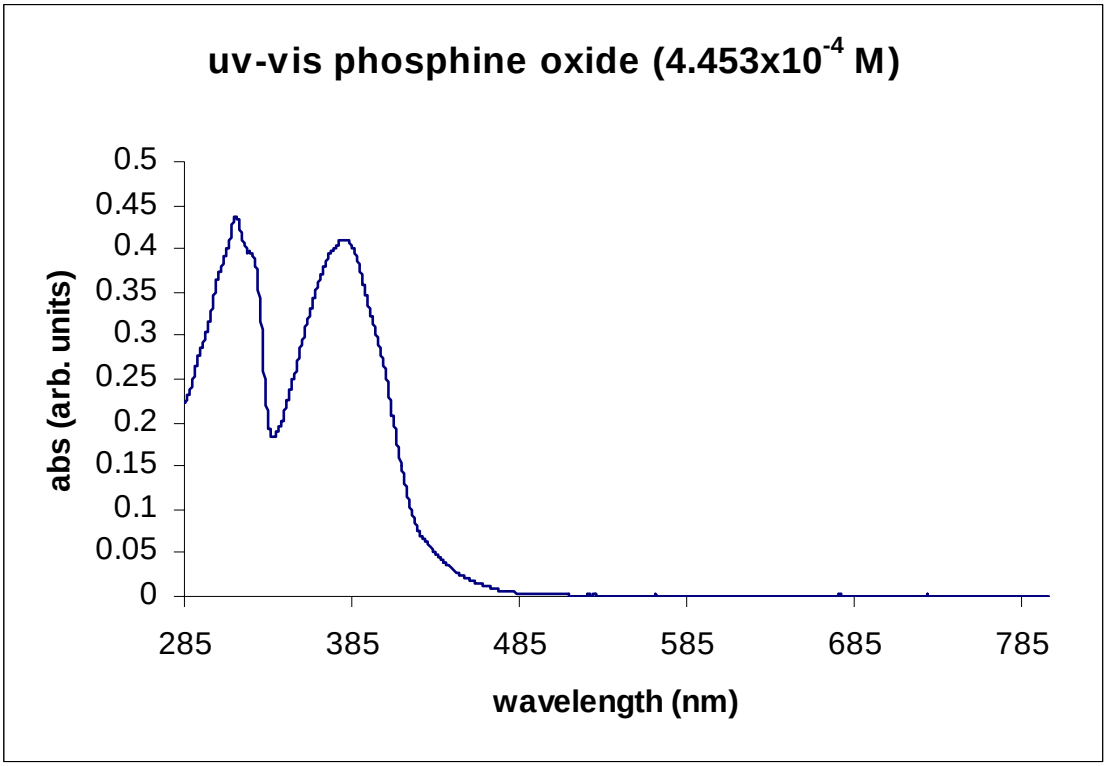

Figure B-4: Absorption spectrum for linear phosphine oxide **18** showing a maximum absorbance of ~381 nm.

Linear phosphine oxide **16**; EGT-1-50; 04/03/08

Structure:

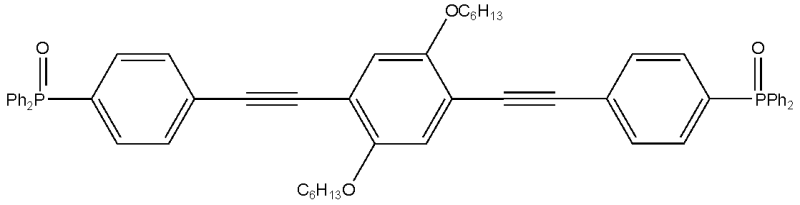

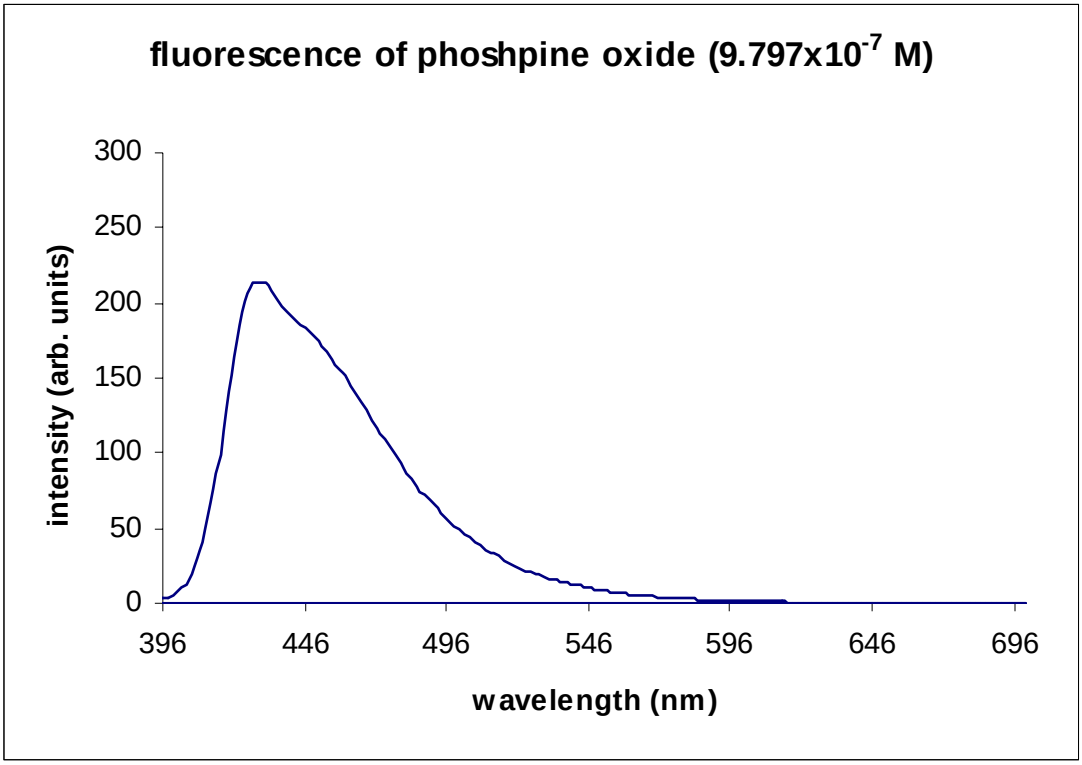

Figure B-5: Photoluminescence emission spectrum for linear phosphine oxide **16** using an excitation wavelength of 381 nm.

Linear phosphine **18**; EGT-1-51; 04/15/08

Structure:

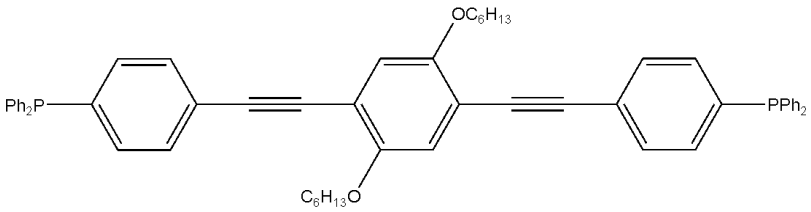

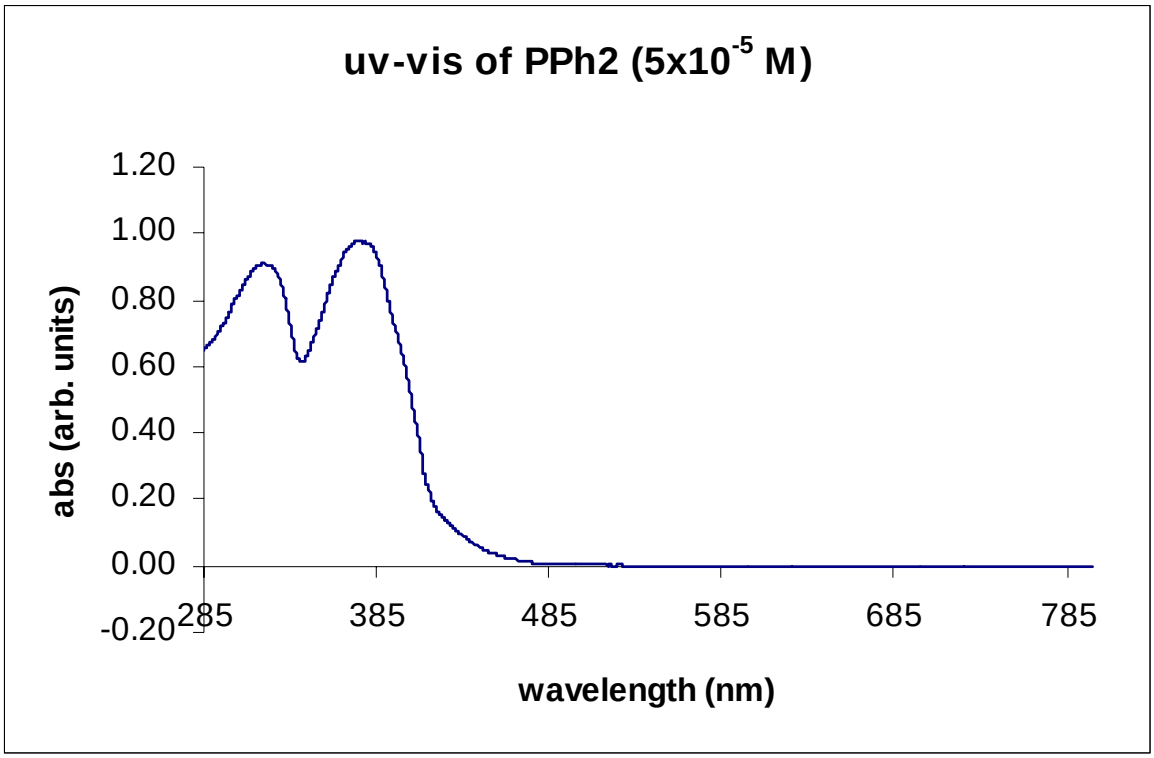

Figure B-6: Absorption spectrum for linear phosphine **18** showing a maximum absorbance of ~376 nm.

Linear phosphine **18**; EGT-1-51; 04/15/08

Structure:

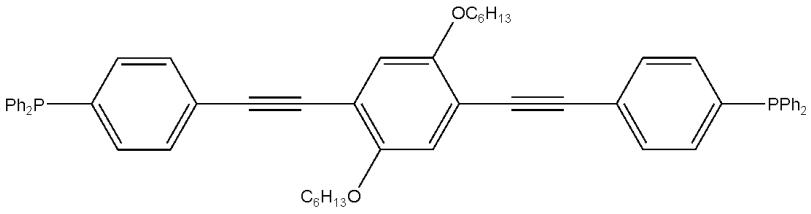

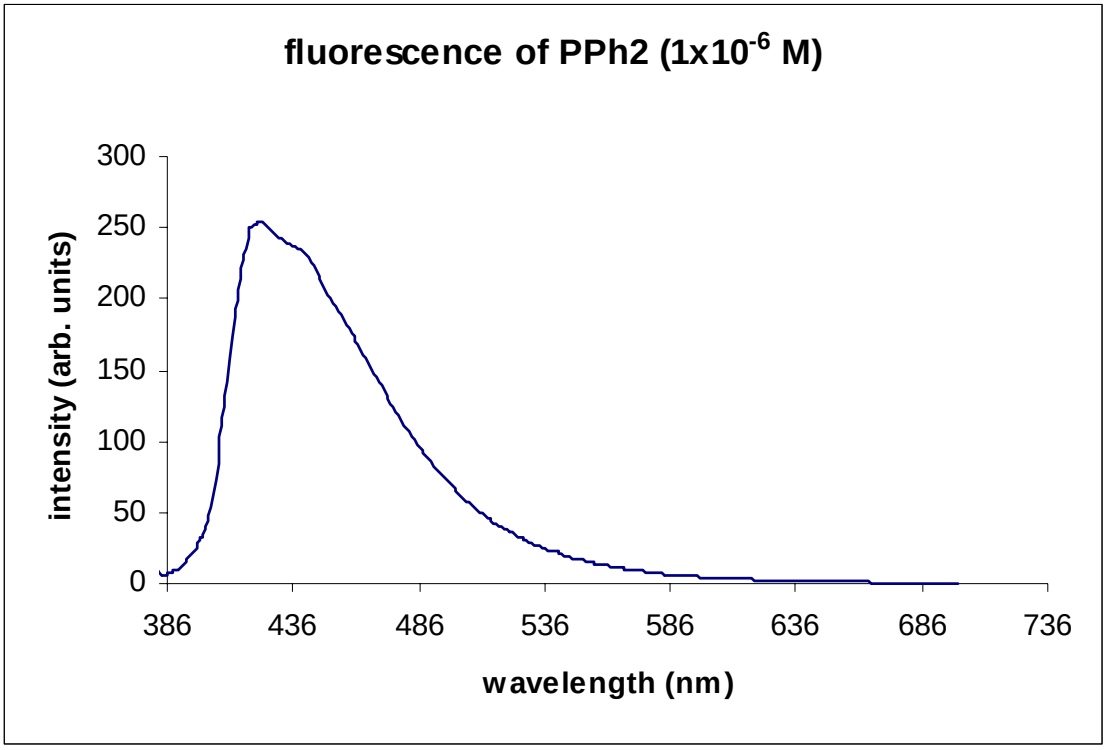

Figure B-7: Photoluminescence emission spectrum for linear phosphine **18** using an excitation wavelength of 376 nm.

Polymer **19**; EGT-1-51; 04/15/08

Structure:

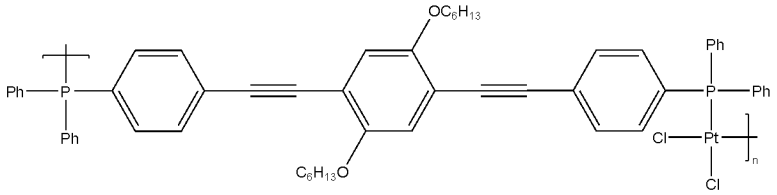

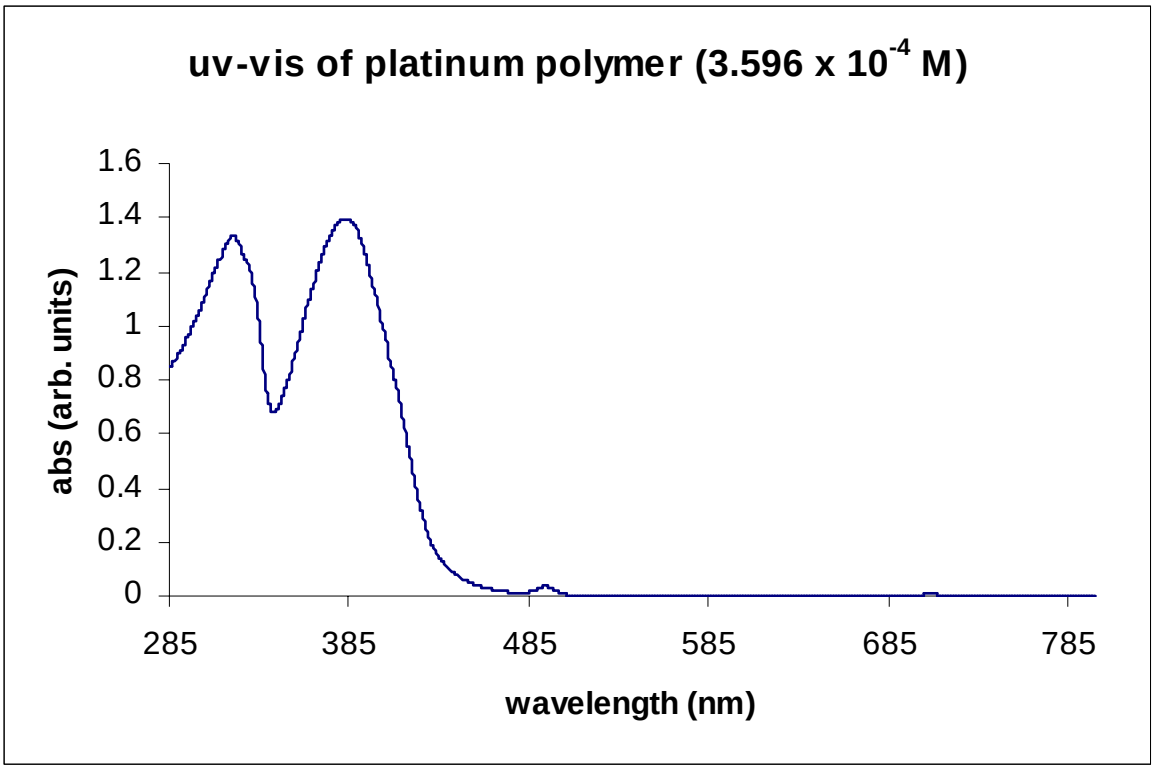

Figure B-8: Absorption spectrum for polymer **19** showing a maximum absorbance of ~384 nm.

Polymer **19**; EGT-1-51; 04/15/08

Structure:

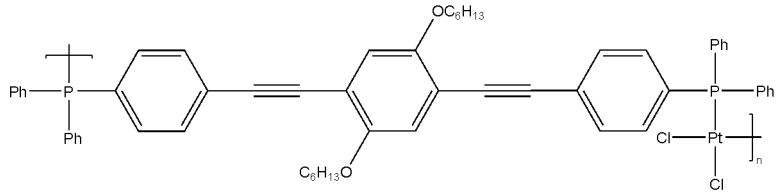

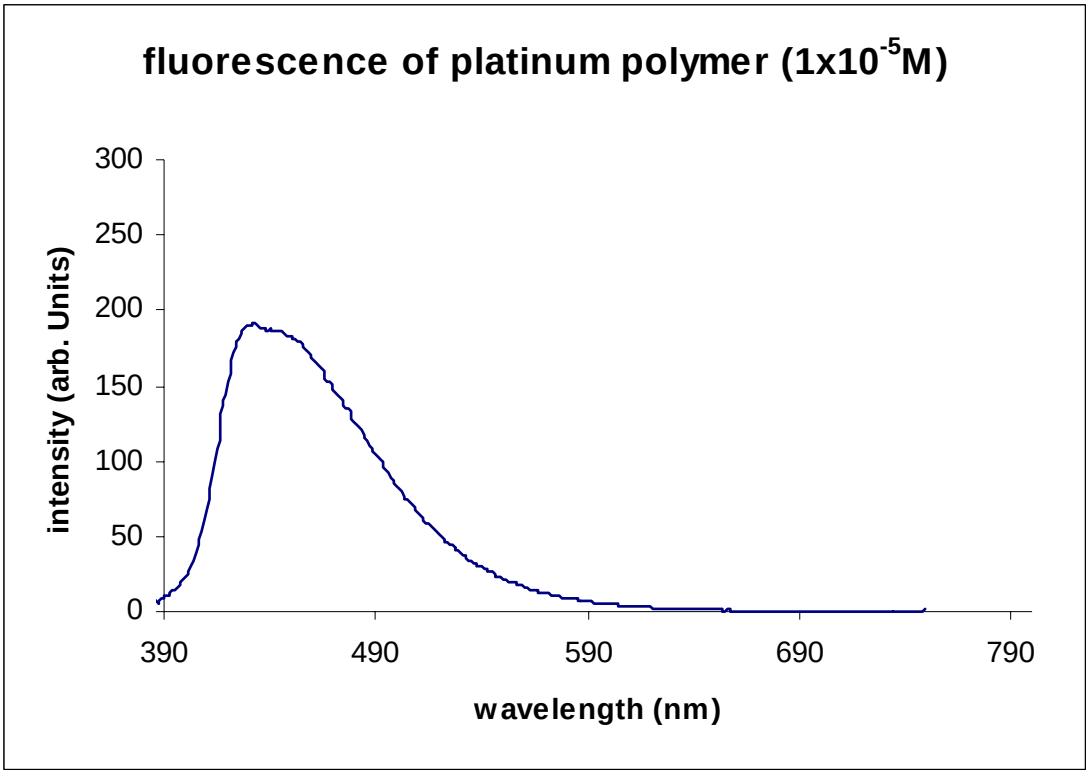

Figure B-9: Photoluminescence emission spectrum for polymer **19** using an excitation wavelength of 384 nm.

Polymer **20**; EGT-1-51; 04/15/08

Structure:

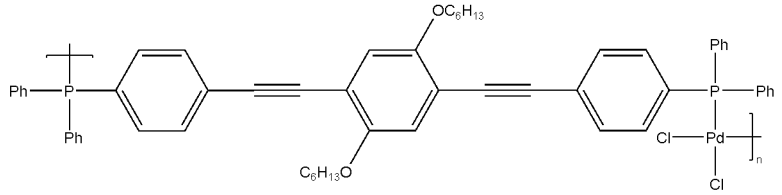

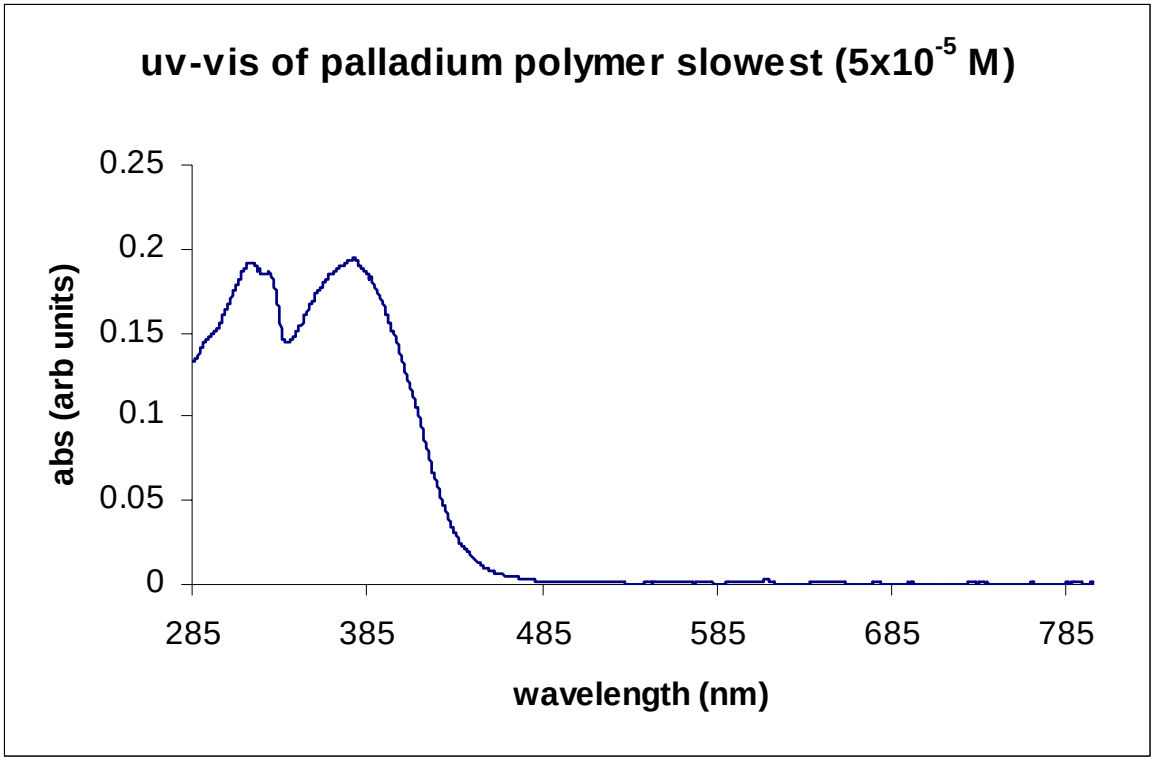

Figure B-10: Absorption spectrum for polymer **20** showing a maximum absorbance of ~378 nm.

Polymer **20**; EGT-1-51; 04/15/08

Structure:

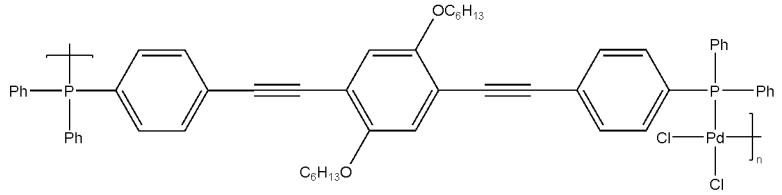

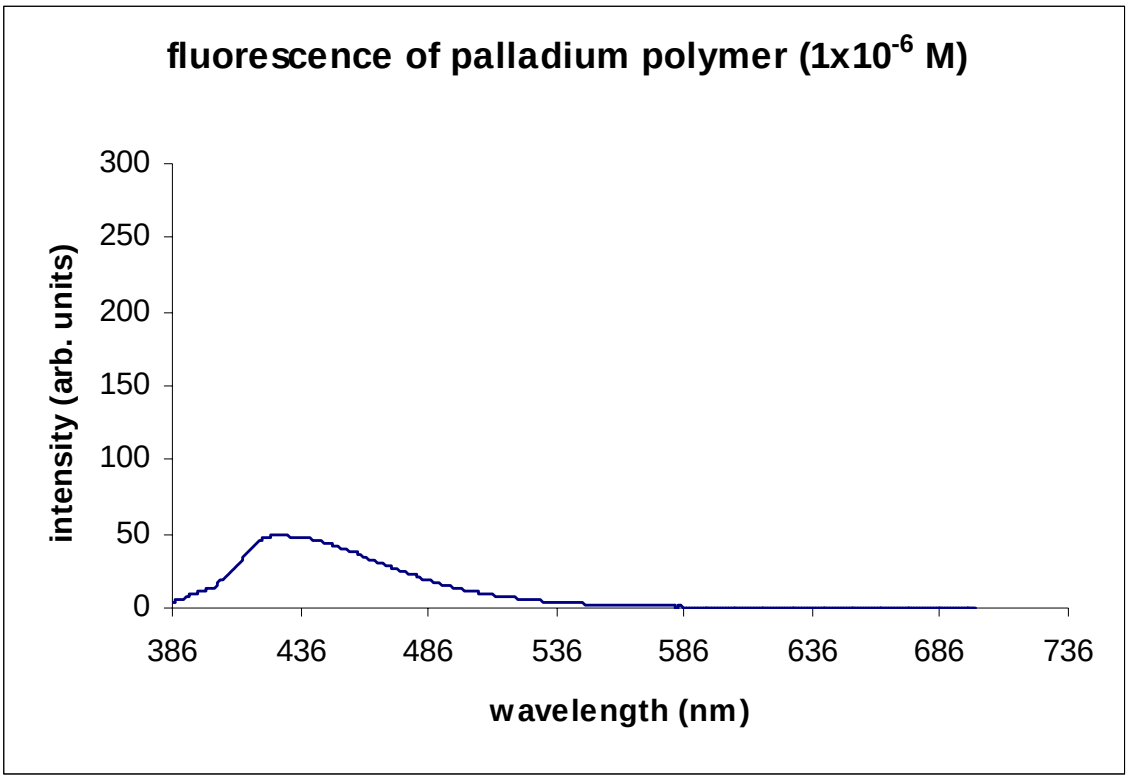

Figure B-11: Photoluminescence emission spectrum for polymer **20** using an excitation wavelength of 378 nm.

LHP1-OHx; EGT-2-1; 10/01/08

Structure:

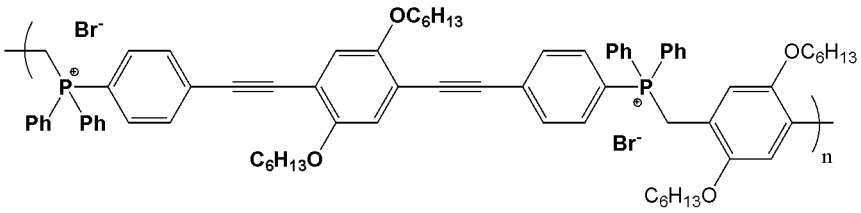

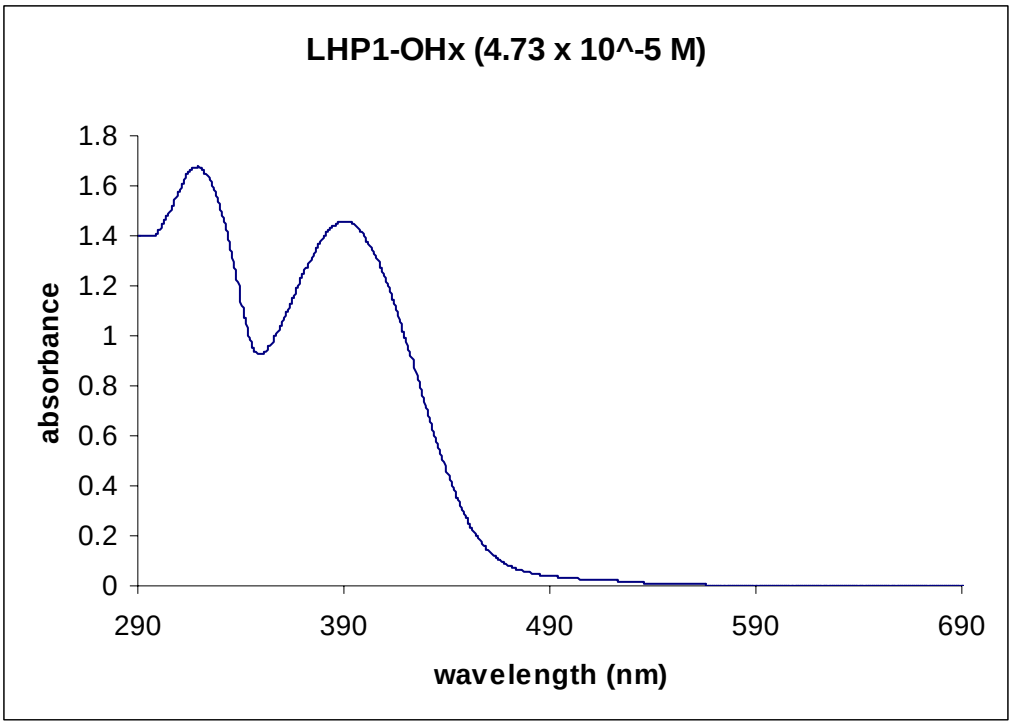

Figure B-12: Absorption spectrum for **LHP1-OHx**.

LHP1-OHx; EGT-2-1; 10/01/08

Structure:

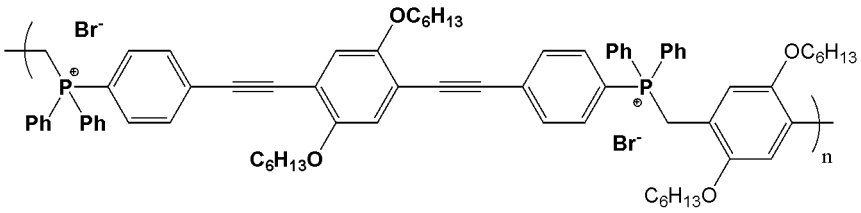

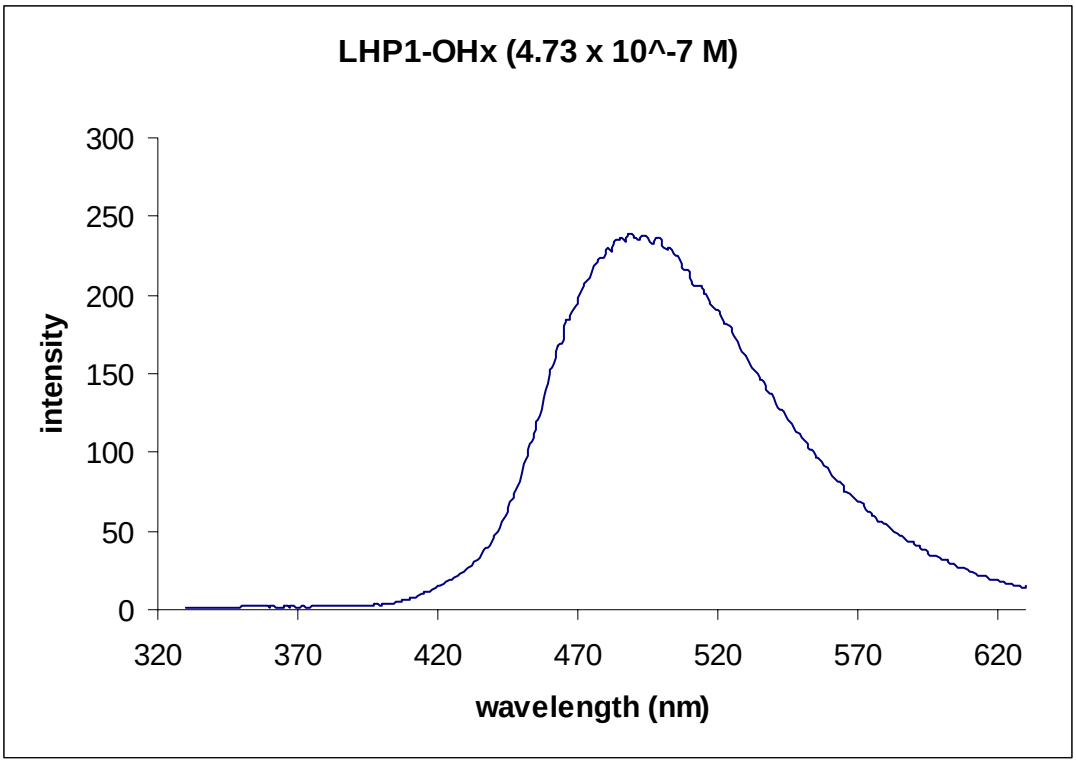

Figure B-13: Photoluminescence emission spectrum for **LHP1-OHx** in acetonitrile after exciting at 390 nm.

LHP1-OHx; EGT-2-2; 10/04/09

Structure:

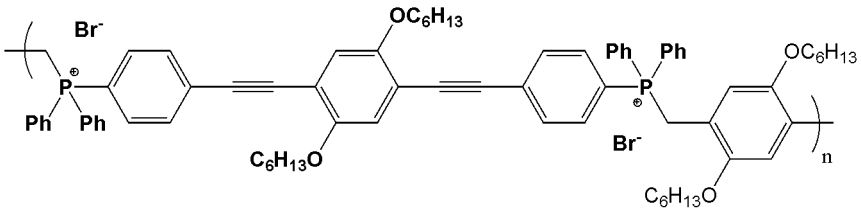

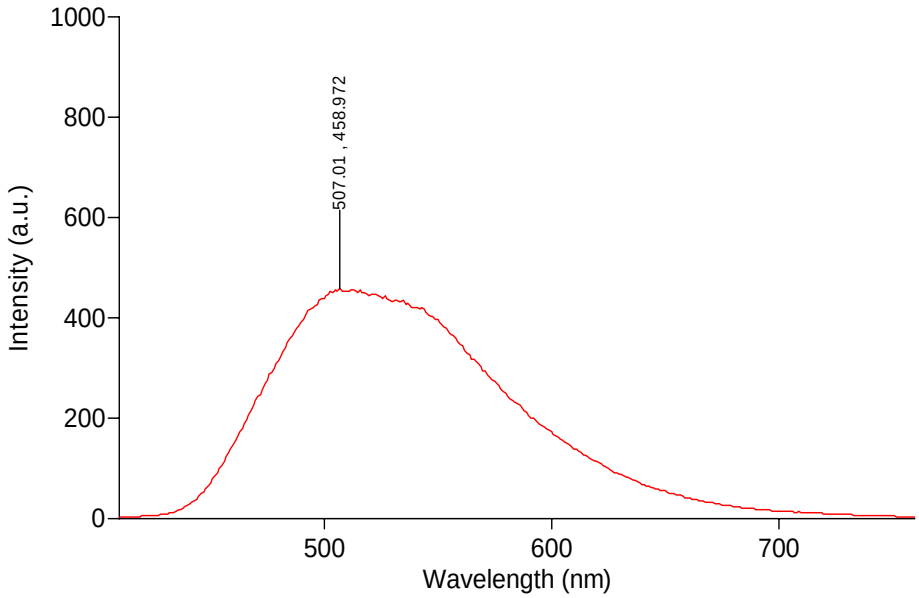

Figure B-14: Fluorescence emission spectrum for **LHP1-OHx** in zero times the critical micelle concentration (0 [CMC]) of SDS after exciting at 390 nm.

LHP1-OHx; EGT-2-2; 10/04/09

Structure:

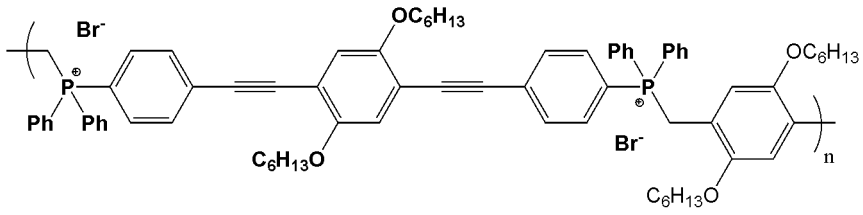

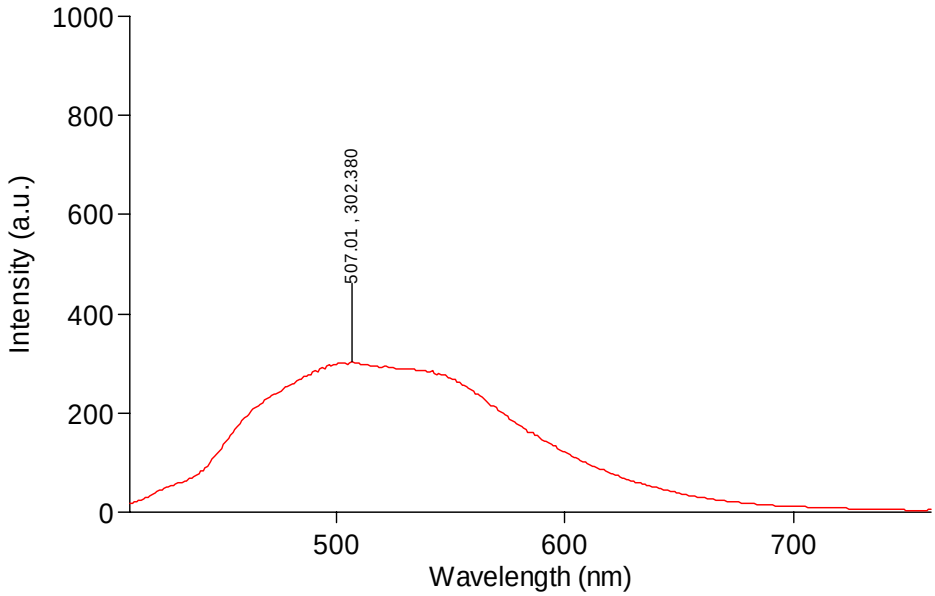

Figure B-15: Fluorescence emission spectrum for **LHP1-OHx** in 0.5 [CMC] of SDS after exciting at 390 nm.

LHP1-OHx; EGT-2-2; 10/04/09

Structure:

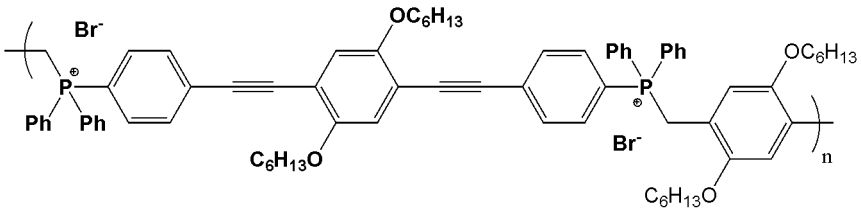

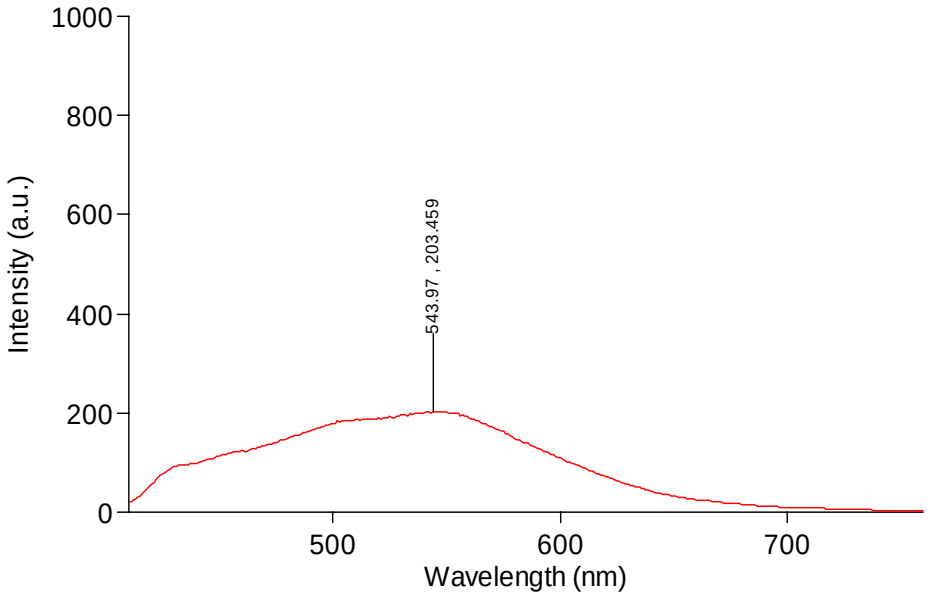

Figure B-16: Fluorescence emission spectrum for **LHP1-OHx** in [CMC] of SDS after exciting at 390 nm.

LHP1-OHx; EGT-2-2; 10/04/09

Structure:

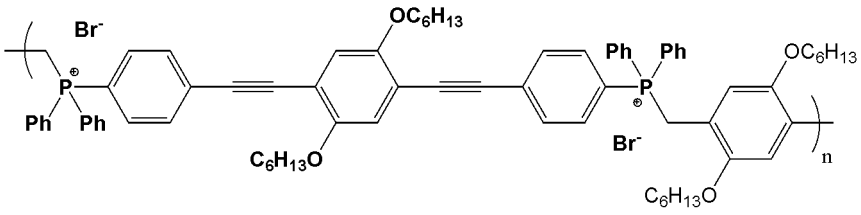

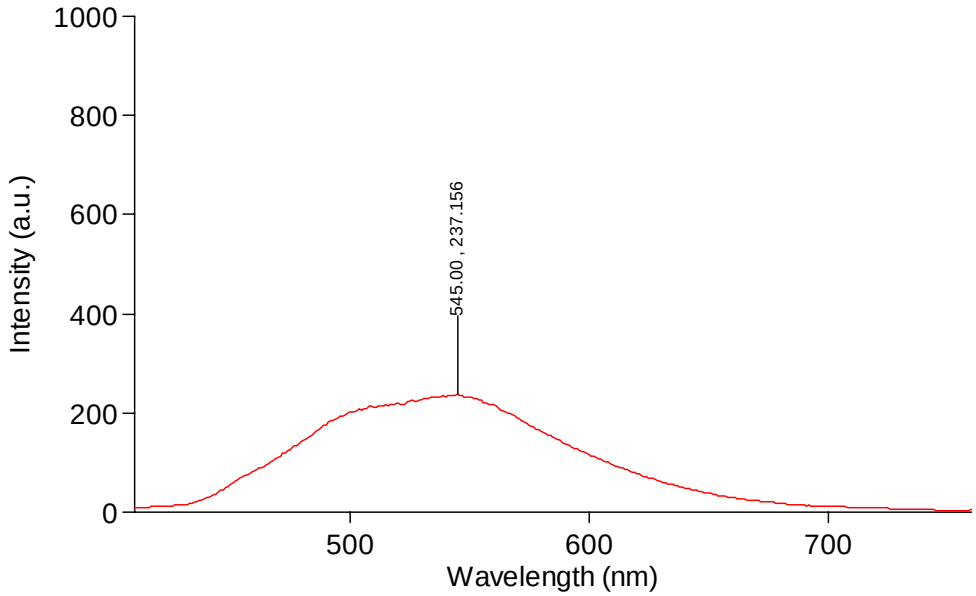

Figure B-17: Fluorescence emission spectrum for **LHP1-OHx** in 2 [CMC] of SDS after exciting at 390 nm.

LHP1-OHx; EGT-2-3; 10/20/09

Structure:

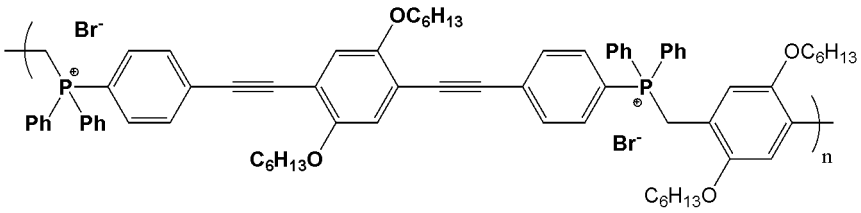

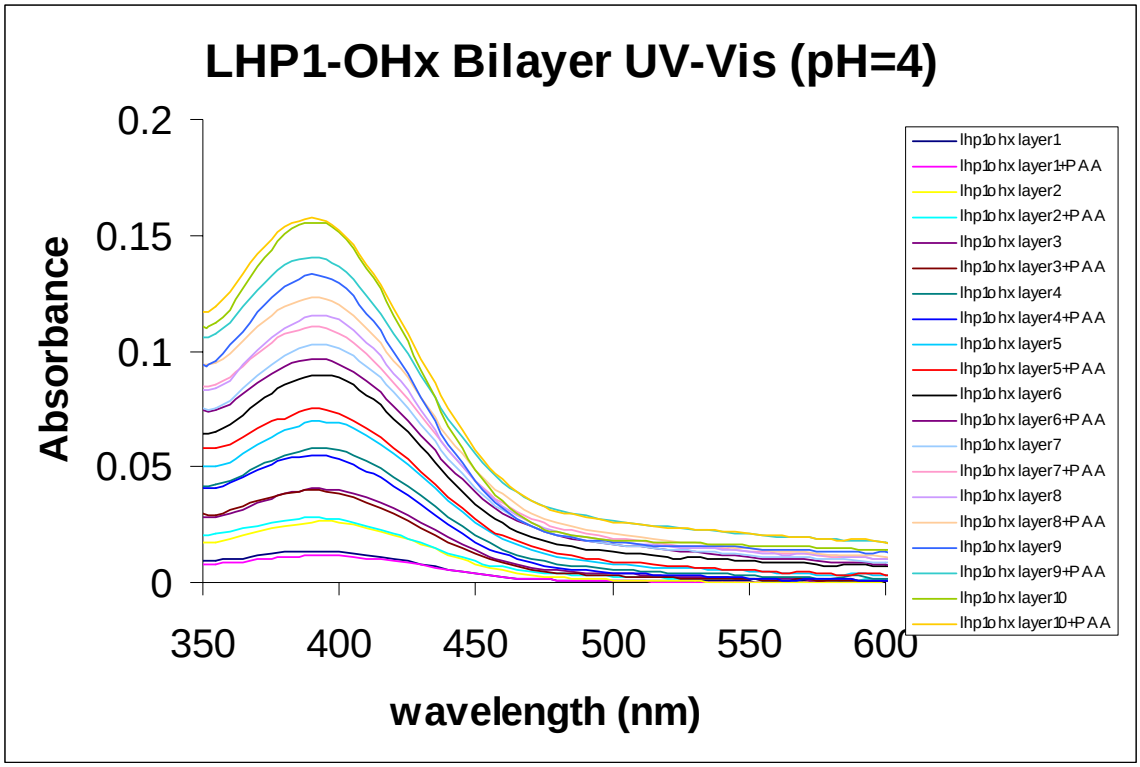

Figure B-18: Absorption data for bilayer study of **LHP1-OHx** and poly(acrylic acid) at pH = 4.

LHP1-OHx; EGT-2-4; 10/20/09

Structure:

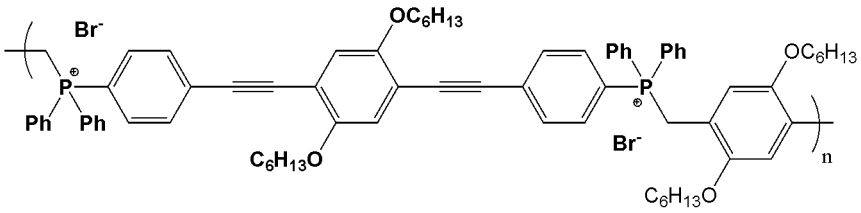

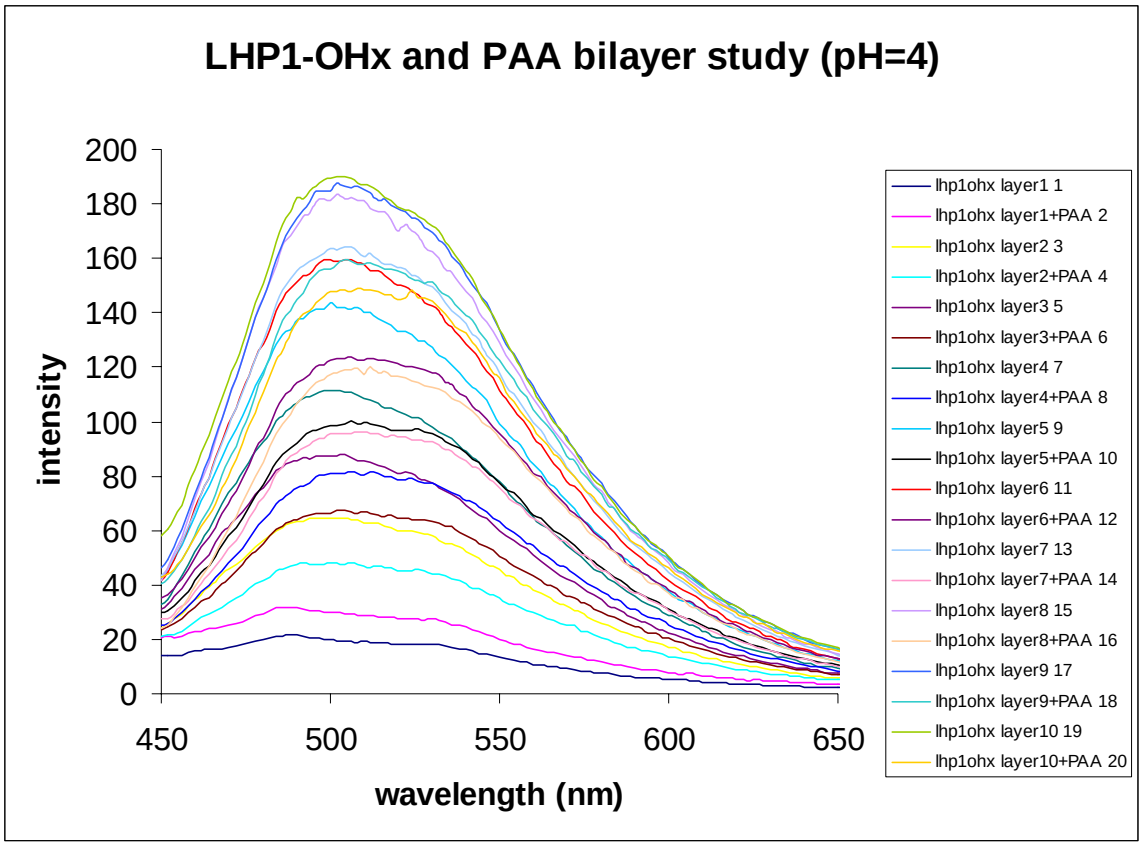

Figure B-19: Fluorescence data for bilayer study of **LHP1-OHx** and poly(acrylic acid) at pH = 4; excitation wavelength is 390 nm.

LHP1-OHx; EGT-2-5; 10/21/08

Structure:

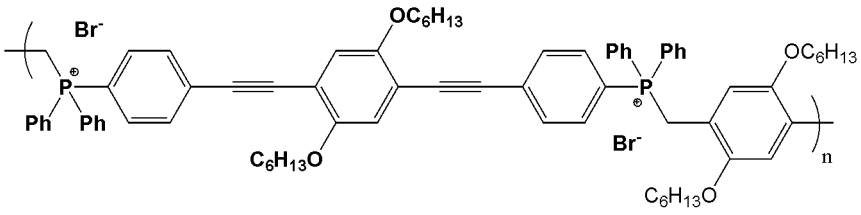

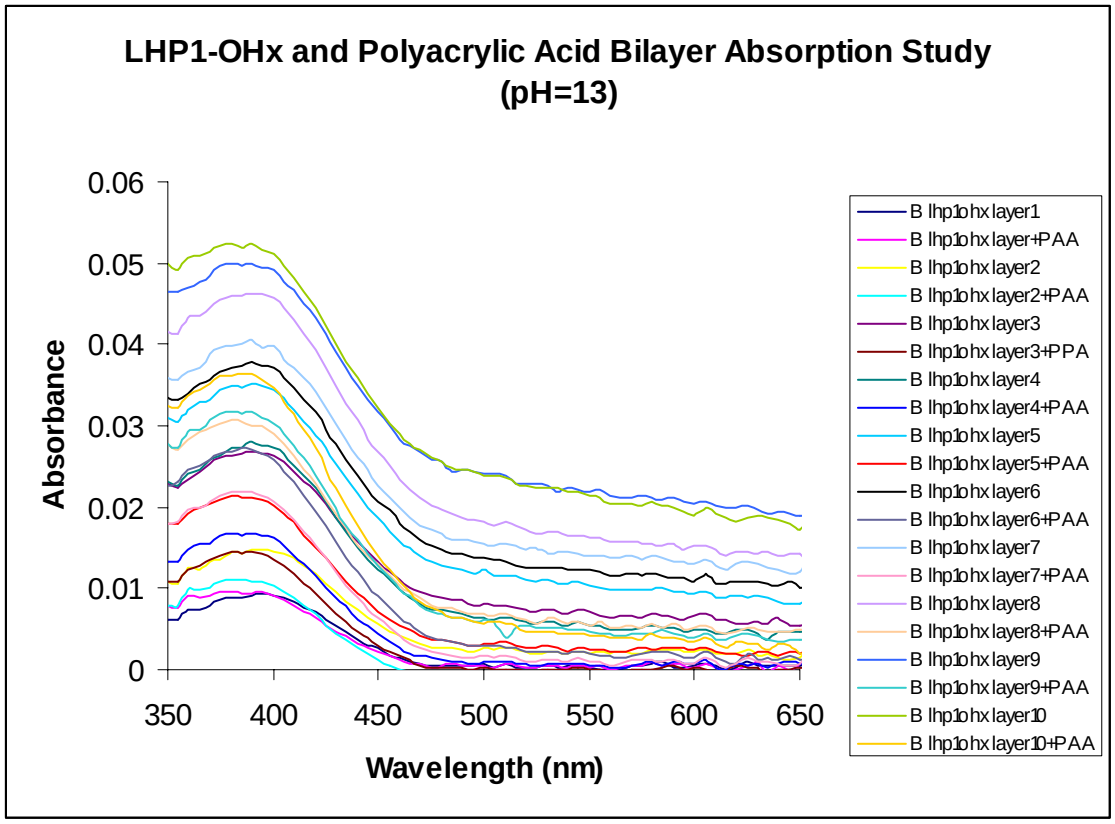

Figure B-20: Absorption data for bilayer study of **LHP1-OHx** and poly(acrylic acid) at pH = 13.

LHP1-OHx; EGT-2-6; 02/10/09

Structure:

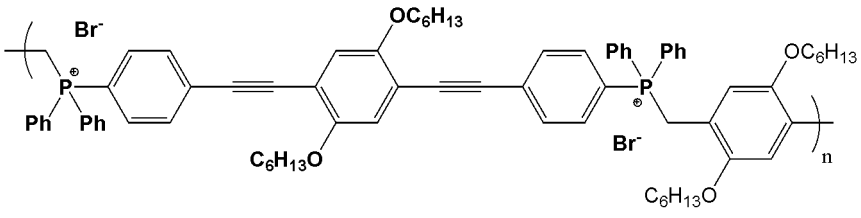

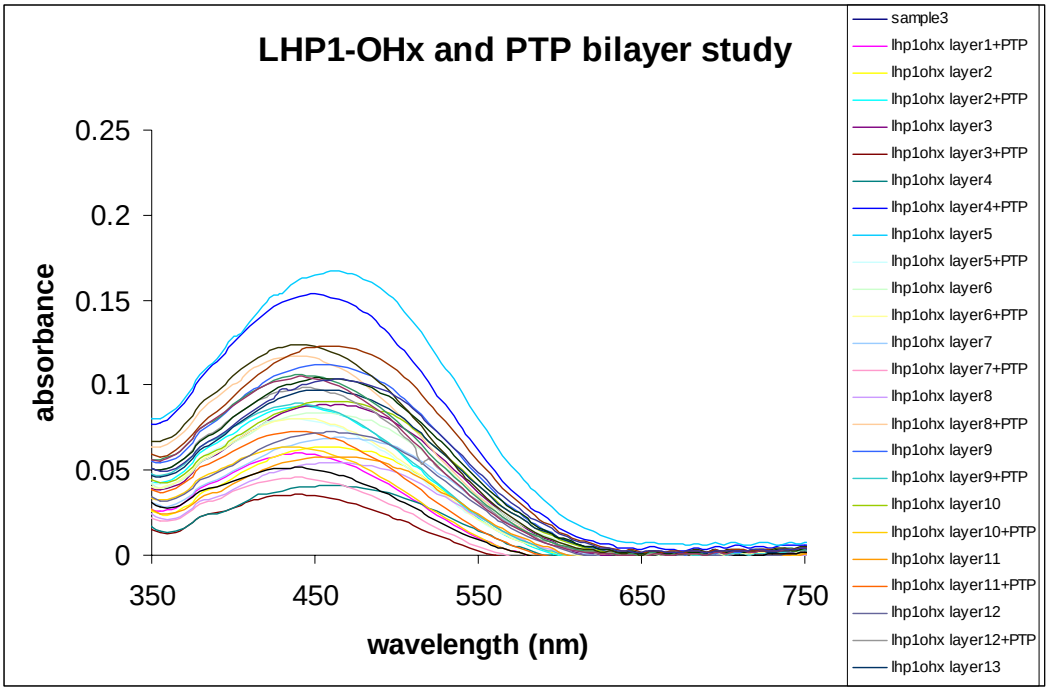

Figure B-20: Absorption data for bilayer study of **LHP1-OHx** and poly[2-(3-thienyl)ethyloxy-4-butylsulfonate] (PTP).

REFERENCES

(1) Morse Potential Diagram from http://upload.wikimedia.org/wikipedia/commons/0/0e/Franck-Condon-diagram.png retrieved on 20 March 2009.

(2) Solar Radiation Spectrum from http://globalwarmingart.com/images/4/4c/Solar_Spectrum.png retrieved on 28 February 2009.

(3) V. Talrose, A.N. Yermakov, A.A. Usov, A.A. Goncharova, A.N. Leskin, N.A. Messineva, N.V. Trusova, M.V. Efimkina, UV/Visible Spectra" in **NIST Chemistry WebBook, NIST Standard Reference Database Number 69**, Eds. P.J. Linstrom and W.G. Mallard, National Institute of Standards and Technology, Gaithersburg MD, 20899, http://webbook.nist.gov, (retrieved February 28, 2009).

(4) Doping Silicon: Diodes and Transistors from http://electronics.howstuffworks.com/diode1.htm retrieved on 20 March 2009.

(5) Albrecht, M.; van Koten, G. "Platinum Group Organometallics Based on 'Pincer' Complexes: Sensors, Switches, and Catalysts" *Angew. Chemie Int. Ed.* **2001**, *40*, 3750-3781.

(6) Autschbach, J.; Le Guennic, B. "Analyzing and Interpreting NMR Spin-Spin Coupling Constants Using Molecular Orbital Calculations" *J. Chem. Educ.* **2007**, *84*, 156-171.

(7) Baldo, M. A.; O'Brien, D. F.; You, Y.; Shoustikov, A.; Sibley, S.; Thompson, M. E.; Forrest, S. R. "Highly Efficient Phosphorescent Emission from Organic Electroluminescent Devices" *Nature* **199**, *395*, 151-154.

(8) Balema, V. P.; Wiench, J. W.; Pruskia, M.; Pecharsky, V. K. "Solvent-Free Mechanochemical Synthesis of Two Pt complexes: *cis*-$(Ph_3P)_2PtCl_2$ and *cis*-$(Ph_3P)_2PtCO_3$" *Chemical Commun.* **2002**, 1606-1607.

(9) Barker, J. "An Electrochemical Investigation of the Doping Processes in Poly(thienylene vinylene)" *Synthetic Metals* **1989**, *32*, 43-50.

(10) Bazan, G. C. "Novel Organic Materials through Control of Multichromophore Interactions" *J. Org. Chem.* **2007**, *72*, 8615-8635.

(11) Beljonne, D.; Wittman, F.; Kohler, A.; Graham, S.; Younus, M.; Lewis, J.; Raithby, P. R.; Khan, M. S.; Friend, R. H.; Bredas, J. L. "Spacial Extent of the Singlet and Triplet State Excitons in Transition Metal Containing Poly-ynes" *J. Chem. Phys.* **1996**, *105*, 3868-3877.

(12) Bemi, L.; Clark, H. C.; Davies, J. A.; Fyfe, C. A.; Wasylishen, R. E. "Studies of Phosphorus(III) Ligands and Their Complexes of Nickel(II), Palladium(II), and Platinum(II) Immobilized on Insoluble Supports by High-Resolution Solid-State Phosphorus-31 NMR Using Magic-Angle Spinning Techniques" *J. Am. Chem. Soc.* **1982**, *104*, 438-445.

(13) Blochwitz, J.; Pfeiffer, M.; Fritz, T.; Leo, K. "Low Voltage Organic Light Emitting Diodes Featuring Doped Phthalocyanine as Hole Transport Material" *Appl. Phys. Lett.* **1998**, *73*, 729-731.

(14) Bruice, P. Y. *Organic Chemistry*, Third ed.; Prentice Hall: New Jersey, 2001.

(15) Burn, P. L.; Kraft, A.; Baigent, D. R.; Bradley, D. D. C.; Brown, A. R.; Friend, R. H.; Gymer, R. W.; Holmes, A. B.; Jackson, R. W. "Chemical Tuning of the Electronic Properties of Poly(*p*-phenylenevinylene)-Based Copolymers" *J. Am. Chem. Soc.* **1993**, *115*, 10117-10124.

(16) Burroughes, J. H.; Bradley, D. D. C.; Brown, A. R.; Marks, R. N.; Mackay, K.; Friend, R. H.; Burns, P. L.; Holmes, A. B. "Light-emitting Diodes Based on Conjugated Polymers" *Nature* **1990**, *347*, 539-541.

(17) Cairns, M. A.; Dixon, K. R.; Smith, M. A. R. "A New Synthesis of Platinum-Carbon Bonds" *J. Organomet. Chem.* **1977**, *135*, C33-C34.

(18) Chawdhury, N.; Kohler, A.; Friend, R. H.; Wong, W.-Y.; Lewis, J.; Younus, M.; Raithby, R. R.; Corcoran, T. C.; Al-Mandhary, M. R. A.; Khan, M. S. "Evolution of Lowest Singlet and Triplet Excited States with Number of Thienyl RIngs in Platinum Poly-ynes" *J. Chem. Phys.* **1999**, *110*, 4963-4970.

(19) Chiang, C. K.; Heeger, A. J.; MacDiarmid, A. G. "Effect of Uniaxial Stress on Electrical Conductivity of Sulphur Nitride Polymer" *Physical Letters A* **1977**, *60*, 375-377.

(20) Cimrova, V.; Schmidt, W.; Rulkens, R.; Schulze, M.; Meyer, W.; Neher, D. "Efficient Blue Light Emitting Devices Based on Rigid-Rod Polyelectrolytes" *Adv. Mater.* **1996**, *8*, 585-588.

(21) Clarke, M. L.; Ellis, D.; Mason, K. L.; Orpen, A. G.; Pringle, P. G.; Wingad, R. L.; Zahera, D. A.; Baker, R. T. "The Electron-Poor Phosphines $(C_6F_5)_3P$ and $(3,5\text{-}(CF_3)_2C_6H_3)_3P$ Do Not mimic Phosphites as Ligands for Hydroformylation. A Comparision of the Coordination Chemistry of $(C_6F_5)_3P$ and $(3,5\text{-}(CF_3)_2C_6H_3)_3P$ and the Low Hydroformylation Activity of Their Rhodium Complexes" *Dalton Trans.* **2005**, 1294-1130.

(22) Clyburne, J. A. C.; McMullen, N. "Unusual Structures of Main Group Organometallic Compounds Containing *m*-Terphenyl Ligands" *Coord. Chem. Rev.* **2000**, *210*, 73-99.

(23) Decher, G.; Hong, J. D. "Buildup of Ultrathin Multilayer Films by a Self-Assembly Process: III. Consecutively Alternating Adsorption of Anionic and Cationic Polyelectrolytes on Charged Surfaces" *Thin Solid Films* **1992**, *210-211*, 831-835.

(24) Decher, G. "Fuzzy Nanoassemblies: Toward Layered Polymeric Multicomposites" *Science* **1997**, *227*, 1232-1237.

(25) Dray, A. E.; Wittmann, F.; Friend, R. H.; Donald, A. M.; Khan, M. S.; Lewis, J.; Johnson, B. F. G. "Structure and Electronic Properties of Transition Metal-Containing Poly-ynes" *Synthetic Metals* **1991**, *41*, 871-874.

(26) Eckhardt, H.; Shacklette, L. W.; Jen, K. Y.; Elsenbaumer, R. L. "The Electronic and Electrochemical Properties of Poly(phenylenevinylene) and Poly(thienylenevinylenes): An Experimental Study" *J. Chem. Phys.* **1989**, *91*, 1303-1315.

(27) Einstein, A. "Concerning an Heuristic Point of View toward the Emission and Transformation of Light" *Am. J. Phys.* **1965**, *33*, 1-16.

(28) Friend, R. H.; Gymer, R. W.; Holmes, A. B.; Burroughes, J. H.; Marks, R. N.; Taliana, C.; Bradley, D. D. C.; dos Santos, D. A.; Bredas, J. L.; Logdlund, M.; Salaneck, W. R. "Electroluminescence in Conjugated Polymers" *Nature* **1999**, *397*, 121-128.

(29) Gasparro, F. P.; Kolodny, N. H. "NMR Determination of the Rotational Barrier in *N,N*-dimethylacetamide" *J. Chem. Educ.* **1977**, *54*, 258-261.

(30) Glenis, S.; Horowitz, G.; Tourillon, G.; Garnier, F. "Electrochemically Grown Polythiophene and Poly(3-methylthiophene) Organic Photovoltaic Cell" *Thin Solid Films* **1984**, *111*, 93-103.

(31) Glusac, K.; Kose, M. E.; Jiang, H.; Schanze, K. S. "Triplet Excited State in Platinum-Acetylide Oligomers: Triplet Localization and Effects of Conformation" *J. Phys. Chem.* **2997**, 929-940.

(32) Grim, S. O.; Keiter, R. L.; McFarlane, W. "A Phosphorous-31 Nuclear Magnetic Resonance Study of Tertiary Phosphine Complexes of Platinum(II)" *Inorg. Chem.* **1967**, *6*, 1133-1137.

(33) Grimsdale, A. C.; Chan, K. L.; Martin, R. E.; Jokisz, P. G.; Holmes, A. B. "Synthesis of Light-Emitting Conjugated Polymers for Applications in Electroluminescent Devices" *Chem. Rev.* **2009**, *109*, 897-1091.

(34) Guo, F.; Kim, Y.-G.; Reynolds, J. R.; Schanze, K. S. "Platinum-acetylide Polymer Based Solar Cells: Involvement of the Triplet State for Energy Conversion" *Chemical Commun.* **2006**, 1887-1889.

(35) Hiriyama, S.; Steer, R. P. "Solvatochromism and Barochromism Revisited and Revealed" *J. Chem. Educ.* **2008**, *85*, 317-319.

(36) Ho, P. K. H.; Kim, J.-S.; Burroughes, J. H.; Becker, H.; Li, S. F. Y.; Brown, T. M.; Cacialli, F.; Friend, R. H. "Molecular-Scale Interface Engineering for Polymer Light-Emitting Diodes" *Nature* **2000**, *404*, 481-484.

(37) Huheey, J. E.; Keiter, E. A.; Keter, R. L. *Inorganic Chemistry: Principles of Structure and Reactivity*, Fourth ed.; HarperCollins: New York, 1993.

(38) Kazan, B. "Material Aspects of Display Devices" *Nature* **1980**, *208*, 927-936.

(39) Khan, M. S.; Kakkar, A. K.; Long, N. J.; Lewis, J.; Raithby, P.; P., N.; Marder, T. B.; Wittmann, F.; Friend, R. H. "Synthesis and Optical Spectroscopy of Linear Long-Chain Di-terminal Alkynes and Their Pt-σ-acetylide Polymeric Complexes" *J. Mater. Chem.* **1994**, *4*, 1227-1232.

(40) Khan, M. S.; Al-Mandhary, M. R. A.; Al-Suti, M. K.; Corcoran, T. C.; Al-Mahrooqi, Y.; Attfield, J. P.; Feeder, N.; David, W. I. E.; Shankland, K.; Friend, R. H.; Kohler, A.; Marseglia, E. A.; Tedesco, E.; Tang, C. C.; Raithby, P. R.; Collings, J. C.; Roscoe, K. P.; Batsanov, A. S.; Stimson, L. M.; Marder, T. D. "Synthesis and Optical Characterization of Platinum(II) Poly-yne Polymers Incorporating Substituted 1,4-Diethynylbenzene Derivatives and an Investigation of the Intermolecular Interactions in the Diethynylbenzene Molecular Precursors" *New J. Chem.* **2003**, *27*, 140-149.

(41) Kim, M.; Sandman, D. J. "Polycation Effects on Electronic Spectra of Conjugated Poymers in Programmed Electrostatic Assemblies" *J. Macromol. Sci. A* **2001**, *38*, 1291-1304.

(42) Komorski, R. A. "Line Broadening in the ^{13}C NMR Spectra of Bulk Polymers Above T_g" *J.Poly. Sci. B* **1983**, *21*, 2551-2559.

(43) Koziar, J. C.; Cowan, D. O. "Photochemical Heavy-Atom Effects" *Acc. Chem. Res.* **1978**, *11*, 334-341.

(44) Kraft, A.; Grimsdale, A. C.; Holmes, A. B. "Electroluminescent Conjugated Polymers--Seeing Polymers in a New Light" *Angew. Chemie Int. Ed.* **1998**, *37*, 402-428.

(45) Lakowicz, J. R. *Principles of Fluorescence Spectroscopy*, Third ed.; Springer Science and Business Media: New York, 2006.

(46) Lee, H.; Lee, Y.; Statz, A. R.; Rho, J.; Park, T. G.; Messersmith, P. B. "Substrate-Independent Layer-by-Layer Assembly by Using Mussel-Adhesive-Inspired Polymers" *Adv. Mater.* **2008**, *20*, 1619-1623.

(47) Lee, J.-I.; Kang, I.-N.; Hwang, D.-H.; Shim, H.-K.; Jeoung, S. C.; Kim, D. "Energy Transfer in a Blend of Electroluminescent Polymers" *Chem. Mater.* **1996**, *8*, 1925-1929.

(48) Liu, Y.; Jiang, S.; Glusac, K.; Powell, D. H.; Anderson, D. F.; Schanze, K. S. "Photophysics of Monodisperse Platinum-Acetylide Oligomers: Delocalization in the Singlet and Triplet Excited States" *J. Am. Chem. Soc.* **2002**, *124*, 12412-12413.

(49) Lower, S. K.; El-Sayed, M. A. "The Triplet State and Molecular Electronic Processes in Organic Molecules" *Chem. Rev.* **1966**, *66*, 199-241.

(50) Lucht, B. L.; St. Onge, N. O. "Synthesis and Characterization of Poly(*p*-phenylenephosphine)s" *Chemical Commun.* **2007**, 2097-2098.

(51) Ma, L.; Woloszynek, R. A.; Chen, W.; Ren, T.; Protasiewicz, J. D. "A New Twist on Pincer Ligands and Complexes" *Organometallics* **2006**, *25*, 3301-3304.

(52) Martens, J. F.; Marseglia, E. A.; Bradley, D. D. C.; Friend, R. H.; Burn, P. L.; Holmes, A. B. "The Effect of Side Groups on the Structure and Ordering of Poly(*p*-phenylenevinylene) Derivatives" *Synthetic Metals* **1993**, *55*, 449-452.

(53) Maxwell, J. C. "A Dynamical Theory of the Electromagnetic Field" *Philos. Trans. R. Soc. London, A* **1865**, *155*, 459-512.

(54) McClure, D. S. "Triplet-Singlet Emissions in Organic Molecules" *J. Chem. Phys.* **1949**, *17*, 905-913.

(55) McQuarrie, D. A.; Simon, J. D. *Physical Chemistry: A Molecular Approach*; University Science Books: Sausalito, California, 1997.

(56) Mei, J.; Ogawa, K.; Kim, Y.-G.; Heston, N. C.; Arenas, D. J.; Nasrollahi, Z.; McCarley, T. D.; Tanner, D. B.; Reynolds, J. R.; Schanze, K. S. "Low-band-gap Platinum Acetylide Polymers as Active Materials for Organic Solar Cells" *Appl. Phys. Interfaces* **2009**, *1*, 150-161.

(57) Nguyen, P.; Gmez-Elipe, P.; Manners, I. "Organometallic Polymers with Transition Metals in the Main Chain" *Chem. Rev.* **1999**, *99*, 1515-1548.

(58) Pilar, F. L. *Elementary Quantum Chemistry*, Second ed.; Courier Dover Publications: Massachusetts, 2006.

(59) Pollino, J. M.; Weck, M. "Tandem Catalysis and Self-Assembly: A One-Pot Approach to Functionalized Polymers" *Org. Lett.* **2002**, *4*, 753-756.

(60) Power, P. P. "Persistent and Stable Radicals of the Heavier Main Group Elements and Related Species" *Chem. Rev.* **2003**, *103*, 789-810.

(61) Remmers, M.; Neher, D.; Grner, J.; Friend, R. H.; Gelinck, G. H.; Warman, J. M.; Quattrocchi, C.; dos Santos, D. A.; Brdas, J.-L. "The Opticals, Electronic, and Electroluminescent Properties of Novel Poly(*p*-phenylenevinylene)-Related Polymers" *Macromolecules* **1996**, *29*, 7432-7445.

(62) Roncali, J. "Synthetic Principles for Bandgap Control in Linear π-Conjugated Systems" *Chem. Rev.* **1997**, *97*, 173-206.

(63) Sariciftci, N. S.; Braun, D.; Zhang, C.; Srdanov, V. I.; Heeger, A. J.; Stucky, G.; Wudl, F. "Semiconducting Polymer-Buckminsterfullerene Heterojunctions: Diodes, Photodiodes, and Photovoltaic Cells" *Appl. Phys. Lett.* **1993**, *68*, 585-587.

(64) Shah, A.; Torres, P.; Tscharner, R.; Wyrsch, N.; Keppner, H. "Photovoltaic Technology: The Case for Thin-Film Solar Cells" *Science* **1999**, *285*, 692-698.

(65) Silverman, E. E.; Cardolaccia, T.; Zhao, X.; Kim, K.-Y.; Haskins-Glusac, K.; Schanze, K. S. "The Triplet State in Pt-Acetylide Oligomers, Polymers and Copolymers" *Coord. Chem. Rev.* **2005**, *249*, 1491-1500.

(66) Smith, R. C.; Protasiewicz, J. D. "A Trans-Spanning Diphosphine Ligand Based on a *m*-Terphenyl Scaffold and Its Palladium and Nickel Complexes" *Organometallics* **2004**, *23*, 4215-4222.

(67) Son, S.; Dodabalapur, A.; Lovinger, A. J.; Galvin, M. E. "Luminescence Enhancement by the Introduction of Disorder into Poly(*p*-phenylenevinylene)" *Science* **1995**, *269*, 376-378.

(68) Sonogashira, K.; Takahashi, S.; Hagihara, N. "A New Extended Chain Polymer, Poly[*trans*-bis(tri-*n*-butylphosphine)platinum 1,4-butadiynediyl]" *Macromolecules* **1977**, *10*.

(69) South, C. R.; Weck, M. "Bridged Coordination Polymer Multilayers with Tunable Properties" *Langmuir* **2008**, *24*, 7506-7511.

(70) Swager, T. M.; Gil, C. J.; Wrighton, M. S. "Fluorescence Studies of Poly(*p*-phenyleneethynylene)s: The Effect of Anthracene Substitution" *J. Phys. Chem.* **1995**, *99*, 4886-4893.

(71) Taranekar, P.; Qiao, Q.; Jiang, H.; Ghiviriga, I.; Schanze, K. S.; Reynolds, J. R. "Hyperbranched Conjugated Polyelectrolyte Bilayers for Solar-Cell Applications" *J. Am. Chem. Soc.* **2007**, *129*, 8958-8959.

(72) Thnemann, A. F.; Ruppelt, D. "Electroluminescent Polyelectrolyte-Surfactant Complexes" *Langmuir* **2001**, *17*, 5098-5102.

(73) Thompson, B. C.; Frechét, J. M. J. "Polymer-Fullerene Composite Solar Cells" *Angew. Chemie Int. Ed.* **2008**, *47*, 58-77.

(74) Tipathy, S. K.; Kumar, J.; Nalwa, H. S. *Handbook of Polyelectrolytes and Their Applications*, First ed.; American Scientific Publishers: Stevenson Ranch, CA, 2002.

(75) Tourillon, G.; Garnier, F. "Effect of Dopant on the Physicochemical and Electrical Properties of Organic Conducting Polymers" *J. Phys. Chem.* **1983**, *87*, 2289-2292.

(76) van der Boom, M. E.; Milstein, D. "Cyclometalated Phosphine-Based Pincer Complexes: Mechanistic Insight in Catalysis, Coordination, and Bond Activation" *Chem. Rev.* **2003**, *103*, 1759-1792.

(77) Wang, Y.; Ranasinghe, M. I.; Goodson III, T. "Ultrafast Fluorescence Investigation of Excitation Energy Transfer in Different Dendritic Core Branched Structures" *J. Am. Chem. Soc.* **2003**, *125*, 9562-9563.

(78) Weinberger, B. R.; Gau, S. C.; Kiss, Z. "A Polyacetylene:Aluminum Diode" *Appl. Phys. Lett.* **1981**, *38*, 555-558.

(79) Williams, D. H.; Fleming, I. *Spectroscopic Methods in Organic Chemistry*, Fourth ed.; McGraw-Hill Book Company: UK, 1989.

(80) Wilson, J. S.; Chawdhury, N.; Al-Mandhary, M. R. A.; Younus, M.; Khan, M. S.; Raithby, P. R.; Kohler, A.; Friend, R. H. "The Energy Gap Law for Triplet States in Pt-Containing Conjugated Polymers and Monomers" *J. Am. Chem. Soc.* **2001**, *123*, 9412-9417.

(81) Wilson, J. S.; Dhoot, A. S.; Seeley, A. J. A. B.; Khan, M. S.; Kohler, A.; Friend, R. H. "Spin-Dependent Exciton Formation in π-Conjugated Compounds" *Nature* **2001**, *413*, 828-831.

(82) Wolf, C. *Dynamic Stereochemistry of Chiral Compounds*; RSC Publishing: Cambridge, UK, 2008.

(83) Wong, W.-Y.; Zhou, G.-J.; He, Z.; Cheung, K.-Y.; Ng, A. M.-C.; Djurisic, A. B.; Chan, W.-K. "Organometallic Polymer Light-Emitting Diodes Derived from a Platinum(II) Polyyne Containing the Bithiazole Ring" *Macromolecular Chemistry and Physics* **2008**, *209*, 1319-1322.

(84) Xu, B.; Holdcroft, S. "First Observation of Phosphorescence from π-Conjugated Polymers" *J. Am. Chem. Soc.* **1993**, *115*, 8447-8448.

(85) Yang, N. C.; Gaoni, Y. "Charge-Transfer Interaction in Organic Polymers" *J. Am. Chem. Soc.* **1964**, *86*, 5022-5023.

(86) Yassar, A.; Roncali, J.; Garnier, F. "Conductivity and Conjugation Length in Poly(3-methylthiophene) Thin Films" *Macromolecules* **1989**, *22*, 804-809.